



UNIVERSITAT DE
BARCELONA

Computational Study of the Mechanisms that Stabilize Organic Molecule-Based Magnets

María Pilar Lafuente Hernández

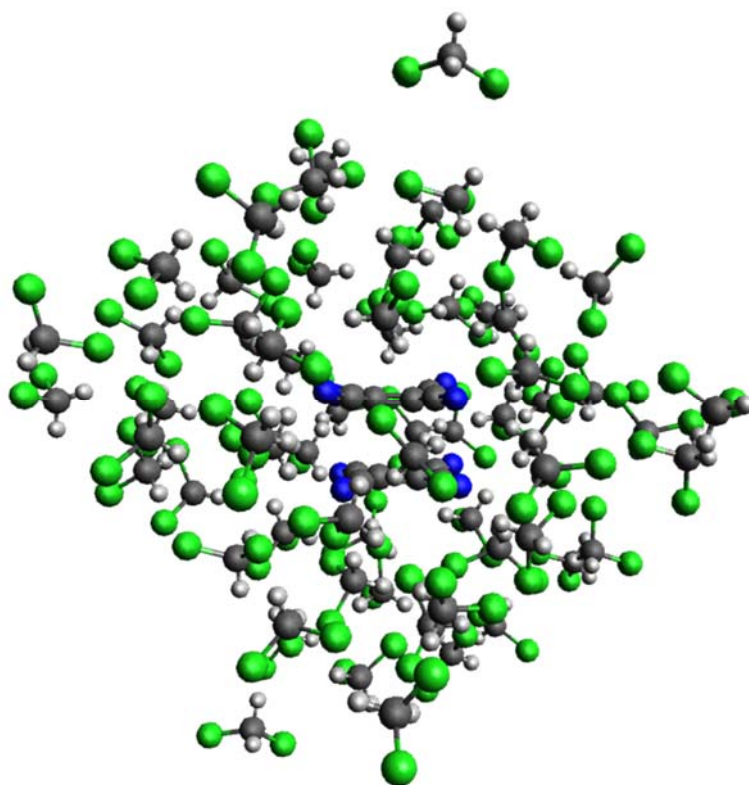
ADVERTIMENT. La consulta d'aquesta tesi queda condicionada a l'acceptació de les següents condicions d'ús: La difusió d'aquesta tesi per mitjà del servei TDX (www.tdx.cat) i a través del Dipòsit Digital de la UB (diposit.ub.edu) ha estat autoritzada pels titulars dels drets de propietat intel·lectual únicament per a usos privats emmarcats en activitats d'investigació i docència. No s'autoritza la seva reproducció amb finalitats de lucre ni la seva difusió i posada a disposició des d'un lloc aliè al servei TDX ni al Dipòsit Digital de la UB. No s'autoritza la presentació del seu contingut en una finestra o marc aliè a TDX o al Dipòsit Digital de la UB (framing). Aquesta reserva de drets afecta tant al resum de presentació de la tesi com als seus continguts. En la utilització o cita de parts de la tesi és obligat indicar el nom de la persona autora.

ADVERTENCIA. La consulta de esta tesis queda condicionada a la aceptación de las siguientes condiciones de uso: La difusión de esta tesis por medio del servicio TDR (www.tdx.cat) y a través del Repositorio Digital de la UB (diposit.ub.edu) ha sido autorizada por los titulares de los derechos de propiedad intelectual únicamente para usos privados enmarcados en actividades de investigación y docencia. No se autoriza su reproducción con finalidades de lucro ni su difusión y puesta a disposición desde un sitio ajeno al servicio TDR o al Repositorio Digital de la UB. No se autoriza la presentación de su contenido en una ventana o marco ajeno a TDR o al Repositorio Digital de la UB (framing). Esta reserva de derechos afecta tanto al resumen de presentación de la tesis como a sus contenidos. En la utilización o cita de partes de la tesis es obligado indicar el nombre de la persona autora.

WARNING. On having consulted this thesis you're accepting the following use conditions: Spreading this thesis by the TDX (www.tdx.cat) service and by the UB Digital Repository (diposit.ub.edu) has been authorized by the titular of the intellectual property rights only for private uses placed in investigation and teaching activities. Reproduction with lucrative aims is not authorized nor its spreading and availability from a site foreign to the TDX service or to the UB Digital Repository. Introducing its content in a window or frame foreign to the TDX service or to the UB Digital Repository is not authorized (framing). Those rights affect to the presentation summary of the thesis as well as to its contents. In the using or citation of parts of the thesis it's obliged to indicate the name of the author.

Computational Study of the Mechanisms that Stabilize Organic Molecule-Based Magnets

Maria Pilar Lafuente Hernández



UNIVERSITAT DE
BARCELONA

Secció de Química Física
Departament de Ciència de Materials i Química Física
Facultat de Química



UNIVERSITAT DE
BARCELONA

Programa de Doctorat de Química Teòrica i Computacional

Computational Study of the Mechanisms that Stabilize Organic Molecule-Based Magnets

Memòria de tesi presentada per Maria Pilar Lafuente Hernández per aspirar al grau de Doctor en Ciències Químiques

Dirigida per:

Dr. Juan José Novoa Vide
Secció Química Física, Facultat Química
Universitat de Barcelona

Dra. Mercè Deumal i Solé
Secció Química Física, Facultat Química
Universitat de Barcelona

Tutor:

Dr. Fernando Mota Valeri
Secció Química Física, Facultat Química
Universitat de Barcelona

Barcelona, Setembre 2016

*A Sergio, por su apoyo incondicional, su perseverancia y su convicción,
A Laura e Irene, por todos esos momentos que me he perdido,
A mis padres, por su insistencia y por enseñarme que nada es imposible,*

'It is difficult to say what is impossible, for the dream of yesterday is the hope of today and the reality of tomorrow.'

Robert H. Goddard.

Acknowledgements

Quisiera agradecer el apoyo de todos aquellos que han “sufrido” conmigo y me han animado durante este largo proceso.

A todos aquellos con los que he compartido horas de cafés y despachos: Toni, Mercè, Carme, Ramón, Maite, Paco, Eva, Mari Àngels, Jordi y muchos otros que también estuvieron allí. Gisela, gracias por ser un ejemplo estos últimos años.

Mike, thanks for guiding me my first years of research. You were a great inspiration and it was a great honor and privilege working with you and your team in London.

Muchas gracias Juan por haber confiado en mí durante todos estos años. Gracias por todas nuestras conversaciones, la mayoría sobre ciencia, pero también sobre la vida. Ha sido un proceso de aprendizaje largo y una gran experiencia que finalmente ha culminado en esta memoria de tesis.

Mercè, sense tu aquesta tesi mai hauria estat una realitat. Tu has estat una persona fonamental durant tot el procés. Des dels principis, a Londres, fins al final, en el laboriós procés de preparació d'aquesta memòria de tesi. Mai podré expressar amb paraules lo agraïda que t'estic. Gràcies es massa poc.

A mis padres, Tomás y M^a Pilar por no dejar de preguntar cómo iba la tesis. Por su ayuda, su insistencia y su apoyo.

A Sergio por su convicción de que esta tesis iba a ser una realidad. Por haberme ayudado a encontrar esos momentos imposibles para poderme dedicar a ella y por su apoyo incondicional y su fuerza en los momentos bajos. Esta tesis es en parte tuya.

Y a Laura e Irene. Porque me perdí muchos momentos con vosotras, pero tuvisteis la paciencia y la comprensión de regalarme esos ratitos. Os lo debía. Recordad que los sueños se cumplen.

Index

1	INTRODUCTION AND OBJECTIVES.....	1
2	MAGNETISM AND MAGNETIC MATERIALS.....	8
2.1	EXPERIMENTAL CLASSICAL APPROACH.....	8
2.2	QUANTUM APPROXIMATION.....	13
2.3	MAGNETIC MECHANISM.....	17
3	METHODS.....	30
3.1	AB-INITIO METHODS.....	30
3.2	DENSITY FUNCTIONAL THEORY (DFT).....	33
3.3	MOLECULAR MECHANICS VALENCE BOND (MMVB) METHOD.....	40
3.4	ATOMS IN MOLECULES (AIM) METHOD.....	44
4	INTRAMOLECULAR INTERACTIONS.....	49
4.1	METHODS.....	49
4.2	HISTORICAL REFERENCES.....	53
4.3	STUDY OF THE STABILIZATION OF THE HIGH-SPIN STATE IN BIRADICALS.....	54
4.4	POLYMERIZATION OF BIRADICALS IN ONE MAGNETIC DIMENSIONALITY (1D SYSTEMS).....	67
4.5	CONCLUSIONS.....	79
5	CHARACTERIZATION OF THROUGH-SPACE INTERACTIONS IN BIMOLECULAR SYSTEMS.....	83
5.1	CHARACTERIZATION OF THE INTERMOLECULAR INTERACTIONS WITH <i>ATOMS IN MOLECULES</i> (AIM): HYDROGEN BOND FORMATION.....	83
5.2	EFFECT OF THE ORIENTATION IN RADICAL-RADICAL INTERMOLECULAR INTERACTIONS: ANALYSIS OF MCCONNELL THEORY.....	90
5.3	CONCLUSIONS.....	116
6	CRYSTAL PACKING IN MOLECULAR MAGNETISM.....	118
6.1	CRYSTAL PACKING: STUDY OF HNOBEN AND YIMWIA CRYSTALS.....	118
6.2	MAGNETO STRUCTURAL STUDY ON THE MOLECULAR α -NITRONYL NITROXIDE CRYSTALS.....	129
7	STUDY OF π-[TCNE]₂²⁻ DIMERS IN MOLECULAR CRYSTALS.....	154
7.1	INTRODUCTION.....	154
7.2	GEOMETRY OF THE [TCNE] ₂ ²⁻ DIMER.....	158
7.3	THE POTENTIAL ENERGY CURVE OF THE [TCNE] ₂ ²⁻ DIMER.....	159
7.4	NATURE OF THE INTERMOLECULAR INTERACTIONS WITHIN THE [TCNE] ₂ ²⁻ DIMER.....	170
7.5	EXPERIMENTAL EVIDENCE OF THE LONG INTERMOLECULAR CC BOND.....	176
7.6	CONCLUSIONS.....	180
7.7	COMPUTATIONAL AND EXPERIMENTAL DETAILS.....	181
8	CONCLUSIONS.....	187
9	RESUMEN.....	191
9.1	OBJETIVO.....	191
9.2	INTRODUCCIÓN.....	191
9.3	MÉTODOS.....	193
9.4	RESULTADOS.....	194
9.5	CONCLUSIONES.....	212

CHAPTER 1

INTRODUCTION

1 Introduction and objectives

The focus of our research has been the study of molecule-based organic magnets. The synthesis of this kind of materials is particularly challenging as their building blocks are organic molecules with free electrons (radicals) that usually are not stable. Since magnetism is a macroscopic property, the contacts between the constitutive radicals need to be ferromagnetic (with parallel spin moments), which is especially difficult since free radicals tend to interact forming bonds and cancel the spin moments. A third condition sought is that the intermolecular ferromagnetic interaction is permanent and expands throughout the crystal.

The first known magnetic materials and the most studied so far are solid inorganic systems. Their magnetic properties are determined by the spin of the unpaired electrons located on their constitutive metal atoms. However, since the last decades of the 20th century, the interest for molecular magnetic materials has increased exponentially. Compounds whose magnetic properties are modulated by organic molecules have very interesting characteristics that the inorganic magnets lack¹⁻⁵. Unlike the synthesis of classic magnets, organic magnets can be prepared at low temperature, have low spin density and high molecular weight. In addition, organic synthesis allows controlling the physical properties of the compound and makes possible to combine in the same product magnetism with optics, plasticity or conductivity properties. Organic compounds can also be biocompatible. As a consequence of that interest, many theoretical and experimental studies have arisen in the last years related to molecular magnets that have organic molecules or organic complexes in their structure^{3,4,6-10}. Although there are many examples of molecules with stable high spin ground states, organic magnets known so far only exhibit magnetic properties at very low temperatures. Despite the fact that these solids do not have a technological applicability up to now, given these low temperatures, there is a great interest to study them due to the possible properties that this kind of materials could present as transparency, insulating behavior, etc^{9,11-13}.

Organic molecular magnets can be classified into three groups considering the nature of their constituents⁵:

- (1) Pure organic molecular magnets, constituted by open-shell organic molecules (neutral radicals, radical ions, transfer charge salts, etc.);
- (2) Organometallic systems, that contain both organic molecules and metal atoms (whether transition metals or rare earth), being both spin containing centers;
- (3) And a third class, that contain organic molecules, but they do not have unpaired electrons. The metal atoms are the spin containing units and the organic molecules have an important structural role.

Pure organic magnetic molecular materials can also be classified into two major groups, considering the structural aspect¹: (a) *polymer magnetic materials* and (b) *molecular magnetic crystals*:

- a. *Polymer magnetic materials* with one or more molecular units that bond to form structures in one, two or three dimensions of space. Depending on the characteristics of the constitutive units, the spin centers, and the **intramolecular interaction** between them, the resulting macromolecule may have a permanent magnetic moment and therefore magnetic properties. Despite the studies conducted in this field^{14–20}, no polymeric material with these properties has been synthesized yet.
- b. The *molecular magnetic crystals* present a crystal structure based on stable high spin radicals that interact among themselves at intermolecular level. The structure of these molecular solids is defined by the **intermolecular interactions** present (ionic, hydrogen bond or Van der Waals interaction)²¹. The structure of a crystal is based on a unit cell that is repeated by translation in the space. The unit cell has certain symmetry properties and, in many cases, these properties are the ones that determine the behavior of the solid. The understanding of these interactions in the context of crystal packing and its use in the design of new crystals is known as *Crystal Engineering*^{5,22–24}.

Some basic concepts about magnetism and molecular magnetic materials will be introduced in **Chapter 2**.

We have used computational chemistry methods in the research performed. The hybrid method *Molecular Mechanical - Valence Bond* (MMVB) developed in M.A. Robb and coworkers²⁵ was selected for qualitative energy calculations on large planar hydrocarbon systems. When more complex *ab initio* methods were required, different methodologies were evaluated to discriminate the one suitable to the system studied. We have used configuration interaction methods **CASSCF(*m,n*)** when it was needed to introduce correlation and more than one configuration to describe the system, especially for open-shell systems like the ones we are working with. We have also used perturbational methods **MP2** when the interaction we studied needed dynamic correlation. In addition, some calculations were done combining the configuration interaction and MP2 (**CASMP2**). Whenever it has been possible, we have used the density functional methods (**UB3LYP**, **M06L**), especially for large and complex systems, due to their simplicity and calculation speed, always evaluating the spin contamination and using Broken Symmetry to minimize it. The basis sets chosen include polarization to add flexibility and allow the molecular orbitals involving the active atoms to have more asymmetry and adapt better to the molecular environment. In the description of anions or radicals, we also needed to introduce diffuse functions to the basis sets to better describe the distant parts from the nuclei. The adequate basis set has been evaluated for each system studied. Additionally, we have used the methodology *Atoms in Molecules*²⁶ (AIM) proposed by Bader to describe the characteristics of the intermolecular interaction. These methods are discussed with detail in **Chapter 3**.

As mentioned, the constitutive molecules of molecular magnets must have a permanent spin moment different from zero. Then, these molecules need to interact so that the interaction is ferromagnetic (favor the parallel distribution of the spin moments) and stable throughout the crystal. Thus, our studies about the design of organic molecule-based magnets had a threefold approach: first, we characterized stable, high spin radicals, second, we analyzed the intermolecular interactions that result in a zero magnetic moment and third, we examined interactions within the crystal that stabilize its structure. Additionally,

we have investigated the causes of the loss of magnetism observed in some experimental transfer salt crystals that were expected to have magnetic behavior.

To begin with, we studied radical hydrocarbons with high spin ground state (**Chapter 4**). In these systems, the free electrons are placed in the π -framework of the molecule, which is basically constituted by the π -orbitals. Depending on whether the π -orbitals are delocalized or localized, these molecules are categorized as alternant or non-alternant hydrocarbons, respectively. As a results of our studies, we observed that, in the molecules that are alternant systems, the through-bond (TB) intramolecular interactions are predominant between active electrons. On the contrary, the gap of energy between the ground and first excited spin states in the non-alternant systems is determined by through-space interaction (TS) between the electrons in the localized orbitals. In the systems studied, the gap of energy between high and low spin states is found to be higher in the alternant systems than in the non-alternant ones, and, therefore, the high spin state is more stable in the former molecules.

Once potential magnetic building blocks were characterized, we evaluated the possibility of designing high spin macromolecules constituted by these high spin organic radicals. One approach evaluated was the polymerization of the previously identified high spin molecules¹⁴. On that regard, we have observed that the gap of energy between the two spin states lower in energy decreases when the number of molecules that are bonded increases. Another approach considered was the strategy followed by Dougherty²⁷⁻²⁹ consisting on the heterogeneous synthesis of spin containing units (SU) coupled through coupling units (CU): SU-CU-SU. We established that the gap of energy between the high and low spin states of the macromolecule is defined by the spin states of the constitutive units. These studies were mainly carried-out using the hybrid method *Molecular Mechanics - Valence Bond* (MMVB)⁶ and CAS calculations³⁰.

Going from high spin molecules to magnetic compounds implies the study of the intermolecular interactions. The method *atoms in molecules* (AIM), proposed by Bader²⁶, is a helpful tool to characterize the existence of connections between atoms based on the topological features of the electron density. However, some discrepancies exist regarding if this description is enough to characterize the intermolecular contacts³¹. In our studies, we challenged this method to verify if the only presence of intermolecular Bond Critical Points (BCPs) can distinguish an attractive intermolecular interaction (**Chapter 5**). We observed that BCP appeared between two molecules even when the interaction between them was repulsive, possibly as a consequence of the overlap of the electronic densities. accordingly, it is recommended to perform the AIM analysis together with an energy evaluation of the interaction to verify whether it is attractive or not.

Within the study of the intermolecular interactions, McConnell proposed a mechanism that intended to predict in a simple way when the interaction is ferromagnetic or antiferromagnetic³². This theory stated that when the main interaction is between atoms or groups of atoms with opposite spin densities, the interaction would be preferably ferromagnetic, while it would be antiferromagnetic when the interaction is between spin densities of the same sign. To assess this theory, we studied through-space interactions in several systems (**Chapter 5**): H₂NO, methyl-allyl and allyl-allyl, constituted by well-known radicals that represent, in a simplified way, some of the intermolecular contacts found in

organic molecular crystals. We evaluated the interaction between two radical molecules at different orientations and we observed that either the high spin or low spin states can be favored depending on how the two molecules are oriented and how the active electrons interact³³. McConnell I model described correctly the spin preference of the interaction when the two molecules were placed in parallel planes and there was a clear predominant interaction between the two molecules. However, McConnell failed if there were several competing intermolecular interactions involved and/or the orientation between the interacting radicals was not in parallel planes. Therefore, the magneto-structural relationship of the interaction between two molecules is not as easy as initially expected³³.

In the crystal design it is important to understand the forces that define the crystal packing of the molecules. For that reason, we characterized the crystal packing in two experimental crystals: hexanitrobenzene (HNOBEN³⁴) and the crystal YIMWIA³⁵, constituted 1:1 by trimethyl isocyanurate (TMIC) and 1,3,5-trinitrobenzene (1,3,5-TNB). The investigation was carried out using the fragment analysis and AIMs methods. With the fragment analysis we tried to identify the interactions that stabilize the crystal structure studying the main intermolecular contacts present in the crystal, both intra- and inter-layer (**Chapter 6**).

Our group has carried out extensive studies to confirm any possible magneto-structural relationship in α -nitronyl nitroxide crystals^{36–40}. On that context and, as part of my research, we studied the α - nitronyl nitroxide crystals that experimentally had shown ferromagnetic behavior. We carried out ab-initio calculations for the intermolecular interactions between the ONCNO groupsⁱ that were closer in space, using the atom coordinates obtained crystallographically. As a result of these calculations (**Chapter 6**), we observed that the spin multiplicity obtained for the intermolecular interactions examined did not always correspond to the experiential macroscopic magnetism. Therefore, this study illustrated that an analysis limited to these interactions is not enough to describe the magnetic property observed. Additionally, we performed a detailed clustering analysis to evaluate if the parameters that identify the intermolecular interaction could group separately the ferromagnetic or antiferromagnetic interactions. The results indicated that there is no clear relationship between the geometric parameters analyzed and the preference for a ferro-/antiferromagnetic interaction³⁹.

An example of an organic-based magnet is $[\text{Fe}(\text{C}_5\text{Me}_5)_2]^+[\text{TCNE}]^-$ (TCNE = tetracyanoethylene) whose ferromagnetic ordering was detected below its T_c of 4.8 K⁴¹. This is an electron transfer salt whose structure consists in alternating parallel chains of the cation and the anion. Since that first magnet, many different crystals have been synthesized based on the structure and characteristics of D^+A^- (D=electron donor, A=electron acceptor). However, sometimes, a loss of magnetism is observed when synthesizing this kind of magnetic materials. It is important to study these cases to better understand the mechanisms that lead to a loss of magnetic properties. As a part of our investigation, we have done an extensive description of the dimerization of TCNE^- radical molecules trying to figure out which conditions favor the dimerization^{42–44} (**Chapter 7**). We rationalized the loss of magnetism, due to the formation of dimers that are metastable in vacuum^{42–44} and are only stabilized in the presence of counterions or molecules of polar solvents.

ⁱ Oxygen-Nitrogen-Carbon-Nitrogen-Oxygen (ONCNO) atoms within the α -nitronyl nitroxide ring

As a conclusion, quantum chemistry is a valuable tool to understand and design molecular magnets. Although, many compounds designed theoretically are impossible to be synthesized for various reasons, the theoretical study provides the necessary knowledge to confirm, interpret and/or predict experimental results. Computational calculations help to minimize cost and effort by establishing potential candidates when designing new materials. The synthesis of light magnetic materials and the possibility of combining physical properties such as photo-magnetic effects, thermal induced magnetic properties or magnetic-pole reversal is something widely desired. However, there are still many challenges to overcome in the synthesis of organic molecule-based magnets. Computational chemistry can bring the tools to understand how the intra- and intermolecular forces stabilize high spin units and how intermolecular interactions that expanded in the crystal structure can bring the desired properties. We are still working on finding the right building blocks of the materials, evaluating their magnetic intermolecular interaction and confirming the right crystal packing, so that the property is extended in the final material.

Bibliography

- (1) *Magnetic Molecular Materials*; Gatteschi, D., Kahn, O., Miller, J. S., Palacio, F., Eds.; Springer Netherlands: Dordrecht, 1991.
- (2) Iwamura, H.; Nakamura, N.; Koga, N.; Sasaki, S. *Mol. Cryst. Liq. Cryst. Sci. Technol. Sect. Mol. Cryst. Liq. Cryst.* **1992**, *218* (1), 207–212.
- (3) Kahn, O. *Molecular Magnetism*, 1 edition.; Wiley-VCH: New York, 1993.
- (4) Miller, J. S.; Epstein, A. J. *Angew. Chem. Int. Ed. Engl.* **1994**, *33* (4), 385–415.
- (5) Day, P.; Underhill, A. E. *Metal-organic and Organic Molecular Magnets*; Royal Society of Chemistry, 1999.
- (6) Manriquez, J. M.; Yee, G. T.; Mclean, R. S.; Epstein, A. J.; Miller, J. S. *Science* **1991**, *252* (5011), 1415–1417.
- (7) Tamura, M.; Nakazawa, Y.; Shiomi, D.; Nozawa, K.; Hosokoshi, Y.; Ishikawa, M.; Takahashi, M.; Kinoshita, M. *Chem. Phys. Lett.* **1991**, *186* (4–5), 401–404.
- (8) Lahti, P. M. In *Molecule-Based Magnetic Materials*; ACS Symposium Series; American Chemical Society, 1996; Vol. 644, pp 218–235.
- (9) Coronado, E.; Gatteschi, D. *J. Mater. Chem.* **2006**, *16* (26), 2513–2515.
- (10) Ratera, I.; Veciana, J. *Chem. Soc. Rev.* **2011**, *41* (1), 303–349.
- (11) Coronado, E.; Delhaès, P.; Gatteschi, D.; Miller, J. *Molecular Magnetism: From Molecular Assemblies to the Devices*; Springer Science & Business Media, 2013.
- (12) Miller, J. S.; Gatteschi, D. *Chem. Soc. Rev.* **2011**, *40* (6), 3065–3066.
- (13) Miller, J. S.; Drillon, M. *Magnetism: Molecules to Materials V*; John Wiley & Sons, 2006.
- (14) Itoh, K. *Pure Appl. Chem.* **1978**, *50* (11–12), 1251–1259.
- (15) Klein, D. J.; Nelin, C. J.; Alexander, S.; Matsen, F. A. *J. Chem. Phys.* **1982**, *77* (6), 3101–3108.
- (16) Alexander, S. A.; Klein, D. J. *J. Am. Chem. Soc.* **1988**, *110* (11), 3401–3405.
- (17) Klein, D. J.; Alexander, S. A.; Randić, M. *Mol. Cryst. Liq. Cryst. Inc. Nonlinear Opt.* **1989**, *176* (1), 109–114.
- (18) Nakamura, N.; Inoue, K.; Iwamura, H.; Fujioka, T.; Sawaki, Y. *J. Am. Chem. Soc.* **1992**, *114* (4), 1484–1485.
- (19) Matsuda, K.; Nakamura, N.; Inoue, K.; Koga, N.; Iwamura, H. *Chem. – Eur. J.* **1996**, *2* (3), 259–264.
- (20) Masi, J. V. In *2007 Electrical Insulation Conference and Electrical Manufacturing Expo*; 2007; pp 352–355.
- (21) Lahti, P. M. *Magnetic Properties of Organic Materials*; CRC Press, 1999.
- (22) Novoa, J. J.; Deumal, M.; Veciana, J. *Synth. Met.* **1999**, *103* (1), 2283–2286.
- (23) Rovira, C.; Veciana, J. *CrystEngComm* **2009**, *11* (10), 2031–2031.
- (24) Yoshioka, N. In *Advances in Organic Crystal Chemistry*; Tamura, R., Miyata, M., Eds.; Springer Japan, 2015; pp 669–688.
- (25) Bearpark, M. J.; Robb, M. A.; Bernardi, F.; Olivucci, M. *Chem. Phys. Lett.* **1994**, *217* (5–6), 513–519.
- (26) Bader, R. F. W. *Atoms in Molecules, Clarendon*; Oxford, 1990.
- (27) Dougherty, D. A. *Acc. Chem. Res.* **1991**, *24* (3), 88–94.
- (28) Novak, J. A.; Jain, R.; Dougherty, D. A. *J. Am. Chem. Soc.* **1989**, *111* (19), 7618–7619.
- (29) Pranata, J.; Dougherty, D. A. *J. Am. Chem. Soc.* **1987**, *109* (6), 1621–1627.
- (30) Lafuente, P.; Novoa, J. J.; Bearpark, M. J.; Celani, P.; Olivucci, M.; Robb, M. A. *Theor. Chem. Acc.* **1999**, *102* (1–6), 309–316.

- (31) Novoa, J. J.; Lafuente, P.; Mota, F. *Chem. Phys. Lett.* **1998**, *290* (4), 519–525.
- (32) McConnell, H. M. *J. Chem. Phys.* **1963**, *39* (7), 1910–1910.
- (33) Novoa, J. J.; Deumal, M.; Lafuente, P.; Robb, M. A. *Mol. Cryst. Liq. Cryst. Sci. Technol. Sect. Mol. Cryst. Liq. Cryst.* **1999**, *335* (1), 603–612.
- (34) Akopyan, Z. A.; Struchkov, Y. T.; Dashevskii, V. G. *J. Struct. Chem.* **1966**, *7* (3), 385–392.
- (35) Thalladi, V. R.; Panneerselvam, K.; Carrell, C. J.; Carrell, H. L.; Desiraju, G. R. *J. Chem. Soc. Chem. Commun.* **1995**, No. 3, 341–342.
- (36) Novoa, J. J.; Deumal, M.; Kinoshita, M.; Hosokishi, Y.; Veciana, J.; Cirujeda, J. *Mol. Cryst. Liq. Cryst. Sci. Technol. Sect. Mol. Cryst. Liq. Cryst.* **1997**, *305* (1), 129–141.
- (37) Deumal i Solé, Mercè. *Estudi Teòric del magnetisme en cristalls moleculars: Mecanismes d'interacció i empaquetament.*, Universitat de Barcelona: Barcelona, 1999.
- (38) Deumal, M.; Cirujeda, J.; Veciana, J.; Novoa, J. J. *Chem. – Eur. J.* **1999**, *5* (5), 1631–1642.
- (39) Deumal, M.; Lafuente, P.; Mota, F.; Novoa, J. J. *Synth. Met.* **2001**, *122* (3), 477–483.
- (40) Deumal, M.; Mota, F.; Bearpark, M. J.; Robb, M. A.; Novoa, J. J. *Mol. Phys.* **2006**, *104* (5–7), 857–873.
- (41) Miller, J. S.; Calabrese, J. C.; Rommelmann, H.; Chittipeddi, S. R.; Zhang, J. H.; Reiff, W. M.; Epstein, A. J. *J. Am. Chem. Soc.* **1987**, *109* (3), 769–781.
- (42) Novoa, J. J.; Lafuente, P.; Del Sesto, R. E.; Miller, J. S. *Angew. Chem. Int. Ed.* **2001**, *40* (13), 2540–2545.
- (43) Miller, J. S.; Del Sesto, R. E.; Lafuente, P.; Novoa, J. J. *Chem. Weinh. Bergstr. Ger.* **2002**, *8* (21), 4894–4908.
- (44) Novoa, J. J.; Lafuente, P.; Sesto, R. E. D.; Miller, J. S. *CrystEngComm* **2002**, *4* (65), 373–377.

CHAPTER 2

MAGNETISM AND MAGNETIC MATERIALS

2 Magnetism and magnetic materials

2.1 Experimental classical approach

Magnetism is a cumulative property of the solid state which is based on the behavior of unpaired electrons in the system^{1,2}. All the electrons have associated an internal angular momentum, also called *spin*. Normally, electrons tend to pair so that two electrons occupy the same orbital. When this happens, their spins are oriented in opposite directions, according to the *Pauli exclusion principle*^{3,4} (\uparrow : positive spin, \downarrow : negative spin) canceling the net magnetic spin moment. In the case of unpaired electrons that interact such that their spin moments are not cancelled, the net spin magnetic moment is different from zero. It is then considered that the system has a high spin multiplicity ground state and the solid acquires a *magnetization* M responsible for the magnetic properties of the system.

The magnetic behavior of a solid can be characterized from the molar magnetization M that the solid acquires after the application of a magnetic field H ^{1,2} (Figure 2.1). The different magnetic properties of the solids can be classified into two groups depending on the interaction between the unpaired electrons: (1) the *non-cooperative* properties, which occur in compounds in which there are no unpaired electrons (*diamagnetism*) or they do not interact (*paramagnetism*), and (2) the *cooperative* properties, which are those observed in materials whose unpaired electrons interact. Within the *cooperative* properties, different behaviors can be observed: when the unpaired electrons interact with parallel spins (*ferromagnetism*) the net magnetic moment is different from zero; if the spin moments are antiparallel, the net spin magnetic moment is zero if the individual spin moments are of the same magnitude (*antiferromagnetism*) or different from zero if the individual spin moments have different magnitude (*ferrimagnetism*).

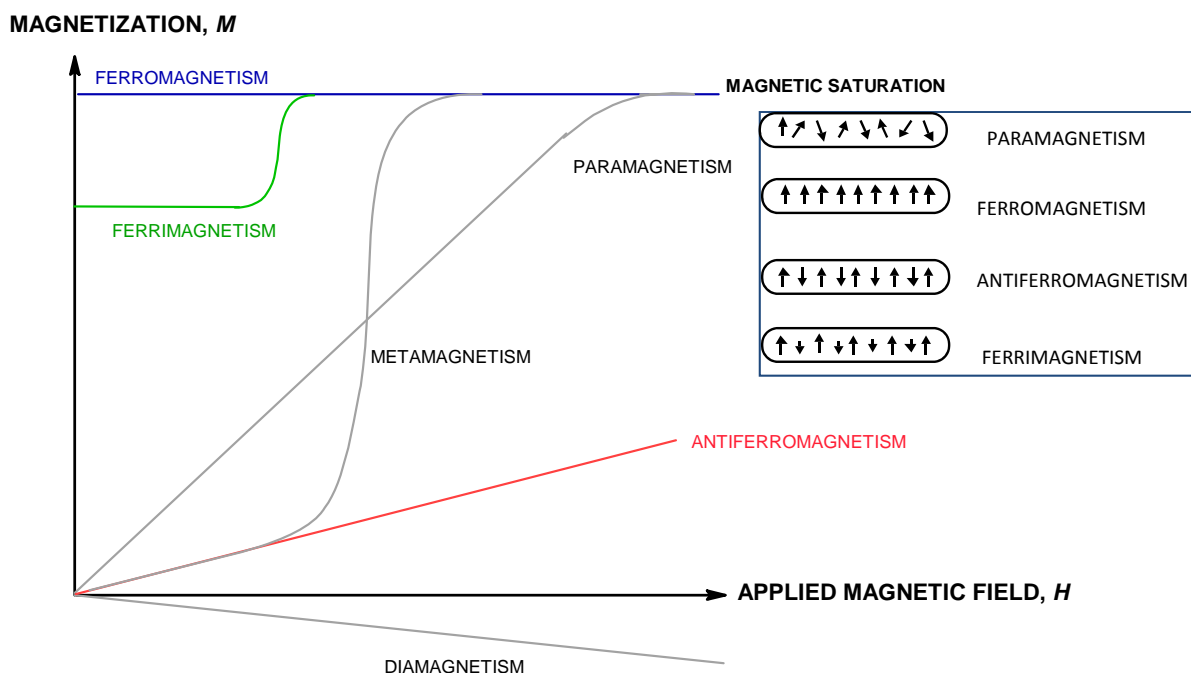


Figure 2.1 Representation of the magnetization M vs the applied magnetic field H for the different responses depending on the characteristics of the solid: diamagnetism, metamagnetism, paramagnetism, ferromagnetism, antiferromagnetism and ferrimagnetism².

Diamagnetism is an intrinsic property of the matter that occurs when applying a magnetic field H as a consequence of the interaction of the magnetic field with the angular moment of the electrons. The observed effect is opposite to the applied field H and has a value of *ca.* 10^{-9} eV.

The phenomenon called *paramagnetism* occurs in systems with unpaired electrons whose coupling energy is lower than the thermal energy. At temperatures above the so-called critical temperature (T_C), the spins do not pair and orient randomly. When a magnetic field H is applied, the magnetic moment μ associated with the electron spin tends to align in the same direction, increasing the magnetization M of the solid. The magnetization can only increase up to a maximum value, called the **saturation magnetization** M_S , which depends on the total number of unpaired electrons that contains the system [Figure 2.1, equation (2.9)]. The *paramagnetic* response is orders of magnitude greater than the *diamagnetic* one, so when *paramagnetic* phenomena exist, the *diamagnetic* effect is negligible (except in cases of biomagnetism, for example in metalloproteins).

Non-cooperative phenomena like *diamagnetism* and *paramagnetism* are characterized by the linear relationship between the molar magnetization M and the applied field H [equation (2.1)]:

$$M = \chi H \quad (2.1)$$

where χ is the magnetic susceptibility and represents the response of the substance to an applied field. The magnetic susceptibility χ has two components, $\chi = \chi^D + \chi^P$: the diamagnetic contribution χ^D is always negative and the paramagnetic χ^P that is positive. Depending on what contribution prevails, the magnetization M acquired by the substance will be opposite or in the same direction than the applied field H .

In the case of **non-cooperative** phenomena (non-coupling spins), when S is a valid quantum number, the susceptibility of the materials is inversely proportional to the temperature and the material follows what is called the **Curie law** [equation (2.2)]:

$$\chi = \frac{C}{T} \quad (2.2)$$

The Curie constant C in emu K mol⁻¹ is expressed as:

$$C = \frac{Ng^2\mu_B^2S(S+1)}{3k_B} \quad (2.3)$$

where S is the spin quantum number, N is the Avogadro's number, g is the Landé g-factor, μ_B is the Bohr magneton and k_B is the Boltzmann constant.

The Curie law assumes that the ground state is not degenerated, the magnetic susceptibility is due to the electron spin and that only the ground state is thermally populated.

When materials with unpaired electrons are at temperatures below certain *critical temperature* T_C , the thermal energy is lower than the magnetic energy and there is a coupling of the electronic spins that gives place to the **cooperative** phenomena. The *critical temperature* T_C is characteristic of each substance and defines what is called the Curie point. **Cooperative** phenomena include *ferromagnetism*, *antiferromagnetism* and *ferrimagnetism* (Figure 2.1). If the spins tend to align in parallel, the observed phenomenon is **ferromagnetism** and the critical temperature is called *Curie temperature* T_C . In the event that the alignment of the spins is antiparallel, the observed phenomenon is **antiferromagnetism**, and the critical temperature is referred to as *Néel temperature* T_N . A special case of antiferromagnetism is *ferrimagnetism*, which occurs when the moments of spin-aligned electrons are of different magnitudes, and, therefore the cancellation is incomplete and the net magnetic moment, although reduced, is non-zero. In the case of *ferrimagnetism* the critical temperature is also referred as *Néel temperature* T_N .

When **cooperative** interactions between the electronic spins exist, a field of effective exchange is introduced to modify the magnetic susceptibility [equation (2.2)]. In that case, the Curie-Weiss law [equation (2.4)] describes the susceptibility of the material above the Curie point ($T \gg T_C$). This law predicts a singularity when the temperature T reaches the critical temperature T_C and does not hold at temperatures close to the Curie point.

$$\chi = \frac{C}{T - T_C} \quad (2.4)$$

where

$$T_C = \frac{C\lambda}{\mu_0} \quad (2.5)$$

λ is the Weiss molecular field constant and μ_0 is the permeability of free space (in CGS units is equal to one).

For products that follow the Curie law, the susceptibility χ increases with the quantum spin number S , the product χT is constant and μ_{eff} is independent of temperature [equations (2.6) in emu K mol⁻¹ units and (2.7) in Bohr magneton units]. However, in the case of **cooperative** phenomena the effective magnetic moment μ_{eff} is temperature dependent, but this dependency is small at low temperatures when the Curie-Weiss law holds.

$$\mu_{eff} = \sqrt{\frac{3\chi k_B T}{N}} = 2.83\sqrt{\chi T} \quad (2.6)$$

$$\mu_{eff} = \mu_B \sqrt{g^2 S(S+1)} \quad (2.7)$$

The **critical temperature** is positive when the spins are oriented in parallel (*ferromagnetic* interactions), while when they are antiparallel (*antiferromagnetic*) is negative. Consequently, the behavior of the susceptibility χ with respect to temperature will differ depending on whether the substance is ferromagnetic or antiferromagnetic (Figure 2.2). The representations χT or effective moment μ_{eff} vs temperature (T) are commonly used in chemistry to characterize the magnetic behavior of a compound.

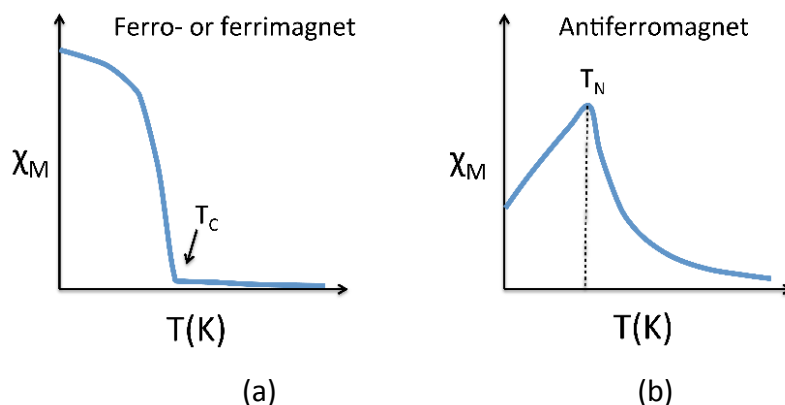


Figure 2.2 Representations χ vs T in (a) ferro- or ferrimagnetic and (b) antiferromagnetic materialsⁱⁱ.

Within the **cooperative** phenomena, we are especially interested in *ferromagnetism*. Ferromagnetic materials show a spontaneous magnetization at zero applied magnetic field [$M(H=0) \neq 0$]. On the contrary, in the case of *antiferromagnetism*, there is no magnetization at field $H=0$, but when applying a magnetic field H the magnetization M increases. In case of *ferrimagnetism* the magnetization at field zero ($H=0$) is different from zero and when applying a H -field the magnetization increases to reach the value of saturation magnetization M_S (Figure 2.1).

From equations (2.1), (2.2) and (2.5) it can be seen that the magnetization M depends on the temperature since the magnetic susceptibility χ does. Such dependency is applicable in cases of *ferro* - and *antiferromagnetism* only when $T \gg 0$, replacing T with an effective temperature $T_{eff} = T - T_C$ [equation (2.8)].

$$M = \frac{C}{T_{eff}} H = \frac{Ng^2 S(S+1) \mu_B^2}{3k_B T_{eff}} H \quad (2.8)$$

At low temperatures and with a high applied magnetic field H , the magnitudes of the thermal and magnetic energies are comparable [$E_M (= gS\mu_B H) \cong E_T (= k_B T)$]. In that case, the saturation magnetization M_S is reached and its value depends on the number of unpaired electrons [equation (2.9)]:

ⁱⁱ Extracted from *imageTemp5psu*.

$$M_s = \mu_B N S g \quad (2.9)$$

Usually in ferromagnetic materials, there are several zones or regions, called **domains**, where the local magnetization is oriented in one direction, but the different areas are oriented in different directions and the total magnetic moment is reduced or zero. When applying a magnetic field, these zones orient in the direction of the magnetic moment and the magnetization of the substance increases (Figure 2.3). To study the relative orientation of the magnetic moments between neighboring domains two factors must be taken into account: (1) the energy from the magnetic field generated by the paired electrons within the domains and (2) the cost of creating the walls between domains. The existence of these walls can be eliminated by the effect of an external magnetic field, to form a single domain. As mentioned before, in the absence of field ($H=0$), a material can have its domains oriented so that the magnetization is zero ($M=0$). Increasing H , M increases up to a maximum value called saturation magnetization. When the external magnetic field decreases from this point down to zero, it is observed that a magnetization different from zero is observed at $H=0$ and it is said that the material has magnetic memory. It is necessary to apply an external magnetic field in the other direction to have again magnetization zero. This is called the hysteresis cycle (Figure 2.3). The *coercive field* H_c is the magnetic field needed to orient the local regions or domains and represents the "memory" of the magnet. Depending on the magnitude of the coercive field of the substance, the magnets are classified as "hard" (when $H_c > 100$ Oe, these materials are used to store information) or "soft" ($H_c < 10$ Oe, these materials allow a quick change of polarity).

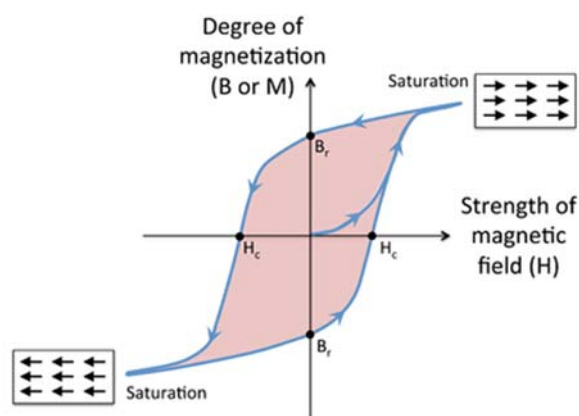


Figure 2.3 Graphical representation of a magnetic hysteresis cycleⁱⁱⁱ.

Apart from magnetic behaviors described above, there are other possible magnetic phenomena: *canted ferromagnetism*, *metamagnetism* and the so-called *spin glass*. *Canted ferromagnetism* is found in ferromagnetic materials that experience a decrease in the magnetic moment due to the inclination of the interacting chains (Figure 2.4a). The *metamagnetism* consists of the transformation from an antiferromagnetic system into ferromagnetic by the action of an external magnetic field (Figure 2.1). Finally, the *spin glass*

ⁱⁱⁱ Extracted from "Magnetic hysteresis" by Tem5psu.

phenomenon occurs when there is a local spatial correlation at close range in the direction of neighboring spins (Figure 2.4b).

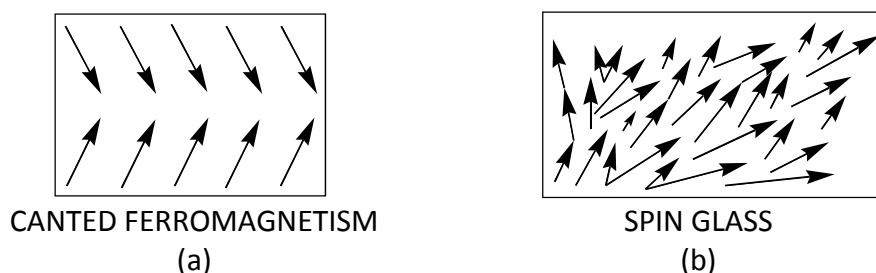


Figure 2.4 Graphical representation of the phenomena of (a) *canted ferromagnetism* and (b) *spin glass*².

2.2 Quantum approximation

As mentioned previously, the magnetic properties of a compound are characterized by the unpaired electrons present in the material. It is therefore essential to introduce concepts of quantum chemistry and, more specifically, the spin electron property and the mechanisms of the exchange interaction between unpaired electrons to explain magnetism⁵⁻⁷.

The energy of a system can be calculated as the expectation value of the Hamiltonian applied on the wave function Ψ that describes the system, using the well-known Schrödinger equation:

$$\hat{H}\Psi(\bar{x}_1, \bar{x}_2, \dots, \bar{x}_N, \bar{R}_1, \bar{R}_2, \dots, \bar{R}_M) = E\Psi(\bar{x}_1, \bar{x}_2, \dots, \bar{x}_N, \bar{R}_1, \bar{R}_2, \dots, \bar{R}_M) \quad (2.10)$$

$$E[\Psi] = \frac{\langle \Psi | \hat{H} | \Psi \rangle}{\langle \Psi | \Psi \rangle} \quad \text{where} \quad \langle \Psi | \hat{H} | \Psi \rangle = \int \Psi^* \hat{H} \Psi d\bar{x} \quad (2.11)$$

For a system with N electrons and M nuclei, the expression of the Hamiltonian in equation (2.10) includes the kinetic terms of the movement of the nuclei and the electrons, the attractive electrostatic interactions between nuclei and electrons and the repulsive potentials due to the electron-electron and the nucleus-nucleus interactions [equation (2.12)].

$$\hat{H} = -\frac{1}{2} \sum_{A=1}^M \frac{1}{M_A} \nabla_A^2 - \frac{1}{2} \sum_{i=1}^N \nabla_i^2 - \sum_{i=1}^N \sum_{A=1}^M \frac{Z_A}{r_{iA}} + \sum_{i=1}^N \sum_{j>i}^N \frac{1}{r_{ij}} + \sum_{A=1}^M \sum_{B>A}^M \frac{Z_A Z_B}{R_{AB}} \quad (2.12)$$

The Born-Oppenheimer approximation assumes that nuclei are much heavier than electrons and their movement is extremely slow compared to the electrons. Consequently, it is presumed that the motion of electrons and nuclei can be separated and it is considered that electrons are moving in the field of fixed nuclei, where the kinetic energy of the nuclei is basically zero and the repulsive potential energy of the nucleus-nucleus interaction is a constant. This leads to an electronic Hamiltonian \hat{H}_{elec} that only includes the electronic

terms: kinetic energy of the electrons (\hat{T}), attractive interaction nucleus-electron (\hat{V}_{Ne}) and repulsive electron-electron interaction (\hat{V}_{ee}) [equation (2.13)]:

$$\hat{H}_{elec} = -\frac{1}{2} \sum_i^N \nabla_i^2 - \sum_{i=1}^N \sum_{A=1}^M \frac{Z_A}{r_{iA}} + \sum_{i=1}^N \sum_{j>i}^N \frac{1}{r_{ij}} = \hat{T} + \hat{V}_{Ne} + \hat{V}_{ee} \quad (2.13)$$

The solution of the Schrödinger equation of the electronic hamiltonian \hat{H}_{elec} on the electronic wavefunction Ψ_{elec} gives the electronic energy E_{elec} . The total energy will be then the sum of the electronic energy and the constant nuclear repulsion term E_{nuc} [equations (2.14) and (2.15)].

$$E_{tot} = E_{elec} + E_{nuc} \quad (2.14)$$

$$E_{nuc} = \sum_{A=1}^A \sum_{B>A}^B \frac{Z_A Z_B}{r_{AB}} \quad (2.15)$$

It is not easy to find the exact wave function that describes the exact ground state of a system Ψ_0 . For that reason, to calculate the energy of a defined state, it is needed to start defining an approximate wave function Ψ to describe the state. This function can be constructed as product of the spin-orbitals ψ_i containing the N electrons of the system [equation (2.16)].

$$\Psi = \psi_1(1)\psi_2(2)\dots\psi_N(N) \quad (2.16)$$

The spin-orbitals ψ_i can be written as a product of the space orbital ϕ_i and the spin orbital σ_i of the particle i ($\psi_i = \phi_i \sigma_i$).

The function Ψ needs to be normalized and be antisymmetric with respect to particle interchange (Pauli's principle) [equation (2.17)].

$$\Psi = \hat{A}\Psi = |\psi_1(1)\psi_2(2)\dots\psi_N(N)| \quad (2.17)$$

The variational principle states that the energy computed from an approximated wave function Ψ is an upper-bound to the true ground-state energy Ψ_0 . To find a better wave function and a closer energy to the ground state, the energy needs to be minimized with respect to all the orbitals [equation (2.18)].

$$E_0 = \min_{\Psi \rightarrow N} E[\Psi] = \min_{\Psi \rightarrow N} \langle \Psi | \hat{T} + \hat{V}_{Ne} + \hat{V}_{ee} | \Psi \rangle \quad (2.18)$$

As mentioned above, charged particles in movement generate magnetic moments; consequently electrons have magnetic moments associated with their movement. These are called spin intrinsic angular momentum and have an associated magnetic moment M_S [equation (2.19)]

$$M_S = \frac{g\mu_B}{\hbar} \hat{S} \quad (2.19)$$

where \hat{S} is the spin operator, g is the gyromagnetic constant, μ_B is the Bohr magneton and \hbar is the Planck constant.

The operator \hat{S} , that describes the spin properties, is a vector of operators $\hat{S} = (\hat{S}_x, \hat{S}_y, \hat{S}_z)$. These operators satisfy the commutation rules. Like an angular momentum, there is a Hilbert space associated with the spin that supports the spin eigenstates. A set of basis vectors for this Hilbert space can be constructed out of simultaneous eigenvectors of the operators $\hat{S}^2 = \hat{S}_x^2 + \hat{S}_y^2 + \hat{S}_z^2$ and \hat{S}_z . The associated eigenvalues that satisfy the eigenvalue equations are $S(S+1)$ and M_S respectively.

Usually, electrons occupying the same orbitals have opposite spin moments (Pauli's Exclusion Principle) that cancel their magnetic moment. However, if there are free electrons in partially occupied orbitals, their magnetic moments are not cancelled and there will be an orbital magnetic moment different from zero.

The model space that describes the different spin states (different multiplicity) of a particular system with the same configuration consists of $2S+1$ functions Ψ^{M_S} with $M_S = S, S-1, \dots, -S$ (magnetic sublevels) that belong to the lowest eigenvalue, E_0 , of the \hat{H}_0 Hamiltonian.

The splitting of different states with the same configuration but different multiplicity is related to the electron-electron interaction and the asymmetry of the N-particle wavefunction. Therefore, the spin properties of this system could be described by a Hamiltonian that only includes the electron-electron interaction terms.

Effective Hamiltonians are Hamiltonians that act in a reduced space and only describe a part of the eigenvalue of the true (or complete) Hamiltonian. Therefore, the effective Hamiltonians are simpler and their eigensystems can be determined easier. To describe the different spin states of a particular system, the effective-spin Hamiltonian \hat{H}_S ⁶ [equation (2.20)] was introduced:

$$\hat{H}_S = Q - \sum_{i=1}^N \sum_{j>i}^N J_{ij} \left(2\hat{S}_i \cdot \hat{S}_j + \frac{1}{2} \hat{I}_{ij} \right) \quad (2.20)$$

where \hat{S}_i and \hat{S}_j are the spin operators associated with the electrons of the molecule, \hat{I}_{ij} is the spin identity operator, the parameter Q represents the Coulomb energy and J_{ij} is the exchange integral between the spin-orbital i, j [equation (2.21)].

$$J_{ij} = \int \psi_a^*(i) \psi_b^*(j) \hat{H} \psi_a(j) \psi_b(i) d\bar{x}_i d\bar{x}_j \quad (2.21)$$

The parameter J_{ij} correlates with the spin coupling of the electrons. In the case of two electrons, in terms of the Heitler-London electronic distribution the parameter J_{ij} can be expressed as:

$$J_{ij} = [ij|ji] + 2S_{ij} \langle i|\hat{h}|j \rangle \quad (2.22)$$

where $[ij|ji]$ is the bielectronic repulsion integral or exchange integral, of small and positive value; S_{ij} is the overlap between i and j , which is always positive; and $\langle i|\hat{h}|j \rangle$ is the monoelectronic integral, that has a negative sign. The magnitude of the parameter J_{ij} is usually dominated by the monoelectronic term and, therefore, tends to be negative, but when overlap tends to zero, this term takes a small and positive value.

One ways to express the expected value of the spin Hamiltonian of the equation (2.20) would be:

$$\langle \hat{H}_S \rangle = Q + \sum_{ij} J_{ij} P_{ij} \quad (2.23)$$

where P_{ij} represent the elements of the exchange density matrix \mathbf{P}^{8-10} :

$$P_{ij} = \left\langle - \left(2\hat{S}_i \cdot \hat{S}_j + \frac{1}{2} \hat{I}_{ij} \right) \right\rangle \quad (2.24)$$

From equation (2.23) and considering that the Coulomb term Q will not change in the two different spin states, the gap of energy between a low spin (LS) and a high spin (HS) states can be expressed as:

$$\Delta E^{LS-HS} = \langle \hat{H}_S \rangle^{LS} - \langle \hat{H}_S \rangle^{HS} = \left(\sum_{ij} J_{ij} P_{ij} \right)^{LS} - \left(\sum_{ij} J_{ij} P_{ij} \right)^{HS} \quad (2.25)$$

The parameter J_{ij} is highly dependent on the geometry of the system. In the case that the two spin states are considered to have similar geometries, the J_{ij} values are supposed to be equivalent in both LS and HS states. Then the equation (2.25) can be rewritten as:

$$\Delta E^{LS-HS} = \sum_{ij} J_{ij} \Delta P_{ij}^{LS-HS} \quad (2.26)$$

Consequently, the difference of energy between two different spin states, with similar geometric distribution of the atoms, will be defined by the parameters J_{ij} and P_{ij} of the active electrons. This expression is similar to the Heisenberg Exchange Hamiltonian [Heisenberg-Dirac-Van Vleck (HDVV)] that is an empirical operator that models the interaction (coupling) of unpaired electrons [equation (2.27)]. Within this approximation, the parameter J_{ij} is supposed to be a constant $J_{ij} = J_{eff}$ when the two i,j electrons are interacting and $J_{ij} = 0$ otherwise.

$$\hat{H}_{HDVV} = -2 \sum_{ij} J_{ij} \hat{S}_i \cdot \hat{S}_j = -2 J_{eff} \sum_{ij} \hat{S}_i \cdot \hat{S}_j \quad (2.27)$$

The difference between two spin multiplicity states ΔE_{HDVV}^{LS-HS} will depend on the value of J_{eff} and the multiplicity difference between both states [equation (2.28)]. Thus, the J_{eff} effective parameter is defined to include the multiplicity difference of the two states and, in a way, expresses half of the difference of energy between both of them [equation (2.29)].

$$\Delta E_{HDVV}^{LS-HS} = -2 J_{eff} \left(\sum_{ij} \langle \vec{S}_i \cdot \vec{S}_j \rangle^{LS} - \sum_{ij} \langle \vec{S}_i \cdot \vec{S}_j \rangle^{HS} \right) \quad (2.28)$$

$$J_{eff} = \frac{1}{2} \Delta E_{HDVV}^{LS-HS} \quad (2.29)$$

Do not confuse the **exchange integral** J_{ij} [equation (2.21)] with the **exchange parameter** J_{eff} in equation (2.29). The J_{eff} is extrapolated as an effective parameter of the multielectronic system and determines the preference for the different spin states: when J_{eff} is positive, the lowest energy state is the high spin (ferromagnetic state), however if it is negative the low spin state is lower in energy (antiferromagnetism). The magnitude of the exchange parameter, J_{eff} , embodies all the interactions that determine the ground state spin preference.

2.3 Magnetic mechanism

In the design of **organic molecular materials** with magnetic properties, it is essential to understand the different mechanisms that stabilize high spin molecules (*intramolecular interactions*, section 2.3.1) and favor the ferromagnetic interaction between these high spin containing units (*intermolecular interactions*, section 2.3.3).

2.3.1 Intramolecular interactions

The existing mechanisms^{2,11-17} to explain and predict the magnetic behavior of a material are directly related to the characteristics of the material itself. Some of the mechanisms

proposed to explain the stabilization of high spin states (**intramolecular ferromagnetic interactions**) are: (1) the Hund's-like rule that explains the preference for high spin states in atoms with unpaired electrons placed in *orthogonal orbitals* (section 2.3.1.1); (2) the so-called *spin polarization* mechanism (section 2.3.1.2) and (3) the *superexchange* mechanism (section 2.3.1.3).

A special case of intramolecular interaction we have studied is the polymerization of high spin containing units, in the attempt of synthesizing high spin macromolecules and polymeric magnetic materials (2.3.2).

2.3.1.1 Ferromagnetic exchange between orthogonal orbitals in the same spatial space.

Based on the Pauli's exclusion principle, the *Hund's rule* states that the existence of unpaired electrons located in orthogonal orbitals that reside in the same spatial region leads to the stabilization of the high spin ground state (Figure 2.5). When the overlap between the orbitals is zero but the electrons are close enough in space, the exchange integral is different from zero and positive, favoring the ferromagnetic interaction between the electrons and the stabilization of the high spin state. These electrons interact maximizing the spin moment to minimize the Coulomb interaction.

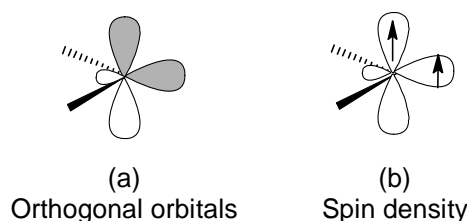


Figure 2.5 Representation of (a) orthogonal orbitals and (b) spin densities of two electrons located in the same atom.

Examples of the extrapolation of the *Hund's rule* for atoms to materials are observed in two-dimensional networks, such as Rb_2CrCl_4 ^{18,19}, where there are a large number of unpaired electrons residing in orthogonal orbitals that, in turn, couple ferromagnetically by different intermolecular mechanisms. Multiple high-spin compounds, such as carbenes and nitrenes (Figure 2.6), have been studied based in this concept²⁰⁻²³.

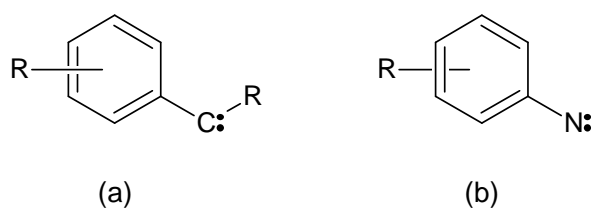


Figure 2.6 Examples of (a) carbene and (b) nitrene.

To predict the ferromagnetism based on this model, only the electronic structure of the radical and the symmetry of the orbitals where the unpaired electrons reside are required. In the case that the electrons are not in the same spatial region, Hund's rule is not applicable.

2.3.1.2 Spin polarization (*Through-Bond* interaction, TB).

Spin polarization is an intramolecular mechanism according to which the unpaired electrons polarize the pair of electrons in the neighbor bonding orbitals. One unpaired electron interact with the adjacent pair of electrons such that, one of them is closer to the unpaired electron than the other. The interaction between these two electrons is preferably antiferromagnetic and this interaction is spread through the different bonds of the molecule, causing the spin polarization. Depending on the geometry of the molecule (number of bonds connecting the spin centers), the spin polarization will set the preference for high or low spin state of the whole molecule.

An example of spin polarization can be found in the *m*-xylylene (1,3-quinodimethane) and *p*-xylylene (1,4-quinodimethane) systems, which have different spin multiplicity namely triplet and singlet ground states, respectively (Figure 2.7).

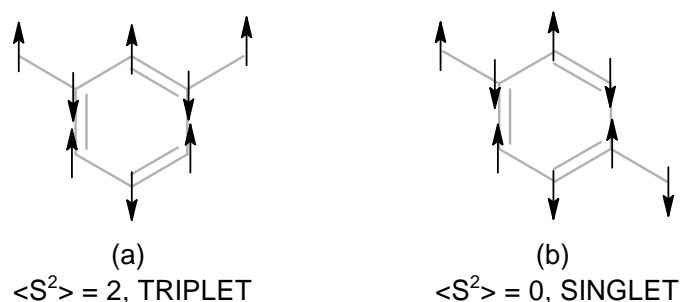


Figure 2.7 Example of spin polarization and spin multiplicity in: (a) *m*-xylylene (1,3-quinodimethane), with a triplet ground state, and (b) *p*-xylylene (1,4-quinodimethane) with a singlet ground state.

Although, usually, valence bond (VB) configurations are used to describe this phenomenon, in fact, it is an intramolecular mechanism of interaction of configurations.

Many high spin molecules used as building blocks in high-spin oligomers stabilize the high-spin state by through bond interactions^{24–35} (Figure 2.8).

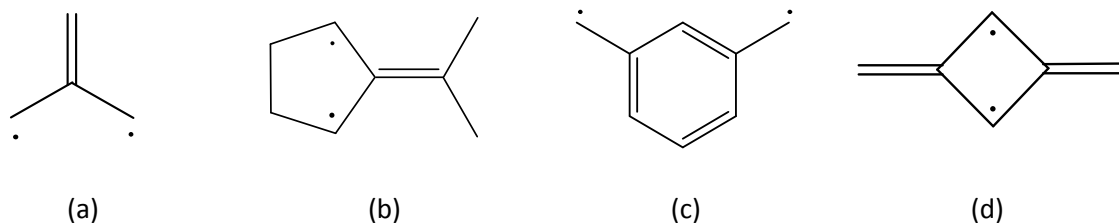


Figure 2.8 (a) trimethylenemethane (TMM) (b) 2-alkylidene-1,3-cyclopentenediyl (c) *m*-xylylene (d) 2,4-dimethylene-1,3-cyclobutanediyl, DM CBD.

2.3.1.3 Super-exchange (*Through-Space* interaction, TS).

This mechanism, also described as dipole-dipole interaction, consists of a through-space spin-spin interaction without an overlap of orbitals or spin densities. It is believed that it

relies on a weak magnetic interaction between the magnetic moments associated with each spin. This mechanism allows explaining the interaction between unpaired electrons that are far away in space. An example of super-exchange is illustrated by the tanol suberate system³⁶ (Figure 2.9), among other examples^{37,38}, which has a flat crystal structure. This material presents a Curie-Weiss behavior at $\theta = 0.7$ K and metamagnetism below $T_C = 0.38$ K. Below the critical field $H_C = 100$, the tanol system is antiferromagnetic and above presents a state of high spin moment.

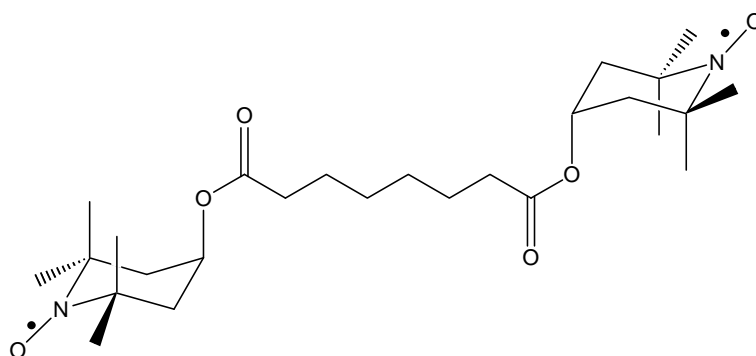


Figure 2.9 Tanol suberate, example of stabilization of the high spin state by a super-exchange mechanism.

2.3.2 High spin macromolecular systems.

As mentioned before, magnetism is a macromolecular property. Therefore, in order to observe magnetism the molecular high spin moment must expand throughout the space. One approach is based in the covalent bonding of high spin molecules^{39,24,40,25,26,41–45}. On one hand, there have been some attempts of building macromolecular systems by homogeneous polymerization of high spin molecules. Another methodology is based on the heterogeneous synthesis of two spin containing units (SU) that are connected through coupling units (CU), being SU and CU high spin molecules.

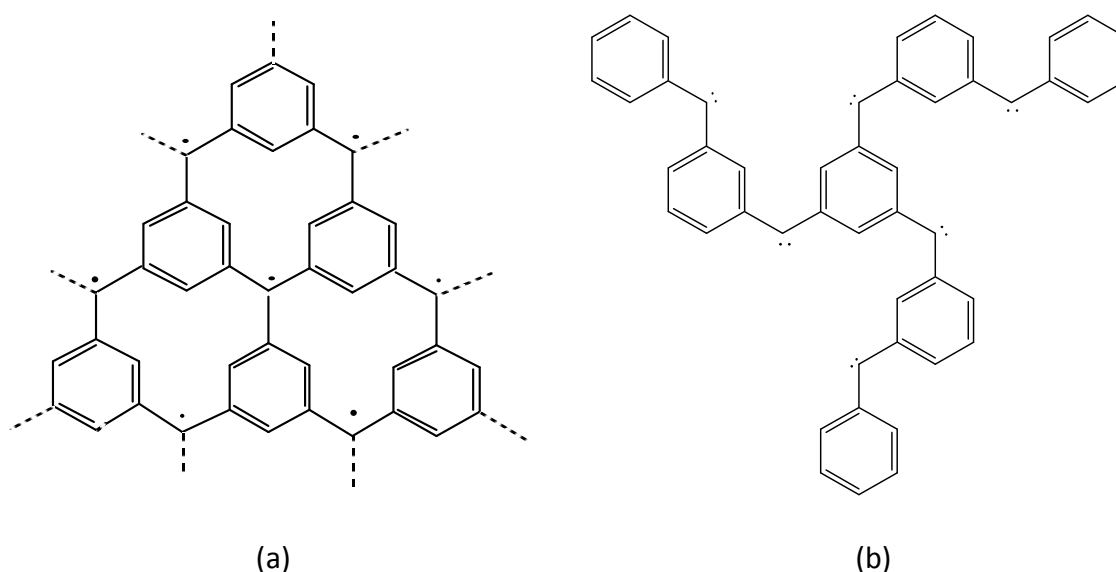


Figure 2.10 Systems (a) and (b) are respectively a spin-polarized polyradical [poly(m-xylylene)] and a polycarbene where centers that contain the unpaired electrons are interconnected through a mechanism of spin polarization.

The so-called *polymeric magnetic materials* class is composed of high spin molecules that connect each other through covalent bonds resulting in a macromolecular polymer system. The bond between these units must be such that favors the ferromagnetic interaction between the constitutive units, in order to expand the high spin multiplicity through the whole system^{17,46–58}. High spin organic systems that present a polymerization mechanism are shown in examples (a)⁵⁹ and (b)⁶⁰ in Figure 2.10. These polymers present radical centers (spin units) ferromagnetically coupled through aromatic rings (*m*-xylylene).

As mentioned, another proposed mechanism in the synthesis of high spin organic molecules consists of the combination of **spin containing units** (SU) through **coupling unit** (CU) that favors the ferromagnetic coupling of the SUs (Figure 2.11). SU and CU constituent units must be molecules that have ground states with high spin moment^{25,26,40,61}.

In both SU and CU systems, two types of coupling between the unpaired electrons can be found: (a) through-space (TS) when the direct interaction between the spin units (SU) is predominant, or (b) through-bond (TB), when occurs through the bonds that connect both spin units and are part of the coupling unit, CU.

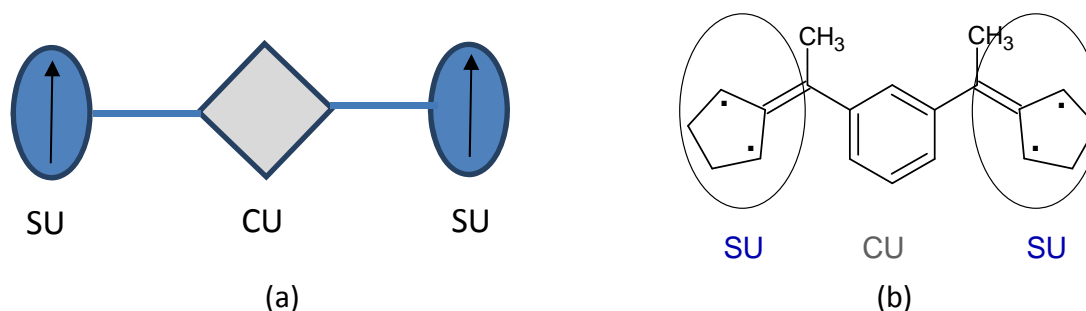


Figure 2.11 –(a) Scheme of the SU-CU-SU model, where SU represent the spin containing units and CU are the coupling units. (b) Example of a SU-CU-SU macromolecule.

A disadvantage that these systems have is their difficult preparation due to the tendency of the free electrons to form covalent bonds. Consequently, it is sometimes complicated to synthesize these macromolecular systems than, on theory, would show magnetization. However, in the last years, new techniques have been proposed to avoid the formation of bonds between the spin centers and important studies have been carried out on molecular coupling, or the formation of copolymers between conjugated oligomers and ferromagnetic centers^{62,63}.

2.3.3 Intermolecular interactions in organic systems.

The **intermolecular interactions** between the unpaired electrons of the spin containing atoms/molecules constituents of the compound will determine the magnetic properties of the material. Therefore, when designing organic molecular magnets, we will look for the **intermolecular interactions** that favor the ferromagnetic coupling of these spin containing centers.

Among the mechanisms that exist to explain the preference for the ferromagnetic interactions between the *spin units* are: the *McConnell I* (section 2.3.3.1) and the *McConnell II* (section 2.3.3.2) theories.

2.3.3.1 McConnell I theory.

One of the theories most widely used for the design of high spin materials is the so-called **McConnell I theory**⁶⁴. This theory is based on the property of *spin density* ($\rho_i^\alpha, \rho_i^\beta$ spatial distribution of the spin electron) of the unpaired electron. In a model where each spin-orbital is occupied by a single electron and it can be solved either for positive (α) and negative (β) spin densities, regions in a molecule with excess of spins α and β (positive and negative regions respectively) can be determined. McConnell I theory, postulated in 1963, proposes that organic radicals, which are ordered such that positive spin density of one molecule interact with the negative spin density of the neighboring interacting molecule (Figure 2.12), give rise to a global ferromagnetic exchange interaction.

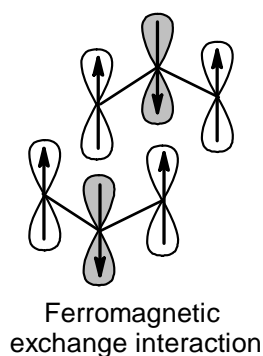


Figure 2.12 Diagram of the first (I) mechanism proposed by McConnell where positive spin densities interact with negatives resulting in a system with global high-spin multiplicity.

The methodological Hamiltonian proposed for the study of this class of systems is shown in equation (2.30):

$$\hat{H}^{AB} = - \sum_{i \in A, j \in B} J_{ij}^{AB} \hat{S}_i^A \cdot \hat{S}_j^B \quad (2.30)$$

where J_{ij}^{AB} is the integral of exchange between two centers i, j that belong to different fragments A and B . $\hat{S}_i^A \cdot \hat{S}_j^B$ is the product of the electron spin operators of the electrons i, j in radicals A and B , respectively. The Hamiltonian in equation (2.30) is approximated as the effective Hamiltonian in equation (2.31):

$$\hat{H}^{AB} = -J_{eff} (\hat{S}^A \cdot \hat{S}^B) \quad (2.31)$$

in which J_{eff} is the effective coupling constant and the terms $\hat{S}^A \cdot \hat{S}^B$ are the total spin operators of the fragments A and B .

This theory has been extensively applied in the study of molecule-based magnets, such as the nitronyl nitroxide crystals family^{65–67} (Figure 2.13). However, this methodology requires certain conditions of the systems to be strictly true: interacting molecules must be planar and they must be placed in parallel planes. Although, it allows to predict and describe the results for systems like the bis(phenylmethylene)[2,2]cyclophane⁶⁸ (Figure 2.14), some studies showed that when small displacement of the McConnell systems occurs, the preferred magnetic interaction proposed by this mechanism is not the observed^{69,70}.

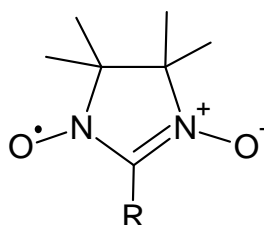


Figure 2.13 Nitronyl nitroxide.

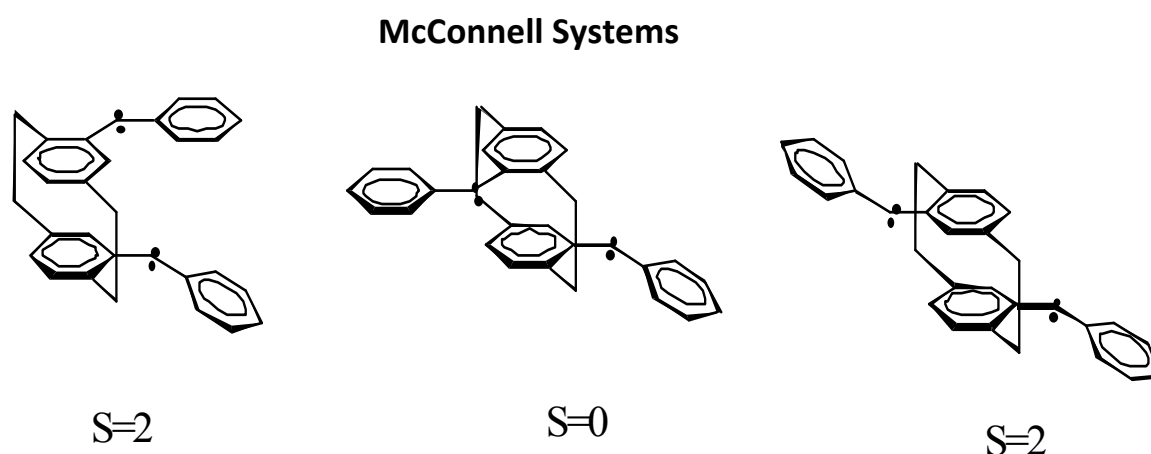


Figure 2.14 Example of the bis(phenylmethylene)[2,2]cyclophane at positions ortho-, meta -, and para-respectively. The multiplicity observed experimentally and shown under each one of the systems can be explained easily with the McConnell I theory¹⁶.

2.3.3.2 McConnell II theory. Transfer salts and frontier orbitals.

The transfer salts systems are constituted by two species: a Donor (D) and an Acceptor (A). These two molecules interact such that the donor species gives an electron to the acceptor one and both become charged radicals (positively charged the donor and negatively charged the acceptor). If the unpaired electrons of the resulting ions interact ferromagnetically the substance shows magnetic properties.

To describe the magnetic behavior of these systems, two important aspects should be considered: (1) the electron configuration within each species; and (b) the Donor/Acceptor interaction that stabilizes the ferromagnetic coupling.

The description of the mechanism of interaction between Donor/Acceptor involves excited states of both species. Therefore, the wave function of the system should be evaluated as configuration interaction.

One of the mechanisms that explains the high spin state in such systems proposes that this stabilization occurs via interaction with higher states of dianion-dication chains (Figure 2.15). This theory is still widely discussed and it has been observed that it is not always valid.

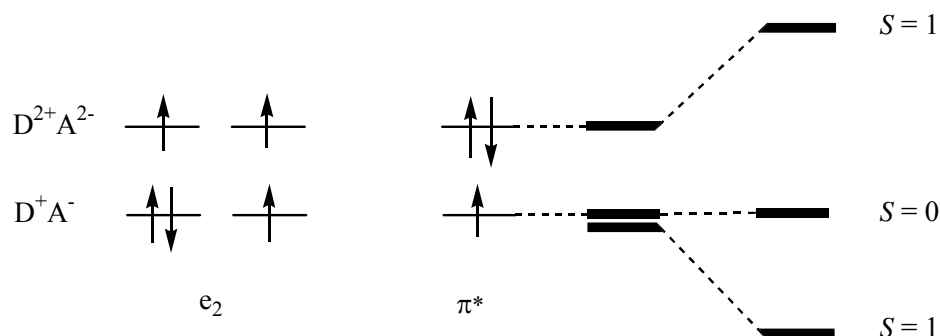


Figure 2.15 Mechanism that explains the stabilization of the high spin state in the charge transfer salts by interaction of D^+A^- with higher energy $D^{2+}A^{2-}$. This interaction would stabilize the high spin state.

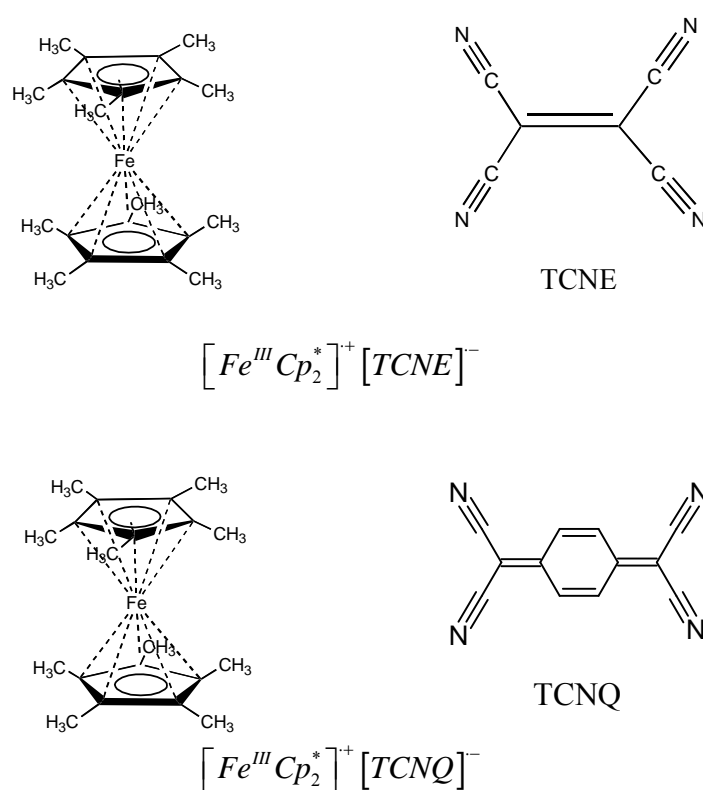


Figure 2.16 Constituent units of $[Fe(Cp)_2]^+[TCNE]^-$ and $[Fe(Cp)_2]^+[TCNQ]^-$, where the donor specie D is the ferrocene and the acceptor, A, are the TCNE/TCNQ respectively.

Examples of charge-transfer systems are $[Fe^{III} Cp_2^*]^+[TCNE]^-$ salt and its analog $[Fe^{III} Cp_2^*]^+[TCNQ]^-$, where $Cp = 1,2,3,4,5$ -pentamethyl (Me_5C_5), $TCNE =$ tetracyanoethylene and $TCNQ = 7,7,8,8$ -tetracyanoquinodimethane (Figure 2.16). The

molecular complex $[Fe^{III}Cp_2^*]^+[TCNE]^-$ was one of the first materials for which bulk ferromagnetism was detected⁷¹. These systems are metamagnetic, *i.e.*, in the presence of a certain field (16000Oe for the first case and *ca.* the Earth's magnetic field for the second) the ground state is ferromagnetic. As mentioned previously, in these examples, the donor specie $[FeCp_2]$ is charged positively and negatively the two acceptors $TCNQ$ and $TCNE$ after the electron transfer. In the final state, two unpaired electrons are located in different orbitals (Figure 2.17).

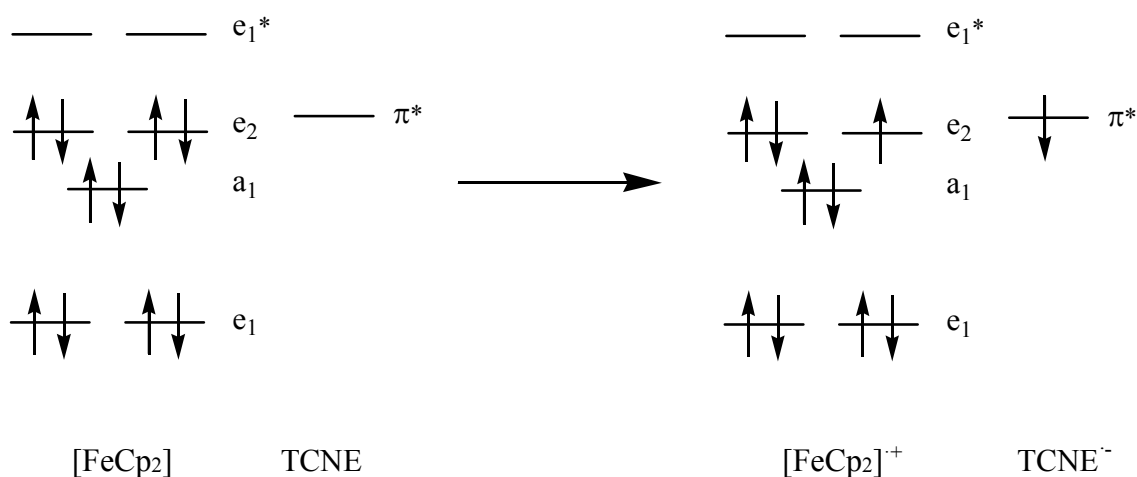


Figure 2.17 Orbital scheme for the charge transfer salt $[FeCp_2]^+[TCNE]^-$.

The structure observed in this type of salts is based on chains $\cdots D^+A^-D^+A^- \cdots$ that stack on top of each other. The distances and orientation of the species, as well as the type and distribution of the chains, depends on the constitutive species.

It has been observed experimentally that some of these charge transfer salts lose their magnetic properties due to the dimerization of their constitutive species. The study of the mechanism that favor this dimerization would help to avoid the loss of magnetism in the synthesis of these compounds.

2.3.4 Simulating magnetic properties from microscopic information. First-Principles Bottom-Up working strategy.

The magnetic exchange coupling, that has been studied at a radical level, can be used to estimate the observable magnetic properties, such as magnetic susceptibility $\chi(T)$, heat capacity $C_p(T)$ and/or magnetization (M). For this extrapolation, appropriate statistical mechanics expressions are used.

A systematic procedure to go from the study of molecular-molecular interactions to the magnetism observed at solid state is described in the bottom-up principle proposed by M. Deumal et al.⁷². This procedure consist in:

Step 1: The crystal structure is analyzed looking for all the possible A-B radical-radical whose interactions could be responsible for the macroscopic magnetic properties. This is performed by selecting one symmetry-unique A radical and choosing all the A-B pairs that are placed at a shorter distance than a given threshold value.

Step 2: The microscopic J_{AB} are computed for the interactions between all selected A-B pairs.

Step 3: From the obtained J_{AB} values, those with a $|J_{AB}|$ higher than a threshold value are selected. The interactions represented by these selected J_{AB} and how these propagate along the crystal axes are considered the magnetic topology of the crystal. The minimal magnetic model is defined as the smallest set of radicals that include all the non-negligible J_{AB} interactions. The representation of the minimal model along the crystallographic axes (a, b and c) direction should regenerate the magnetic topology of the full crystal. The spin states used to compute the matrix representation of the corresponding Heisenberg Hamiltonian are formed by the radical centers that define the minimal magnetic model.

Step 4: The energy of all possible spin states is then calculated by diagonalizing the Heisenberg Hamiltonian matrix. The only parameters required to compute the matrix representation of the Heisenberg Hamiltonian are the J_{AB} interactions obtained in step 2. The macroscopic magnetic properties as the magnetic susceptibility χ , the heat capacity C_p , or the magnetization M can be then estimated from the obtained energies using expressions from statistical mechanics.

Bibliography

- (1) Kahn, O. *Molecular Magnetism*, 1 edition.; Wiley-VCH: New York, 1993.
- (2) Miller, J. S.; Epstein, A. J. *Angew. Chem. Int. Ed. Engl.* **1994**, *33* (4), 385–415.
- (3) Wood, R. *Understanding Magnetism*; Tab Books Inc., Blue Ridge Summit, PA, 1988.
- (4) Mattis, D. C. *The Theory of Magnetism I: Statics and Dynamics*; Springer Science & Business Media, 1981.
- (5) Szabo, A.; Ostlund, N. S. *McGraw-Hill N. Y.* **1989**.
- (6) McWeeny, R.; Sutcliffe, B. T. *Methods of Molecular Quantum Mechanics*; Academic Press, 1976.
- (7) McWeeny, R. *Spins in Chemistry*; Academic Press, 1970.
- (8) Bearpark, M. J.; Robb, M. A.; Bernardi, F.; Olivucci, M. *Chem. Phys. Lett.* **1994**, *217* (5–6), 513–519.
- (9) Bernardi, F.; Olivucci, M.; McDouall, J. J. W.; Robb, M. A. *J. Chem. Phys.* **1988**, *89* (10), 6365–6375.
- (10) Bernardi, F.; Olivucci, M.; Robb, M. A. *J. Am. Chem. Soc.* **1992**, *114* (5), 1606–1616.
- (11) Gatteschi, D. *Adv. Mater.* **1994**, *6* (9), 635–645.
- (12) *Proceedings of the Conference on Chemistry & Physics of Molecule Based Magnetic Materials.*; Iwamura, H., Miller, J. S., Eds.; Mol. Cryst., Liq. Cryst.; 1993.
- (13) *Proceedings of the Conference on Molecular Magnetic Materials: NATO ARW Molecular Magnetic Materials*; Kahn, O., Gatteschi, D., Miller, J. S., Eds.; Kluwer Academic publishers, E198: London, 1991.
- (14) Kinoshita, M. *Jpn. J. Appl. Phys.* **1994**, *33* (Part 1, No. 10), 5718–5733.
- (15) *Proceedings of the Conference on Ferromagnetic & High-Spin Molecular-Based Magnets*; Miller, Joel S., Dougherty, Dennis A., Eds.; Mol. Cryst., Liq. Cryst.; 1989.
- (16) *Proceedings of the Conference on Molecule-Based Magnets*; Miller, Joel S., Epstein, Arthur J., Eds.; Mol. Cryst., Liq. Cryst.; 1995.
- (17) Rajca, A. *Chem. Rev.* **1994**, *94* (4), 871–893.
- (18) Day, P. *Acc. Chem. Res.* **1979**, *12* (7), 236–243.
- (19) Bellitto, C.; Day, P. *J. Mater. Chem.* **1992**, *2* (3), 265–271.
- (20) Iwamura, H.; Sugawara, T.; Itoh, K.; Takui, T. *Mol. Cryst. Liq. Cryst.* **1985**, *125* (1), 251–260.
- (21) Iwamura, H. *Pure Appl. Chem.* **1993**, *65* (1), 57–64.
- (22) Itoh, K. In *Magnetic Molecular Materials*; Gatteschi, D., Kahn, O., Miller, J. S., Palacio, F., Eds.; NATO ASI Series; Springer Netherlands, 1991; pp 67–86.
- (23) Dannenberg, J. J.; Liotard, D.; Halvick, P.; Rayez, J. C. *J. Phys. Chem.* **1996**, *100* (23), 9631–9637.
- (24) Dougherty, D. A. *Acc. Chem. Res.* **1991**, *24* (3), 88–94.
- (25) Pranata, J.; Marudarajan, V. S.; Dougherty, D. A. *J. Am. Chem. Soc.* **1989**, *111* (6), 2026–2030.
- (26) Pranata, J.; Dougherty, D. A. *J. Am. Chem. Soc.* **1987**, *109* (6), 1621–1627.
- (27) Dowd, P. *J. Am. Chem. Soc.* **1966**, *88* (11), 2587–2589.
- (28) Baseman, R. J.; Pratt, D. W.; Chow, M.; Dowd, P. *J. Am. Chem. Soc.* **1976**, *98* (18), 5726–5727.
- (29) Geib, S. J.; Vicent, C.; Fan, E.; Hamilton, A. D. *Angew. Chem. Int. Ed. Engl.* **1993**, *32* (1), 119–121.
- (30) Dixon, D. A.; Dunning, T. H.; Eades, R. A.; Kleier, D. A. *J. Am. Chem. Soc.* **1981**, *103* (10), 2878–2880.

- (31) Platz, M. S.; Berson, J. A. *J. Am. Chem. Soc.* **1977**, *99* (15), 5178–5180.
- (32) Berson, J. A. *Acc. Chem. Res.* **1978**, *11* (12), 446–453.
- (33) Goodman, J. L.; Berson, J. A. *J. Am. Chem. Soc.* **1985**, *107* (19), 5409–5424.
- (34) Wright, B. B.; Platz, M. S. *J. Am. Chem. Soc.* **1983**, *105* (3), 628–630.
- (35) Inoue, K. In *π -Electron Magnetism*; Veciana, P. J., Arçon, D., Deumal, M., Inoue, K., Kinoshita, M., Novoa, J. J., Palacio, F., Prassides, K., Rawson, J. M., Rovira, C., Eds.; Structure and Bonding; Springer Berlin Heidelberg, 2001; pp 61–91.
- (36) Chouteau, G.; Veyret-Jeandey, C. *J. Phys.* **1981**, *42* (10), 1441–1444.
- (37) Wang, J.; Hou, L.; Browne, W. R.; Feringa, B. L. *J. Am. Chem. Soc.* **2011**, *133* (21), 8162–8164.
- (38) Rajca, A.; Mukherjee, S.; Pink, M.; Rajca, S. *J. Am. Chem. Soc.* **2006**, *128* (41), 13497–13507.
- (39) Itoh, K. *Pure Appl. Chem.* **1978**, *50* (11–12), 1251–1259.
- (40) Jacobs, S. J.; Shultz, D. A.; Jain, R.; Novak, J.; Dougherty, D. A. *J. Am. Chem. Soc.* **1993**, *115* (5), 1744–1753.
- (41) Jacobs, S. J.; Dougherty, D. A. *Angew. Chem. Int. Ed. Engl.* **1994**, *33* (10), 1104–1106.
- (42) Silverman, S. K.; Dougherty, D. A. *J. Phys. Chem.* **1993**, *97* (50), 13273–13283.
- (43) Novak, J. A.; Jain, R.; Dougherty, D. A. *J. Am. Chem. Soc.* **1989**, *111* (19), 7618–7619.
- (44) Goldberg, A. H.; Dougherty, D. A. *J. Am. Chem. Soc.* **1983**, *105* (2), 284–290.
- (45) Adam, W.; van Barneveld, C.; Bottle, S. E.; Engert, H.; Hanson, G. R.; Harrer, H. M.; Heim, C.; Nau, W. M.; Wang, D. *J. Am. Chem. Soc.* **1996**, *118* (16), 3974–3975.
- (46) Lahti, P. M. *Magnetic Properties of Organic Materials*; CRC Press, 1999.
- (47) Itoh, K.; Kinoshita, M. *MRS Bull.* **2002**, *27* (8), 1–1.
- (48) Rajca, A.; Utamapanya, S. *J. Am. Chem. Soc.* **1993**, *115* (23), 10688–10694.
- (49) Wienk, M. M.; Janssen, R. A. J. *J. Am. Chem. Soc.* **1997**, *119* (19), 4492–4501.
- (50) Wienk, M. M.; Janssen, R. A. J. *Synth. Met.* **1997**, *85* (1), 1725–1726.
- (51) Ishida, T.; Iwamura, H. *J. Am. Chem. Soc.* **1991**, *113* (11), 4238–4241.
- (52) Kanno, F.; Inoue, K.; Koga, N.; Iwamura, H. *J. Phys. Chem.* **1993**, *97* (50), 13267–13272.
- (53) Inoue, K.; Iwamura, H. *J. Am. Chem. Soc.* **1994**, *116* (7), 3173–3174.
- (54) Iwamura, H.; Inoue, K. *Adv. Mater.* **1996**, *8* (1), 73–76.
- (55) Rajca, A.; Lu, K.; Rajca, S. *J. Am. Chem. Soc.* **1997**, *119* (43), 10335–10345.
- (56) Rajca, A.; Rajca, S.; Wongsriratanakul, J. *J. Am. Chem. Soc.* **1999**, *121* (26), 6308–6309.
- (57) Rajca, A.; Wongsriratanakul, J.; Rajca, S. *Science* **2001**, *294* (5546), 1503–1505.
- (58) Teki, Y.; Nakatsuji, M.; Miura, Y. *Mol. Phys.* **2002**, *100* (9), 1385–1394.
- (59) Mataga, N. *Theor. Chim. Acta* **1968**, *10* (4), 372–376.
- (60) Nakamura, N.; Inoue, K.; Iwamura, H.; Fujioka, T.; Sawaki, Y. *J. Am. Chem. Soc.* **1992**, *114* (4), 1484–1485.
- (61) Jacobs, S. J.; Dougherty, D. A. *Angew. Chem. Int. Ed. Engl.* **1994**, *33* (10), 1104–1106.
- (62) Fukutome, H.; Takahashi, A.; Ozaki, M. *Chem. Phys. Lett.* **1987**, *133* (1), 34–38.
- (63) Kaisaki, D. A.; Chang, W.; Dougherty, D. A. *J. Am. Chem. Soc.* **1991**, *113* (7), 2764–2766.
- (64) McConnell, H. M. *J. Chem. Phys.* **1963**, *39* (7), 1910–1910.
- (65) Tamura, M.; Nakazawa, Y.; Shiomi, D.; Nozawa, K.; Hosokoshi, Y.; Ishikawa, M.; Takahashi, M.; Kinoshita, M. *Chem. Phys. Lett.* **1991**, *186* (4–5), 401–404.
- (66) Kinoshita, M. *Philos. Trans. R. Soc. Lond. Math. Phys. Eng. Sci.* **1999**, *357* (1762), 2855–2872.
- (67) Teki, Y.; Miyamoto, S.; Iimura, K.; Nakatsuji, M.; Miura, Y. *J. Am. Chem. Soc.* **2000**, *122* (5), 984–985.

-
- (68) Izuoka, A.; Murata, S.; Sugawara, T.; Iwamura, H. *J. Am. Chem. Soc.* **1985**, *107* (6), 1786–1787.
- (69) Deumal, M.; Novoa, J. J.; Bearpark, M. J.; Celani, P.; Olivucci, M.; Robb, M. A. *J. Phys. Chem. A* **1998**, *102* (43), 8404–8412.
- (70) Novoa, J. J.; Lafuente, P.; Mota, F. *Chem. Phys. Lett.* **1998**, *290* (4–6), 519–525.
- (71) Chittipeddi, S.; Cromack, K. R.; Miller, J. S.; Epstein, A. J. *Phys. Rev. Lett.* **1987**, *58* (25), 2695–2698.
- (72) Deumal, M.; Mota, F.; Bearpark, M. J.; Robb, M. A.; Novoa, J. J. *Mol. Phys.* **2006**, *104* (5–7), 857–873.

CHAPTER 3

METHODS

3 Methods

The methods^{1,2} of calculation selected to estimate the properties of the studied systems depend on the type of molecules involved. We are basically interested in organic molecules with free electrons and we need to describe correctly ground and excited states with different spin multiplicities. To describe these systems, we have used: **MP2** methods when studying interaction where the *dynamic correlation* is important (section 3.1.1); **CASSCF(*m,n*)**, when it is essential to introduce correlation and the systems need to be described with more than one configuration (section 3.1.2); and, in some cases, we have evaluated if it was necessary to introduce both contributions, so **CASMP2 (*m,n*)** calculations were run in parallel and compared to MP2 and CASSCF results. Whenever it has been possible, the method chosen was **UB3LYP** due to its simplicity and speed of calculation (section 3.2).

To describe correctly the high spin molecules the basis set selected usually included polarization (so the molecular orbitals can adapt to the molecular environment) and diffuse functions (to better describe the distant parts from the nuclei).

One of the methods used for the description of specific systems (planar alternant hydrocarbons) is the hybrid method, **Molecular Mechanics - Valence Bond (MMVB)** which will be detailed in section 3.3. This method allows a quick qualitative description of the spin states of organic molecules with high number of electrons in the active space, but it also has some limitations that will be discussed.

To characterize the intermolecular interactions we evaluated the use of the methodology **Atoms in Molecules (AIM)** proposed by Bader that is described in section 3.4.

3.1 Ab-initio methods

Since the studied systems are radicals with unpaired electrons, it is necessary to use computational methods that describe correctly open-shell molecules. The simplest method to do so is the restricted open-shell Hartree-Fock (ROHF), whose wavefunction is defined by a single determinant. This method allows to obtain the shape of the orbitals, which will have occupation numbers that are integers: 2, 1, 0. However, it does not allow the partial occupation of the orbitals and, consequently, is not valid to describe the polarization of spin which is needed to compute correctly some of the systems we are interested in. An unrestricted Hartree-Fock (UHF) methodology allows this fractional occupancy of the orbital, similar to that obtained in methods of configuration interaction (CI). Nevertheless, in many cases, UHF wavefunctions are not eigenfunctions of the spin operator and spin contamination may occur. In these cases, UHF calculations can lead to incorrect spin distribution and sign, although the optimized geometry at UHF level can be acceptable. Examples of this spin contamination are seen in the family of the α -nitronyl nitroxide (α -NN). Consequently, it is necessary to introduce dynamic correlation to properly study this type of systems. In our studies, initial UHF calculations have been carried out to obtain the initial wavefunction, orbitals and geometries from which more extended calculations were made. UHF calculations have also been very useful to find the starting geometries for subsequent optimizations, and perform an initial analysis on the fractional population of the orbitals to choose the active spaces in the multiconfigurational methods.

There are many methods that introduce the correlation energy: on one hand, there are the **Møller-Plesset** perturbation methods³⁻⁷ (MP n) that are *size consistent*⁴ but not *variational*⁵; on the other hand, there are the **Configuration Interaction** (CI) methods, whose wavefunction is formed by multiple Slater determinants^{1,8}. These last methods are *variational* but they are only *size consistent*⁴ if all the possible excitations from the ground state determinant are incorporated into the wavefunction (*full CI*) which is impossible for the majority of our systems. There is a hybrid methodology called CASPT2 (CASMP2), which is a many body perturbation method where the perturbation is performed on a multiconfigurational wavefunction^{9,10}.

3.1.1 Møller-Plesset perturbational methods (MP n)

As we have mentioned above, the perturbation methodology is one of the possible ways of introducing the correlation in the calculations. The Hamiltonian \hat{H} considered is the result of the sum of a zero order Hamiltonian, \hat{H}_0 , whose values and functions are known, and a perturbation \hat{V} that may be of 2,3,... n order (MP2, MP3...MP n).

$$\hat{H} = \hat{H}_0 + \hat{V} \quad (3.1)$$

The resulting energy is expressed as the sum of both contributions. When we have used this approach as calculation method, we have chosen the second order perturbation Møller - Plesset³⁻⁷ method applied to an N - electronic system (MP2).

Since this is a monoreference method, spin contamination is observed in some systems that need their wavefunction to be expressed as contribution of various configurations. A way to eliminate the spin contamination is to use methods in which some components (usually the next in multiplicity, since they represent the largest contribution to the spin contamination) are projected. Another way to solve the problem consisting in using the methodology CASPT2 (CASMP2, Complete Active Space Perturbation Theory), where the perturbation is performed on a multiconfigurational optimized CASSCF wavefunction. CASPT2(CASMP2) is a more elaborated method and with higher computational complexity

3.1.2 Complete Active Space (CASSCF) methods

In order to describe correctly some systems (*e.g.*: for molecular ground states which are quasi-degenerate with low-lying excited states, dissociation processes with open-shell products), it is necessary to introduce more than one configuration into the wavefunction. In those cases, the so-called multi-configurational self-consistent field (MCSCF)^{1,8} approach

⁴ *Size consistent*: It is a property that guarantees the consistency of the energy behavior when the interaction between the involved molecular systems is nullified (*i.e.* by distance) and describes what has been referred as the "additive-separability" of the wave-function. A method that is size-consistent should describe correctly the entire process of fragmentation, including the fragmentation limit of a molecule.

⁵ *Variational*: A variational method is the one that follows the variational principle and therefore, any trial function different from the ground state will have a higher energy (upper bound) to the true ground state energy.

is used. In these methods, the wavefunction is constructed as a linear combination of the configuration state functions, CSF, or configuration [equation (3.2)].

$$\Phi_{CAS} = \sum_K A_K \Psi_K \quad (3.2)$$

Ψ_K is the wavefunction with spin-correct, symmetry-correct configuration and A_K is the weight (coefficient) of each of these configurations (also called expansion coefficients).

For each electronic state M , the energy can be estimated using equation (3.3), where K and L represent different configurations that describe the electronic state M and $A_{K,M}$, $A_{L,M}$ the corresponding coefficients for each configuration. These coefficients are determined variationally using the linear variation principle [equations (3.4)].

$$E_M = \langle \Phi_M | \hat{H} | \Phi_M \rangle = \sum_{K,L} A_{K,M} A_{L,M} \langle \Psi_{K,M} | \hat{H} | \Psi_{L,M} \rangle \quad (3.3)$$

$$\frac{\partial E_M}{\partial A_{K,M}} = 0, \dots \quad (3.4)$$

Both the orbitals, defined by the basis functions, and the weight of each configuration are optimized for each state. The solution of this matrix equations yields to MCSCF energies E_M [equation (3.3)] for each electronic state M and the corresponding coefficients $A_{K,M}$ of each K configuration [equations (3.4)].

Among the MCSCF methods, the CASSCF (m,n) is one of the most popular, being m the number of electrons and n the number of orbitals within the *active* space. The excitations considered as possible configurations are of electrons belonging mostly to the active space into orbitals in turn considered into the active space. Consequently, in this methodology it is necessary to specify the number of active electrons m and orbitals n that constitute the active space.

One of the difficulties presented by CASSCF methodology lies in the choice of the adequate active space. A first criterion for choosing the active space consists of performing a preliminary analysis to evaluate the occupied orbitals with higher energy and the empty orbitals with lower energy. Knowing the chemical problem that we want to solve and considering the shape of these orbitals, we can choose those that interest us for our analysis and include them into the active space. Many times, this criterion of *chemical intuition* is not enough to properly describe the system and it is necessary to introduce a greater number of orbitals. In this case, an initial UHF natural orbital calculation is performed to estimate the orbital occupation. After this analysis, the orbitals with occupancy 2.0 are considered inactive, the ones with occupancy 0.0 belong to the virtual space and the ones with occupancy between 1.99-0.01 belong to the active space^{11,12}.

It is important to take into account both criteria since the active space must contain the orbitals of *chemical interest* and those which are necessary for a good description of the system. Sometimes it is difficult to find the right active space and in these cases the convergence of the calculation is difficult.

These methods can deal with extremely complex chemical situations and, if computing capacity permits, may be used to reliably calculate molecular ground- and excited states if all other methods fail.

3.2 Density Functional Theory (DFT)

The methods based on the density functional theory (DFT)¹³⁻¹⁶ are very controversial. On one hand, they have become one of the most popular computational quantum mechanical methods due to their low computational costs. However, they also have many detractors due to the difficulties to describe correctly the exchange and correlation interaction.

In the case of open-shell systems, the DFT prediction of their energies, geometries, molecular properties and spin densities has some limitations. These inaccuracies need to be considered when using DFT as the method to describe spin states in radicals.

3.2.1 Electron density and energy potentials

The electron density function $\rho(\vec{r})$ is defined as the integral over the spin coordinates of all electrons and all but one of the spatial variables ($\vec{x} \equiv \vec{r} \cdot s$) and represents the probability density of finding any electron at position \vec{r} [equation (3.5)]. This approach allows decreasing the computational cost by reducing the many-body problem of N electrons with $3N$ spatial coordinates to 3 spatial coordinates.

$$\rho(\vec{r}) = N \int \cdots \int |\psi(\vec{x}_1, \vec{x}_2, \cdots, \vec{x}_N)|^2 ds_1 d\vec{x}_2 \cdots \vec{x}_N \quad (3.5)$$

The expression of the Hamiltonian for N electrons [equation (3.6)] is written as a function of the kinetic energy of the N -electrons \hat{T} [equation (3.7)], the electron-electron interaction energy \hat{V}_{ee} [equation (3.8)] and an external potential \hat{V} [equation (3.9)].

$$\hat{H} = \hat{T} + \hat{V}_{ee} + \hat{V} \quad (3.6)$$

$$\hat{T} = -\frac{1}{2} \sum_{i=1}^N \nabla_i^2 \quad (3.7)$$

$$\hat{V}_{ee} = \sum_{i=1}^N \sum_{j>i}^N \frac{1}{r_{ij}} \quad \text{where } r_{ij} = |\vec{r}_i - \vec{r}_j| \quad (3.8)$$

$$\hat{V} = \sum_{i=1}^N v(\vec{r}_i) \quad (3.9)$$

Often, the external potential is the electron-nucleus attraction potential:

$$v(\vec{r}_i) = v_{Ne}(\vec{r}_i) = -\sum_{A=1}^M \frac{Z_A}{r_{iA}} \quad \text{where} \quad r_{iA} = |\vec{r}_i - \vec{R}_A| \quad (3.10)$$

$$\hat{V} = \hat{V}_{Ne} = -\sum_{i=1}^N \sum_{A=1}^M \frac{Z_A}{r_{iA}} \quad (3.11)$$

The energy expectation value is then calculated as the sum of the eigenvalues values of the kinetic energy and the electron-electron interaction and external potentials:

$$\langle \Psi | \hat{H} | \Psi \rangle = \langle \Psi | \hat{T} | \Psi \rangle + \langle \Psi | \hat{V}_{ee} | \Psi \rangle + \langle \Psi | \hat{V} | \Psi \rangle \quad (3.12)$$

The kinetic energy \hat{T} and the electron-electron term \hat{V}_{ee} are the same for any N -electron system. For that reason, the ground state of the system and its properties are completely determined by the external potential \hat{V} and the number of electrons N .

3.2.2 Hohenberg-Kohn theorems and Kohn-Sham approximation

DFT methods are based on the Hohenberg-Kohn (HK) theorems¹³. The **first HK theorem** demonstrates that the external potential $\hat{V}(\vec{r})$ is, to within a constant, a unique functional of the electron density $\rho(\vec{r})$. Consequently, since $\hat{V}(\vec{r})$ and N define the Hamiltonian, the ground state of a many-body electron system and its properties are defined by $\rho(\vec{r})$.

The expression of the energy functional according to the DFT methodology, $E_{DFT}[\rho]$, is written as a function of the kinetic energy functional $T[\rho]$, the electron-electron interaction functional $E_{ee}[\rho]$ and the contribution of the external potential $v(\vec{r})$:

$$E_{DFT}[\rho] = T[\rho] + E_{ee}[\rho] + \int \rho(\vec{r})v(\vec{r})d^3\vec{r} \quad (3.13)$$

To simplify the expression of the DFT energy, Hohenberg-Kohn introduced the functional $F_{HK}[\rho]$ that contains the two electronic terms $T[\rho]$ and $E_{ee}[\rho]$:

$$F_{HK}[\rho] = T[\rho] + E_{ee}[\rho] \quad (3.14)$$

If the electron-electron interaction $E_{ee}[\rho]$ is expressed in terms of the classical Coulomb interactions $J[\rho]$ and the non-classical contribution to the electron-electron exchange interaction $E_{ex}[\rho]$ [equation (3.15)], the HK functional can be rewritten as equation (3.16).

$$E_{ee}[\rho] = \frac{1}{2} \iint \frac{\rho(\vec{r}_1)\rho(\vec{r}_2)}{r_{12}} d\vec{r}_1 d\vec{r}_2 + E_{ex}[\rho] = J[\rho] + E_{ex}[\rho] \quad (3.15)$$

$$F_{HK}[\rho] = T[\rho] + J[\rho] + E_{ex}[\rho] \quad (3.16)$$

The **second HK theorem** states that the ground state energy can be obtained variationally. That is to say, the density that minimizes the total energy is the exact ground state density ρ_0 .

If the Hohenberg-Kohn functional $F_{HK}[\rho]$ was known, it would be possible to solve exactly the Schrödinger equation. However, only $J[\rho]$ can be calculated exactly and the explicit form of $T[\rho]$ and $E_{ex}[\rho]$ functionals is the major challenge of DFT methodology. To solve that problem, Kohn and Sham proposed in 1965¹⁴ to calculate the exact kinetic energy T_s of a non-interacting reference systems (the subscript 's' is introduced to denote the 'single particle' in the non-interacting system) with the same density as the real interacting system. The corresponding kinetic energy $T_s[\rho]$ is not the true energy of the system and a new term needs to be introduced to account for it (correlation term). For that, an exchange-correlation functional $E_{XC}[\rho]$ was defined, which includes everything that is unknown, *i.e.* both the exchange $E_{ex}[\rho]$ and the correlation $(T[\rho] - T_s[\rho])$ contributions [equation (3.17)].

$$E_{XC}[\rho] \equiv (T[\rho] - T_s[\rho]) + (E_{ex}[\rho] - J[\rho]) = (T[\rho] - T_s[\rho]) + E_{ex}[\rho] \quad (3.17)$$

The resulting energy is then expressed as in equation (3.18) where only the term $E_{XC}[\rho]$ has no explicit form.

$$E_{DFT}[\rho] = T_s[\rho] + J[\rho] + E_{XC}[\rho] + \int \rho(\vec{r})v(\vec{r})d^3\vec{r} \quad (3.18)$$

The exchange-correlation functional $E_{XC}[\rho]$ is defined in term of integrals of functions of the density and the density gradient. If the functional depends only on the density, it is referred to as local, while if it also depends on the gradient of the density, it is called non-local. There are many different functionals proposed to determine the parts of exchange and correlation. Experience has shown that non-local functionals give best results in chemical systems, notably the so-called B3LYP functional¹⁷⁻¹⁹.

Since we are considering a non-interacting reference system, the Hamiltonian to be applied can be expressed as function of operators acting on non-interacting particles [equation (3.19)]. This Hamiltonian does not contain electron-electron interaction terms. Therefore the Schrödinger equation can be solved and the exact wavefunction is represented as a single Slater determinant $\Phi_s = |\varphi_1\varphi_2 \cdots \varphi_N|$ (anti-symmetrized product of one-electron functions).

$$\hat{H}_s = \hat{T} + \hat{V}_s = -\frac{1}{2} \sum_{i=1}^N \nabla_i^2 + \sum_{i=1}^N v_s(\hat{r}_i) \quad (3.19)$$

Once the variational principle is applied, the solution of the Schrödinger equation $\hat{H}_s \Phi_s = E_s \Phi_s$ (with $E_s = \sum_i \varepsilon_i$) results to be the φ_i orbitals that minimize the energy expression under the $\langle \varphi_i | \varphi_j \rangle = \delta_{ij}$ constrain, being $\delta_{ij} = 1$ when $i = j$ and $\delta_{ij} = 0$ when $i \neq j$. The external potential $v_s(\hat{r}_i)$ in equation (3.19) is named the Kohn-Sham potential and the orbitals φ_i that solve the Schrödinger equation are referred as the Kohn-Sham orbitals.

The applicability of HF theorems is limited to the ground state. Therefore, this strategy cannot easily be transferred to excited states.

3.2.3 Spin treatment in Density Functional Theory

When the electron density is explicitly integrated over the corresponding spin variable, we can obtain the corresponding α - and β -spin densities [equations (3.20) and (3.21), respectively]. The number of α and β electrons can then be calculated by integrating the corresponding α - and β -electron densities: $N_\alpha = \int \rho_\alpha(\vec{r}) d\vec{r}$ and $N_\beta = \int \rho_\beta(\vec{r}) d\vec{r}$.

$$\rho_\alpha(\vec{r}) = N \int \cdots \int |\psi(\vec{r}_1, +\frac{1}{2}, \vec{x}_2, \cdots, \vec{x}_N)|^2 d\vec{x}_2 \cdots \vec{x}_N \quad (3.20)$$

$$\rho_\beta(\vec{r}) = N \int \cdots \int |\psi(\vec{r}_1, -\frac{1}{2}, \vec{x}_2, \cdots, \vec{x}_N)|^2 d\vec{x}_2 \cdots \vec{x}_N \quad (3.21)$$

The total electron density is the sum of the α - and β -electron densities [$\rho(\vec{r}) = \rho_\alpha(\vec{r}) + \rho_\beta(\vec{r})$] and the spin density $Q(\vec{r})$ is defined as the excess of the α -electrons at a given point [$Q(\vec{r}) = \rho_\alpha(\vec{r}) - \rho_\beta(\vec{r})$]. As the electron density $\rho(\vec{r})$, the spin density $Q(\vec{r})$ is an observable.

When the spin operators \hat{S}^2 and \hat{S}_z commute with the Hamiltonian \hat{H} , the eigenfunctions Ψ of the Hamiltonian are eigenfunctions of the two spin operators \hat{S}^2 and \hat{S}_z with eigenvalues $S(S+1)$ and M_S , respectively. An eigenfunction of the \hat{S}^2 operator with eigenvalue $S(S+1)$ will be $(2S+1)$ -fold degenerated in the $(2S+1)$ eigenstates of \hat{S}_z .

The spin operator \hat{S}_z is a one-electron operator than can be expressed only in terms of σ_z , therefore, its expectation values M_S can be obtained directly from the spin density [equation (3.22)]. The eigenfunction of the spin operator \hat{S}_z with eigenvalue M_S is represented as $\Psi^{M_S}[\rho]$. In the spin-restricted DFT formulation these degenerated eigenstates $\Psi^{M_S}[\rho]$ share the same electron density [$\rho^{M_S}(\vec{r}) = \rho^{M_S=S}(\vec{r})$, where $\rho^{M_S=S}(\vec{r})$ is the total electron density of the state with higher M_S] but have different spin densities. The spin densities of the M_S states have the same functional form and are connected by a simple scaling factor [equation (3.23), where $Q^{M_S=S}(\vec{r})$ represents the total spin density of the state with highest M_S . It can be seen that $Q^{M_S}(\vec{r}) = -Q^{-M_S}(\vec{r})$ and $Q^{M_S=0}(\vec{r}) = 0$].

$$M_s = \frac{1}{2} \int Q(\vec{r}) d\vec{r} = \frac{1}{2} (N_\alpha - N_\beta) \quad (3.22)$$

$$Q^{M_s}(\vec{r}) = \left(\frac{M_s}{S} \right) Q^{M_s=S}(\vec{r}) \quad (3.23)$$

According to the first HK theorem, only the electron density $\rho(\vec{r})$, and not the spin density $Q(\vec{r})$, is required for obtaining the ground state energy $E[\rho]$. Consequently, the minimization of $E[\rho]$ will lead to a unique ground state density ρ_0 and the ground state spin density $Q_0(\vec{r})$ will not be directly available. For that reason, several approximations need to be introduced to treat open-shell systems.

3.2.4 Treatment of open-shell systems in the Kohn-Sham approximation

Within the Kohn-Sham DFT formulation, there are two different options to deal with open-shell molecules: the **spin-restricted** and the **spin-unrestricted** spin formulations.

In the **restricted** approximation the wavefunctions are given by the antisymmetrized product of one-electron functions [Slater single determinant $\Phi_s(\vec{x}_1, \dots, \vec{x}_N) = |\varphi_1\alpha, \varphi_1\beta, \varphi_2\alpha, \varphi_2\beta, \dots|$]. As seen before, the orbitals φ_i that represent the spatial part of this function can be obtained as the solution of one-electron Schrödinger equations. In that case, the corresponding one-electron Hamiltonian does not depend on the spin electron and each energy eigenvalue is twofold degenerated (α and β functions) with identical spatial orbitals. Consequently, the resulting Slater determinant is *spin-restricted*.

In the KS theorems, the non-interacting kinetic energy functional $\hat{T}_s[\rho]$ and the Coulomb energy $J[\rho]$ are independent of the spin density and only the exchange-correlation functional $E_{xc}[\rho, Q]$ depends on the spin density Q .

In the interacting system, the minimization of the energy functional $E[\rho]$ with respect to ρ under the constrain that it integrates to the correct number of electrons will lead to the exact ground state electron density $\rho_0(\vec{r})$ and the corresponding exact wavefunction Ψ_0 will be eigenfunction of \hat{S}^2 and \hat{S}_z . However, in the KS non-interacting reference system, its ground state wavefunction $\Psi_{s,0}$ does not necessarily agree with the wavefunction of the interacting system Ψ_0 . Therefore, the multiplicities of the ground state of the non-interacting and the interacting systems can be different. These functions only share the same electronic density, but their corresponding spin densities $Q(\vec{r})$ and $Q_s(\vec{r})$ are in general not equal. It thus follows that the true ground state spin density cannot be calculated from $\Psi_{s,0}$.

However, if a suitable value of M_s is chosen, the wavefunction Ψ^{M_s} is uniquely determined by the electron density $\rho(\vec{r})$. In that case, $\rho_\alpha^{M_s}[\rho](\vec{r})$ and $\rho_\beta^{M_s}[\rho](\vec{r})$ (the ground state α -

electron and β -electron densities, respectively) and the corresponding spin density $Q^{M_s}[\rho](\vec{r}) = \rho_\alpha^{M_s}[\rho](\vec{r}) - \rho_\beta^{M_s}[\rho](\vec{r})$ can be calculated. As mentioned, a specific value of M_s that fixes the number of α and β electrons has to be selected to perform these calculations.

As a consequence, to obtain the spin density in the restricted KS-DFT formulation one has to minimize the spin-resolved HK functional $F_{HK}[\rho_0, Q]$ with respect to $Q(\vec{r})$ under the constrain $\int Q(\vec{r})d^3\vec{r} = 2M_s$. This implies a two-step procedure for determining the spin multiplicity with the restricted KS-DFT: first the total ground state density $\rho_0(\vec{r})$ is determined by solving the KS equations and, then, the spin-density $Q_0(\vec{r})$ is calculated for a chosen value of M_s .

For the **spin-unrestricted solution** the selected reference system of non-interacting electrons has the same α - and β -electron densities as the interacting system. In this case, the Hamiltonian for the reference system differentiates between α and β electrons. The KS exchange potential is then the sum of a component that acts on the total electron density $v_s^{tot}(\vec{r})$ (total exchange-correlation) and another that acts on the spin density $v_s^{spin}(\vec{r})\sigma_z(s_i)$ (spin exchange-correlation). The α and β potentials can be expressed respectively as functions of the total and spin exchange-correlation potentials: $v_s^\alpha(\vec{r}) = v_s^{tot}(\vec{r}) + v_s^{spin}(\vec{r})$ and $v_s^\beta(\vec{r}) = v_s^{tot}(\vec{r}) - v_s^{spin}(\vec{r})$.

The solution of the corresponding spin-unrestricted Hamiltonian $H_s^{(u)}$ (the superscript '(u)' is introduced to denote 'unrestricted') is a single Salter determinant $[\Phi_s(\vec{x}_1, \dots, \vec{x}_N) = |\varphi_1^\alpha \alpha, \varphi_1^\beta \beta, \varphi_2^\alpha \alpha, \varphi_2^\beta \beta, \dots|]$, where the spatial orbitals $\varphi_i^\alpha, \varphi_i^\beta$ are different for α - and β -electrons. The spatial parts can be obtained from the Schrödinger equation of mono-electronic hamiltonians resulting in orthonormal sets of α - and β -orbitals $\langle \varphi_i^\alpha | \varphi_j^\alpha \rangle = \delta_{ij}$, $\langle \varphi_i^\beta | \varphi_j^\beta \rangle = \delta_{ij}$, but α - and β -orbitals are not orthogonal to each other.

This spin-unrestricted Hamiltonian $H_s^{(u)}$ commutes with \hat{S}_z . Consequently, the spin-unrestricted determinants of the reference system are eigenfunctions of \hat{S}_z . In contrast to the spin-restricted treatment, the different \hat{S}_z eigenstates are not restricted and excited state wavefunctions with different values of M_s can be obtained for the corresponding non-interacting reference system.

On the contrary, $H_s^{(u)}$ does not commute with \hat{S}^2 . Therefore, the ground state wavefunction is not an eigenfunction of \hat{S}^2 and larger expected values are obtained. This is referred to as **spin contamination**.

For the unrestricted Slater determinant the total energy functional is given by the kinetic energy functional $T_s^{(u)}[\rho_\alpha, \rho_\beta]$ and the KS potentials v_s^α and v_s^β acting on α - and β -orbitals respectively:

$$E_s^{(u)}[\rho_\alpha, \rho_\beta] = T_s^{(u)}[\rho_\alpha, \rho_\beta] + \int \rho_\alpha(\vec{r}) v_s^\alpha d\vec{r} + \int \rho_\beta(\vec{r}) v_s^\beta d\vec{r} \quad (3.24)$$

The ground state α - and β - densities $\rho_\alpha^0(\vec{r})$ and $\rho_\beta^0(\vec{r})$ of the non-interacting system can be obtained by minimizing the energy functional with respect to ρ_α and ρ_β .

The exchange-correlation functional $F_{HK}[\rho_\alpha, \rho_\beta]$ is expressed as the sum of the kinetic energy of the unrestricted non-interacting system $T_s^{(u)}[\rho_\alpha, \rho_\beta]$, the Coulomb potential $J[\rho]$ and the spin-unrestricted exchange-correlation energy $E_{XC}^{(u)}[\rho_\alpha, \rho_\beta]$. The kinetic energy of the unrestricted non-interacting system $T_s^{(u)}[\rho_\alpha, \rho_\beta]$ is different from the restricted one $T_s[\rho]$, and, as a consequence, the exchange-correlation functional of the unrestricted system $E_{XC}^{(u)}$ is different from the restricted one E_{XC} .

The ground state function $\Psi_{s,0}^{(u)}$ of the KS unrestricted non-interacting reference system is given by the Slater determinants constructed from the orbitals obtained from the corresponding KS equations. Even though the electron density and the spin density calculated from $\Psi_{s,0}^{(u)}$ are equal to those of the fully interacting system, it is important to realize that these wavefunctions do not agree with the ground state wavefunction Ψ_0 of the interacting system. In particular, the wavefunction $\Psi_{s,0}^{(u)}$ is not an eigenfunction of \hat{S}^2 for $S > 0$, while Ψ_0 is. As a result, the unrestricted non-interacting solutions will have spin contamination.

3.2.5 Spin-specific states

So far, we have discussed only the description of the ground state. Targeting the lowest state of a given spin symmetry (with a specific eigenvalue $S(S+1)$ of \hat{S}^2) requires a spin-state specific Hohenberg-Kohn functional $F_{HK}^S[\rho]$ [equation (3.25), the superscript 'S' indicates the spin number of the spin-specific state]:

$$F_{HK}^S[\rho] = \min_{\Psi^S \rightarrow \rho} \langle \Psi^S | \hat{T} + \hat{V}_{ee} | \Psi^S \rangle \quad \text{with} \quad \hat{S}^2 \Psi^S = S(S+1) \Psi^S \quad (3.25)$$

In the spin-restricted formalism, the strategy followed in practice is defining the non-interacting reference system such that it is described by a single Slater determinant with $M_S = S$. In that case, the ground state spin density is not directly available and has to be determined after calculating the ground state electron density.

In the spin-unrestricted KS-DFT the non-interacting reference system is not an eigenfunction of \hat{S}^2 . As a consequence, it is not possible to define a spin-state specific analogue of the unrestricted non-interaction kinetic energy $T_s^{(u)}[\rho, Q]$. It follows that the spin-state dependence is introduced in the exchange-correlation functional $E_{XC}^{(u)}[\rho, Q]$. The strategy

consists in fixing $M_S = S$ when defining the non-interacting reference system (*i.e.* only the maximal eigenvalue of \hat{S}^2 is allowed). The specific exchange-correlation functional can then be expressed as a function of the spin density at the state with $M_S = S$; $E_{XC}^{(u),ss}[\rho, Q^{M_S=S}]$ (where the superscript ‘*ss*’ indicates ‘spin-state’ dependence introduced by $Q^{M_S=S}$). The different spin states can then be distinguished based on the integral of the spin density. However the functional of the spin states $E_{XC}^{(u),ss}[\rho, Q^{M_S=S}]$ does not describe the correct spin density dependence on $E_{xc}^{(u)}[\rho, Q]$ any more, neither $E_{XC}^{(u),S}[\rho, Q]$ that is limited to spin densities corresponding to $M_S = S$. However the spin density $Q^{M_S=S}$ corresponding to other eigenvalues of \hat{S}_z can be obtained from the scaling relation in equation (3.23).

In broken-symmetry (BS) DFT the requirement that the spin density of the non-interacting reference system matches the correct spin density of the fully interacting system is sacrificed in favor of obtaining accurate energies for the low-spin states.

3.2.6 Final considerations about the DFT

Pople et al²⁰ pointed out that a single determinant of Kohn-Sham orbitals probably will show spin contamination when describing open-shell systems, since it is the density, not the orbitals themselves, which have meaning. The wavefunction described by a Kohn-Sham determinant is not a correct wavefunction for the system, and, therefore, is not an eigenfunction of the \hat{S}^2 operator. Consequently, when the eigenvalue of the \hat{S}^2 operator is calculated, the result will present spin contamination. This fact has motivated the application of spin projection methods, or the replacement of the single determinant theory by the multiconfigurational theory. In any case, within the DFT methodology, the KS state must be spin symmetrical to describe the exact wavefunction, *i.e.*, the spin restricted solution should be stable for the description of the singlet in biradicals. Besides, the breaking of symmetry in the KS ground state simply reflects the limitations due to the use of an approximate functional. Considering that the KS density corresponds to a wavefunction of many particles, the broken symmetry function of the KS state represents a state of many particles, which is a mixture of singlet + triplet states, *i.e.*, a state with spin contamination. Thus, instead of spin contamination, the atomic spin density is the property to be used as a diagnostic for the quality of the UDFT calculations.

3.3 Molecular Mechanics Valence Bond (MMVB) method

The Molecular Mechanics Valence Bond (MM-VB) method^{21–23} is a hybrid QM/MM method that uses a Heisenberg Hamiltonian (VB) for the QM part combined with force field (MM) methods. The MM and QM parts are fully parametrized. The use of the VB method allows modeling of the ground and excited state processes.

This method, designed within the group of Michael A. Robb²¹, involves the application of an MM2 force field to describe the part of the system that remains *inactive* (usually the σ skeleton of the molecules). The *active* part (that is involved in chemical reactions and contains the *active* orbitals) is described using ab-initio VB methodology where each electron is located on an atom-based orbital. A CASSCF(n,n)/4-31 g calculation, where n is the number of electrons and active molecular orbitals, is applied to the constructed

wavefunction. Since the calculation time and complexity grow exponentially with n , the maximum number of active electrons n is 24 e^- and orbitals²⁴. The result of the diagonalization of the matrix of molecular orbitals is a matrix constructed by blocks. Within this block matrix, only the blocks that represent covalent configurations are considered and the ionic are obviated (this approach is correct when studying hydrocarbons where the ionic configurations will have very low weight). The Heisenberg Hamiltonian is then applied to the matrix of covalent configurations and the elements of the electron density matrix, \mathbf{P} , and the energy E are obtained.

The basis of the MMVB method consists in the reduction of the complicated MCSCF wavefunction into a simpler VB wavefunction and using the effective Hamiltonian in equation (3.26):

$$\hat{H}_S = Q - \sum_{ij} J_{ij} (2\hat{S}_i \cdot \hat{S}_j + \frac{1}{2} \hat{I}_{ij}) \quad (3.26)$$

where \hat{S}_i is the spin operator associated with the electron i ; \hat{I}_{ij} is the spin identity operator and J_{ij} is the exchange integral between the spin-orbitals i, j ² [equation (3.27)]. This exchange integral is interpreted in terms of electronic distribution as the Heitler-London exchange: $[ij|ij]$ is the bielectronic integral of electron-electron repulsion whose value is always positive and very small, s_{ij} is the overlap between i and j and $\langle i|\hat{h}|j\rangle$ is the monoelectronic integral dominated by the nuclei-electron attraction. The J_{ij} values in this model are empirical parameters that correlate chemical bond effects with spin coupling (despite the fact that there is no a real coupling between the spins)^{21-23,25}. The J_{ij} results in MMVB are obtained from CASSCF computations, however only the $2s_{ij}\langle i|\hat{h}|j\rangle$ term is well represented in this approach^{21,25}.

$$J_{ij} = [ij|ij] + 2s_{ij}\langle i|\hat{h}|j\rangle \quad (3.27)$$

The Coulomb Q term in equation (3.28), represents the antibonding repulsion and steric effects. This has two contributions: $Q_{framework}$, which represents the structure (*framework*) of the molecule and contains more than two effective interactions; and Q_{ij} , the Heitler-London bielectronic parameter [equation (3.29)]. This bielectronic contribution of the *active* electrons includes the term Q_c that represent the closed-shell center (*core*).

$$Q = Q_{framework} + Q_{ij} \quad (3.28)$$

$$Q_{ij} = Q_c + [ii|jj] + \langle i|\hat{h}|i\rangle + \langle j|\hat{h}|j\rangle \quad (3.29)$$

In the algorithm used to model the Heisenberg Hamiltonian \hat{H}_S , the force field that includes the potential energy functions of the molecular framework is described by a molecular mechanics (MM) method. A modified potential for the *active* electrons (Q_{ij}) is incorporated to the standard MM potential (V_{MM}), which is applied to the inactive electrons. The Coulomb term Q is then expressed as:

$$Q = V_{MM} + Q_{ij} \quad (3.30)$$

The Heisenberg Hamiltonian of the equation (3.26) can be then understood as an effective Hamiltonian calculated from an exact *full*-CI Hamiltonian, using a model space of neutral VB(K) determinants formed by n electrons in n atomic orbitals^{26–30}.

$$\Psi = \sum_K C_K |K\rangle \quad (3.31)$$

It has been demonstrated^{21–23} that the parameters Q and J_{ij} can be derived from CASSCF calculations through an effective Hamiltonian formalism. In this case, the localized atomic orbitals and these orbitals can be identified with the centers i and j . As a consequence, the equation (3.26) can be rewritten in second quantization as:

$$\hat{H}_S = Q - \sum_{ij} J_{ij} \left\langle i(1)j(2) \left| \hat{s}_i \cdot \hat{s}_j + \frac{1}{2} \hat{I}(1,2) \right| i(1)j(2) \right\rangle a_i^+ a_j^+ a_j a_i \quad (3.32)$$

and the expression of the elements of the matrix according to the Hamiltonian are represented in the equation (3.33):

$$\hat{H}_{KL} = \delta_{KL} Q - \sum_{ij} J_{ij} \langle \mathbf{K} | a_i^+ a_j^+ a_j a_i | \mathbf{L} \rangle \quad (3.33)$$

where i, j represent the spin-orbitals of the *active* electrons.

As is proposed in ref.²¹, this operator connects configurations that share the same space part and differ only in the contribution of spin. Any *full*-CI Hamiltonian can be projected in that space and the subset of the eigenvalues can be reproduced exactly³¹.

The introduction of P_{ij} , as the elements of the exchange density matrix²¹, defined as in equation (3.34), simplifies the expression of the expected value [equation (3.35)] of the Hamiltonian of the equation (3.26).

$$P_{ij} = \left\langle -(2\hat{s}_i \cdot \hat{s}_j + \frac{1}{2} \hat{I}_{ij}) \right\rangle \quad (3.34)$$

$$\langle \hat{H}_S \rangle = Q + \sum_{ij} J_{ij} P_{ij} \quad (3.35)$$

The difference in energy between two states of different spin multiplicity (*LS*: low spin multiplicity state and *HS*: high spin multiplicity state), where the parameters J_{ij} are considered virtually identical between both states can be expressed as in equation (3.36):

$$\Delta E^{LS-HS} = \sum_{ij} J_{ij} \Delta P_{ij}^{LS-HS} \quad (3.36)$$

where ΔP_{ij}^{LS-HS} is the difference of matrix elements P_{ij} between low and high spin states.

For n electrons on n active spin-orbitals, the expected values of the exchange density matrix will be^{21,31}:

$$\begin{aligned} \langle \Psi | \hat{P} | \Psi \rangle &= -\langle \Psi | \sum_{\mu < \nu}^n (2\hat{S}(\mu) \cdot \hat{S}(\nu) + \frac{1}{2}\hat{I}) | \Psi \rangle = \\ &= -S(S+1) - \frac{n(n-4)}{4} \end{aligned} \quad (3.37)$$

Using the formalism of second quantization equation (3.37) can be rewritten as equation (3.38):

$$\begin{aligned} \langle \Psi | \sum_{\mu < \nu}^n (2\hat{S}(\mu) \cdot \hat{S}(\nu) + \frac{1}{2}\hat{I}) | \Psi \rangle &= \\ = \sum_{i,j,k,l}^N \left\langle i(1)j(2) \left| \sum_{\mu < \nu}^n (2\hat{S}(\mu) \cdot \hat{S}(\nu) + \frac{1}{2}\hat{I}) \right| k(1)l(2) \right\rangle \langle \Psi | a_i^+ a_j^+ a_l a_k | \Psi \rangle \end{aligned} \quad (3.38)$$

And considering the orthogonality of the space-orbitals in the CAS wavefunction, the formula is simplified [equation (3.39)]:

$$\langle \Psi | \hat{P} | \Psi \rangle = \sum_{r,s}^M P_{rs} \quad (3.39)$$

and the multiplicity of the system can be then expressed as:

$$S(S+1) = -\frac{n(n-4)}{4} - \sum_{ij}^n P_{ij} \quad (3.40)$$

Within the MMVB methodology, the parameters J_{ij} and P_{ij} have a specific physical meaning. The P_{ij} parameters indicate the nature of the spin coupling between the centers i and j . With a single VB wavefunction configuration, perfectly paired (Rumer functions³²), the value of $P_{ij} = -1$ when electrons i and j have parallel spins (ferromagnetic coupling), and $P_{ij} = 1$ when the coupling is antiparallel (antiferromagnetic coupling). Note that the calculated P_{ij} values differ from the "ideal" values when there is configuration interaction.

To calculate the P_{ij} components, the equation (3.26) is rewritten³² in terms of standard generators $\hat{E}_{ij}^{\sigma\sigma} = a_{i\sigma}^+ a_{j\sigma}$ of the unitary group $U(n)$ where $\sigma = \alpha, \beta$:

$$\hat{H}_S = Q + \sum_{ij}^M J_{ij} \frac{1}{2} (\hat{E}_{ij}^{\alpha\alpha} \hat{E}_{ji}^{\beta\beta} + \hat{E}_{ij}^{\beta\beta} \hat{E}_{ji}^{\alpha\alpha} + [\hat{E}_{ij}^{\alpha\alpha} \hat{E}_{ji}^{\alpha\alpha} - \hat{E}_{ii}^{\alpha\alpha}] + [\hat{E}_{ij}^{\beta\beta} \hat{E}_{ji}^{\beta\beta} - \hat{E}_{ii}^{\beta\beta}]) \quad (3.41)$$

The equation (3.41) is the basis of the quantum chemistry implementation of the equation (3.26), since the P_{ij} parameters are the expected values of the bilinear forms in equation (3.41).

The Heisenberg Hamiltonian implemented in MMVB corresponds to equation (3.26) and (3.41) and acts on the set of multielectronic neutral VB states built from the active orbital that are occupied by a single electron. The P_{ij} elements are obtained from the CI vectors of MMVB [ref] and provide the values of the exchange spin-density matrix elements for i, j .

3.4 Atoms In Molecules (AIM) method

The method "*Atoms in Molecules*" (AIM), postulated by Bader^{33,34}, describes the molecular structure of a chemical system using the topological properties of the electron density distribution in the real space. The form of such spatial distribution is related to the forces involved in the system, such as the attractive field exerted by the nuclei.

3.4.1 Structural hypothesis

The electron density ρ is a measurable physical quantity at any point in space whose properties determine the characteristics of the chemical system under study. The atoms are considered to be proper open systems than can share energy and electron density. The nuclei are stationary points at which the electron density function is a maximum (attractors). These nuclei are connected by gradient paths of the electron density that originate and terminate on them. A bond is then identified when there is a maximum of the electron density within the interatomic surface that corresponds to the internuclear saddle point, which also lies at the minimum of the ridge between the corresponding pair of nuclei. Thus, the properties of the system are described by the topological properties of the electron density distribution: **the density gradient** ($\nabla\rho$), the **Hessian** ($\frac{\nabla^2\rho}{\nabla q_i \nabla q_j}$) and the

Laplacian, ($\nabla^2\rho$).

3.4.1.1 The density gradient

The gradient of the electron density is the spatial variation of the density over an area. It is described by the vector of the partial first derivatives of the function regarding the three space coordinates, which represent the **trajectories of the function** or "*gradient paths*":

$$\nabla\rho(r) = i\frac{\partial\rho}{\partial x} + j\frac{\partial\rho}{\partial y} + k\frac{\partial\rho}{\partial z} \quad (3.42)$$

Critical points are defined as the points in the space where the gradient of the function is zero, $\nabla\rho(r) = 0$, and can correspond to minimum, maximum, and saddle points of the density function, being the electron density function a maximum at the local nuclei positions.

The gradient of a function is perpendicular to the contour lines of the function (points where the function has a constant value) and indicates the direction of the greatest rate of increase of the function. All path must begin or end in a critical point ($\nabla\rho(r) = 0$) and the trajectories define a unique direction for each r and must not cross each other.

3.4.1.2 Hessian of the density

The Hessian matrix is a 3 x 3 matrix of second derivatives of the density function with respect to the spatial coordinates [equation (3.43)].

$$\begin{pmatrix} \frac{\partial^2 \rho}{\partial^2 x} & \frac{\partial^2 \rho}{\partial x \partial y} & \frac{\partial^2 \rho}{\partial x \partial z} \\ \frac{\partial^2 \rho}{\partial y \partial x} & \frac{\partial^2 \rho}{\partial^2 y} & \frac{\partial^2 \rho}{\partial y \partial z} \\ \frac{\partial^2 \rho}{\partial z \partial x} & \frac{\partial^2 \rho}{\partial z \partial y} & \frac{\partial^2 \rho}{\partial^2 z} \end{pmatrix} \quad (3.43)$$

It is a real and symmetric matrix and, therefore, diagonalizable [equation (3.44)].

$$\begin{pmatrix} \lambda_1 & 0 & 0 \\ 0 & \lambda_2 & 0 \\ 0 & 0 & \lambda_3 \end{pmatrix} \quad (3.44)$$

Diagonalization of the Hessian matrix yields eigenvalues, which are the diagonal matrix elements $\lambda_1, \lambda_2, \lambda_3$, and correspond to the principal symmetry axes of the system. The number of these eigenvalues that are different from zero and their sign characterize the critical points found.

3.4.1.3 Laplacian of the density ($\nabla^2 \rho$)

The Laplacian of a function is defined as the trace of its Hessian matrix and represents the divergence of the gradient of the density on the Euclidean space:

$$\nabla^2 \rho = \frac{\partial^2 \rho}{\partial^2 x} + \frac{\partial^2 \rho}{\partial^2 y} + \frac{\partial^2 \rho}{\partial^2 z} \quad (3.45)$$

The Laplacian of a scalar field determines the distribution of the electronic charge since it is located where the field is locally concentrated or absent. A negative value of the Laplacian $\nabla^2 \rho < 0$ implies a concentration of charge density, while if the value is positive $\nabla^2 \rho > 0$ the implication is, conversely, a reduction of the charge.

The gradient, Hessian and Laplacian are used in AIMs to characterize the atoms within the molecule as well as the bonds between them, based on the topological properties of the electron density functions.

3.4.2 Critical points and trajectories

The eigenvalues or curvatures obtained by the Hessian matrix help to characterize the critical points as maxima, minima or saddle points. For that, two new parameters are

defined: the **range** (ω) which is the number of the Hessian eigenvalues different from zero and the **character** (σ) that is the sum of the signs of these eigenvalues. All critical points are characterized by its range and character (ω, σ). The critical points that are relevant to us have a range $\omega = 3$ and their classification will be determined by their character. A critical point **(3,-3)** is a maximum function in three directions and defines an **attractor (nucleus)**; a point **(3,-1)** represents a maximum function in two directions and a minimum in one direction and it is characteristic of a **bond critical point** between two nuclei or attractors; a point **(3,1)** presents two positive curvature and therefore is a minimum in two directions and maximum in one direction, characteristic of the **ring critical point** since it is found in the middle of several bonds forming a ring. Finally the point **(3,3)** represents that the function is minimum in the three directions of space and is called **cage critical point**. It is found when several rings form a cage.

A relationship between the electron density distribution and the conventional chemical structure can be established based on the number and class of critical points present in the system. Thus, an **atom** is defined as an attractor [critical point (3,-3)] in a **basin of trajectories**. A basin of trajectories is defined as the region of the space where the gradient flow is invariant, *i.e.*, all the trajectories with origin in the basin end in the attractor. The **interatomic surface** is defined as the surface that separates the basins of neighboring atoms. It is characterized by a zero flow of the gradient vector $\nabla\rho(r)$ [equation (3.46)] and differentiates the atoms that constitute a molecule. This characteristic of zero flow is a natural boundary condition for systems in the real space. The intersection of the interatomic surface with the plane takes place through trajectories that end at the bond critical point (the negative eigenvalues). The vector gradient $\nabla\rho(r)$ is always tangent to that surface. From this interatomic surface, characterized by the presence of a bond critical point, the atomic surface that defines the field lines associated with each atom can be defined. This, together with the nucleus and the basin, determine the topological definition of atom.

$$\nabla\rho(r) \cdot n(r) = 0 \quad (3.46)$$

The chemical structure of the molecule is then defined by the nuclei or attractors (3,-3) that are linked through the critical points (3,-1) located between neighboring atoms. The **bond path** is the lines of atomic interaction that connects two nuclei and is defined by the path that represents the unique positive eigenvalue of the bond critical point (3, -1). It is always between two nuclei whose basins share an interatomic surface. The electronic density accumulates between the bonded nuclei. The presence of the line of atomic interaction in a geometry of equilibrium (minimum of energy) is a necessary and sufficient condition to establish a bond between the atoms. The **molecular graph** is defined by the conjunction of all the atomic interactions lines or bond paths, which are a direct result of the main topological properties.

The type and kind of bonds that are identified by the bond critical points are classified through the Laplacian and the **expansion ratio**. The Laplacian of a scalar field locates the points where this field is locally concentrated ($\nabla^2\rho(r_c) < 0$) or reduced ($\nabla^2\rho(r_c) > 0$). The **expansion ratio** ($|\lambda_1|/\lambda_3$) indicates the direction of expansion or contraction of the field.

Thus, a **covalent bond** is defined by $\nabla^2 \rho(r_c) < 0$, large density $\rho(r_c)$ value and expansion ratio $|\lambda_1|/\lambda_3 > 1$ that implies an *accumulation of charge* at the bond critical point located between the nuclei. On the other hand, closed shell interactions such as **ionic bond** or weak bonds such as the **hydrogen bond** are characterized by positive Laplacian $\nabla^2 \rho(r_c) > 0$, small density $\rho(r_c)$ value and expansion ratio $|\lambda_1|/\lambda_3 < 1$ that indicate a *reduction of charge* in the interatomic surface.

Therefore the formation of a chemical bond and the interatomic surface associated with it are the result of two competitive effects: the perpendicular contraction of ρ towards the bond path, which leads to the concentration of charge along this line, and the parallel expansion of ρ away from the surfaces, resulting in the separate concentration of charge within each atomic basin.

Bibliography

- (1) Szabo, A.; Ostlund, N. S. *Modern Quantum Chemistry: Introduction to Advanced Electronic Structure Theory*; Courier Corporation, 1989.
- (2) McWeeny, R.; Sutcliffe, B. T. *Methods of Molecular Quantum Mechanics*; Academic Press, 1976.
- (3) Møller, C.; Plesset, M. S. *Phys. Rev.* **1934**, *46* (7), 618–622.
- (4) Head-Gordon, M.; Pople, J. A.; Frisch, M. J. *Chem. Phys. Lett.* **1988**, *153* (6), 503–506.
- (5) Sæbø, S.; Almlöf, J. *Chem. Phys. Lett.* **1989**, *154* (1), 83–89.
- (6) Frisch, M. J.; Head-Gordon, M.; Pople, J. A. *Chem. Phys. Lett.* **1990**, *166* (3), 281–289.
- (7) Head-Gordon, M.; Head-Gordon, T. *Chem. Phys. Lett.* **1994**, *220* (1), 122–128.
- (8) Malmqvist, P.-Å.; Roos, B. O. *Chem. Phys. Lett.* **1989**, *155* (2), 189–194.
- (9) Andersson, K.; Malmqvist, P.-Å.; Roos, B. O.; Sadlej, A. J.; Wolinski, K. *J. Phys. Chem.* **1990**, *94* (14), 5483–5488.
- (10) Andersson, K.; Malmqvist, P.-Å.; Roos, B. O. *J. Chem. Phys.* **1992**, *96* (2), 1218–1226.
- (11) Pulay, P.; Hamilton, T. P. *J. Chem. Phys.* **1988**, *88* (8), 4926–4933.
- (12) Bofill, J. M.; Pulay, P. *J. Chem. Phys.* **1989**, *90* (7), 3637–3646.
- (13) Hohenberg, P.; Kohn, W. *Phys. Rev.* **1964**, *136* (3B), B864–B871.
- (14) Kohn, W.; Sham, L. J. *Phys. Rev.* **1965**, *140* (4A), A1133–A1138.
- (15) Parr, R. G.; Yang, W. *Density-functional theory of atoms and molecules—Oxford: Oxford Univ; Press*, 1989.
- (16) Jacob, C. R.; Reiher, M. *Int. J. Quantum Chem.* **2012**, *112* (23), 3661–3684.
- (17) Becke, A. D. *Phys. Rev. A* **1988**, *38* (6), 3098–3100.
- (18) Lee, C.; Yang, W.; Parr, R. G. *Phys. Rev. B* **1988**, *37* (2), 785–789.
- (19) Miehlich, B.; Savin, A.; Stoll, H.; Preuss, H. *Chem. Phys. Lett.* **1989**, *157* (3), 200–206.
- (20) Pople, J. A.; Gill, P. M. W.; Handy, N. C. *Int. J. Quantum Chem.* **1995**, *56* (4), 303–305.
- (21) Bearpark, M. J.; Robb, M. A.; Bernardi, F.; Olivucci, M. *Chem. Phys. Lett.* **1994**, *217* (5–6), 513–519.
- (22) Bernardi, F.; Olivucci, M.; McDouall, J. J. W.; Robb, M. A. *J. Chem. Phys.* **1988**, *89* (10), 6365–6375.
- (23) Bernardi, F.; Olivucci, M.; Robb, M. A. *J. Am. Chem. Soc.* **1992**, *114* (5), 1606–1616.
- (24) Bearpark, M. J.; Smith, B. R.; Bernardi, F.; Olivucci, M.; Robb, M. A. In *Combined Quantum Mechanical and Molecular Mechanical Methods*; ACS Symposium Series; American Chemical Society, 1998; Vol. 712, pp 148–158.
- (25) Lafuente, P.; Novoa, J. J. *Theor. Chem. Acc. - THEOR CHEM ACC* **1999**, *102* (1), 309–316.
- (26) Anderson, P. W. *Phys. Rev.* **1959**, *115* (1), 2–13.
- (27) Said, M.; Maynau, D.; Malrieu, J. P. *J. Am. Chem. Soc.* **1984**, *106* (3), 580–587.
- (28) Maynau, D.; Durand, P.; Daudey, J. P.; Malrieu, J. P. *Phys. Rev. A* **1983**, *28* (6), 3193–3206.
- (29) Durand, P.; Malrieu, J.-P. *Adv Chem Phys* **1987**, *67*, 321.
- (30) Durand, P.; Malrieu, J.-P. In *Advances in Chemical Physics*; Lawley, K. P., Ed.; John Wiley & Sons, Inc., 1987; pp 321–412.
- (31) Pauncz, R. *Spin Eigenfunctions*; Springer US, 1979.
- (32) McWeeny, R. *Spins in chemistry*; Academic Press, 1970.
- (33) Bader, R. F. W. *Atoms in Molecules, Clarendon*; Oxford, 1990.
- (34) Bader, R. F. W. *Atoms in Molecules: A Quantum Theory*, 1st Paperback Edition edition.; Clarendon Press: Oxford England : New York, 1994.

CHAPTER 4

CHARACTERIZATION OF INTERMOLECULAR INTERACTIONS

4 Intramolecular interactions

Molecular magnetic organic systems are composed by high-spin organic molecules¹⁻⁷. It is unusual for this type of radicals to be stable, since the unpaired electrons tend to form bonds. With the objective of understanding the mechanisms that favor the stabilization of high-spin radicals we studied several known molecules that have this characteristic.

The systems we studied are organic molecules formed by carbon (C), hydrogen (H), nitrogen (N), and oxygen (O) atoms that contain unpaired electrons. The interactions between the electrons that constitute the so-called "active space" determine the spin states of the molecules/macromolecules⁸. Two main types of interactions between the active electrons within the molecule are distinguished: (a) the through-space interactions (**TS**), via a super-exchange electron transfer mechanism, and (b) the through-bond interactions (**TB**), by a spin polarization mechanism. The preference for a high multiplicity state can be evaluated according to one and/or another contribution.

This PhD thesis describes the spin state of some organic molecules that are acknowledged to have high-spin ground states. For that, we used the J_{ij} and P_{ij} parameters, which represent the exchange integral and the spin-exchange density matrix elements between the electrons.

In addition, we explored the possibility of designing high-spin macromolecules formed by polymerization or heterogeneous synthesis of the high-spin radicals as building blocks. The molecules that show high-spin multiplicity in the ground state are considered possible building blocks for larger systems with probable macroscopic magnetism. Two kinds of approaches are examined in this chapter: (a) the polymerization of the high-spin radicals to form polymers with magnetic properties, and (b) the heterogeneous synthesis of different high-spin radicals following the scheme SU-CU-SU with two spin containing units (SU) which are ferromagnetically coupled due to a third molecule, known as coupling unit (CU).

4.1 Methods

First of all, in this study we analyzed how the interactions between the electrons belonging to the active space of the molecule determines the multiplicity of the system. Considering the effective Heisenberg spin Hamiltonian [equation (4.1)], the ground state has high-spin multiplicity when the energy difference between two spin states (LS: low-spin, HS: high-spin) of the same molecule ΔE^{LS-HS} is positive [equation (4.2)].

$$\hat{H}_S = Q - \sum_{ij} J_{ij} (2\hat{S}_i \cdot \hat{S}_j + \frac{1}{2} \hat{I}_{ij}) \quad (4.1)$$

$$\Delta E^{LS-HS} = \sum_{ij} \Delta(J_{ij} P_{ij})^{LS-HS} \quad (4.2)$$

The energy gap ΔE^{LS-HS} depends on two parameters: (a) the exchange integrals J_{ij} [equation (4.3)] and (b) the spin-exchange density matrix elements P_{ij} [equation (4.4)].

$$J_{ij} = [ij|ji] + 2S_{ij} \langle i | \hat{h} | j \rangle \quad (4.3)$$

$$P_{ij} = \left\langle - (2\hat{s}_i \cdot \hat{s}_i + \frac{1}{2} \hat{I}_{ij}) \right\rangle \quad (4.4)$$

To estimate the energy gap between the two spin states, we used the P_{ij} and J_{ij} parameters calculated at CASVB(n,n) and MMVB^{9,10} levels, and using a simple program denominated *J*-code, developed by the M.A. Robb group, which is described more in detail below. MMVB calculations are limited to systems with an even number of electrons. Therefore, most of the systems chosen for this study will have an even number ($2n$) of active electrons.

For the CASVB(n,n) calculations (where n is the number of active electrons and orbitals), we followed the methodology proposed by Pulay et al.¹¹ to define the active space and the starting orbitals for the MCSCF computation. Initially, we run UHF calculations with natural orbitals and we selected as active space those orbitals whose occupancies ranged between 0 and 2:

- 1) UHF/*basis-set*: geometry optimization for the high-spin state.
- 2) UHF/*basis-set*: selection of the natural orbitals (occupancy 0 – 2).
- 3) CASSCF(n,n)/*basis-set*: calculation of P_{ij} and J_{ij} parameters and estimation of the energy gap between the two spin states.

In CASVB, the number of active orbitals is the same than active electrons, and every orbital is related to one electron. This fact simplifies the interpretation of the parameters P_{ij} and J_{ij} and the description of the spin preference of the molecule.

Generally, the basis set used in CASVB calculation was 6-31g(d). However, when compared to MMVB and *J*-code, the 4-31g(d) basis was used, since this is the basis set implemented in MMVB.

4.1.1 *J*-code

When an effective spin Hamiltonian on a valence bond space (VB) is used to estimate the energy values, the parameters J_{ij} and P_{ij} (orbitals i,j being assigned to active-space electrons) have physical meaning^{9,12-14}. The exchange integral J_{ij} is generally negative for two bonding ij orbitals, and only when the overlap of the two ij orbitals tends to zero, but there is still interaction between them, J_{ij} has a small positive value. The value of P_{ij} is +1, 1/2 and -1 for pairs of paired, uncoupled and parallel spins, respectively.

A qualitative analysis can be done using the J_{ij} and P_{ij} parameters to calculate the spin multiplicity of the ground and excited states in a molecular system based on the topology of the molecule.

First, a topological J -matrix is built similarly to the Ovchinnikov's theory¹⁵. This matrix is triangular and based on J_{ij} parameters, which are strongly dependent on the geometry. That is, J_{ij} are different from zero when i,j represent pairs of neighbor electrons close in space, and $J_{ij} = 0$ for i,j pairs distantly located (Figure 4.1). A similar technique has been previously proposed and successfully applied in alternating conjugated hydrocarbons^{16–19}.

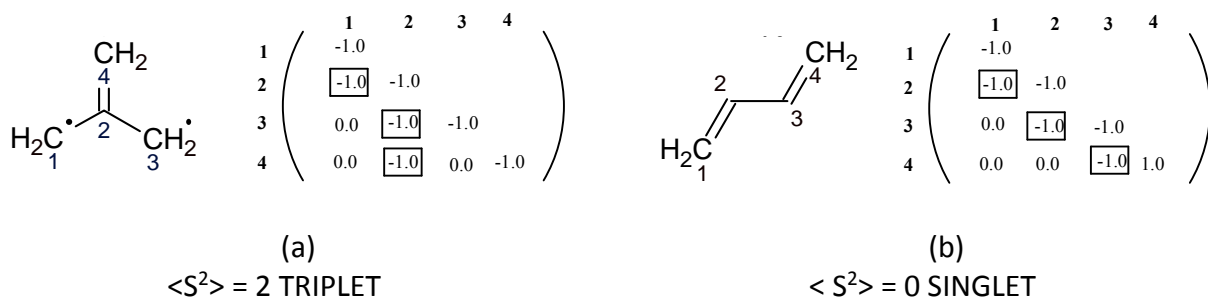


Figure 4.1 J -matrix constructed with values $J_{ij} = -1.0$ a.u. for bonded i,j atoms and $J_{ij} = 0.0$ a.u. for non-bonded i,j atoms for the molecules (a) trimethylenemethane (TMM) and (b) butadiene. Systems (a) and (b) have the same atoms but different connectivity, and show different ground state spin multiplicity.

To build the J -matrix, one needs to know the value of the J_{ij} elements. For that, we have used three possible approaches:

- I. Values $J_{ij} = -1.0$ a.u. are given when i,j are connected and $J_{ij} = 0.0$ a.u. when they are not (Figure 4.1). With this J -matrix, we just obtain qualitative energy results from the expected values of the Hamiltonian. It is a method based purely on connectivity, which allows us to estimate the energy order of the different spin states of the system.
- II. Values J_{ij} are previously calculated with MMVB^{9,12,13}. These values can be used as generic values for a class of i,j interacting atoms. For example, if i,j electrons belong to the carbon π -orbitals, such as in the alternant hydrocarbons, the value of the parameter J_{ij} between two centers i,j is $J_{ij} = -0.06$ a.u. The expected eigenvalues of the spin Hamiltonian obtained from this J -matrix are a better estimation, as well as the energy gap between the different spin multiplicity states.
- III. Values J_{ij} previously obtained from CASVB(n,n) calculations. In CASSCF, parameters J_{ij} are calculated by applying an effective Hamiltonian²⁰ and the P_{ij} matrix is obtained from an active space composed of localized orbital. It thus follows that the calculation is restricted to small active spaces.

The expected value of the spin Hamiltonian for different spin states of the molecule can be then calculated from the constructed J -matrix and the P -matrix. Note that the P -matrix is computed using an in-house code developed by the research group of Professor M.A. Robb.

The multiplicity of each state can be then calculated using the equation (4.5), where n is the number of the π -electrons in the active space.

$$S(S+1) = -\frac{n(n-4)}{4} - \sum_{ij} P_{ij} \quad (4.5)$$

To check the applicability of the code that uses the topological J -matrix, a series of calculations were conducted on well-known alternant hydrocarbon (AH) molecules where the active electrons belong to the π -framework of the C atoms (Figure 4.2). The topological J -matrix used in the calculations is type (I), thus $J_{ij} = -1.0$ a.u. for neighbor i, j centers and $J_{ij} = 0.0$ a.u. when i, j are distant in space. An exception is the value of J_{ij} between the two atoms within the ring of the system (3) [Figure 4.2]. In this case, the J_{ij} value is positive and lower in magnitude ($J_{ij} = 0.05$ a.u.) than any other two i, j connected atoms, due to the distance and kind of interaction between the two centers (the magnitude and sign of the parameter were confirmed by previous CASSCF calculations).

In all cases the multiplicity calculated for the ground state is the same than observed experimentally^{7,21-30}. However, the values for the energy gap between the high and low-spin states are higher than the experimental ones (Figure 4.2).

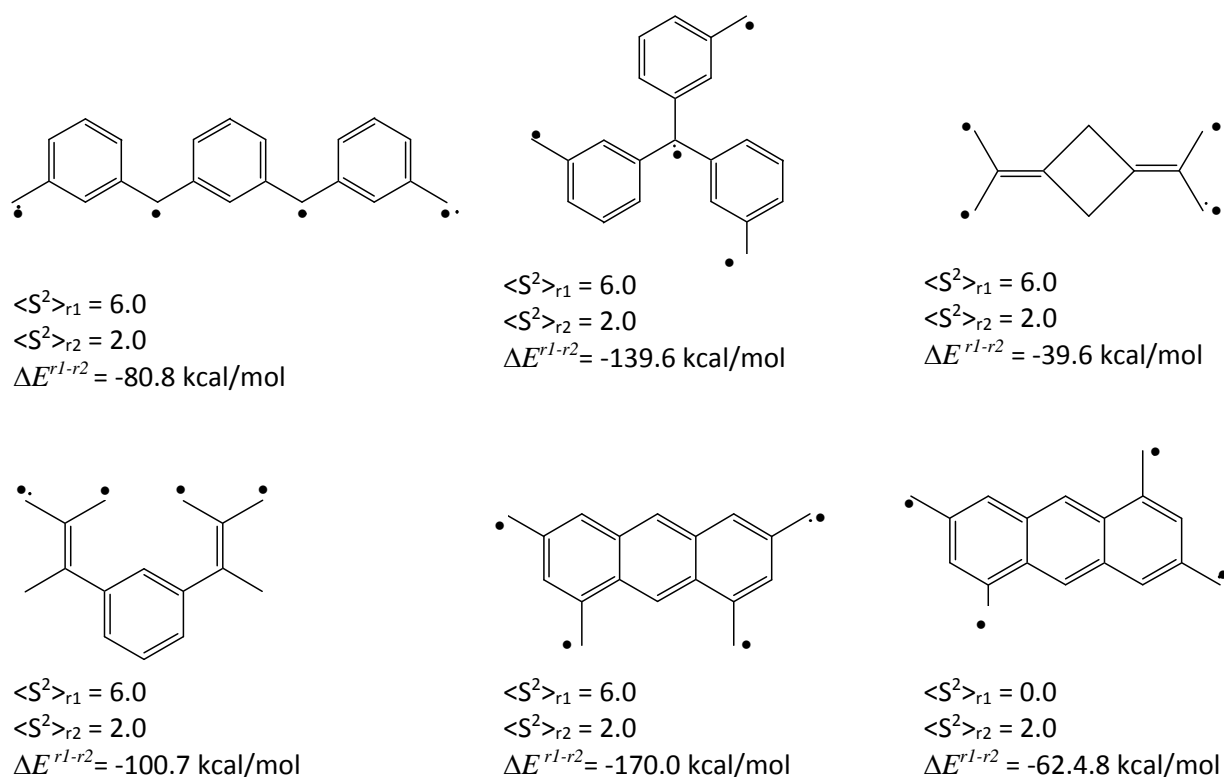


Figure 4.2 Example of alternant hydrocarbon (AH) molecules. For each system the multiplicity of the ground (root 1, r1) and first excited (root2, r2) states and the calculated value for the energy gap between both states are shown. For all the systems, the ground state multiplicity has been estimated correctly when compared to experimental observations^{7,21-30}.

The relationship between topology and spin multiplicity in the alternant hydrocarbons is highlighted by the different multiplicity observed for system (5), a quintet, and system (6), a singlet, while these two molecules differ only in the position of two substituent methyl radicals.

These J -matrices and the in-house computation code used allow the fast and efficient determination of the stability and multiplicity of the different energy states of the molecules.

4.2 Historical references.

Due to the high interest in molecule-based magnets, several theoretical models arised^{31,15,32-39} to explain the mechanism that favor the stabilization of states with spin moment different from zero in organic radicals.

One of the first rules that tried to predict the spin multiplicity in biradical alternate hydrocarbons was based on the molecular orbital (MO) approach. Biradical alternate hydrocarbons are characterized by a pair of non-bonding molecular orbitals (NBMO^{31,40}) containing unpaired electrons. The multiplicity of the ground-state of these molecules was explained as an extension of the Hund's rule of maximum multiplicity for atoms (Longuet-Higgins' model³¹). Based on this principle, Borden and Davidson^{16,17} proposed that there should be as many non-bonding molecular orbitals (NBMOs) as free electrons to stabilize a high-spin ground state. If these NBMO were degenerate or quasi-degenerate, the free electrons would tend to be arranged according to a rule of maximum multiplicity (comparable to the Hund's theory for atoms). This degeneration (or quasi-degeneration) occurs when different NBMOs constructed by linear combination of atomic orbitals (LCAO) include common atomic orbitals (AO). These systems are called *non-disjoin systems*. According to this approach, the multiplicity of the ground state is predicted to be half of the number of NBMOs³¹.

The Huckel⁴¹⁻⁴⁴ molecular orbital method (HMO) provides a simple mechanism for determining the energy of the MOs of the π -electrons of conjugated hydrocarbons. According to HMO, the MOs are simple LCAO. The HMO is based on the Schrödinger equation and symmetry orbital considerations. An extended version was developed by Hoffman and included σ orbitals⁴⁵.

Beyond the Hückel method, the semi-empirical Hamiltonians as the Pariser-Parr-Popel (PPP)⁴⁶⁻⁴⁸ and Hubbard⁴⁹ (simplification of the former where the Coulomb interactions are limited to the π -electrons of the same atom) appeared to study molecules with many unpaired electrons. These Hamiltonians have been widely applied to large systems (about 14 π centers) and can correctly describe the multiplicity of their ground state^{18,33-36,50-52}.

Within the VB description, the Ovchinnikov theory¹⁵ (based on the demonstration of Lieb and Mattis³²) is widely known and used for systems of alternating hydrocarbon (AH) with conjugated bonds. The Ovchinnikov rule to predict the spin multiplicity in planar alternant hydrocarbon consists in dividing the C-sp² active atoms (π system of the molecule) into two sets: the so-called *starred* (*) and the *unstarred* (o). In order to be able to apply this rule, two adjacent atoms must belong to two different sub-groups, *i.e.*, neighbor atoms have to be *-o and never *-* or o-o to avoid breaking the alternation (for example see Figure 4.3). If the alternant hydrocarbon contains an odd number of atoms there must be an unpaired orbital with zero bonding energy (a non-bonding orbital)⁵³. The spin multiplicity estimated for these systems is then calculated according to equation (4.6).

$$S = \frac{(n^o - n^*)}{2} \quad (4.6)$$

This methodology allows to distinguish the different multiplicity observed for two systems that only differs in connectivity, like *m*-xylylene (1,3-quinodimethane) and *p*-xylylene (1,4-quinodimethane) with a triplet and singlet ground state respectively (Figure 4.3).

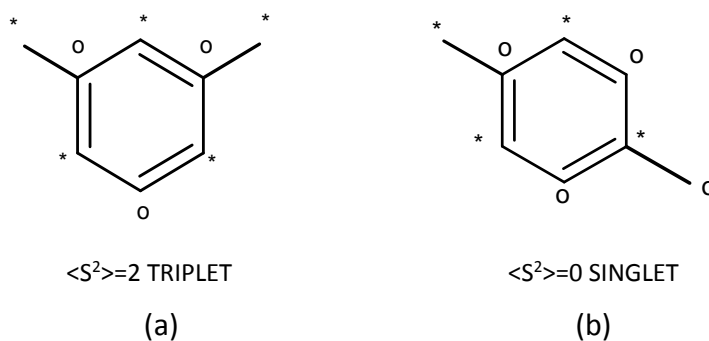


Figure 4.3 Example of multiplicity calculation using Ochivnnikov topology method: (a) *m*-xylylene (1,3-quinodimethane), with a triplet ground state; (b) *p*-xylylene (1,4-quinodimethane) with a singlet ground state.

Ovchinnikov's theory, in spite of its many limitations, allows to predict the multiplicity of numerous radical systems. Correspondingly, it shows the direct relationship between the topology (spatial distribution of the active orbitals) and the multiplicity of the system.

In the early 1980s, Malrieu and Maynau^{54–58} proposed a VB method derived from the Hubbard Hamiltonian and applied *many-body* perturbation theory up to fourth-order correction. Following this technique several conjugated hydrocarbons were studied with success^{51,18,59,60,16,17}.

From different calculations for several systems, it has been observed that, generally speaking, the multiplicity calculated with VB methods is smaller and the MO multiplicity is higher than the experimental ones: $S(\text{VB}) < S(\text{experimental}) < S(\text{MO})$ ^{33–36}. In addition, it should be noted that, usually, the theory that best predicts the multiplicity of the system is the VB theory. Likewise, the MO description often tends to refer to VB to rationalize the results. Despite these advantages, the VB theory implies complex calculations since it involves a large number of configurations to consider and, therefore, it is difficult to be used for large systems.

4.3 Study of the stabilization of the high-spin state in biradicals

4.3.1 Case study of the σ,σ -didehydronaphthalene isomers

Molecules like σ,σ -didehydronaphthalene isomers (Figure 4.4) are systems of great interest from several points of view⁶¹. In these molecules, two unpaired electrons are located in two σ orbitals of the naphthalene structure; the different isomers exist depending on where these σ orbitals are to be found (1,2-; 1,3-; 1,4-; 1,5-; 1,6-; 1,7-; 1,8-; 2,3-; 2,6-; 2,7-). Some of these isomers have a high-spin ground state (triplet) while others stabilize the singlet. As part of this PhD thesis, we intended to describe the intramolecular interactions that regulate the preference for the low or high-spin state.

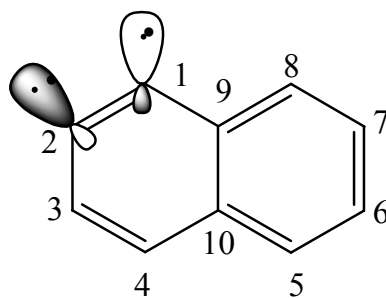


Figure 4.4 Generic example of σ,σ -didehydronaphthalene; namely the 1,2-didehydronaphthalene.

The active space of the molecule is considered to be constituted by two free electrons located in two σ orbitals (radical centers) and ten electrons belonging to the π -framework of the naphthalene. On a valence bond (VB) analysis, where all the active electrons are placed in atomic orbitals (OAs), the spin distribution of the active electrons is expected to be: (1) parallel (α - α or β - β) between the σ and π electrons located in the same radical atoms, following the Hund's rule of two unpaired electrons in a same atom, and (2) antiparallel (α - β) between neighbor electrons within the π -framework, due to the spin polarization (Figure 4.5, see 1,2-didehydronaphthalene as an example).

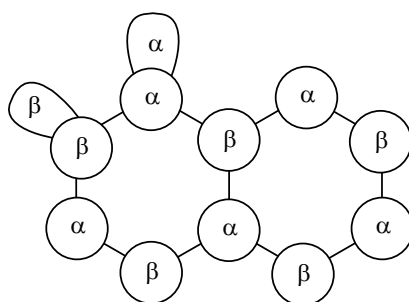


Figure 4.5 Spin distribution for 1,2-didehydronaphthalene.

Cramer *et al*⁶¹ studied at CASPT2 (12,12) level the energy gap between the singlet (S) and triplet (T) states for the σ,σ -didehydronaphthalene isomers. We will use their results as control values to our calculations. Cramer postulated that the energy gap can be partitioned into three different contributions: (a) through-space (**TS**), (b) through-bond within the π -framework (**T π B**), and (c) through-bond via the σ -bond (**T σ B**). This last contribution (**T σ B**) is practically negligible in most cases.

The **TS** (σ - σ) interaction represents the direct overlap of the σ orbitals in which the two radical centers are located. If the two σ radical centers are close enough to overlap, the antiferromagnetic (AFM) α - β interaction between the two free electrons is energetically favored. However, such overlap is only important at short distances and at certain orientations of these orbitals. Thus, when the **TS** interaction is practically zero, the decisive contribution to the final multiplicity of the state is **T π B** (π - π), which is ruled by the spin polarization through the π -framework of the molecule.

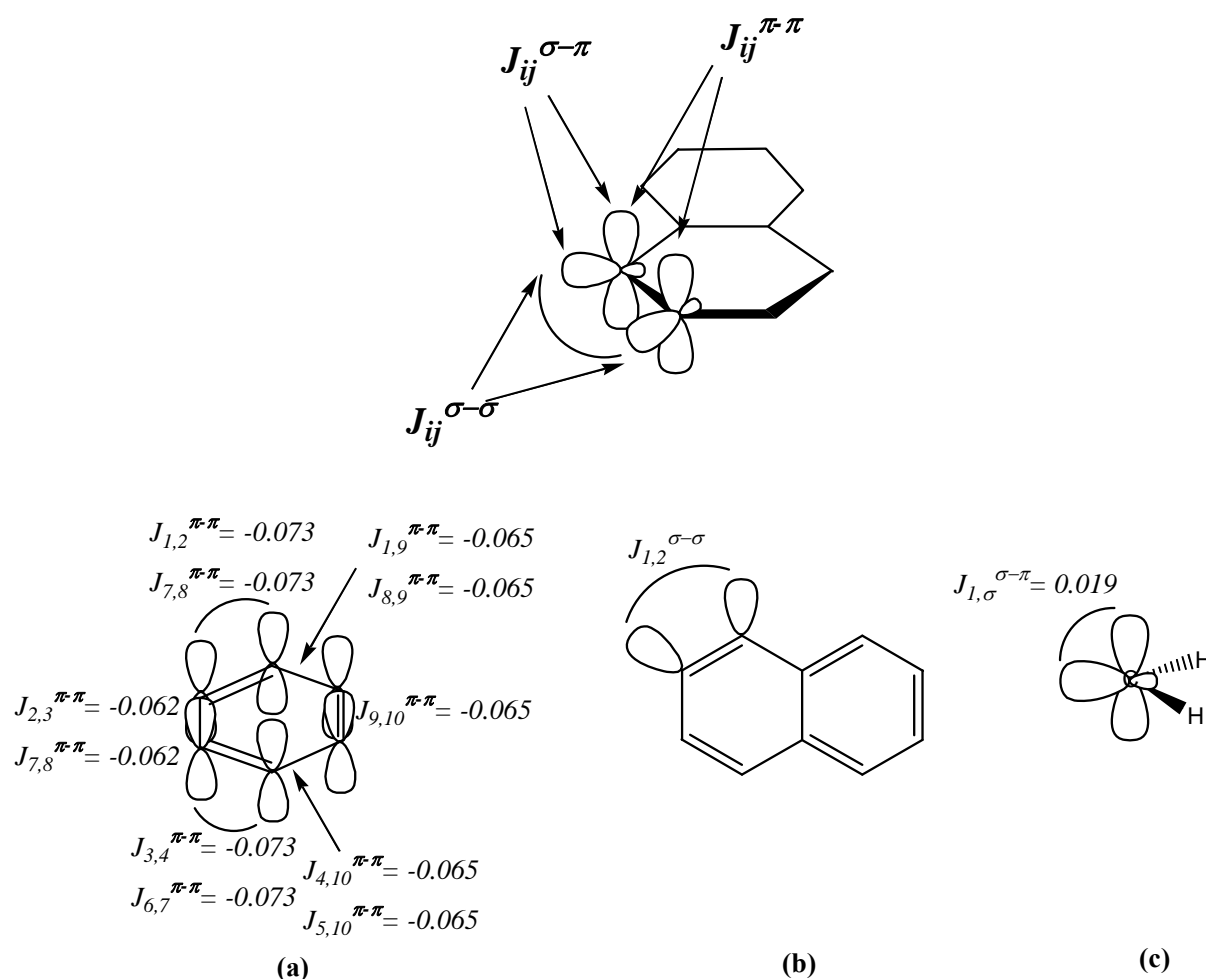


Figure 4.6 (a) π - π , (b) σ - σ and (c) σ - π contributions for 1,2-didehydronaphthalene. The J values have been calculated: (a) $J^{\pi-\pi}$ with MMVB (b) $J^{\sigma-\sigma}$ with CAS(2,2)/4-31g for each isomer and (c) $J^{\sigma-\pi} = 0.019$ a.u. as the energy difference between the singlet and triplet states of the biradical carbene $:\text{CH}_2$. See Figure 4.4 for atom labeling.

We used the J -topological matrix to evaluate the **TS** and **T π B** contributions using the geometries optimized by Cramer⁶¹, and then compared our results to those calculated by Cramer. The J_{ij} terms of the different contributions of the electrons in the active space (π - π , σ - σ , π - σ) were estimated according to three different methods (Figure 4.6):

- $J^{\pi-\pi}$:** Values $J_{ij}^{\pi-\pi} = -0.062$ a.u. and $J_{ij}^{\pi-\pi} = -0.073$ a.u. values were computed with MMVB using the geometry obtained by Cramer in their calculations (Figure 4.6a). These interactions are classified as through-bond interactions **T π B** within the π -framework.
- $J^{\sigma-\sigma}$:** Contribution $J_{ij}^{\sigma-\sigma}$ was estimated with a CAS(2,2)/4-31g calculation, where the active space is constituted by two σ -electrons occupying two σ -orbitals located in the two radical centers (Figure 4.6b). These interactions are the ones considered as through-space **TS** interactions. This value will be different for each isomer, depending on the σ - σ interaction.
- $J^{\sigma-\pi}$:** The $J_{ij}^{\sigma-\pi} = 0.019$ a.u. values were calculated as the energy difference between the singlet and triplet states of the biradical methylene (methylidene): CH_2 (Figure 4.6c). The interaction of the two electrons located in the σ and π orbitals within the

same atom is always ferromagnetic (Hund's rule). It has been included in the through-bond $\mathbf{T}\pi\mathbf{B}$ contribution.

With all these parameters, the topological \mathbf{J} -matrix is built based on connectivity. Distributing the active centers in π or σ blocks, the \mathbf{J} -matrix is a symmetric matrix that can be divided into π - π , π - σ or σ - σ sectors (Figure 4.7).

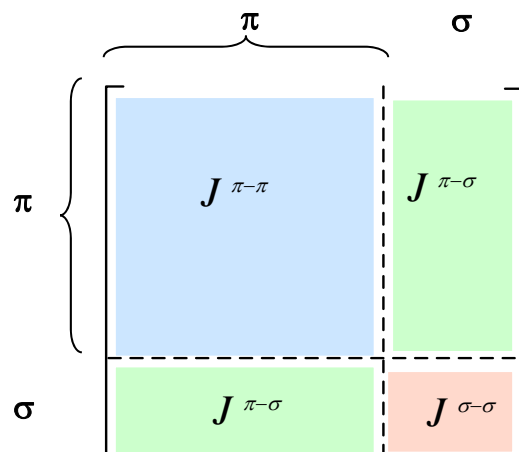


Figure 4.7 Topological \mathbf{J} -matrix. The active electrons have been distributed in rows and columns such that the matrix can be divided into blocks $J^{\pi-\pi}$, $J^{\sigma-\pi}$, $J^{\sigma-\sigma}$.

Using the in-house code developed by M.A. Robb and coworkers, the values of P_{ij} were calculated for each state and isomer. The energy and the energy gap (ΔE^{LS-HS}) between states of low (LS) and high (HS) spin was then estimated using the equation (4.2). This gap can then be partitioned [equation (4.7)] into the contribution TS [equation (4.8)] and $\mathbf{T}\pi\mathbf{B}$ [equation (4.9)] for each σ - σ isomer (Table 4.1). The through-space (\mathbf{TS}) and through- π -bond ($\mathbf{T}\pi\mathbf{B}$) contributions represent two out of the three mechanisms suggested by Cramer⁶¹ to interpret the multiplicity of the different didehydronaphthalene biradicals. The third mechanism used by Cramer to explain the stabilization of the singlet as ground state of the 2,7-didehydronaphthalene, the so-called $\mathbf{T}\sigma\mathbf{B}$, has not been evaluated as it has been considered of small significance for most of the isomers.

$$\begin{aligned}
 \Delta E^{LS-HS} &= \sum_{ij} \Delta(J_{ij} P_{ij})^{LS-HS} = \\
 &= \sum_{ij}^{\sigma-\sigma} \Delta(J_{ij} P_{ij})^{LS-HS} + \sum_{ij}^{\sigma-\pi} \Delta(J_{ij} P_{ij})^{LS-HS} + \sum_{ij}^{\pi-\pi} \Delta(J_{ij} P_{ij})^{LS-HS} = \\
 &= J^{\sigma-\sigma} + J^{\sigma-\pi} + J^{\pi-\pi} \\
 &= J_{TS} + J_{T\pi B}
 \end{aligned} \tag{4.7}$$

$$J_{TS} = J^{\sigma-\sigma} = \sum_{ij}^{\sigma-\sigma} \Delta(J_{ij} P_{ij})^{LS-HS} \tag{4.8}$$

$$J_{T\pi B} = J^{\sigma-\pi} + J^{\pi-\pi} = \sum_{ij}^{\sigma-\pi} \Delta(J_{ij}P_{ij})^{LS-HS} + \sum_{ij}^{\pi-\pi} \Delta(J_{ij}P_{ij})^{LS-HS} \quad (4.9)$$

Table 4.1 Results obtained for all possible didehydronaphthalene isomers. The two first rows show the results of the J_{ij} parameters between σ radical centers. The three following rows show $\Delta(J_{ij}P_{ij})$ results for the σ - σ , π - π and σ - π contributions. These values are used to calculate J_{TS} and $J_{T\pi B}$ shown in the 6th and 7th rows. The energy gap between the singlet and the triplet ΔE^{S-T} calculated from these two results is shown in 8th row. The last row shows the values reported by Cramer *et al.* at CASPT2(12,12) level⁶¹.

	1,2	1,3	1,4	1,5	1,6	1,7	1,8	2,3	2,6	2,7
$J_{ij}^S(\sigma_1-\sigma_2)$ a.u.	-0.051	-0.019	-0.001	-0.002	0	-0.0003	-0.0001	-0.0486	0	-0.0008
$J_{ij}^T(\sigma_1-\sigma_2)$ a.u.	-0.014	-0.007	-0.002	-0.0025	0	-0.0002	-0.0011	-0.0087	0	-0.0006
$\Delta(J_{ij}P_{ij})^{\sigma-\sigma}$ (kcal/mol)	-39.0	-16.2	-1.8	-2.7	0.00	-0.3	-0.8	-34.8	0.0	-0.9
$\Sigma\Delta(J_{ij}P_{ij})^{\pi-\pi}$ (kcal/mol)	-2.2	-1.6	0.2	0.2	-0.9	0.5	-1.0	-1.3	0.4	-0.7
$\Sigma\Delta(J_{ij}P_{ij})^{\sigma-\pi}$ (kcal/mol)	0.5	3.7	-2.0	-1.3	1.9	-1.6	2.2	0.4	-1.5	1.8
J_{TS} (kcal/mol)	-39.0	-16.2	-1.8	-2.7	0.0	-0.3	-0.8	-34.8	0.0	-0.9
$J_{T\pi B}$ (kcal/mol)	-1.7	2.1	-1.8	-1.1	1.0	-1.1	1.2	-0.9	-1.1	1.1
ΔE^{S-T} (kcal/mol)	-40.6	-14.6	-3.3	-3.8	1.1	-1.3	0.5	-36.2	-1.0	0.2
ΔE^{S-T} (kcal/mol) CASPT2 ⁶¹	-41.1	-20.2	-3.8	-5.8	0.7	-0.3	0.8	-34.8	-0.2	-1.2

In the analysis of **TS** and **T π B** mechanisms (Table 4.1), negative values mean contribution for stabilization of the low-spin state, while positive values denote a preference for the high-spin state. It is noted that **TS** values depend strongly on the distance and orientation between the two σ - σ orbitals and are always negative or zero. On the contrary, **T π B** effect is either negative or positive, depending on the topology of the system, and of similar magnitude. For **1,2-**; **1,4-**; **1,5-**; **1,7-**; **2,3-** and **2,6-** isomers (Table 4.1, rows 6 and 7) both contributions are negative or zero. Consequently, the energy gap is negative and the ground state is a singlet. The positive **T π B** contribution in **1,3-**; **1,6-**; **1,8-** and **2,7-** isomers (Table 4.1, row 7) favors the stabilization of the high-spin state. However, the ground state of the **1,3-** isomer is a singlet (Table 4.1, row 8), due to the large negative **TS** value (**TS** = -16.2 kcal/mol) that overcomes the positive **T π B** contribution (**T π B** = 2.1 kcal/mol). Systems **1,3-** and **1,8-** are topologically similar since there is only one C atom between the two radical centers (Figure 4.8). However, as observed in Table 4.1, the singlet is energetically stabilized (ΔE = -14.6 kcal/mol) for the **1,3-** system, while for the **1,8-** isomer the triplet is slightly lower in energy (ΔE = 0.5 kcal/mol). The difference between both systems is, mainly, due to the **TS** contribution. In the case of the **1,3-** isomer (Figure 4.8a) the spatial distribution allows a better tail-to-tail overlapping of the σ - σ orbitals and, as a result, the **TS** contribution is larger (**TS** = -16.2 kcal/mol) and favors the singlet. On the contrary, in the case of **1,8** (Figure 4.8b) the parallel orientation of the σ - σ orbitals gives as a result a small **TS** contribution (**TS** = -0.8 kcal/mol) is exceeded by the positive **T π B** contribution **T π B** = 1.2 kcal/mol.

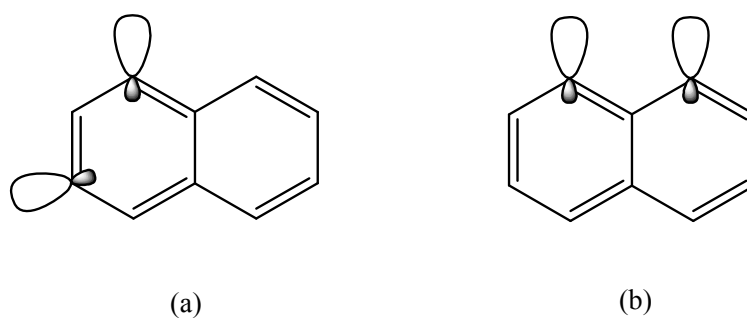


Figure 4.8 (a) 1,3-didehydronaphthalene, and (b) 1,8-didehydronaphthalene isomers σ -orbitals. The spatial orientation allows a higher tail-to-tail overlap between the σ orbitals in the 1,3 isomer compared to the parallel σ - σ orbitals in 1,8 system.

The energy gap between singlet and triplet for the **1,6** isomer is very small, being the triplet slightly lower in energy (Table 4.1, row 8), in agreement with Cramer's CASPT2 results (Table 4.1, row 9). In this case **TS** is zero due to the high distance and orientation between the two σ - σ radical centers and the only appreciable contribution is the positive **T π B** value.

According to our results, for **2,7** isomer there is a quasi-degeneration between the triplet and the singlet states, being the triplet slightly lower in energy ($\Delta E^{S-T} = 0.2$ kcal/mol, Table 4.1), contrary to Cramer's results. In our calculations, the **T π B** contribution (**T π B** = 1.1 kcal/mol) is slightly higher than the **TS** (**TS** = -0.9 kcal/mol) and the triplet is stabilized. Cramer's justification for the stability of the singlet is based on the **T σ B** contribution through the C atoms of the naphthalene framework. Since we have not included this contributions in our calculations, this effect was not evaluated and we cannot assess this statement.

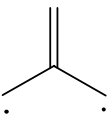
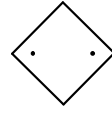
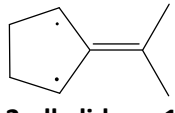
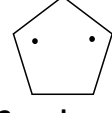
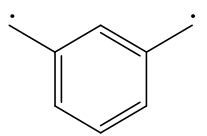
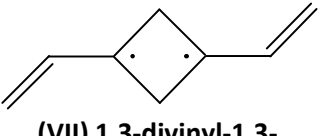
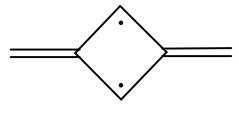
In our calculations, practically all the isomers have singlet ground states, with the exception of **1,6-**; **1,8-** and **2,7-**. As it has been seen, there are two main contributions identified: through-space (**TS**) and through-bond within the π -framework of the naphthalene (**T π B**). When the σ orbitals are close enough and their orientation facilitates their overlapping, the **TS** contribution is the main driving force stabilizing the singlet state. The **TS** contribution is negative in all the studied isomers, favoring the antiferromagnetic coupling of the two radical electrons placed in the σ -orbitals. When the **TS** contribution is very small or practically zero, the **T π B** becomes relevant in the determination of the ground state spin multiplicity. The magnitude of this contribution is similar for all the studied isomers and its sign (negative or positive) depends on the location of the σ electrons within the naphthalene framework. Therefore, the **T π B** multiplicity preference depends on the topology of the system.

Although in these calculations we have estimated all J_{ij} contributions for each ij pair in the active space, the **J π - π** parameters within the π -framework (p_z orbitals of the C atoms) in AH are usually very similar ($J_{ij}^{\pi-\pi} \sim -0.070$ u.a.). Also, **J σ - π** contribution between the σ and p_z orbitals in the same C atom, has generally the same value ($J_{ij}^{\sigma-\pi} = 0.019$ a.u.). Therefore, we could perform the calculations using the estimated parameters $J_{ij}^{\pi-\pi} = -0.070$ u.a., $J_{ij}^{\sigma-\pi} = 0.019$ a.u. and computing only the $J_{ij}^{\sigma-\sigma}$ values with simple CAS(2,2) calculations. With this method we can predict the correct spin multiplicity of the system and estimate the energy gap between the two spin states in a quick and effective way.

4.3.2 High-spin C_{π} biradicals.

The simplest high-spin molecules are systems that have two unpaired electrons interacting ferromagnetically. These molecules are called biradicals. Extensively studied organic biradicals are those whose free electrons belong to the π framework of the molecule. These C_{π} biradicals can be classified into two groups: (a) systems with electrons " π -delocalized" or alternate hydrocarbon (AH) and (b) " π -localized" systems (see Table 4.2a and b, respectively).

Table 4.2 Multiplicity of the ground state as reported in the bibliography: (a) calculated^{3-5,38,39,62-66} and/or observed experimentally^{3-5,62-65,67-70} for the π -delocalized biradicals and (b) calculated^{3-5,26-30} and/or experimentally observed⁷¹⁻⁷³ for the π -localized biradicals.

(a) π -Delocalized biradicals		(b) π -Localized biradicals	
SYSTEMS	MULTIPLICITY BIBLIOGRAPHY	SYSTEMS	MULTIPLICITY BIBLIOGRAPHY
 (I) trimethylenemethane	Triplet	 (V) 1,3-cyclobutanediyl	Triplet
 (II) 2-alkylidene-1,3-cyclopentadienyl	Triplet	 (VI) 1,3-cyclopentadienyl	Triplet
 (III) m-xylylene (m-phenylene)	Triplet	 (VII) 1,3-divinyl-1,3-cyclobutanediyl	Triplet
 (IV) 1,3-dimethylenecyclobutadiene (2,4-dimethylene-1,3-cyclobutanediyl, DMCBD)	Triplet		

4.3.2.1 π -Delocalized Biradical Systems (Alternant Hydrocarbons)

Alternant hydrocarbons (AH) are those whose active electrons are placed on the p_z -orbitals of neighbor C atoms and these p_z -orbitals are delocalized all over the π -system of the molecule.

In the π -delocalized biradicals, the **TS** interactions are expected to be very small compared to the **TB** ones. Consequently, the **TB** interactions are supposed to be the predominant contribution in the determination of the spin multiplicity of the ground state.

Both experimental and computational results^{3-5,62-65,67-70} show that the ground state spin multiplicity for I-IV biradicals in Table 4.2a is the triplet. The calculated energy gap between the singlet and triplet optimized states [calculations performed with MMVB and CAS(n,n)/6-31g(d)] are in accordance with the experimental values (Table 4.3).

Table 4.3 Energy gap between the singlet and triplet states for the systems I, II, III y IV calculated with MMVB and CAS/6-31g(d) compared to the reported values in bibliography^{3-5,38,39,62-66}

SYSTEMS	ΔE^{S-T} MMVB (kcal/mol)	ΔE^{S-T} CAS/6-31g(d) (kcal/mol)	ΔE^{S-T} bibliography (kcal/mol)
I	26.9	25.4	≈ 15 - 20
II	26.1	24.4	≈ 10 - 15
III	22.5	15.9	≈ 9 - 10
IV	24.4	23.5	≈ 10 - 20

Considering that the active space of these molecules is constituted by the p_z -orbitals of the carbon atom, the overlap between two neighbor ij orbitals is not null, and, the parameters J_{ij} are negative (< 0). Accordingly, the state lower in energy will have all the $P_{ij} > 0$ (spins antiparallel, AFM coupling) between all pairs of neighboring ij orbitals [equation (4.2)]. As mentioned, the multiplicity of the state can be estimated by the equation (4.5)⁷⁴, and it depends on the topological arrangement of the active centers (similar to what was postulated by Ovchinnikov for this type of systems).

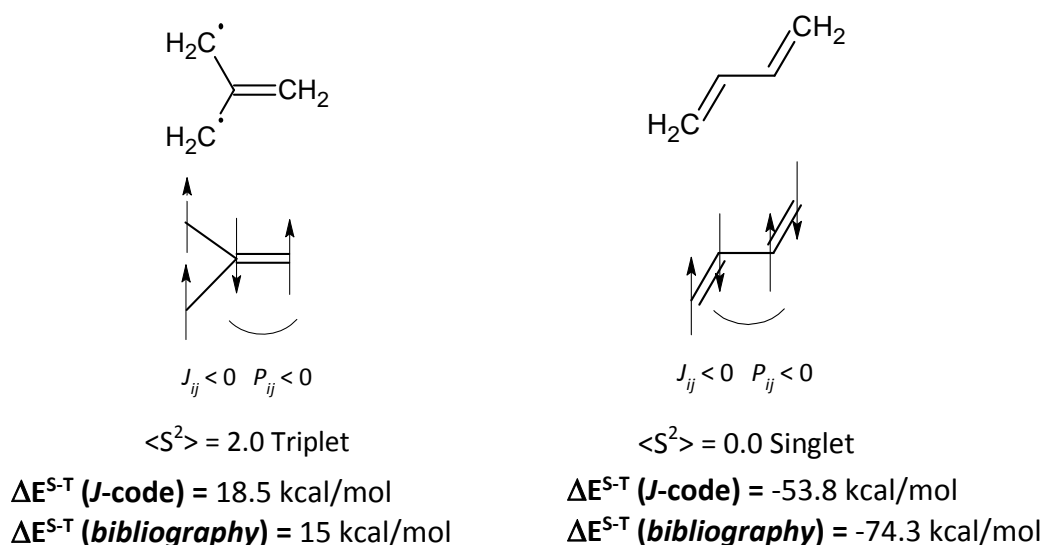


Figure 4.9 Spin distribution of the π electrons on the ground state, ground state multiplicity and energy gap between singlet and triplet states for the systems (a) TMM and (b) 1,3-butadiene.

Trimethylenemethane (TMM) is a simple AH biradical with a triplet as ground state that has been widely studied⁶²⁻⁶⁵ (Figure 4.9a). In order to get a deeper understanding of the TMM, we will compare it with 1,3-butadiene (Figure 4.9b) since it has the same number of atoms and electrons within the π -framework than TMM, but with different connectivity. It is observed that the spin multiplicity of the ground state is completely different, being a singlet for 1,3-butadiene. According to the Ovchinnikov theory, this is due exclusively to the different system topology. By applying Ovchinnikov's rules for alternant hydrocarbons and

the equation (4.6), the multiplicity of the ground states is correctly predicted for both the TMM (triplet) and 1,3-butadiene (singlet).

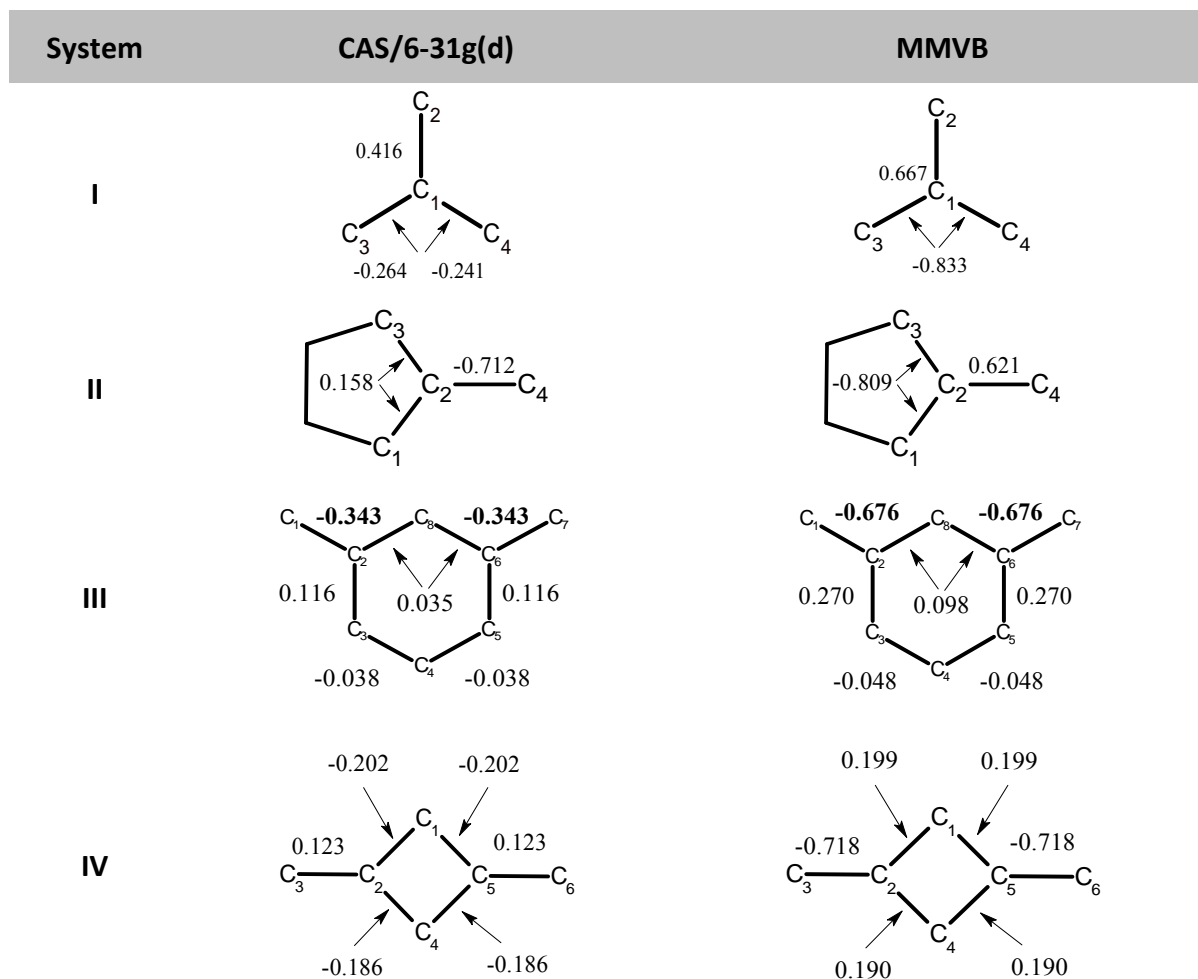


Figure 4.10 Systems I, II, III and IV. ΔP_{ij}^{S-T} values between the active sites according to CAS/6-31g(d) and MMVB calculations.

Considering the active space constituted by the four π -electrons of the molecule, all the J_{ij} parameters between two atomic orbitals ij , both in the singlet and in the triplet states, are negative and equivalent in magnitude. As it has been mentioned before, under these conditions, the state that is stabilized is the one that has all P_{ij} values positive. In TMM, it is noted that two negative P_{ij} contributions in the singlet destabilize the low-spin state. Considering that J_{ij} parameters are negative, negative ΔP_{ij}^{S-T} contributions in Figure 4.10 (**System I**) indicate the destabilization of the singlet.

The observation that the spin distribution framework influences on the spin multiplicity preference is supported by the results obtained when we apply the in-house J -code. This simple methodology, based on the active space topology, estimates correctly the distribution of states, with a value of energy gap $[\Delta E^{S-T}(J\text{-code}) = 18.4 \text{ kcal/mol}]$ in line with those obtained with the CASSCF(4,4)/4-31g $[\Delta E^{S-T}(\text{CAS}) = 20.6 \text{ kcal/mol}]$ and MMVB $[\Delta E^{S-T}(\text{MMVB}) = 26.9 \text{ kcal/mol}]$ calculations.

As for TMM (system **I**), negative ΔP_{ij}^{S-T} values in systems **II**, **III** and **IV** (Figure 4.10) indicate the stabilization of the triplet vs the singlet. In all these cases, the high-spin state has all the P_{ij}^T values positive, being the energy of this state lower than the singlet.

In system **III**, the most significant ΔP_{ij} values are the $\Delta P_{12} = \Delta P_{67}$, which are both negative (Figure 4.10). The 1-2 and 6-7 interactions represent the connection between the methyl radicals and the benzene ring and determine the stability of the high-spin state.

As TMM and 1,3-butadiene, *m*-xylylene (**III**) and *p*-xylylene have the same number of atoms and electrons within the π -framework, but with different connectivity. Likewise, it is observed that, *m*-xylylene and *p*-xylylene have different ground state multiplicity by structural isomerism ($\Delta E^{S-T} = 29.3$ kcal/mol and $\Delta E^{S-T} = -29.7$ kcal/mol for *m*-xylylene and *p*-xylylene respectively, with $J_{ij} = -0.065$ u.a.).

For systems **II** and **IV**, CAS and MMVB ΔP_{ij}^{S-T} values seem to differ (Figure 4.10). For system **II**, the interaction between C₂-C₄ has ΔP_{ij}^{S-T} negative at CAS level ($\Delta P_{2,4}^{S-T} = -0.7$), while at MMVB level ΔP_{ij}^{S-T} are negative inside the ring ($\Delta P_{1,3}^{S-T} = \Delta P_{2,3}^{S-T} = -0.8$). For system **IV**, the central ring shows ΔP_{ij}^{S-T} negative at CAS level ($\Delta P_{1,2}^{S-T}$, $\Delta P_{2,4}^{S-T}$, $\Delta P_{4,5}^{S-T}$, $\Delta P_{1,5}^{S-T}$), while at MMVB level the negative ΔP_{ij}^{S-T} contributions are $\Delta P_{2,3}^{S-T}$ and $\Delta P_{5,6}^{S-T}$. These differences are due to the VB configuration considered for the singlet state description in each calculation and its corresponding spin distribution. However, the final result is calculated correctly at both CASVB and MMVB levels.

4.3.2.2 π -Localized Biradical Systems

The so-called π -localized systems are hydrocarbons whose ground state multiplicity is determined by the interaction between two i,j electrons located in two non-alternant π -orbitals. Some examples are shown in Table 4.2b. Since there is no overlap between the two π -orbitals where the two i,j electrons are located, the J_{ij} values for this i,j pair is expected to be positive. MMVB methodology is not designed to evaluate electronic pairs i,j with $J_{ij} > 0$ values, consequently MMVB calculations have not been carried out on systems **V** and **VI**, that have π -localized electrons. The values for the energy gap between the different spin states for these systems have been calculated with CAS(n,n)/6-31g(d) [Table 4.4].

Biradical systems **V** and **VI** (Table 4.2b) have only two electrons in the active orbital space defined by the π framework of the molecule. Considering similar geometries for the triplet and the singlet states of each molecule, the J_{12} will be equivalent for both states and the energy gap between them can be estimated as:

$$\Delta E = \langle \hat{H}^S \rangle - \langle \hat{H}^T \rangle = 2J_{12}\Delta P_{12} \quad (4.10)$$

For system **V** and **VI**, the parameter J_{12} between the two active centers 1 and 2 has been calculated projecting the CI matrix on the corresponding Slater determinants and applying the effective Hamiltonian. The non-diagonal terms of the resulting matrix correspond directly to the values $J_{ij}^{9,12,13}$. The results obtained from a CAS(2,2) calculation using Slater determinants is $J_{1,2}(\mathbf{V}) = 0.4$ kcal/mol and $J_{1,2}(\mathbf{VI}) = 0.2$ kcal/mol for systems **V** and **VI**

respectively. The $J_{1,2}$ magnitude is slightly lower for system **VI** due to the longer distance between the two active centers. As a consequence, the energy gap between the singlet and the triplet ΔE^{S-T} is higher for system **V** than for system **VI** (1.5 kcal/mol and 0.9 kcal/mol, respectively; see Table 4.4).

Table 4.4 Energy gap between the singlet and the triplet states for systems **V**, **VI** y **VII** calculated at CAS/6-31g(d) level compared to the data reported in the bibliography^{3-5,38,39,62-66}.

SYSTEMS	ΔE^{S-T} CAS/6-31g(d) (kcal/mol)	ΔE^{S-T} BIBLIOGRAPHY (kcal/mol)
V	1.5	≈ 1.7
VI	0.9	≈ 1.2
VII	0.5	

For two interacting electrons (ie. system **V**), the P_{ij} values are $P_{1,2} = 1.0$ for the singlet and $P_{1,2} = -1.0$ for the triplet ($\Delta P_{1,2} \sim 2.0$). Based on the parameters $J_{1,2} = 0.4$ kcal/mol, $\Delta P_{1,2} = 2$ obtained in the calculations, and according to the equation (4.10) the value of the *gap* in energy between the singlet and the triplet is $\Delta E = 1.5$ kcal/mol. Notice that this magnitude is similar to the one obtained as result of CAS/6-31(g) calculations (Table 4.4). The value of $\Delta E > 0$ implies the stability of high-spin against the low-spin state. The positive value of the through-space exchange integral $J_{1,2}$ implies the parallel spin alignment of the two free electrons and, consequently, the stabilization of the triplet state, as has been observed in both experimental and computational simulations (Table 4.4).

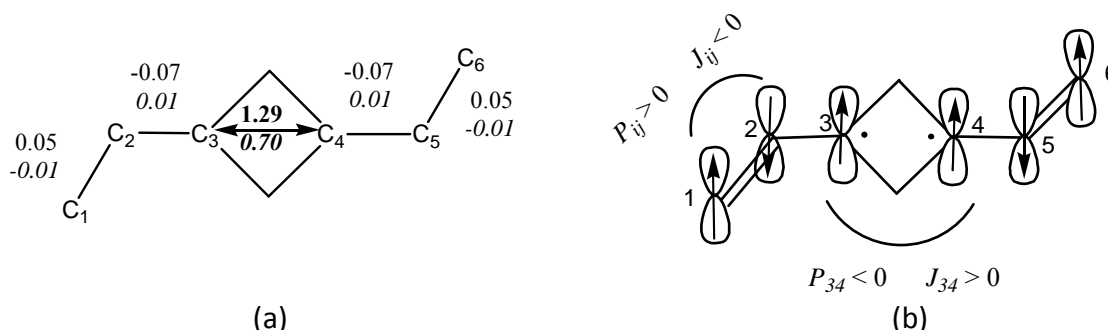


Figure 4.11 System **VI**. (a) ΔP_{ij}^{S-T} calculated with MMVB (above) and CAS (below and in cursive); (b) schematic spin distribution in the triplet state.

System **VII**'s active space is constituted by six electrons (Figure 4.11). The distances between the C atoms that contain the π -electrons reveal a certain delocalization of these electrons among the 1-2-3 and 4-5-6 bonds. The analysis of ΔP_{ij} (Figure 4.11a) shows that the main contribution to the difference between the triplet and the singlet corresponds to the carbons located in the ring C₃-C₄ ($\Delta P_{3,4}^{CAS} = 0.7$), being all the remaining ΔP_{ij} values close to zero. Considering a positive $J_{3,4}$ value ($J_{3,4}^{CAS} \approx 0.3$ kcal/mol, similar to system **V**), the global state of the high-spin triplet is stabilized.

The small ΔP_{ij} values obtained within the 1-2-3 and 4-5-6 fragments (Figure 4.11) imply that the spin distribution is conserved in these fragments for both the singlet and the triplet state. Consequently, the interaction through the ring C₃-C₄ that couples the two fragments is

the main contribution that stabilizes the triplet. The $J_{3,4}$ is lower in magnitude ($J_{3,4}^{CAS} \approx 0.3$ kcal/mol) than the other J_{ij} parameters ($J_{ij} = 40.8$ kcal/mol.).

According to the three π -localized systems analyzed, it has been confirmed that the preference for the high-spin state is due to the through-space (TS) interaction between the electrons within the ring. Since the through-space J_{ij} values are very small, the energy gap between the high and low-spin states for these systems is lower in magnitude than the ones observed in the previously studied AH (π -delocalized biradical) systems in section 4.3.2.1.

4.3.2.3 Biradicals with heteroatoms.

Ovchinnikov theory is only valid for AH, but could it be applied to systems with heteroatoms? In the literature there are several articles that raised this issue and postulated its validity^{7,75}. To evaluate this premise, we considered that the only difference when studying biradicals with heteroatoms lies in the magnitude of J_{ij} that connect the given heteroatom to any other within the biradical. To test this hypothesis we analyzed three systems similar to TMM and *m*-xylylene (see section 4.3.2.1), where the radical carbon atoms have been substituted by oxygen (O) atoms and nitroxide (NO) groups (Figure 4.12).

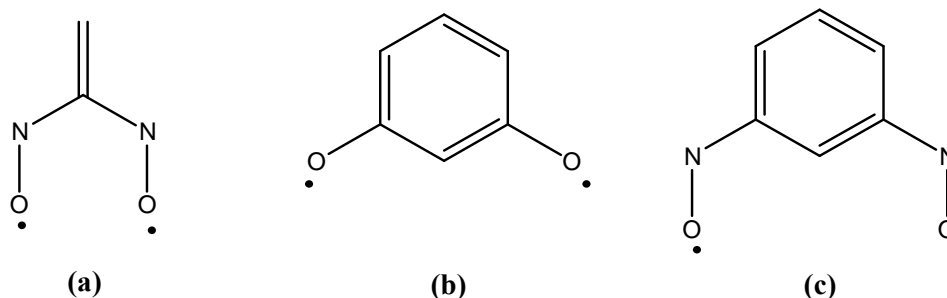


Figure 4.12 (a) DNE, (b) *m*-DOB and (c) *m*-DNB.

Let us mention that MMVB calculations are not possible for systems with heteroatoms. Therefore, only CASVB and *J*-code calculations were performed.

The J_{ij} values between the ij active orbitals in these molecules were calculated using the CASVB methodology (Figure 4.13). The resulting J_{ij} absolute value between a nitroxide group (NO) and a C atom is lower ($J_{NO-C} \sim -0.04$ a.u.) than the computed J_{ij} between two C atoms ($J_{CC} \sim -0.11$ a.u. and -0.09 a.u.) [Figure 4.13a and Figure 4.13c]. On the contrary, $J_{O-C} = -0.11$ a.u. absolute value is slightly higher than the one observed for the aromatic CC ($J_{CC} \sim -0.09$ a.u.) [Figure 4.13b].

Both CASVB and *J*-code calculations estimated the triplet as a ground state for the three molecules (Table 4.5), in agreement with the results found in the literature for *m*-DOB⁶⁶ and *m*-DNB^{75,76}. It is observed that the energy gap is much smaller for DNE (2.1 kcal/mol, Table 4.5) and *m*-DNE (7.2 kcal/mol, Table 4.5) than for TMM (25.4 kcal/mol, Table 4.3) and *m*-xylylene (15.9 kcal/mol, Table 4.3), respectively, as analyzed in the previous section. This can be explained by the smaller absolute value of the $J_{NO-C} = -0.04$ a.u. when compared to the $J_{CC} = -0.09$ a.u. in TMM and *m*-xylylene. This smaller J_{ij} value (in absolute value) implies a lower energetic barrier between the triplet and the singlet states.

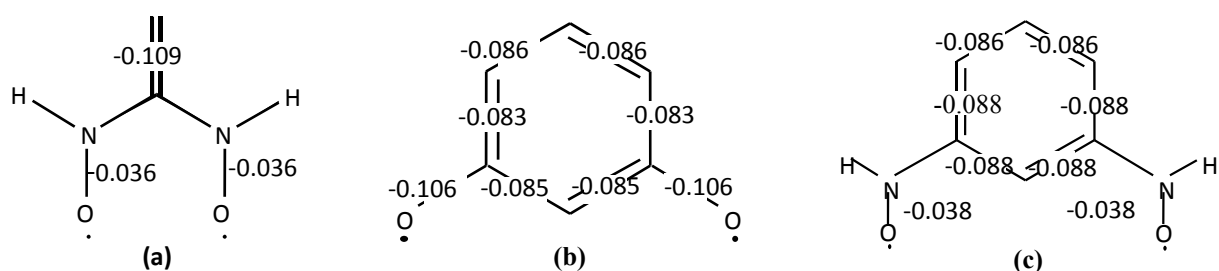


Figure 4.13 J_{ij} values in a.u. calculated for the triplet state with CAS(n,n) for the systems (a) DNE, (b) *m*-DOB and (c) *m*-DNB

Table 4.5 Energy gap in kcal/mol calculated with CAS(n,n)/4-31g and J -code for the systems DNE, *m*-DOB and *m*-DNB.

ΔE^{S-T} (kcal/mol)	DNE	<i>m</i> -DOB	<i>m</i> -DNB
CAS (n,n)/4-31g	2.1	18.2	7.2
J -code	6.3 ⁽¹⁾	45.4 ⁽²⁾	8.3 ⁽³⁾

⁽¹⁾ $J_{CC} = -0.109$ a.u., $J_{NO-C} = -0.036$ a.u.

⁽²⁾ $J_{CC} = -0.085$ a.u. (average value), $J_{O-C} = -0.106$ a.u.

⁽³⁾ $J_{CC} = -0.087$ a.u. (average value), $J_{NO-C} = -0.038$ a.u.

However, the energy gap ΔE^{S-T} between both spin states in *m*-DOB (18.2 kcal/mol, Table 4.5) is similar to that in *m*-xylylene (15.4 kcal/mol, Table 4.3), since the J_{ij} parameters are very similar ($J_{O-C} = -0.11$ and $J_{CC} = -0.09$). Comparing DNE and *m*-DNB to *m*-DOB, it is observed that the energy gap for the latter is higher than for the two former ones, fact that can be attributed to the difference in magnitude of the J_{ij} parameters.

As mentioned before, it is expected that the interactions that define the energy gap between the ground state and the first excited state are those with lower J_{ij} values. This observation is confirmed by analyzing the ΔP_{ij}^{S-T} contributions for the three systems: DNE, *m*-DOB and *m*-DNB (Figure 4.14). For the systems we are studying, negative ΔP_{ij}^{S-T} values contribute to the stabilization of the triplet.

For DNE and *m*-DNB systems, the higher negative ΔP_{ij}^{S-T} values are those that involve the NO groups (Figure 4.14a, and Figure 4.14c). In contrast, for the *m*-DOB system, the negative ΔP_{ij}^{S-T} contributions are found inside the benzene ring and ΔP_{ij}^{S-T} are positive for the interactions of the oxygens and the benzene (Figure 4.14b). It is noticeable that, although the energy gap of *m*-DOB and *m*-xylylene are similar, for *m*-xylylene the negative ΔP_{ij}^{S-T} contributions are between the methyl radicals and the ring (Figure 4.10 system III). This is because the lower J_{ij} contribution in *m*-DOB are for ij orbitals within the ring.

J_{ij} and P_{ij} parameters have proved to be a valuable tool when describing spin multiplicity in biradicals, both π -delocalized (AH) and π -localized, and in systems with heteroatoms. It has been observed that when the exchange integrals between ij active orbitals are negative, $J_{ij} < 0$, the spin state that is stabilized is the one that have all P_{ij} parameters positive. In the event that any J_{ij} contribution is positive, the preferred interaction for this pair ij will have a

negative P_{ij} value, $P_{ij} < 0$ (parallel spins). Additionally, it has been seen that the difference between the ground and the first excited spin states is determined by the interaction that has the lower J_{ij} value.

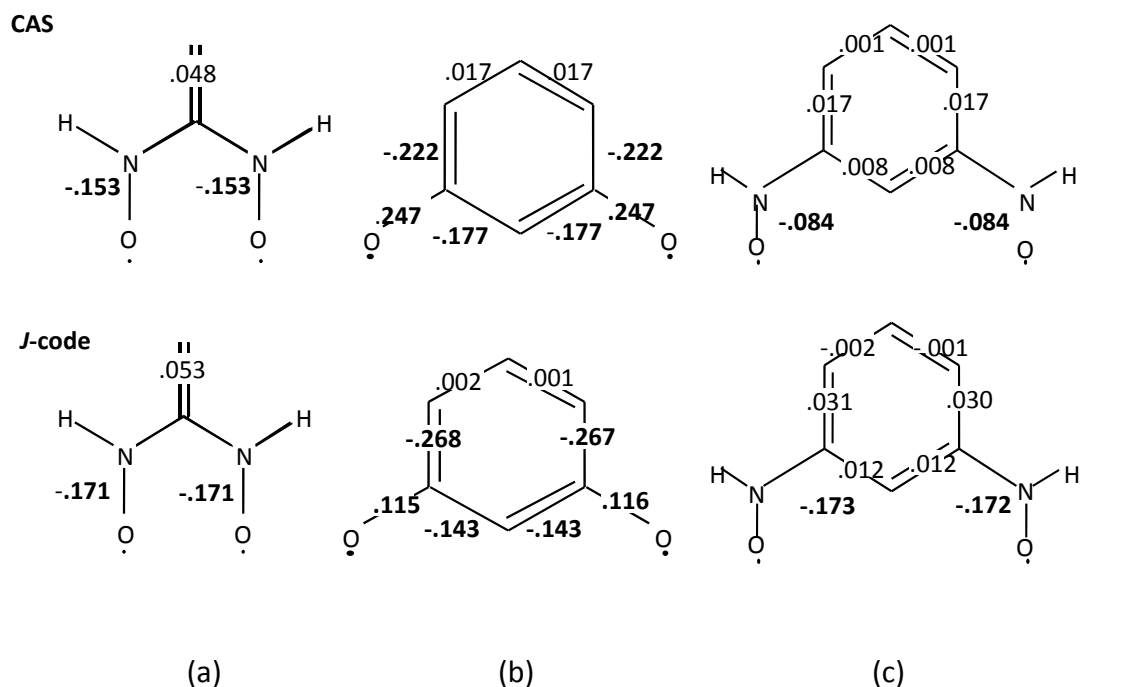


Figure 4.14 Values of ΔP_{ij}^{S-T} calculated with CAS(n,n) and the J-code for systems (a) DNE (b) *m*-DOB and (c) *m*-DNB

4.4 Polymerization of biradicals in one magnetic dimensionality (1D systems)

As mentioned before, the ferromagnetic coupling of high-spin molecules (*building blocks*) could produce high-spin macromolecules or polymers^{7,18,26–30,51,52}. To assess this hypothesis, we calculated the effect of the polymerization of high-spin molecules as the ones studied in section 4.3.2. In a first approach, we evaluated a possible expansion of the high-spin molecules in one dimension, 1-D, forming chains. This study could be extended to two dimensions, 2-D, in the plane or to three dimensions, 3-D, in all the space. A second method considered was the heterogeneous synthesis of high-spin molecules, following the SU-CU-SU scheme proposed by Dougherty^{26,26–30} among others (where SU = spin-containing unit and CU = coupling unit).

4.4.1 Polymers 1-D of high-spin molecules

One of the methodologies proposed for the design of magnetic materials is the polymerization of high-spin molecules. To evaluate this possible strategy, we studied conceivable polymeric macromolecules built from the high-spin molecules studied in the previous section: TMM^{18,33–36,51,52}, DNE, *m*-DOB and *m*-DNB^{75,77–79} (Figure 4.15). The study performed was a qualitative approach applying the J-code. A topological matrix was constructed for each system studied, using J_{ij} values similar to those obtained for the monomer units. With this method, we calculated the multiplicity of the ground and excited states and the qualitative values for the energy gap between both of them.

For the evaluation of the polymerization of these molecules, let us consider a scheme SU-CU-SU; that is, spin containing units (or atoms), SU, connected by coupling units, CU. In the analyzed systems, the SUs are the C atoms, O atoms and the NO groups and the CU units are either the ethane or the benzene ring.

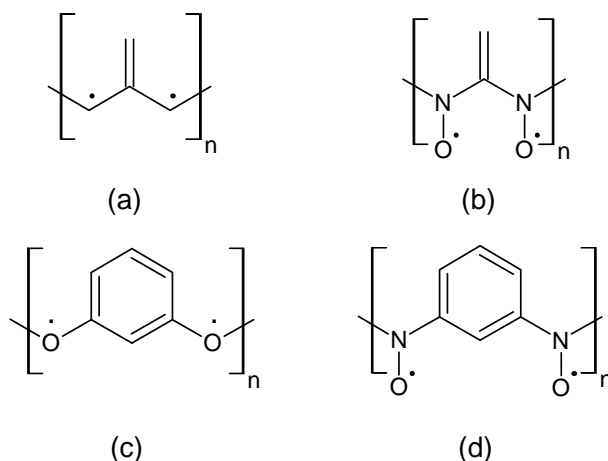


Figure 4.15 Polymer systems from monomers (a) TMM, (b) DNE, (c) *m*-DOB and (d) *m*-DNB.

In the J -code calculations, the J_{ij} parameters considered are divided in two blocks: (a) J_{ij}^{CU} , that are J_{ij} parameters for all the ij contained in the CU units, and (b) J_{ij}^{SU-CU} , that are the J_{ij} parameters for the ij interaction between the SU and the CU units. In the studied systems, the SU units only contain one unpaired electron and, therefore, there are not J_{ij} within the SU unit to be considered. The distance between the SU units is far enough to consider the SU-SU contribution negligible.

Considering the polymerization of the TMM molecule in one dimension, we evaluated macromolecules with two (2TMM), three (3TMM), five (5TMM), seven (7TMM) units (Figure 4.15a). For all these systems, CAS(n,n)/4-31g, MMVB and J -code calculations estimated the high-spin multiplicity state to be the lower in energy (Table 4.6). It was also observed, that the energy gap between the first and second states (first and second root) becomes smaller as the polymer size increases. A similar analysis could be made for DNE (Figure 4.15b). However, for DNE, it is observed that the energy gap between the first and second spin states is smaller (Table 4.7). This is due to the fact that the magnitude of the J_{ij} for DNE is smaller compared to TMM, as it has been seen in previous sections. In both TMM and DNE polymerizations, the energy gap between the two first spin states is negative (high-spin state more stable). This value can be partitioned into two contributions: (1) CU that is positive, and (2) SU-CU that is negative. The SU-CU contribution determines the sign of the energy gap in TMM and DNE polymers.

The ground states of the macromolecules constructed by polymerization of three *m*-DOB (Figure 4.15c) or three *m*-DNB (Figure 4.15d) molecules are quintets (Table 4.8). However, it is noticed that the contribution (CU or SU-CU) that determine the sign of the energy gap differ for both systems. For macromolecules resulting from *m*-DOB polymerization, the negative contributions are both the SU-CU and CU (Table 4.8). However, in the case of *m*-DNB, it is the SU-CU contributions that determine the sign of the energy gap (Table 4.8). This

is as a result of the different magnitude of J_{ij}^{CU} and J_{ij}^{SU-CU} parameters for both systems. It is noted that for the case of *m*-DOB $J_{ij}^{CU} < J_{ij}^{SU-CU}$ ($J_{ij}^{CU} = -0.08$, $J_{ij}^{SU-CU} = -0.12$) while for *m*-DNB the value of parameters $J_{ij}^{CU} > J_{ij}^{SU-CU}$ ($J_{ij}^{CU} = -0.09$, $J_{ij}^{SU-CU} = -0.04$).

In all the analyzed systems, the ground state has the higher spin multiplicity. However, the energy gap between the first and second states decreases with the number of molecules (*i.e.* with the increasing size of the macromolecule). This observation puts a question mark on the viability of constructing magnets based exclusively in the polymerization of high-spin molecules based on alternant hydrocarbons.

Table 4.6 Energy gap ΔE^{r1-r2} (kcal/mol) calculated with CAS(*n,n*)/4-31g, MMVB and *J*-code for the TMM polymers.

		TMM	2TMM	3TMM	5TMM	7TMM
Number of monomers	n	1	2	3	5	7
Number of spin centers	SU	2	3	4	6	8
Ground state (r1)	S(S+1)	2	3.75	6	12	20
First excited state (r2)	S(S+1)	0	0.75	2	6	12
CAS(<i>n,n</i>)/4-31(g) (kcal/mol)	ΔE^{r1-r2}	-20.6	-8.6	-4.9	-	-
	$\Sigma\Delta(J_{ij}P_{ij})^{CU}$	62.4	1.1	3.8	-	-
	$\Sigma\Delta(J_{ij}P_{ij})^{SU-CU}$	-84.9	-14.5	-11.5	-	-
MMVB (kcal/mol)	ΔE^{r1-r2}	-16.7	-	-5.8	-	-
	$\Sigma\Delta(J_{ij}P_{ij})^{CU}$	37.9	-	3.6	-	-
	$\Sigma\Delta(J_{ij}P_{ij})^{SU-CU}$	-59.8	-	-12.1	-	-
<i>J</i>-code⁽¹⁾ (kcal/mol)	ΔE^{r1-r2}	-18.4	-	-9.4	-4.3	-2.5
	$\Sigma J_{ij}\Delta P_{ij}^{CU}$	15.9	-	1.3	1.3	0.9
	$\Sigma J_{ij}\Delta P_{ij}^{SU-CU}$	-34.3	-	-10.5	-5.4	-3.3

(1) J_{ij} values used in the *J*-code were: $J_{ij}^{SU-CU} = -0.06$ and $J_{ij}^{CU} = -0.04$ a.u. for TMM; $J_{ij}^{SU-CU} = J_{ij}^{CU} = -0.07$ a.u. for 3TMM, 5TMM and 7TMM. Note that the J_{ij} values in the macromolecules (3TMM, 5TMM and 7TMM) are different from the monomer ones (TMM). This change was introduced following the observation in the CAS calculations that the delocalization of the electrons increased with the polymerization and the values of the J_{ij} parameters were more similar for all the *ij* pairs involved than the ones in the monomer.

Table 4.7 Energy gap ΔE^{r1-r2} (kcal/mol) calculated with CAS(*n,n*)/4-31g and *J*-code for the DNE polymers.

		DNE	3DNE	5DNE	7DNE
Number of monomers	n	1	3	5	7
Number of radical centers	SU	2	4	6	8
Ground state (r1)	S(S+1)	2	6	12	20
First excited state (r2)	S(S+1)	0	2	6	12
CAS/ 4-31(g) (kcal/mol)	ΔE^{r1-r2}	-2.2	-	-	-
	$\Sigma\Delta(J_{ij}P_{ij})^{CU}$	9.7	-	-	-
	$\Sigma\Delta(J_{ij}P_{ij})^{SU-CU}$	-11.8	-	-	-
<i>J</i>-code⁽¹⁾ (kcal/mol)	ΔE^{r1-r2}	-6.3	-1.8	-0.8	-0.5
	$\Sigma J_{ij}\Delta P_{ij}^{CU}$	6.7	1.6	0.8	0.0
	$\Sigma J_{ij}\Delta P_{ij}^{SU-CU}$	-12.9	-3.5	-1.6	-0.9

(1) *J_{ij}* values used in the *J*-code were: $J_{ij}^{CU} = -0.1$ a.u., $J_{ij}^{SU-CU} = -0.03$ a.u.

Table 4.8 Energy gap ΔE^{r1-r2} (kcal/mol) calculated with CAS(*n,n*)/4-31g and *J*-code for the *m*-DOB and *m*-DNB polymers

		DOB		DNB	
		<i>m</i> -DOB	3 <i>m</i> -DOB	<i>m</i> -DNB	3 <i>m</i> -DNB
Number of monomers	n	1	3	1	3
Number of radical centers	SU	2	4	2	4
Ground state (r1)	S(S+1)	2	6	2	6
First excited state (r2)	S(S+1)	0	2	0	2
CAS(8,8) / 4-31g(d) (kcal/mol)	ΔE^{r1-r2}	-18.2		-7.2	-
	$\Sigma\Delta(J_{ij}P_{ij})^{CU}$	-80.3		5.7	
	$\Sigma\Delta(J_{ij}P_{ij})^{SU-CU}$	65.7		-8.1	
<i>J</i>-code⁽¹⁾ (kcal/mol)	ΔE^{r1-r2}	-45.4	-9.3	-8.3	-2.1
	$\Sigma\Delta(J_{ij}P_{ij})^{CU}$	-81.1	-4.0	4.1	1.7
	$\Sigma\Delta(J_{ij}P_{ij})^{SU-CU}$	35.7	-5.6	-17.3	-4.0

(1) *J_{ij}* values used in the *J*-code were: $J_{ij}^{CU} = -0.08$, $J_{ij}^{SU-CU} = -0.12$ for *m*-DOB and 3*m*-DOB.
 $J_{ij}^{CU} = -0.09$, $J_{ij}^{SU-CU} = -0.04$ for *m*-DNB and 3*m*-DNB.

4.4.2 SU-CU-SU systems

Another design strategy to obtain high-spin systems consists in the combination of different high-spin molecules. In this heterogeneous synthesis, the spin containing units (SU) are ferromagnetically connected through a coupling unit (CU), being SU and CU different molecules. The simplest example of such model would be the scheme SU-CU-SU proposed by Dougherty^{3-5,26-30} based on Itoh pioneering work⁶⁰ (Figure 4.16).

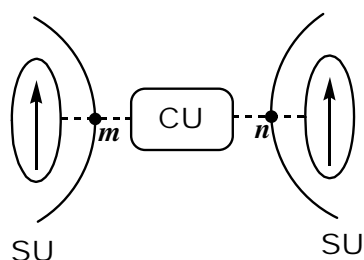


Figure 4.16 SU-CU-SU scheme

Dougherty³⁻⁵ worked on the synthesis of high-spin systems constructed from SU and CU units, being these units biradicals with triplet ground states. To describe the interaction between the two SU units, Dougherty proposed the phenomenological Hamiltonian in equation (4.11):

$$\hat{H} = -2J'_{eff} \hat{S}_1 \cdot \hat{S}_2 \quad (4.11)$$

where \hat{S}_1 and \hat{S}_2 represent the spin operators for each SU unit and J'_{eff} the coupling parameter (or effective exchange integral) that contains the effect of the coupling unit CU.

The energy gap between the low-spin (LS) and high-spin (HS) states is then described in equation (4.12):

$$\Delta E^{LS-HS} = -2J'_{eff} \left(\langle \hat{S}_1 \cdot \hat{S}_2 \rangle^{LS} - \langle \hat{S}_1 \cdot \hat{S}_2 \rangle^{HS} \right) \quad (4.12)$$

being $\langle \hat{S}_1 \cdot \hat{S}_2 \rangle$ the expected value of the product of the total spin operators for each of the SU units, whose value is:

$$\langle \hat{S}_1 \cdot \hat{S}_2 \rangle = \frac{1}{2} [S_{12}(S_{12} + 1) - S_1(S_1 + 1) - S_2(S_2 + 1)] \quad (4.13)$$

where S_1 and S_2 are the spin expected values of the units SU₁ and SU₂ respectively and S_{12} is the expected value of the sum vector of S_1 and S_2 .

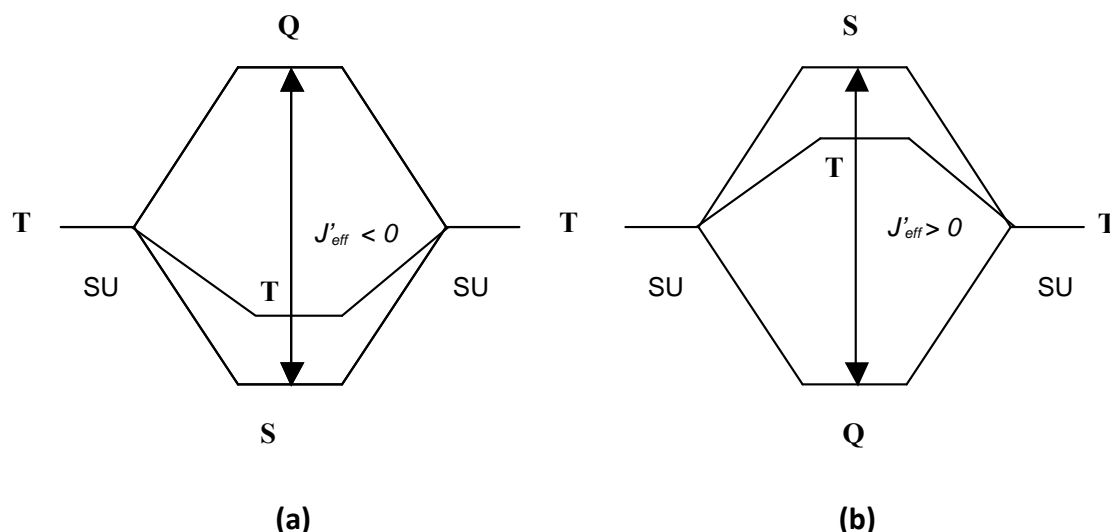


Figure 4.17 Energy diagram that represents the interaction between two SU units with triplet ground states: (a) AFM interaction, $J'_{eff} < 0$, that stabilizes the singlet state, S (b) FM interaction, $J'_{eff} > 0$, that stabilizes a quintet, Q, ground state.

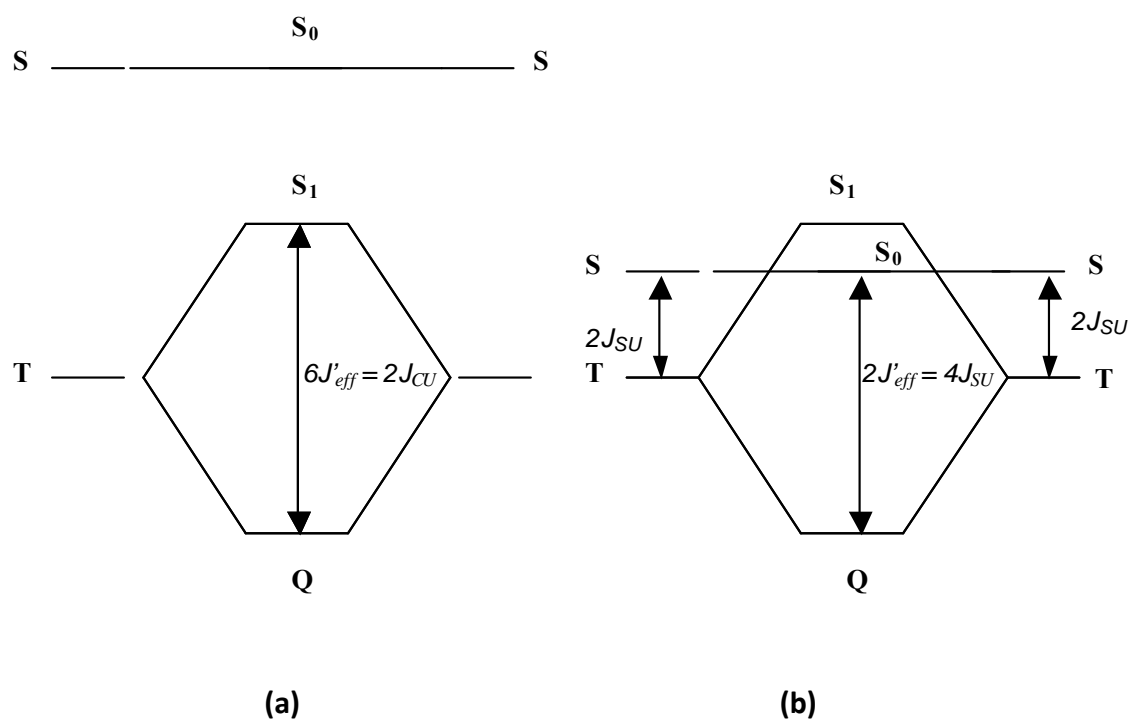


Figure 4.18 Energy diagrams that include the singlet state S_0 (resulting from the interaction of the singlet state of the two SU units) and the singlet state S_1 (resulting from the AFM interaction of the triplet states of the SU units). (a) The state S_1 is lower in energy than S_0 . The energy gap between the quintet ground state, Q, and the first excited singlet state, S_1 , is $\Delta E(S_1-Q) = 6J'_{eff} = 2J_{CU}$. (b) The energy of the singlet state S_0 is lower than the singlet state S_1 , in which case, the energy gap between the quintet ground state and the first excited singlet state is equal to $\Delta E(S_0-Q) = 2J'_{eff} = 4J_{SU}$, (if $4J_{su} < 2J_{CU}$ in absolute value)

In the interaction of two SU triplets, the singlet state is stabilized when the interaction is antiferromagnetic (AFM), defined by a negative effective exchange integral, $J'_{eff} < 0$ (Figure

4.17a). On the other hand, the stabilization of the high-spin state quintet is favored when the exchange parameter is positive, $J'_{eff} > 0$, representing the ferromagnetic (FM) interaction of the two SU units (Figure 4.17b)²⁶⁻³⁰.

This approach assumes that: (1) the two SU units maintain their spin identity when they are part of the SU-CU-SU system, hypothesis that should be tested; and (2) the singlet state is defined by the AFM interaction of two triplet SU units (Figure 4.18a). However, this is not always the case; it could be that the first singlet excited state is the result of the interaction of two singlet SU units (Figure 4.18b). This situation is observed when the gap of energy between the high and low-spin states for the SUs is lower in energy than for the CU.

In the case $E(S_0) < E(S_1)$ as shown in Figure 4.18b, Dougherty²⁶⁻³⁰ proposes the effective Hamiltonian in equation (4.14):

$$\hat{H} = -2J_A \hat{S}_2 \cdot \hat{S}_3 - J_B [(\hat{S}_2 + \hat{S}_3) \cdot (\hat{S}_1 + \hat{S}_4)] \quad (4.14)$$

where J_A represents the mechanism of spin polarization, which was taken into account by the coupling unit J_{CU} , and J_B characterizes the mechanism of superexchange, that is associated with J_{SU-SU} . Numbers 1-4 refer to the molecule radical centers. Dougherty postulated that both J_A and J_B should be positive for the ground state to have high-spin multiplicity (quintet), assuming that they are characteristic parameters of the isolated CU and SU units.

Back to the SU-CU-SU scheme in Figure 4.16, we must point out that m, n carbon atoms in the figure represent the active centers of the connection between the units SU and CU. These atoms are frontier atoms that belong to both the SU and CU units ($m \in SU_1$ and CU; $n \in SU_2$ and CU).

The energy gap between low (LS) and high (HS) spin states in the SU-CU-SU systems [equation (4.15)] can be partitioned into the different contribution SU, CU, SU-CU and SU-SU [equation (4.16)]. In equations (4.16) frontier atoms m, n are included within the terms ΔE^{SU_1} , ΔE^{SU_2} , ΔE^{CU} , and, consequently, they are deleted from the interaction terms ΔE^{SU_1-CU} , ΔE^{SU_2-CU} and $\Delta E^{SU_1-SU_2}$. The remaining interactions evaluated within the ΔE^{SU_1-CU} , ΔE^{SU_2-CU} terms are between $i \in SU$ and $j \in CU$ that are far in space and, consequently, these two contributions have been considered negligible when compared to the other terms of the equation (4.15). Additionally, for the systems studied, the contributions $\Delta E^{SU_1-SU_2}$ have been estimated to be minimal. Parameters J_{ij} are strongly dependent on the distance, and since units SU_1 and SU_2 are far in space, the $\Delta E^{SU_1-SU_2}$ value virtually do not contribute to the total result of ΔE^{LS-HS} . Therefore, the total energy gap ΔE^{LS-HS} for the systems to study can be expressed as $\Delta E^{LS-HS} = \Delta E^{SU_1} + \Delta E^{CU} + \Delta E^{SU_2}$.

$$\Delta E^{LS-HS} = \sum_{ij} J_{ij} \Delta P_{ij} = \Delta E^{SU_1} + \Delta E^{SU_2} + \Delta E^{CU} + \Delta E^{SU_1-SU_2} + \Delta E^{SU_1-CU} + \Delta E^{SU_2-CU} \quad (4.15)$$

$$\begin{aligned}
\Delta E^{SU_1} &= \sum_{i,j \in SU_1}^{SU_1} J_{ij} \Delta P_{ij} \\
\Delta E^{SU_2} &= \sum_{i,j \in SU_2}^{SU_2} J_{ij} \Delta P_{ij} \\
\Delta E^{CU} &= \sum_{i,j \in CU}^{CU} J_{ij} \Delta P_{ij} \\
\Delta E^{SU_1-SU_2} &= \left(\sum_{\substack{i \in SU_1 \\ j \in SU_2}}^{SU_1+SU_2} J_{ij} \Delta P_{ij} - J_{mn} \Delta P_{mn} \right) \\
\Delta E^{SU_1-CU} &= \sum_{\substack{i \in SU_1, i \neq m \\ j \in CU, j \neq m, n}}^{SU_1+CU} J_{ij} \Delta P_{ij} \\
\Delta E^{SU_2-CU} &= \sum_{\substack{i \in SU_2, i \neq n \\ j \in CU, j \neq m, n}}^{SU_2+CU} J_{ij} \Delta P_{ij}
\end{aligned} \tag{4.16}$$

In the case of a singlet state S_1 , that results from the AFM interaction of two triplet units (Figure 4.18a), the two SU units do not change their spin distribution and only the CU changes its multiplicity from triplet (FM coupling) to singlet (AFM coupling) in the quintet and singlet states of the macromolecule respectively. Under this assumption, the two SU units will not change their multiplicity between the high and low spin states of the macromolecule and $\Delta E^{SU_1} = \Delta E^{SU_2} = 0$. The change in multiplicity of the CU molecule between the triplet to singlet is quantified as $\Delta E^{CU} = 2J_{CU}$. As a consequence, the energy difference between the singlet state S_1 and the quintet Q is expressed as $\Delta E^{S_1-Q} = 6J'_{eff} = 2J_{CU}$ [equation (4.17)].

$$\begin{aligned}
\Delta E^{S_1-Q} &= 6J'_{eff} = \sum_{i,j \in SU_1}^{SU_1} J_{ij}^{SU_1} \Delta P_{ij}^{S_1-Q} + \sum_{i,j \in CU}^{CU} J_{ij}^{CU} \Delta P_{ij}^{S_1-Q} + \sum_{i,j \in SU_2}^{SU_2} J_{ij}^{SU_2} \Delta P_{ij}^{S_1-Q} = 2J_{CU} \\
\sum_{i,j \in SU_1}^{SU_1} J_{ij}^{SU_1} \Delta P_{ij}^{S_1-Q} &= \sum_{i,j \in SU_2}^{SU_2} J_{ij}^{SU_2} \Delta P_{ij}^{S_1-Q} = 0 \\
\sum_{i,j \in CU}^{CU} J_{ij}^{CU} \Delta P_{ij}^{S_1-Q} &= \Delta E^{CU} = 2J_{CU}
\end{aligned} \tag{4.17}$$

For the singlet state S_0 , that results from the interaction of two singlet units, as represented in Figure 4.18b, the stabilization of the singlet state S_0 occurs via the SU units. In that case, the difference between the triplet and singlet states for the SU units ($\Delta E^{SU_1} = \Delta E^{SU_2} = 2J_{SU}$) drives the stabilization of the S_0 state and the contribution of the CU unit is negligible [equation (4.18)]:

$$\Delta E^{S_0-Q} = 2J'_{eff} = \sum_{i,j \in SU_1}^{SU_1} J_{ij}^{SU_1} \Delta P_{ij}^{S_0-Q} + \sum_{i,j \in CU}^{CU} J_{ij}^{CU} \Delta P_{ij}^{S_0-Q} + \sum_{i,j \in SU_2}^{SU_2} J_{ij}^{SU_2} \Delta P_{ij}^{S_0-Q} = 4J_{SU} \tag{4.18}$$

$$\sum_{i,j \in CU} J_{ij}^{CU} \Delta P_{ij}^{S_0-Q} = 0$$

$$\sum_{i,j \in SU_1} J_{ij}^{SU_1} \Delta P_{ij}^{S_0-Q} = \sum_{i,j \in SU_2} J_{ij}^{SU_2} \Delta P_{ij}^{S_0-Q} = \Delta E_{SU}^{S-T} = 2J_{SU}$$

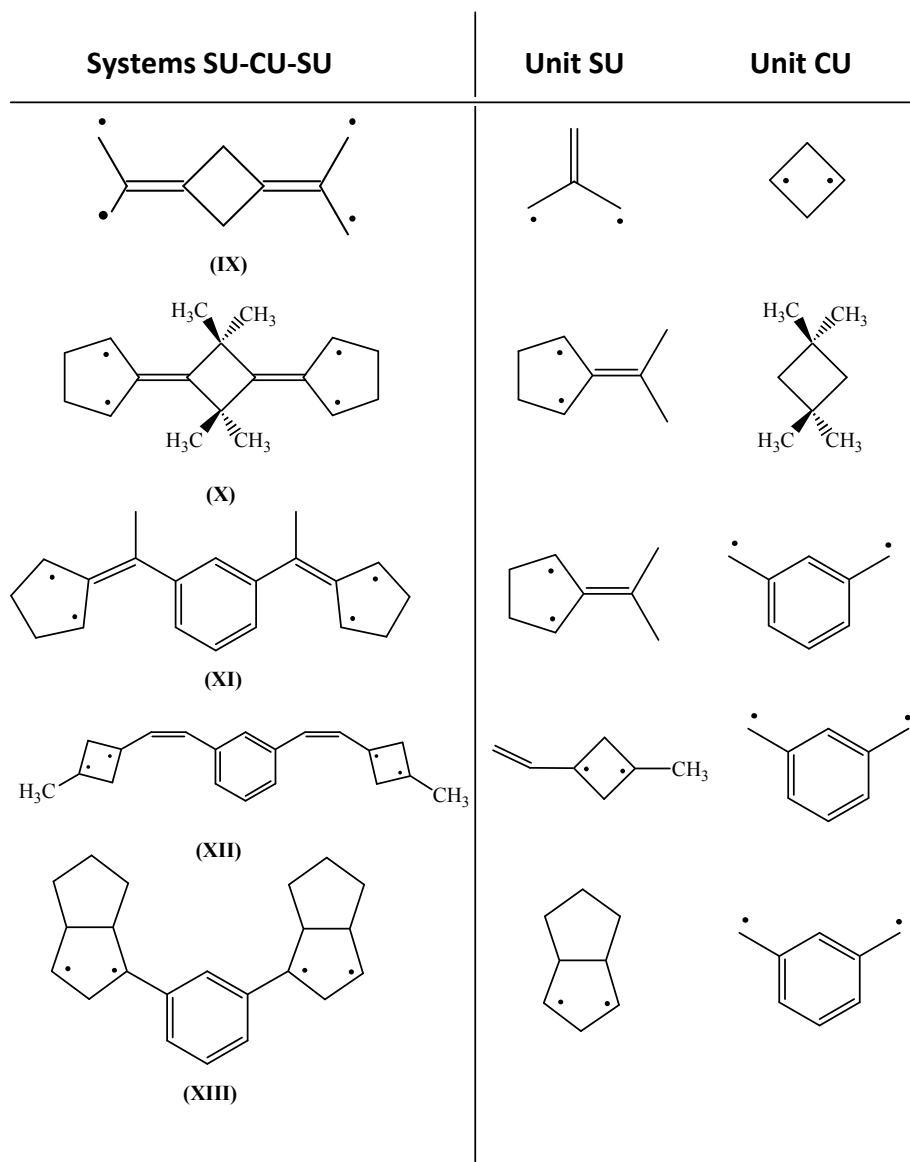


Figure 4.19 Systems SU-CU-SU and their respective constitutive units SU and CU.

In the study of SU-CU-SU materials we analyzed the spin multiplicity of each SU and CU units within the SU-CU-SU system to verify which unit maintain or change its multiplicity and which contributions determine the energy gap between the two spin states. If the energy gap between the low-spin (LS) and high-spin (HS) states for the CU unit is lower than for the SUs, it is expected that the LS, singlet S_1 , corresponds to the AFM interaction of the two SUs triplets, and both HS and LS will differ on the multiplicity of the CU (Figure 4.17a). Otherwise, if the difference of energy between the triplet and the singlet within the SUs is lower than the CUs, the singlet excited state S_0 would be determined by two interacting singlet SUs units and the HS and LS states will differ on the multiplicity of the SUs (Figure

4.17b). In both cases the HS state, quintet Q, will be defined by the FM interaction of two triplets.

We studied high-spin molecules synthesized following the methodology SU-CU-SU proposed by Dougherty^{3-5,26-30} (Figure 4.19 systems **X** and **XI**³⁻⁵ and system **XII**²⁶⁻³⁰) and Adam⁸⁰ (Figure 4.19 system **XIII**), where both SU and CU units are biradical molecules whose ground state spin multiplicity is a triplet. All the geometries of the systems analyzed have been optimized with the MMVB method.

The systems studied present two types of spin transmission mechanisms between the radical centers: the so-called spin polarization **A** and super-exchange **B**. From this distinction, it is postulated that the first two systems (**IX**, **X**) have an **ABA** structure, system **XI** have an **AAA** structure and systems **XII** and **XIII** show a **BAB** scheme.

As seen in the previous section, $\Delta E_{CU}^{S-T} < \Delta E_{SU}^{S-T}$ for systems **IX**, **X** and **XI**. Consequently, it is expected that for these systems, the first singlet excited state S_1 is the result of the AFM interaction of two triplets. Contrarily, for systems **XII** and **XIII**, it has been calculated that $\Delta E_{CU}^{S-T} > \Delta E_{SU}^{S-T}$. As a result, the SU units are expected to change multiplicity in the singlet state compared to the quintet state. Besides, in these cases, the first excited state corresponds to S_0 .

The multiplicity values of each one of the SU and CU units that compose each system can be calculated from the equations (4.19) and (4.20) respectively:

$$[S(S+1)]^{SU} = -\frac{n^{SU}(n^{SU}-4)}{4} - P^{SU} \quad (4.19)$$

$$[S(S+1)]^{CU} = -\frac{n^{CU}(n^{CU}-4)}{4} - P^{CU} \quad (4.20)$$

where n^{SU} and n^{CU} are the number of active electrons within the SU and CU units and P^{SU} and P^{CU} are the sum of the P_{ij} values within each SU [equation (4.21)] and CU [equation (4.22)] units.

$$P^{SU} = \sum_{i,j \in SU}^{SU} P_{ij} \quad (4.21)$$

$$P^{CU} = \sum_{i,j \in CU}^{CU} P_{ij} \quad (4.22)$$

Calculations performed on systems **IX-XIII** for the quintet and the singlet states using equations (4.19) and (4.20) show that the spin multiplicities $(2S+1)$ are preserved within the SU and CU units when forming the SU-CU-SU systems (Table 4.9). According to these results,

for systems **IX**, **X** and **XI**, the CU unit changes multiplicity between the quintet ground state and the first excited singlet state S_1 . Therefore, the energy diagram of these systems would be represented by Figure 4.18a. For systems **XII** and **XIII**, the SU units vary multiplicity in the singlet state, S_0 . This situation is described by the energy diagram of the Figure 4.18b.

Table 4.9 Spin multiplicity ($2S+1$) for SU and CU units within system IX-XIII, for the quintet (HS) and singlet (LS) states.

Systems	Unit SU		Unit CU	
	QUINTET	SINGLET	QUINTET	SINGLET
IX	3	3	3	2
X	3	3	3	2
XI	3	3	3	2
XII	3	2	3	2
XIII	3	2	3	3

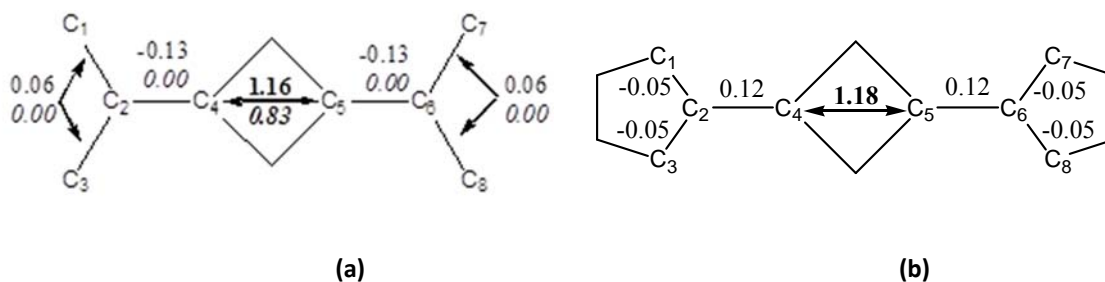


Figure 4.20 ΔP_{ij}^{S-Q} values for the ij active centers according to MMVB (above) and CAS (below and in italics) for systems (a) **IX** and (b) **X**.

Systems **IX** and **X** have similar topology. Their SUs are units which are robust triplets. However, their CU (cyclobutane-1,3-diyl) is known to have a small energy gap between the triplet and the singlet, as discussed in section 4.3.2.2. As expected, CAS(8,8)/6-31g(d) and MMVB calculations showed that the main contribution to the energy gap between high and low-spin states is due to the interaction between active centers 4 and 5 belonging to the CU unit (see Figure 4.20 a and b, respectively). For these system, whose CU unit only contains two active sites, the contribution ΔE^{CU} and, therefore, $\Delta E^{S-Q} \sim 2J_{CU}$, can be approximated as:

$$\Delta E^{S-Q} = 2J_{12}^{CU} \Delta P_{12}^{S-Q} \quad (4.23)$$

Considering the value of $J_{ij} = 0.4$ kcal/mol (obtained by CASSCF calculations using an isolated CU unit) and the ΔP_{45} values [ΔP_{45}^{MMVB} (**IX**) = 1.16, ΔP_{45}^{CAS} (**IX**) = 0.83 (Figure 4.20a) and ΔP_{45}^{MMVB} (**X**) = 1.18 (Figure 4.20b)], the energy gap can be estimated as ΔE^{S-Q} (MMVB) = 0.9 kcal/mol and ΔE^{S-Q} (CAS) = 0.6 kcal/mol for system **IX**, and ΔE^{S-Q} (MMVB) = 0.9 kcal/mol for system **X**.

To sum up, the transition between quintet and singlet states involves the CU unit, which couples antiferromagnetically the two SU triplets (S_1 in Figure 4.18) instead of acting as a FM

coupler as it would do if being isolated. This is due to the fact that this mechanism implies the lowest energy cost.

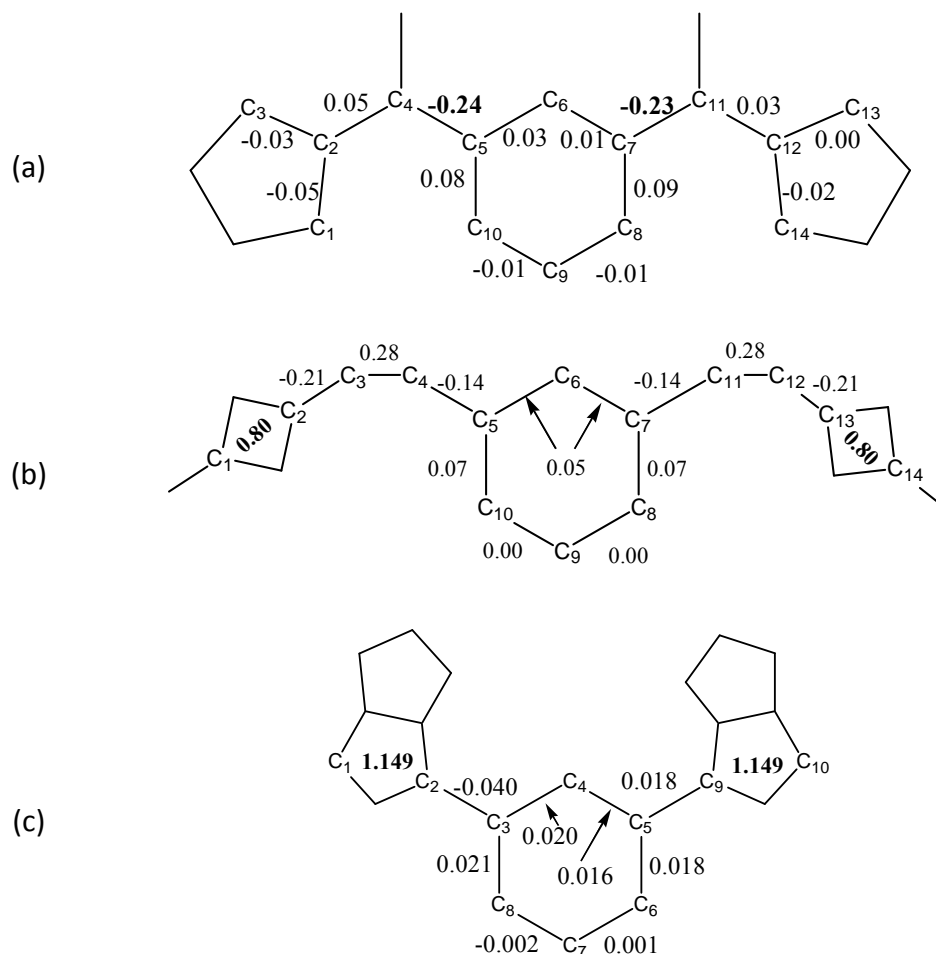


Figure 4.21 ΔP_{ij}^{S-Q} values for the ij active centers according to MMVB for systems (a) **XI** (b) **XII** and (c) **XIII**.

System **XI** is constituted by SU and CU units that are both robust triplets. In this system, all J_{ij}^{MMVB} parameters between neighboring active centers have similar values ($-0.058 \text{ a.u.} \leq J_{ij} \leq -0.070 \text{ a.u.}$). Practically all ΔP_{ij}^{S-Q} values between the singlet and quintet states using the ground state optimized geometry are zero, except $\Delta P_{4,5} = -0.24$ and $\Delta P_{7,11} = -0.23$ (Figure 4.21a). Therefore, the main contribution to the energy gap between the quintet and singlet states is the SU-CU interaction, which is represented by the interaction between centers it is the SU-CU interaction, represented by the interaction between the centers 4-5 and 7-11. Since the implied active centers have been considered within the CU unit, the multiplicity of the CU unit will no longer agree with that of a robust triplet, as it would if being isolated (see Table 4.9). Note that $P_{4,11}^S / P_{4,11}^Q = -0.13 / -0.81$ values clearly indicate a variation in the interaction of these electrons. The P_{ij} value for the quintet state is close to 1 (-0.81), which is typical for two electrons arranged parallel, and to zero in the singlet state (-0.13).

In systems **XII** and **XIII**, the SUs are radicals that have smaller energy gap between the triplet and singlet states when compared to the CU. ΔP_{ij}^{S-Q} values for both systems calculated at

the ground state optimized geometry (Figure 4.21b and c) showed that the larger ΔP_{ij} contributions are within the SU units. Consequently, as expected, the first singlet state results from the FM coupling of the two singlet SU units (S_0 singlet state).

4.5 Conclusions

J_{ij} and P_{ij} parameters are important tools to estimate the energy gap between different spin states. Using these parameters we have been able to identify the main contributions to the energy gap and understand better the mechanisms that stabilize high-spin states. It has been observed that the energy difference between the first and second spin states of a molecule is driven by the contributions that have lower J_{ij} exchange coupling and, therefore, have lower energy barriers.

Several high-spin biradicals have been characterized at CASVB, MVVB and J -code levels. Our study shows that alternant hydrocarbons (π -delocalized radicals) are robust triplets (larger energy gap) compared to the π -localized biradicals. We have confirmed that we can apply a similar methodology to study hydrocarbons with heteroatoms like nitrogen and oxygen.

The analysis of the possible polymerization of alternant hydrocarbons, as a way to design high-spin macromolecules, has led to the observation that the energy gap between the first and second spin states decreases with the size of the macromolecule. Therefore, it does not appear to be good approach to design high-spin macromolecules. On the other hand, we have also examined macromolecules synthesized following the SU-CU-SU scheme: spin containing units (SU) ferromagnetically coupled through a coupling unit (CU). When designing systems like these, we need to consider that the energy difference between the first and second spin states is defined by the energy gap of the constitutive molecules. The building units with lower energy gap between spin states will define the spin energy ordering of the spin states of the macromolecule. Therefore, among all the possibilities we have studied, we conclude that the use of robust high spin radicals, such as alternant hydrocarbons, as SU and CU building blocks is a promising strategy to design new high-spin SU-CU-SU macromolecules.

Bibliography

- (1) Miller, J. S.; Epstein, A. J. *New Aspects of organic chemistry I: Proceedings of the Fourth International Kyoto Conference on New Aspects of Organic Chemistry*; Yoshida, Z. 'ichi, Shiba, T., Oshiro, Y., Eds.; VCH Publishers, New York, 1989.
- (2) Iwamura, Hiizu. *Advances in Physical Organic Chemistry*; Academic Press, 1991; Vol. 26.
- (3) Dougherty, D. A. *Acc. Chem. Res.* **1991**, 24 (3), 88–94.
- (4) Pranata, J.; Marudarajan, V. S.; Dougherty, D. A. *J. Am. Chem. Soc.* **1989**, 111 (6), 2026–2030.
- (5) Pranata, J.; Dougherty, D. A. *J. Am. Chem. Soc.* **1987**, 109 (6), 1621–1627.
- (6) Kahn, O. *Molecular Magnetism*, 1 edition.; Wiley-VCH: New York, 1993.
- (7) Rajca, A. *Chem. Rev.* **1994**, 94 (4), 871–893.
- (8) Rajca, A.; Rajca, S. J. *Am. Chem. Soc.* **1996**, 118 (34), 8121–8126.
- (9) Bearpark, M. J.; Robb, M. A.; Bernardi, F.; Olivucci, M. *Chem. Phys. Lett.* **1994**, 217 (5–6), 513–519.
- (10) Hall, K. F.; Tokmachev, A. M.; Bearpark, M. J.; Boggio-Pasqua, M.; Robb, M. A. *J. Chem. Phys.* **2007**, 127 (13), 134111.
- (11) Pulay, P.; Hamilton, T. P. *J. Chem. Phys.* **1988**, 88 (8), 4926–4933.
- (12) Bernardi, F.; Olivucci, M.; McDouall, J. J. W.; Robb, M. A. *J. Chem. Phys.* **1988**, 89 (10), 6365–6375.
- (13) Bernardi, F.; Olivucci, M.; Robb, M. A. *J. Am. Chem. Soc.* **1992**, 114 (5), 1606–1616.
- (14) McWeeny, R. *Spins in Chemistry*; Academic Press, 1970.
- (15) Ovchinnikov, A. A. *Theor. Chim. Acta* **1978**, 47 (4), 297–304.
- (16) Oguchi, T.; Nishimori, H.; Taguchi, Y. *J. Phys. Soc. Jpn.* **1986**, 55 (1), 323–330.
- (17) Taguchi, Y.; Nishimori, H. *Bussei Kenkyu* **1986**, No. 45, 299.
- (18) Teki, Y.; Takui, T.; Kinoshita, T.; Ichikawa, S.; Yagi, H.; Itoh, K. *Chem. Phys. Lett.* **1987**, 141 (3), 201–205.
- (19) Dannenberg, J. J.; Liotard, D.; Halvick, P.; Rayez, J. C. *J. Phys. Chem.* **1996**, 100 (23), 9631–9637.
- (20) Bernardi, F.; Olivucci, M.; Robb, M. A. In *New Theoretical Concepts for Understanding Organic Reactions*; Beltrán, J., Csizmadia, I. G., Eds.; NATO ASI Series; Springer Netherlands, 1989; pp 147–163.
- (21) Rajca, A. *J. Am. Chem. Soc.* **1990**, 112 (15), 5890–5892.
- (22) Rajca, A.; Utamapanya, S.; Xu, J. J. *Am. Chem. Soc.* **1991**, 113 (24), 9235–9241.
- (23) Rajca, A.; Utamapanya, S.; Thayumanavan, S. J. *Am. Chem. Soc.* **1992**, 114 (5), 1884–1885.
- (24) Rajca, A.; Utamapanya, S. J. *Am. Chem. Soc.* **1993**, 115 (23), 10688–10694.
- (25) Rajca, A.; Rajca, S.; Padmakumar, R. *Angew. Chem. Int. Ed. Engl.* **1994**, 33 (20), 2091–2093.
- (26) Jacobs, S. J.; Shultz, D. A.; Jain, R.; Novak, J.; Dougherty, D. A. *J. Am. Chem. Soc.* **1993**, 115 (5), 1744–1753.
- (27) Jacobs, S. J.; Dougherty, D. A. *Angew. Chem. Int. Ed. Engl.* **1994**, 33 (10), 1104–1106.
- (28) Silverman, S. K.; Dougherty, D. A. *J. Phys. Chem.* **1993**, 97 (50), 13273–13283.
- (29) Novak, J. A.; Jain, R.; Dougherty, D. A. *J. Am. Chem. Soc.* **1989**, 111 (19), 7618–7619.
- (30) Goldberg, A. H.; Dougherty, D. A. *J. Am. Chem. Soc.* **1983**, 105 (2), 284–290.
- (31) Longuet-Higgins, H. C. *J. Chem. Phys.* **1950**, 18 (3), 265–274.
- (32) Lieb, E.; Mattis, D. J. *Math. Phys.* **1962**, 3 (4), 749–751.

- (33) Klein, D. J.; Nelin, C. J.; Alexander, S.; Matsen, F. A. *J. Chem. Phys.* **1982**, 77 (6), 3101–3108.
- (34) Alexander, S. A.; Klein, D. J. *J. Am. Chem. Soc.* **1988**, 110 (11), 3401–3405.
- (35) Klein, D. J.; Alexander, S. A.; Randić, M. *Mol. Cryst. Liq. Cryst. Inc. Nonlinear Opt.* **1989**, 176 (1), 109–114.
- (36) Klein, D. J.; Alexander, S. A. *Mol. Cryst. Liq. Cryst. Sci. Technol. Sect. Mol. Cryst. Liq. Cryst.* **1993**, 232 (1), 219–232.
- (37) Pranata, J. *J. Am. Chem. Soc.* **1992**, 114 (26), 10537–10541.
- (38) Borden, W. T.; Davidson, E. R. *J. Am. Chem. Soc.* **1977**, 99 (14), 4587–4594.
- (39) Davidson, E. R.; Borden, W. T.; Smith, J. J. *J. Am. Chem. Soc.* **1978**, 100 (11), 3299–3302.
- (40) Salem, L. Benjamin N. Y. **1966**.
- (41) Hückel, E. Z. *Für Phys.* **1931**, 70 (3–4), 204–286.
- (42) Hückel, E. Z. *Für Phys.* **1931**, 72 (5–6), 310–337.
- (43) Hückel, E. Z. *Für Phys.* **1932**, 76 (9–10), 628–648.
- (44) Hückel, E. Z. *Für Phys.* **1933**, 83 (9–10), 632–668.
- (45) Hoffmann, R. *J. Chem. Phys.* **1963**, 39 (6), 1397–1412.
- (46) Pariser, R.; Parr, R. G. *J. Chem. Phys.* **1953**, 21 (3), 466–471.
- (47) Pariser, R.; Parr, R. G. *J. Chem. Phys.* **1953**, 21 (5), 767–776.
- (48) Pople, J. A. *Trans. Faraday Soc.* **1953**, 49 (0), 1375–1385.
- (49) Hubbard, J. *Proc. R. Soc. Lond. Math. Phys. Eng. Sci.* **1963**, 276 (1365), 238–257.
- (50) Doehnert, D.; Koutecky, J. *J. Am. Chem. Soc.* **1980**, 102 (6), 1789–1796.
- (51) Li, S.; Ma, J.; Jiang, Y. *J. Phys. Chem. A* **1997**, 101 (30), 5567–5573.
- (52) Teki, Y.; Takui, T.; Itoh, K.; Iwamura, H.; Kobayashi, K. *J. Am. Chem. Soc.* **1986**, 108 (9), 2147–2156.
- (53) Smith, M. B.; March, J. *March's advanced organic chemistry: reactions, mechanisms, and structure*; John Wiley & Sons, 2007.
- (54) Malrieu, J.-P.; Maynau, D. *J. Am. Chem. Soc.* **1982**, 104 (11), 3021–3029.
- (55) Maynau, D.; Malrieu, J. P. *J. Am. Chem. Soc.* **1982**, 104 (11), 3029–3034.
- (56) Maynau, D.; Said, M.; Malrieu, J. P. *J. Am. Chem. Soc.* **1983**, 105 (16), 5244–5252.
- (57) Said, M.; Maynau, D.; Malrieu, J. P.; Garcia-Bach, M. A. *J. Am. Chem. Soc.* **1984**, 106 (3), 571–579.
- (58) Said, M.; Maynau, D.; Malrieu, J. P. *J. Am. Chem. Soc.* **1984**, 106 (3), 580–587.
- (59) Ma, J.; Li, S.; Jiang, Y. *J. Phys. Chem.* **1996**, 100 (37), 15068–15072.
- (60) Itoh, K. *Pure Appl. Chem.* **1978**, 50 (11–12), 1251–1259.
- (61) Squires, R. R.; Cramer, C. J. *J. Phys. Chem. A* **1998**, 102 (45), 9072–9081.
- (62) Dowd, P. J. *J. Am. Chem. Soc.* **1966**, 88 (11), 2587–2589.
- (63) Baseman, R. J.; Pratt, D. W.; Chow, M.; Dowd, P. J. *J. Am. Chem. Soc.* **1976**, 98 (18), 5726–5727.
- (64) Geib, S. J.; Vicent, C.; Fan, E.; Hamilton, A. D. *Angew. Chem. Int. Ed. Engl.* **1993**, 32 (1), 119–121.
- (65) Dixon, D. A.; Dunning, T. H.; Eades, R. A.; Kleier, D. A. *J. Am. Chem. Soc.* **1981**, 103 (10), 2878–2880.
- (66) Fort, R. C.; Getty, S. J.; Hrovat, D. A.; Lahti, P. M.; Borden, W. T. *J. Am. Chem. Soc.* **1992**, 114 (19), 7549–7552.
- (67) Platz, M. S.; Berson, J. A. *J. Am. Chem. Soc.* **1977**, 99 (15), 5178–5180.
- (68) Berson, J. A. *Acc. Chem. Res.* **1978**, 11 (12), 446–453.
- (69) Goodman, J. L.; Berson, J. A. *J. Am. Chem. Soc.* **1985**, 107 (19), 5409–5424.
- (70) Wright, B. B.; Platz, M. S. *J. Am. Chem. Soc.* **1983**, 105 (3), 628–630.

-
- (71) Jain, R.; Snyder, G. J.; Dougherty, D. A. J. *Am. Chem. Soc.* **1984**, 106 (23), 7294–7295.
- (72) Buchwalter, S. L.; Closs, G. L. J. *Am. Chem. Soc.* **1979**, 101 (16), 4688–4694.
- (73) Buchwalter, S. L.; Closs, G. L. J. *Am. Chem. Soc.* **1975**, 97 (13), 3857–3858.
- (74) Pauncz, R. *Spin Eigenfunctions*; Springer US, 1979.
- (75) Ishida, T.; Iwamura, H. J. *Am. Chem. Soc.* **1991**, 113 (11), 4238–4241.
- (76) Calder, A.; Forrester, A. R.; James, P. G.; Luckhurst, G. R. J. *Am. Chem. Soc.* **1969**, 91 (14), 3724–3727.
- (77) Kanno, F.; Inoue, K.; Koga, N.; Iwamura, H. J. *Phys. Chem.* **1993**, 97 (50), 13267–13272.
- (78) Inoue, K.; Iwamura, H. J. *Am. Chem. Soc.* **1994**, 116 (7), 3173–3174.
- (79) Iwamura, H.; Inoue, K. *Adv. Mater.* **1996**, 8 (1), 73–76.
- (80) Adam, W.; van Barneveld, C.; Bottle, S. E.; Engert, H.; Hanson, G. R.; Harrer, H. M.; Heim, C.; Nau, W. M.; Wang, D. J. *Am. Chem. Soc.* **1996**, 118 (16), 3974–3975.

CHAPTER 5

CHARACTERIZATION OF THROUGH-SPACE INTERACTIONS IN BIMOLECULAR SYSTEMS

5 Characterization of through-space interactions in bimolecular systems

In Crystal Engineering, it is important to understand the characteristics of the interactions between the molecules that are the building blocks of the molecule-based magnet^{1,2}. In this chapter we are presenting several studies that we performed to characterize the interaction between two radical molecules at different spatial orientations. The objective was to establish which alignment favors the intermolecular ferromagnetic (FM) coupling with the purpose of using this knowledge when designing crystals with magnetic properties.

5.1 Characterization of the intermolecular interactions with *Atoms in Molecules* (AIM): hydrogen bond formation

In the formation of molecular crystals, an intermolecular interaction as weak as a hydrogen bond can be of great importance, since it may represent the force that stabilizes the global crystal structure³. Bader's Atoms-in-Molecules (AIM) analysis⁴ can be a useful tool to study the weak interactions between two molecules by characterizing the *Bond Critical Point* (BPC) that appears between them. However, we challenged whether the sole presence of a BCP is enough to determine the intermolecular bond formation.

All these methods have been carried out with the *Gaussian* software package⁵ at MP2⁶⁻¹⁰ level using a diffuse basis set with polarization 6-31+G(2d,2p). The electron density function and its Laplacian and Hessian have been used to describe the type of interaction that exists in the analyzed bimolecular systems.

5.1.1 Characterization of hydrogen bond formation between two molecules

To assess whether the AIM analysis is able to characterize weak intermolecular interactions, we studied the interaction between the oxygen atom of one water molecule (H₂O) and the hydrogen of different molecules (namely HF, CH₄ and CHF₃) (Figure 5.1).

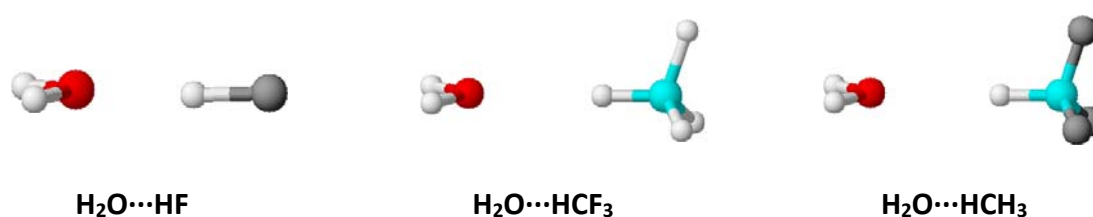


Figure 5.1 Systems H₂O...HF, H₂O...HCH₃, H₂O...HCF₃. Hydrogen atoms are in white, oxygen atoms are in red, carbon atoms are in blue and fluorine atoms are in grey.

The electronegativity of the oxygen atom favors the formation of a hydrogen bond with a neighbor molecule if the distance between them is short enough and the interaction angle is adequate. Since this is a very weak interaction, it is expected that it will depend strongly on the distance between both molecules. We have confirmed this assumption by performing an analysis of the variation of the properties of the electron density function at increasing distance (*r*) between the molecules in each of the studied systems.

Another important factor that characterizes the hydrogen bond formation is the electronegative character of the atom to which the hydrogen is bonded. The hydrogen-

donor molecules included in these analyses differ in the electronegative characteristics of the central atom. We have selected hydrogen fluoride HF, because this molecule is expected to facilitate the transfer of hydrogen and the formation of the hydrogen bond with the neighbor water molecule given the electronegative character of F and the F^- anion stability. In the trifluoromethane, HCF_3 , the presence of three atoms of F increases the ability of the molecule to stabilize a negative charge and, consequently, the donation of the hydrogen. Finally, the third selected molecule, methane CH_4 , is anticipated not to form strong hydrogen bonds.

According to Bader⁴, a weak interaction, such as a hydrogen bond, is characterized by several features. It is a closed shell interaction whose bond critical point shows (1) a small electron density, (2) a positive Laplacian and (3) an expansion ratio or ellipticity $|\lambda_1|/\lambda_3 < 1$. In the three systems studied, the intermolecular hydrogen bond, which is identified as BCPs (3, -1) with the above mentioned characteristics, appears localized between the two interacting molecules.

Bearing in mind that our objective is to investigate the formation of hydrogen bonds between H_2O and any of the three molecules listed above (namely, HF, CHF_3 and CH_4), we performed a twofold study. Firstly, we focused on the **interaction energy** (E_{int}), which allows to characterize the interaction and to see at which distance the minimum in E_{int} is observed. Secondly, we analyzed the intermolecular BCPs found between the two molecules. The parameters studied to characterize the hydrogen bonds were the **electron density** and **Laplacian** of the BCP at different distances (r) between both molecules.

The E_{int} calculated (Figure 5.2a) for the interaction of a water molecule (H_2O) with a molecule of HF shows that this interaction has the highest stabilization ($E_{int} = -8.5$ kcal/mol) at a shorter distance (1.6 Å) compared to CHF_3 and CH_4 . As it was expected, the presence of F atoms in the trifluoromethane CHF_3 increases the stabilization of the interaction ($E_{int} = -3.5$ kcal/mol) between the H_2O and CHF_3 molecules when compared to methane, CH_4 , ($E_{int} = -0.7$ kcal/mol). This is probably due to the stronger hydrogen bond that is formed between the two former molecules. Both systems show a minimum at similar intermolecular distance: 2.5 Å and 2.7 Å for CHF_3 and CH_4 respectively.

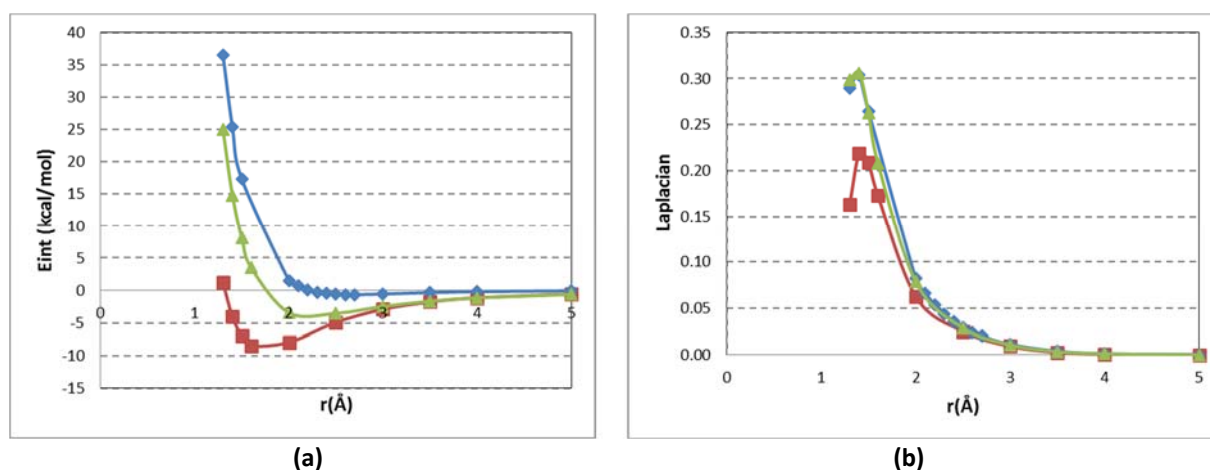


Figure 5.2 (a) E_{int} (kcal/mol) vs r (Å) and (b) Laplacian (a.u.) vs r (Å) for the systems $H_2O \cdots HF$ (in red), $H_2O \cdots HCH_3$ (in blue), $H_2O \cdots HCF_3$ (in green).

The value of the **critical point density**, ρ_{CP} , found in the minimum of the curve is one order of magnitude higher for the interaction of H₂O with HF [$\rho_{CP}(1.6 \text{ \AA}) = 0.0539 \text{ a.u.}$] than for the other two systems [CHF₃ $\rho_{CP}(2.5 \text{ \AA}) = 0.0076 \text{ a.u.}$; CH₄ $\rho_{CP}(2.7 \text{ \AA}) = 0.0053 \text{ a.u.}$] indicating a stronger hydrogen bond formation. The typical electron density value for the intermolecular BCP in a hydrogen bond is $\rho_{CP} < 0.1 \text{ a.u.}$ ¹¹. In the three cases, the electron densities of the intermolecular hydrogen interaction are one or two orders of magnitude lower than the electron densities corresponding to the intramolecular bonds.

The three Laplacian values are positive (Figure 5.2b). A positive value of the Laplacian indicates a depletion of density and it is characteristic of closed-shell interactions (*e.g.* ionic, hydrogen-bonding, van der Waals)¹¹. At the distance at which the minimum has been identified, the values of the Laplacian are: $\nabla^2 \rho_{CP}(1.6 \text{ \AA}) = 0.173 \text{ a.u.}$ for HF, $\nabla^2 \rho_{CP}(2.5 \text{ \AA}) = 0.0287 \text{ a.u.}$ for CHF₃, and $\nabla^2 \rho_{CP}(2.7 \text{ \AA}) = 0.0201 \text{ a.u.}$ for CH₄. Usually, the $\nabla^2 \rho_{CP}$ value for an open shell contact is *c.a.* 0.03 a.u. ¹¹. The three expansion ratios obtained for these intermolecular BCPs are < 1 (Table 5.1).

Table 5.1 Distance (r), interaction energy (E_{int}), BCP density (ρ_{CP}), **Laplacian** and **expansion ratio** ($|\lambda_1/\lambda_3|$) at the minimum of the energy potential surface.

	r_{min} (\AA)	E_{int} (kcal/mol)	ρ_{CP} (a.u.)	Laplacian (a.u.)	$ \lambda_1/\lambda_3 $
H ₂ O...HF	1.6	-8.5	0.0539	0.173	0.031
H ₂ O...CHF ₃	2.5	-3.5	0.0076	0.0287	0.029
H ₂ O...CH ₄	2.7	-0.7	0.0053	0.0201	0.104

Considering (1) the existence of a E_{int} minimum that indicates the stabilization of the dimer vs separate molecules; (2) the small value of the critical point electron density, ρ_{CP} , that indicates a weak bond; (3) the positive value of the Laplacian, $\nabla^2 \rho_{CP} > 0$; and (4) an expansion ratio $|\lambda_1/\lambda_3| < 1$ for all three systems, that indicates a closed shell weak interaction, we conclude that the intermolecular critical points, BCPs (3, -1), found between the two studied molecules can be categorized as **hydrogen bonds**.

5.1.2 Variation of the interaction between two water molecules with the intermolecular angle α

When two water molecules placed on the same plane change their relative orientation by rotating one of the molecules vs the other (Figure 5.3, at $\alpha = 0^\circ$ the intermolecular interaction takes place between the hydrogen of one molecule and the oxygen of the other and at $\alpha = 120^\circ$ the intermolecular interaction takes place between the two oxygen atoms), it is expected that the intramolecular interaction gradually changes from being attractive to repulsive. In this study, we evaluated the intermolecular bond critical point, BCP, between the two molecules at different angles α with a constant oxygen-oxygen intermolecular distance $r(\text{O-O}) = 2.5 \text{ \AA}$ (Figure 5.3).

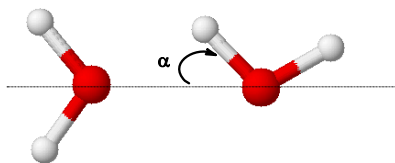


Figure 5.3 Intermolecular angle α between two water molecules at fixed O-O distance $r(\text{O-O}) = 2.5 \text{ \AA}$.

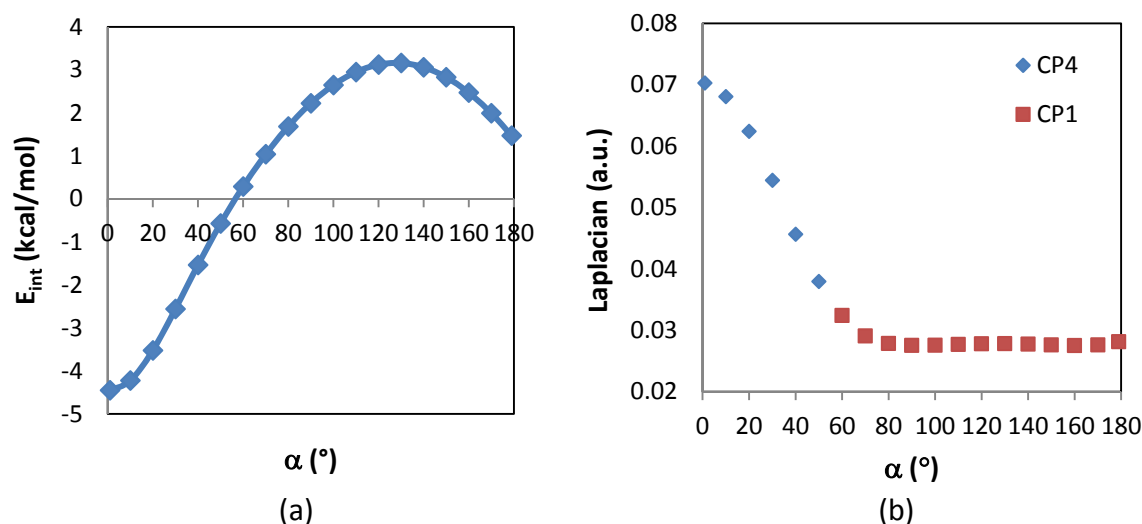


Figure 5.4 (a) E_{int} and (b) Laplacian of the critical point between the two water molecules at different angles (α).

Along this angular variation (see Figure 5.4a), the interaction between two H_2O molecules indeed changes from being attractive ($E_{int} < 0$), at intermolecular angles $0^\circ \leq \alpha \leq 50^\circ$, to repulsive ($E_{int} > 0$) at angles $60^\circ \leq \alpha \leq 180^\circ$. At small angles ($\alpha \leq 50^\circ$), the shortest intermolecular distance takes place between the oxygen of one molecule and the hydrogen of the other. This orientation favors the formation of a hydrogen bond between the two molecules. However, at larger angles ($\alpha \geq 60^\circ$), the intermolecular interaction takes place between the two oxygen atoms and the intermolecular interaction becomes repulsive. The Laplacian value of the intermolecular BCP decreases from 0.07 a.u. to 0.03 a.u. between 0° - 50° (critical point CP4) and for angles $\alpha > 50^\circ$ the value of this magnitude (critical point CP1) remains more or less constant at 0.02 – 0.03 a.u. (Figure 5.4b).

The electron density gradient paths $\nabla\rho$ illustrate that the intermolecular BCP (3,- 1) between the atoms $\text{O}_2[\text{H}_2\text{O}(1)]$ and $\text{H}_5[\text{H}_2\text{O}(2)]$ changes with the angle α (Figure 5.5). It is observed that the critical point between the two water molecules changes from being between the oxygen of one molecule and the hydrogen of the other (CP4), representing an hydrogen bond, to appear between the two oxygen atoms $\text{O}_2[\text{H}_2\text{O}(1)] - \text{O}_1[\text{H}_2\text{O}(2)]$ at $\alpha \geq 50^\circ$ (CP1). The isodensity surfaces between two water molecules at angles 40° , 48° , 50° and 120° (Figure 5.6) show that the isodensity line seen between the two molecules, where the critical point is located, closes at increasing angles. The value of the critical point density decreases from 0.02 a.u. to 0.008 a.u. with increasing values of angle. All these factors together with the negative value of the E_{int} , indicate that, between $\alpha = 0^\circ - 50^\circ$, the BCP that appears between the two water molecules characterizes a weak intermolecular bond formation (hydrogen bond). However, there is no stabilization of the bimolecular system at

angles ranging from 50° to 180° ($E_{int} > 0$). At this angles, it is suspected that the intermolecular critical point indicates an overlap of the electron densities of both molecules.

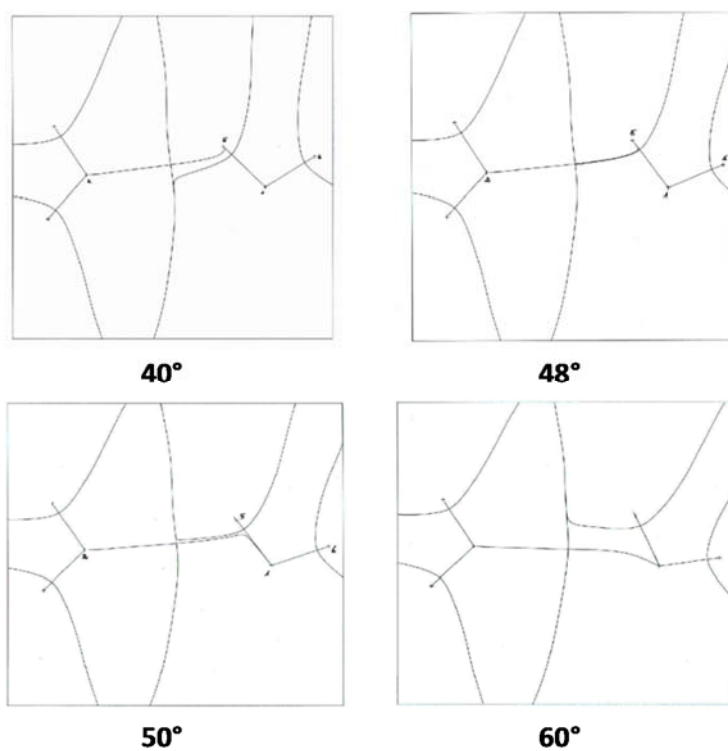


Figure 5.5 Bond critical point paths at $\alpha = 40^\circ, 48^\circ, 50^\circ$ and 60° between two water molecules.

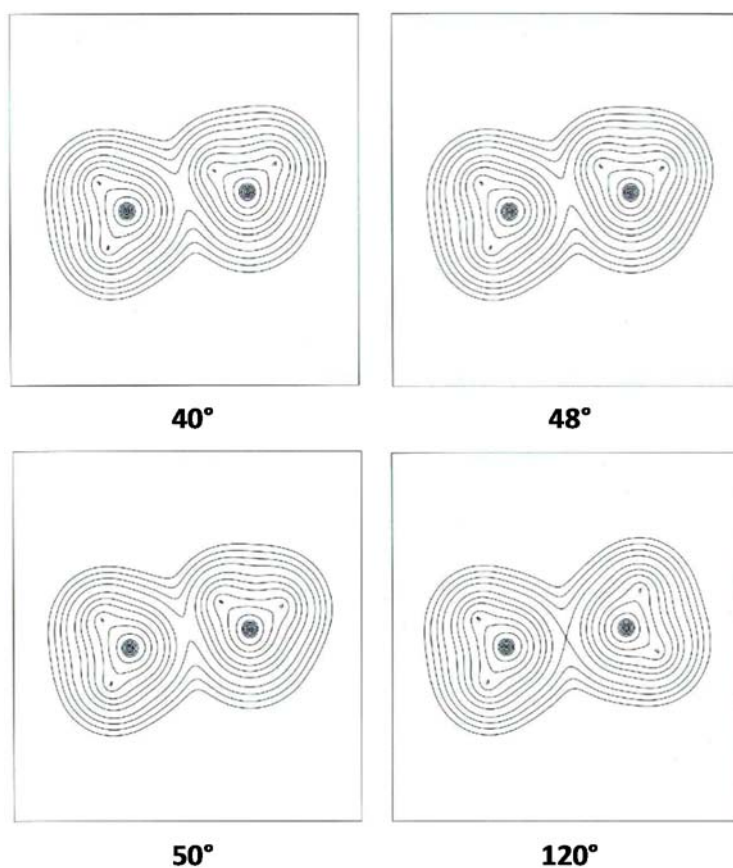


Figure 5.6 Isodensity surfaces at angles $\alpha = 40^\circ, 48^\circ, 50^\circ$ and 120° between two water molecules.

We conclude that an AIM analysis of intermolecular critical points is a useful tool to determine whether there is an interaction between the molecules and describe its nature. However, it has been observed that the presence of an intermolecular bond critical point is not always indicative of attractive interaction between the molecules and a complementary analysis of the interaction energy E_{int} is needed to determine the bonding nature of the interaction.

5.1.3 Characterization of repulsive interactions

As it has been discussed in the previous section, intermolecular BCPs exist even if the interaction between the two molecules is not attractive. To characterize these BCPs, we analyzed the interaction of two oxygen atoms from two different molecules. The selected systems are arranged on a plane and the oxygen atoms are placed one in front of the other. In all cases, the oxygen atoms have sp^2 hybridization and all their electrons are placed in filled orbitals. The systems studied are classified into two groups according to the type of intramolecular binding of the oxygen:

I.- In the first class of systems studied (systems I), the oxygen atoms in the molecule are bound to different groups R and R'. The hybridization of the oxygen in these molecules is sp^3 with two unbound lone pairs. The R, R' groups have been chosen to have different electronegativity and volume (Figure 5.7a). The only exception in this group is for the CO molecule, where the O atom has a hybridization sp forming a triple bond with the carbon atom.

II- In the second class of systems studied (systems II), the oxygen atoms are bound to a single atom X, either C or N. The C and N atoms are bound to different groups R and R' that, as for Systems I, differ in electronegativity and volume (Figure 5.7b). In these cases, both the O and the C or N atoms have sp^2 hybridization and the O atom two double occupied lone pairs.

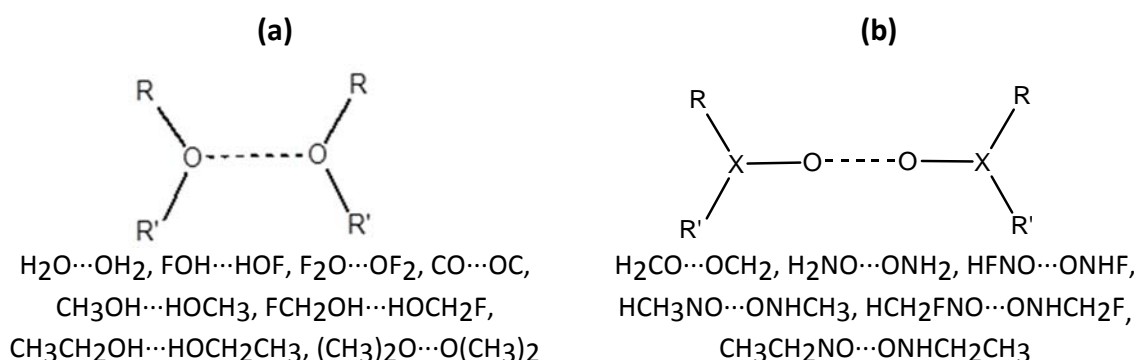


Figure 5.7 (a) Systems I consisting of two molecules ROR' and (b) systems II consisting of two molecules R'RX-O. The molecules are oriented so that the oxygen atoms of each molecule are placed one in front of the other, being the intermolecular interaction repulsive.

The interaction energy (E_{int}) for systems I and II is mainly repulsive, except for systems F₂O and CO (Figure 5.8.). On the other hand, the electron density [ρ_{cp}] and Laplacian [L_{cp}] of the intermolecular critical point increase as closer the two molecules are (Figure 5.8). Given the

different properties of the R and R' groups, we were expecting to observe different characteristics of the intermolecular BCP depending on the system being either I or II.

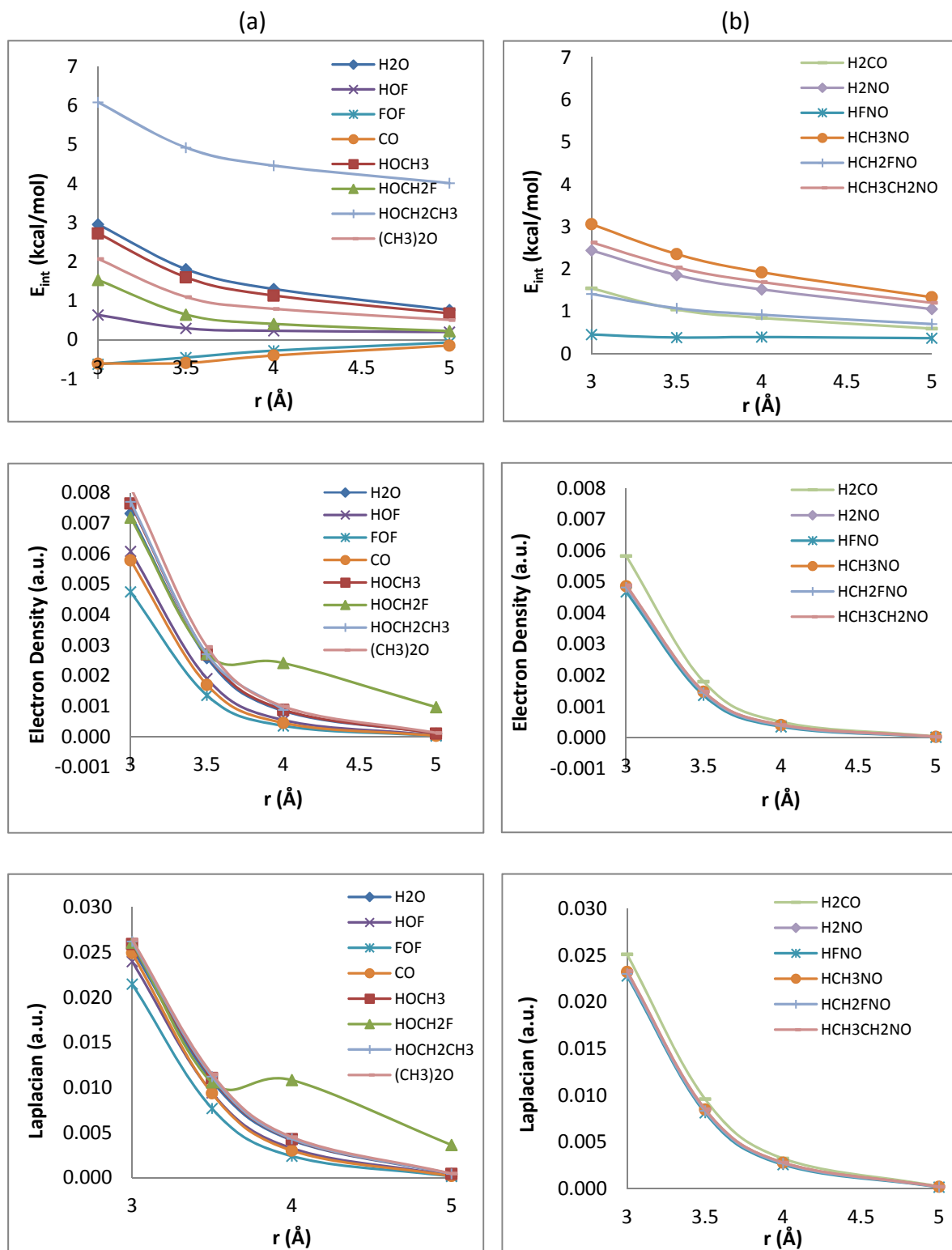


Figure 5.8 Representation of the E_{int} (kcal/mol), electron density (ρ_{cp}) and the Laplacian values at the intermolecular critical point for (a) systems I and (b) systems II.

Although the intermolecular interaction is repulsive for most of them, a bond critical point (3,-1) appears between the interacting molecules with very small values of the electron density (ranging from 0.005 a.u. to 0.008 a.u.) and small positive Laplacian (ranging between 0.02 a.u. and 0.03 a.u.). The presence of these BCPs is thought to be a consequence of the superposition of electron densities of the atoms.

At a fixed intermolecular oxygen-oxygen distance of $r(\text{O-O}) = 3 \text{ \AA}$, we analyzed the parameters E_{int} (kcal/mol), dipole, polarizability and the electron density [ρ_{cp}] and Laplacian [L_{cp}] at the intermolecular critical point for all these different systems (Table 5.2). There is no clear correlation between the studied parameters and the stability of the dimer. Consequently consequently, we did not find a simple way to discriminate which BCP are true bond critical points and which ones appear solely due to the superposition of electron density of the molecules.

Table 5.2 Values of E_{int} , dipole, polarizability, electron density (ρ_{cp}) and Laplacian (L_{cp}) at the intermolecular critical point for the systems (a) type I and (b) type II.

System	E_{int} (MP2) kcal/mol	Dipole moment	Polarizability	ρ_{cp} a.u.	L_{cp} a.u.
SYSTEMS I					
H ₂ O	2.96	2.084	1.154	$7.33 \cdot 10^{-3}$	$2.54 \cdot 10^{-2}$
HOF	0.64	2.263	1.551	$6.08 \cdot 10^{-3}$	$2.40 \cdot 10^{-2}$
FOF	-0.63	0.253	1.955	$4.75 \cdot 10^{-3}$	$2.15 \cdot 10^{-2}$
CO	-0.61	0.340	1.842	$5.79 \cdot 10^{-3}$	$2.49 \cdot 10^{-2}$
HOCH ₃	2.73	1.956	2.760	$7.65 \cdot 10^{-3}$	$2.59 \cdot 10^{-2}$
(CH ₃) ₂ O	2.07	1.628	4.510	$8.19 \cdot 10^{-3}$	$2.64 \cdot 10^{-2}$
HOCH ₂ F	1.53	0.365	2.930	$7.19 \cdot 10^{-3}$	$2.61 \cdot 10^{-2}$
HOCH ₂ CH ₃	6.09	1.821	4.483	$7.71 \cdot 10^{-3}$	$2.62 \cdot 10^{-2}$
SYSTEMS II					
H ₂ CO	1.55	3.303	2.758	$5.83 \cdot 10^{-3}$	$2.51 \cdot 10^{-2}$
H ₂ NO	2.44	2.913	2.379	$4.85 \cdot 10^{-3}$	$2.30 \cdot 10^{-2}$
HFNO	0.45	2.883	2.496	$4.68 \cdot 10^{-3}$	$2.28 \cdot 10^{-2}$
HCH ₃ NO	3.06			$4.86 \cdot 10^{-3}$	$2.32 \cdot 10^{-2}$
HCH ₂ FNO	1.41			$4.82 \cdot 10^{-3}$	$2.30 \cdot 10^{-2}$
HCH ₂ CH ₃ NO	2.63	3.084	5.613	$4.89 \cdot 10^{-3}$	$2.33 \cdot 10^{-2}$

Since an analysis based only on the electron density and its Laplacian at the CP is not sufficient to establish the nature of the interaction, it is advisable to complement the study of BCPs always with an interaction energy calculation^{12,13}.

5.2 Effect of the orientation in radical-radical intermolecular interactions: analysis of McConnell theory

McConnell¹⁴ and Yamaguchi^{15,16}, among others¹⁷⁻²⁰, postulated that there is a magneto-structural relationship associated to the interaction between two radical molecules. Accordingly, the spatial orientation of the constituent units of the crystal would define the magnetic properties of the crystal. Previous works have been carried out following this idea,

accentuating the important contribution made by Yamaguchi in relation to studies performed on two interacting radicals at different orientations^{15–17}.

McConnell^{14,21} proposed an effective Hamiltonian to study the interaction of two radicals A and B [equation (5.1)] where it was assumed that only the intermolecular terms are relevant to describe the spin multiplicity of the system. Assuming that the spin operators \hat{S}_i^A, \hat{S}_j^B on orbitals i, j in the molecules A and B respectively, can be calculated as described in equations (5.2) and (5.3), the energy gap between the low-spin (LS) and high-spin (HS) states can then be estimated using equation (5.4):

$$\hat{H}^{AB} = -\sum_{\substack{i \in A \\ j \in B}} J_{ij}^{AB} \hat{S}_i^A \cdot \hat{S}_j^B \quad (5.1)$$

$$\hat{S}_i^A = \hat{S}^A \rho_i \quad (5.2)$$

$$\hat{S}_j^B = \hat{S}^B \rho_j \quad (5.3)$$

$$\begin{aligned} \Delta E^{LS-HS} &= \langle \hat{H}^{AB} \rangle^{LS} - \langle \hat{H}^{AB} \rangle^{HS} = -\sum_{\substack{i \in A \\ j \in B}} J_{ij}^{AB} \left[\langle \hat{S}_i^A \cdot \hat{S}_j^B \rangle^{LS} - \langle \hat{S}_i^A \cdot \hat{S}_j^B \rangle^{HS} \right] = \\ &= -\left[\langle \hat{S}^A \cdot \hat{S}^B \rangle^{LS} - \langle \hat{S}^A \cdot \hat{S}^B \rangle^{HS} \right] \sum_{\substack{i \in A \\ j \in B}} J_{ij}^{AB} (\rho_i^A \rho_j^B) \end{aligned} \quad (5.4)$$

The value of $\left[\langle \hat{S}^A \cdot \hat{S}^B \rangle^{LS} - \langle \hat{S}^A \cdot \hat{S}^B \rangle^{HS} \right]$ is a negative number since $\langle \hat{S}^A \cdot \hat{S}^B \rangle^{LS} < \langle \hat{S}^A \cdot \hat{S}^B \rangle^{HS}$ [according to equation (5.5)].

$$\langle \hat{S}^A \cdot \hat{S}^B \rangle = \frac{1}{2} [S(S+1) - S_A(S_A+1) - S_B(S_B+1)] \quad (5.5)$$

Then, assuming that $J_{ij}^{AB} < 0$, the antiferromagnetic interaction between the two molecules will be favored when the interaction between two spin densities ρ are of the same sign ($\rho_i^A \rho_j^B > 0$), while it will be ferromagnetic if such spin densities ρ are of opposite sign ($\rho_i^A \rho_j^B < 0$) [equation (5.4)]. On the other hand, it will be the other way round if $J_{ij}^{AB} > 0$, which happens when the overlap between the molecular orbitals containing the unpaired electrons is null or almost null, but the exchange energy is different from zero.

5.2.1 Methodology

In order to evaluate this approach, we investigated the interaction of two radicals at different orientations. The systems studied were: (a) two dihydronitroxide (H_2NO) molecules and the interactions between the organic radicals (b) methyl-allyl and (c) allyl-allyl. These

are well-known and characterized organic radicals^{21,22} that intend to represent, in a simplified way, intermolecular connections commonly found in organic molecular crystals.

The calculation of the energy gap between the low and high-spin states ΔE^{S-T} was performed using B3LYP, CAS, CASPT2 methods and 6-31+g(d,p) and 6-31+g(2d,2p) basis sets, although additional basis sets and methods were used in specific systems when it was required. To evaluate McConnell theory, we used J_{ij} and P_{ij} parameters. These parameters were estimated projecting CASSCF calculations in a Valence Bond space constituted by the ij orbitals that belong to the active space.

5.2.2 Analysis of the interaction between two H₂NO molecules at different orientations

To investigate whether there is a magneto-structural relationship between the magnetic interaction and the orientations of two H₂NO molecules, we explore the preference of energy for high-spin (triplet) and low-spin (singlet) states according to, first, the variation of the distance, and, second, the angle between the two H₂NO molecules.

5.2.2.1 Variation of the interaction between two molecules with the intermolecular distance r

To study the importance of the orientation of two H₂N-O···O-NH₂ molecules, we analyzed the intermolecular interaction along two different approaching paths (Figure 5.9): (a) *ss* and (b) *pp*. In the interaction of two H₂NO molecules a different behavior is observed when the two molecules approach along the orientations *ss* or *pp*. In the first, E_{int} is always > 0 , which indicates that the interaction between the two molecules is always repulsive (see H₂NO-*ss* graph in Figure 5.10a). However, in the orientation *pp* a small minimum of energy is observed at $r \sim 3 - 4 \text{ \AA}$ indicative of a slight stabilization of the dimer (Figure 5.10a, H₂NO-*pp* graph).

Both CAS and UB3LYP calculations estimated that in the case of the *ss* orientation the energy gap between the singlet and the triplet is always negative $\Delta E^{S-T} < 0$ (Figure 5.10b, H₂NO - *ss* graph). Therefore, the singlet is always lower in energy than the triplet. Conversely, for orientation *pp* (Figure 5.10b, H₂NO - *pp* graph), the curve shows an inflection and values change from being slightly negative ($E^S < E^T$) to be positive ($E^S > E^T$) at $r \leq 3 \text{ \AA}$ (UB3LYP) and $r \leq 4 \text{ \AA}$ (CAS) close to the minimum of energy, which is found at 4 \AA at both CAS and UB3LYP levels. Comparing the results obtained according to CAS and B3LYP calculations, it is seen that in both cases the curve obtained has a very similar shape, although there is a shift of ca. 50-100 cm^{-1} .

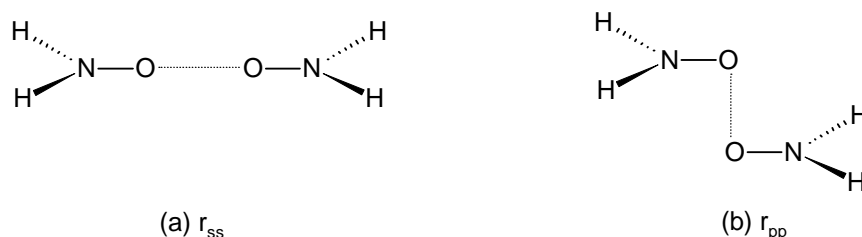


Figure 5.9 Two H₂N-O···O-NH₂ molecules approaching along the paths: (a) *ss*, intermolecular distance r_{ss} , and (b) *pp*, intermolecular distance r_{pp} .

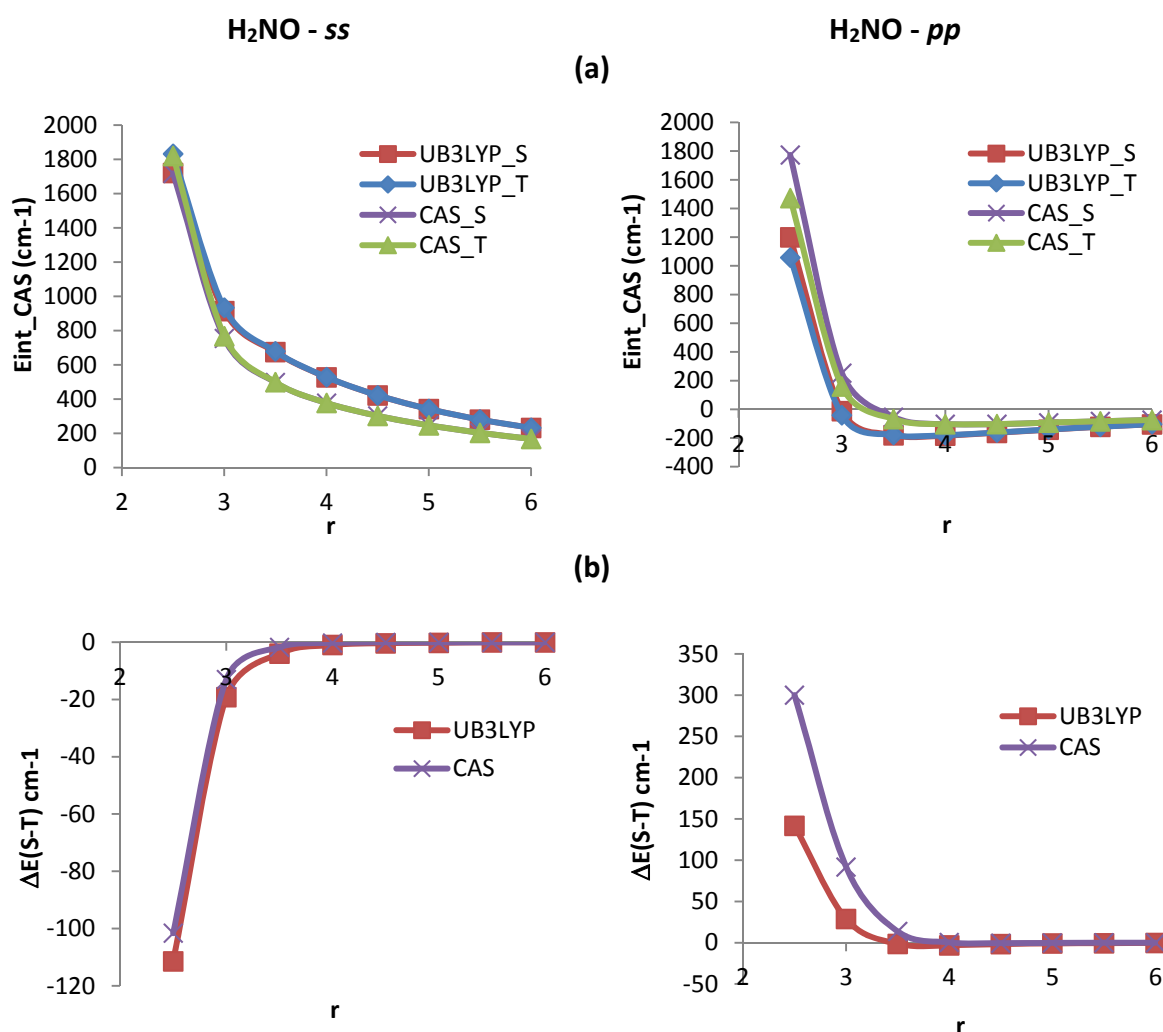


Figure 5.10 (a) Interaction energy (E_{int}) and (b) energy gap (ΔE^{S-T}), both in cm⁻¹, for two H_2NO molecules at different distances along the paths ss and pp . The calculations were performed with UB3LYP and CASSCF(6,4) methods and 6-31+g (2d,2p) basis set.

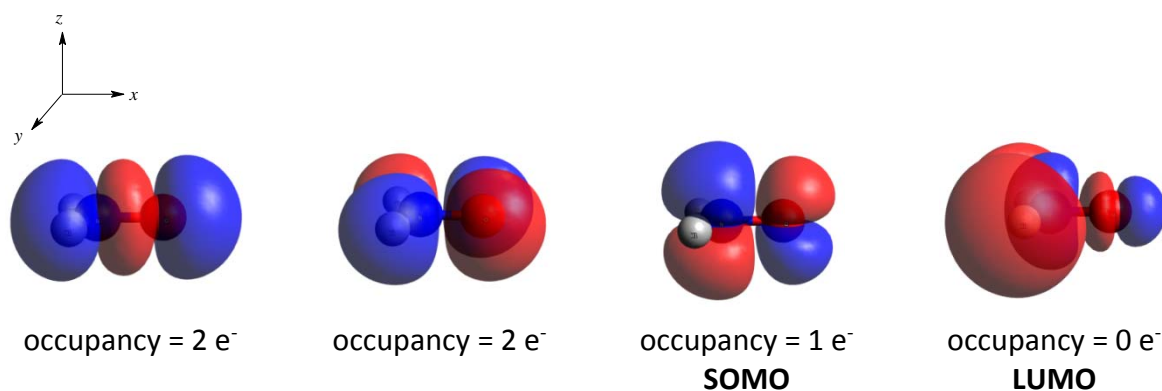


Figure 5.11 H_2NO molecular orbitals and their occupancy.

In H_2NO , the nitrogen (N) has a hybridization sp^2 . The singly occupied molecular orbital (SOMO) that contains the unpaired electron $\pi^* = p_z(N) - p_z(O)$ is delocalized between atoms of N and O, [considering x the coordinate along the direction of the nitrogen-oxygen bond, y

the coordinate in the H_2NO plane perpendicular to x , and z the coordinate perpendicular to the plane containing the molecule]. The highest-occupied (HOMOs), singly-occupied (SOMO) and lowest-unoccupied (LUMO) molecular orbitals of H_2NO are the combination of the sp^2 orbitals of the N and H atoms and the p orbitals of the O atom as shown in Figure 5.11.

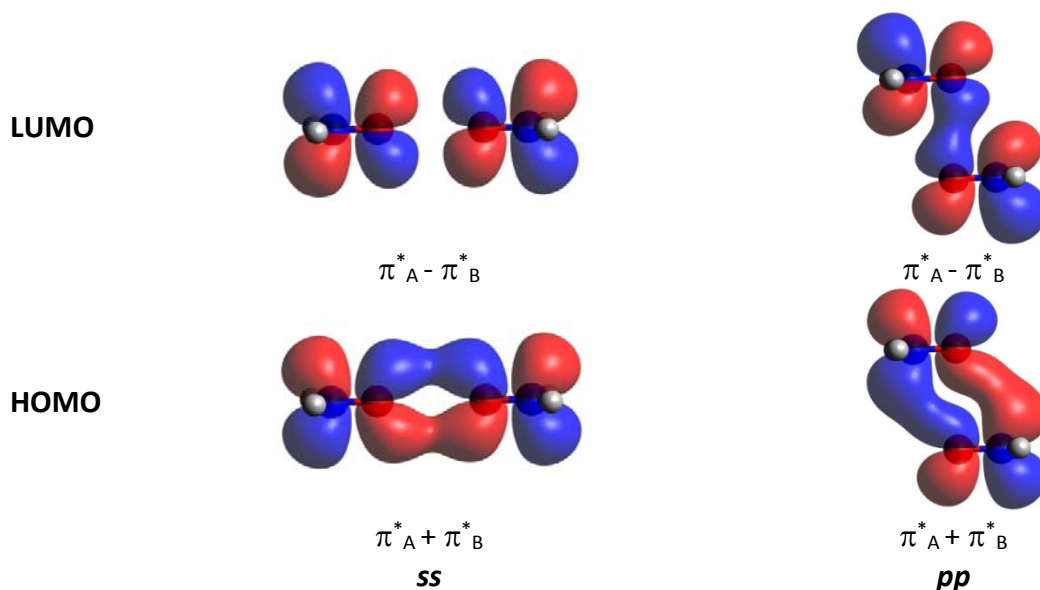


Figure 5.12 HOMO and LUMO of two interacting H_2NO radicals in the orientations ss and pp .

Along the paths ss and pp the two SOMOs π^*_A and π^*_B of two interacting H_2NO radicals A and B combine to form the $\pi^*_A + \pi^*_B$ (HOMO) and $\pi^*_A - \pi^*_B$ (LUMO) molecular orbitals (Figure 5.12). For the orientation ss , there is no stabilization of the dimeric system due to the repulsion between the two electronegative oxygen atoms that have full-occupied σ orbitals. Consequently, there is no attractive interaction between both molecules. In this alignment, the open-shell (OS) singlet is lower in energy and more stable than the triplet and the closed-shell singlet states. On the other hand, in the orientation pp , the interaction between the two free electrons is a π -stacking contact through the two SOMO orbitals resulting in the combinations of the SOMOs, $\pi^*_A + \pi^*_B$ and $\pi^*_A - \pi^*_B$ (Figure 5.12). At short distances ($< 3 \text{ \AA}$) the two molecular orbitals $\pi^*_A + \pi^*_B$ and $\pi^*_A - \pi^*_B$ where the unpaired electrons are located are quasi-degenerated which favors the stabilization of the triplet state²¹.

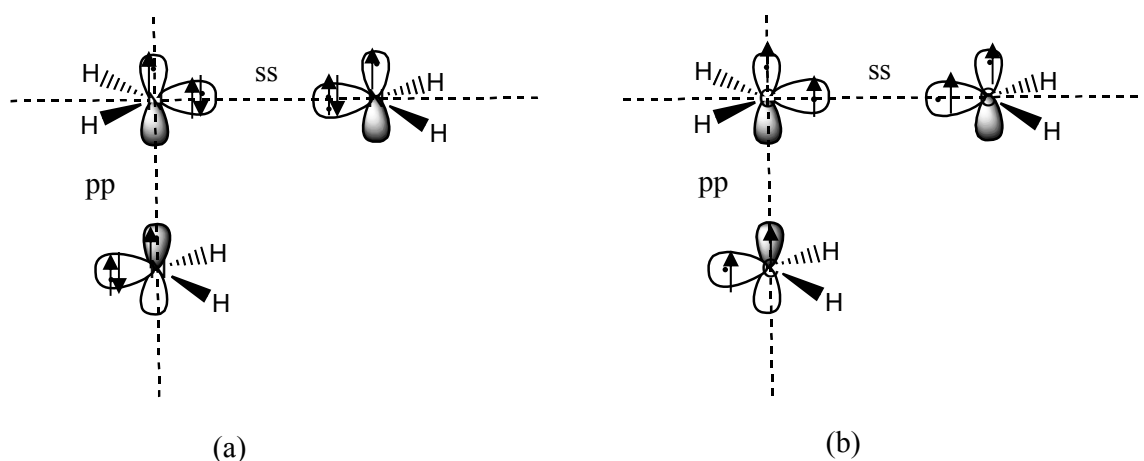


Figure 5.13 Interaction of two molecules (a) H_2N and (b) H_2C along the orientations ss and pp .

In order to evaluate the effect of the repulsion caused by the doubly occupied σ orbitals of the oxygen atom, we studied the interaction of the radicals nitrene NH_2 (Figure 5.13a) and carbene CH_2 : (Figure 5.13b) along the same paths ss and pp . The N and C atoms in this two molecules have a sp^2 hybridization. The nitrene radical has two electrons occupying the sp^2 orbital and one free electron in the p_z orbital, while the carbene radical has a singly-occupied sp^2 orbital and another free electron in the p_z orbital (Figure 5.13).

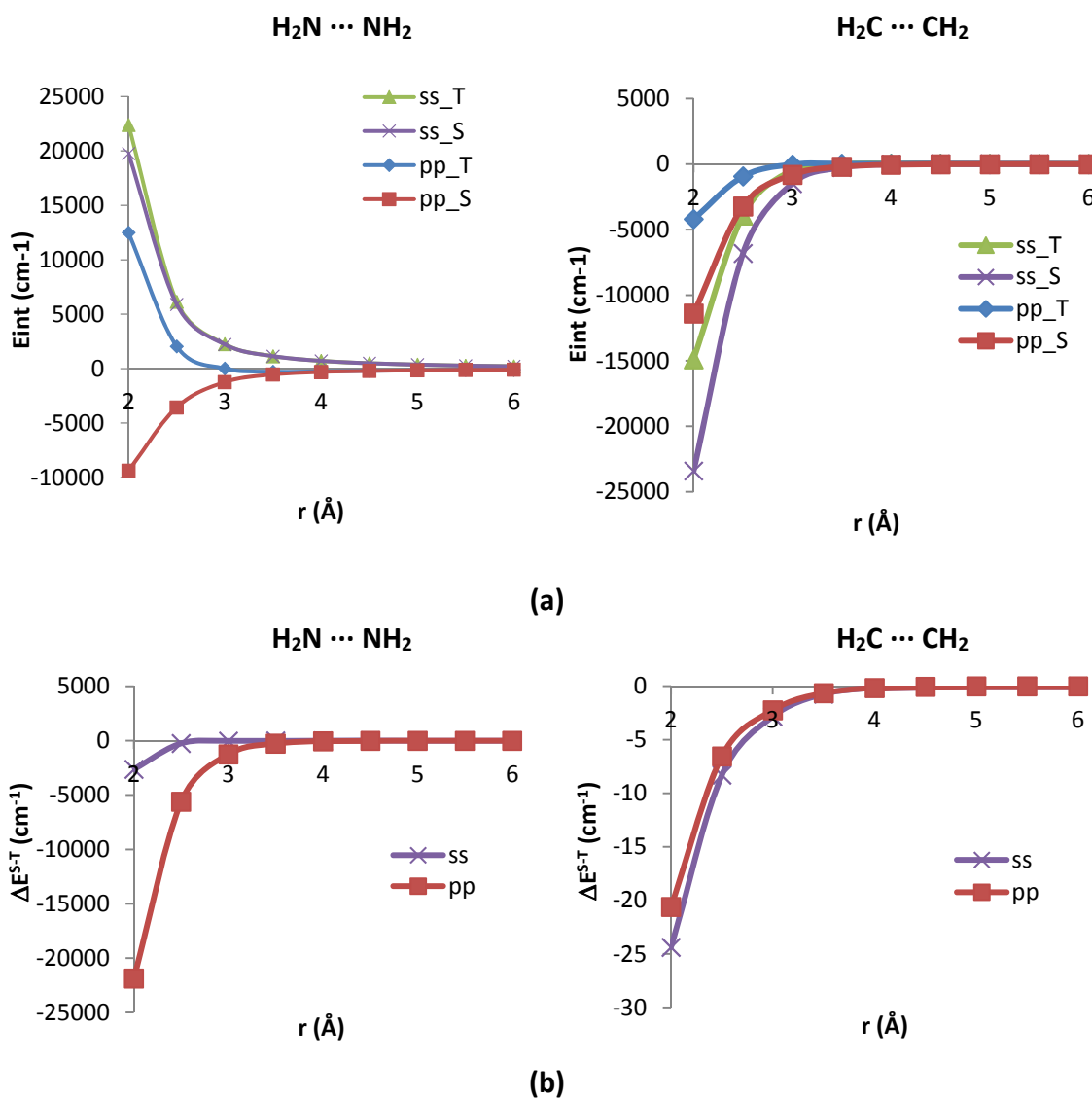


Figure 5.14 (a) Interaction energy (E_{int}) and (b) energy gap (ΔE^{S-T}), both in cm^{-1} , for the systems $\text{H}_2\text{N} \cdots \text{NH}_2$ and $\text{H}_2\text{C} \cdots \text{CH}_2$ along the paths ss and pp . The calculation were performed at CAS(6,4)/6-31+g(2d,2p) and CAS(4,4)/6-31+g(2d,2p) level for $\text{H}_2\text{N} \cdots \text{NH}_2$ and $\text{H}_2\text{C} \cdots \text{CH}_2$ respectively.

Calculations CAS(6,4)/6-31+g(2d,2p) for the interaction of two NH_2 units estimated that, while in the orientation ss the interaction is always repulsive (both for the triplet and the singlet), the pp interaction is attractive. Along the pp orientation there is a small minimum at $r = 3.5$ Å for the triplet, while for the singlet the E_{int} always is < 0 (Figure 5.14a, $\text{NH}_2 \cdots \text{NH}_2$ graph). Similarly to H_2NO , in the ss orientation the doubly occupied sp^2 orbitals have a steric repulsion effect that destabilize the interaction. The unpaired electron in the NH_2 molecule

is located in orbital $p_z(N)$. Thus, in the pp path, the orientation of the orbitals $p_z - p_z$ of both molecules favors the attractive intermolecular interaction and, at short distances, the bond formation $H_2N \cdots NH_2$ (N_2H_4).

The interaction between two CH_2 molecules is attractive for all orientations and all spin states [Figure 5.14a $CH_2 \cdots CH_2$ graph, calculations performed at CAS(4,4)/6-31+g(2d,2p) level]. The CH_2 monomer is a diradical with two unpaired electrons, one in a semioccupied sp^2 orbital and the other in a p_z orbital (Figure 5.13b), that within the molecule interact ferromagnetically (Hund's rule) stabilizing the triplet state. The unpaired electrons in both orbitals, sp^2 and p_z favor that the intermolecular interactions to be attractive in both orientations ss and pp .

In both systems, NH_2 and CH_2 , the spin multiplicity state energetically favored is the singlet ($\Delta E^{S-T} < 0$) at all the intermolecular distances analyzed for the interactions of two molecules along the ss and pp paths (Figure 5.14).

In the ss orientation of two H_2N molecules, the occupation of the active molecular orbitals in the ground state is close to 2 for MO1 and MO2 and close to 1 for MO3 and MO4 at all the distances from 6 to 2 Å (Table 5.3), that indicates a ground state with an OS singlet multiplicity. However, for orientation pp , the occupancies are close to 1 for MO3 and MO4 at long distances (4-6 Å), while they decrease for MO3 and increase for MO4 at short intermolecular distances ($r \leq 3$ Å). This indicates that at $r \leq 3$ Å the intermolecular interaction is stabilized and the electrons tend to form a closed-shell singlet.

Table 5.3 Electron population in the active orbitals for two units $H_2N \cdots NH_2$ approaching according to orientations ss and pp calculated with CAS(6,4)/6-31+g(2d,2p)] for the ground state (singlet).

Intermonomer distance (Å)	<i>ss</i>				<i>pp</i>			
	MO1	MO2	MO2	MO4	MO1	MO2	MO2	MO4
6	2.00	2.00	1.00	1.00	2.00	2.00	1.00	1.00
5	2.00	2.00	1.00	1.00	2.00	2.00	0.99	1.01
4	2.00	2.00	0.99	1.01	2.00	2.00	0.94	1.06
3	2.00	2.00	0.96	1.04	2.00	2.00	0.74	1.26
2	1.74	1.98	0.82	1.46	2.00	2.00	0.20	1.80

Table 5.4 Electron population in the active orbitals for two units $H_2C \cdots CH_2$ approaching according to orientations ss and pp CAS(4,4)/6-31+g(2d,2p)] for the ground state (singlet).

Intermonomer distance (Å)	<i>ss</i>				<i>pp</i>			
	MO1	MO2	MO2	MO4	MO1	MO2	MO2	MO4
6	1.00	1.00	1.00	1.00	1.00	1.01	0.99	1.00
5	1.02	0.98	1.00	1.00	1.00	1.01	0.99	1.00
4	1.09	0.91	1.02	0.98	0.99	1.09	0.91	1.01
3	1.37	0.63	1.10	0.90	0.92	1.34	0.66	1.08
2	1.90	0.10	1.66	0.34	0.40	1.87	0.13	1.60

On the other hand, in the interaction of two CH_2 molecules (Table 5.4), at short intermolecular distance in both orientations ss and pp , the occupancy of two MOs (MO2 and MO4 in ss and MO1 and MO2 in pp) is reduced and the occupancy of the other two MOs (MO1 and MO2 in ss and MO2 and MO4 in pp) increase, indicating the formation of the intermolecular bond.

5.2.2.2 Interaction between two H_2NO molecules as a function of the intermolecular angle α

Once the inter-nuclear distance has been analyzed, we explored the preference of energy for high-spin (triplet) and low-spin (singlet) states according to the variation of the angle between the two H_2NO molecules at a fixed intermolecular distance 3 Å and along with the orientations: SS-PP, XY, XZ, and YZ (Figure 5.15).

All the calculations were carried out at B3LYP, MP2 and CASPT2 level and 6-31+g(2d,2p) basis set. The profiles resulted from CASPT2 and UB3LYP calculations were similar (see Figure 5.16), unlike MP2 that was not able to describe correctly the energy gap between the two spin states.

In almost all the points of the displacement of both H_2NO molecules on the **XY**-plane, the singlet results slightly lower in energy than the triplet ($\Delta E^{S-T} < 0$, Figure 5.16). In the interaction between both monomers there is an overlap between the two partially occupied MOs π_A^* and π_B^* that stabilizes the combination $\pi_A^* + \pi_B^*$ vs $\pi_A^* - \pi_B^*$ (similar to the ss orientation analyzed previously). The electrons occupying the orbital $\pi_A^* + \pi_B^*$ with antiparallel spins determine the AFM character of the interaction. The energy gap between the singlet and the triplet decreases along the path and at angles 80° - 90° both states are practically degenerated in energy.

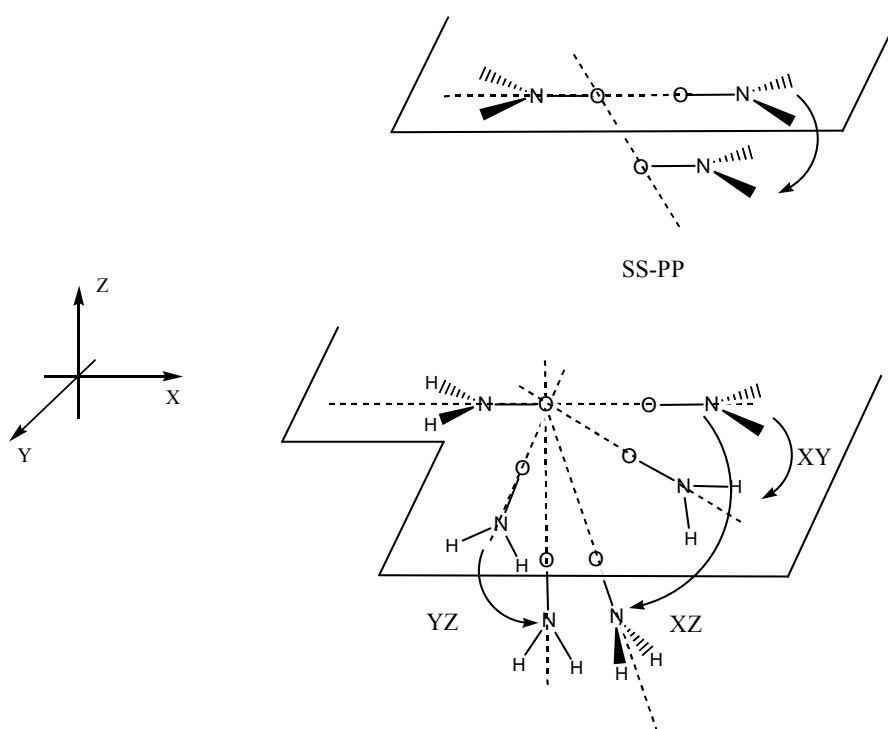


Figure 5.15 Angle variation between two $\text{H}_2\text{N-O}\cdots\text{O-NH}_2$ molecules along the orientations SS-PP, XY, XZ and YZ.

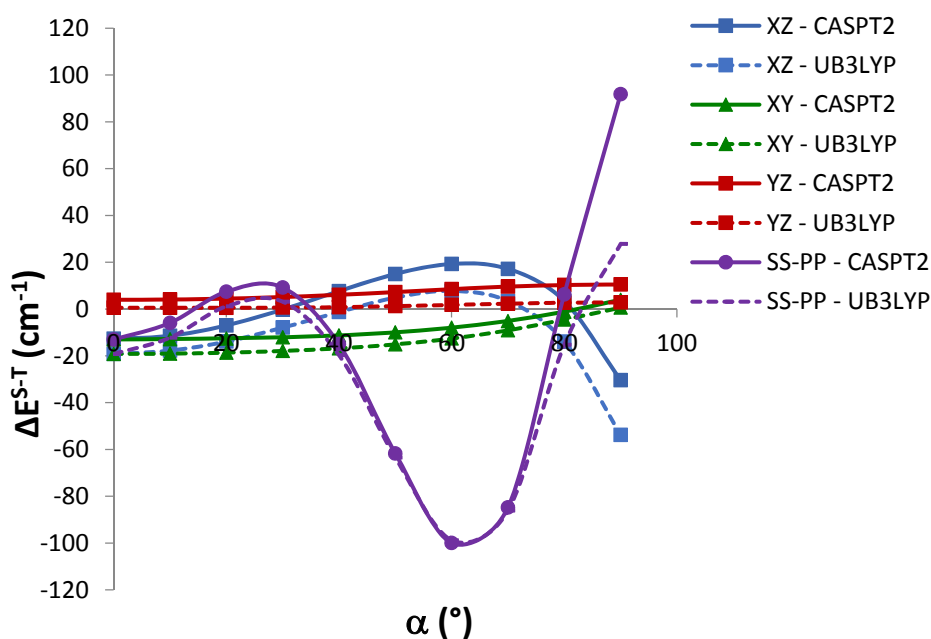


Figure 5.16 Energy gap ΔE^{S-T} (cm^{-1}) between the singlet and triplet states for the interaction of two H_2NO molecules along the paths XY, XZ, YZ and SS-PP (Figure 5.15). Calculations have been performed at CASPT2(6,4) and UB3LYP level with 6-31+g(2d,2p) basis set.

The translation of the two H_2NO molecules on the **YZ** plane starts (Figure 5.16, $\alpha = 0^\circ$ in YZ) at the end point of the previous **XY** curve (Figure 5.16, $\alpha = 90^\circ$ in XY). At angles $\alpha < 40^\circ$ both states singlet and triplet are almost degenerated in energy (Figure 5.16). The gap ΔE^{S-T} increases to some extent with α , showing a slight preference for the triplet state at angles $\alpha > 40^\circ$. In the angular displacement on the YZ plane, the interaction of the π^* orbitals of each molecule changes from being parallel to perpendicular. In this perpendicular alignment there is no overlap between the orbitals, and the value of the exchange integral is positive and very small, which favors the triplet state. However favored the triplet, the difference between both spin states is minimal.

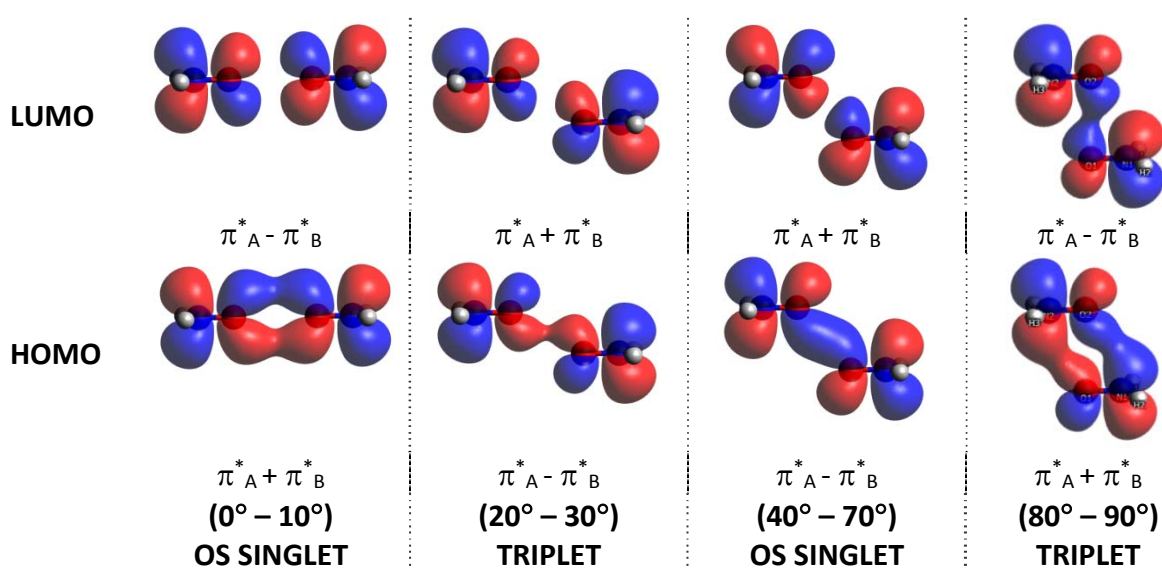


Figure 5.17 HOMO and LUMO of two H_2NO radicals interacting along the orientation SS-PP.

The two orientations that provide the higher energy gaps between the singlet and the triplet are the **SS-PP** and **XZ**.

The orientation of the two H₂NO molecules along the **SS-PP** path changes from the *ss* orientation, analyzed previously, to the *pp* alignment with a π -stacked interaction of the partially occupied SOMOs, which has been discussed above (Figure 5.17). At angles between 0° - 10°, the OS singlet is lower in energy than the triplet. When the two molecules are placed at angles 20° - 30° there is a quasi-degeneracy of the HOMO and LUMO that favors the triplet as a ground state. This degeneracy is lifted at angles 40° - 70°, at which the singlet is favored. At 80° - 90° the preference is again for a triplet as the ground state, as discussed previously for the orientation *pp* (Figure 5.16).

Previous calculation performed by Yamaguchi²³ concluded that the fundamental state is a triplet for the interaction between two H₂NO in parallel planes and both molecules oriented *trans* ($\theta = 180^\circ$, the N atom of one molecule over O atom of the other and the O of the first on N of the second the second) the fundamental state is a triplet.

Extended calculations were performed for the orientation **XZ** using at UB3LYP, CASPT2(6,4), MP2, CCSD(T)^{vi}, DDCI2^{vii}, DDCI3 and full-CI (FCI) level using a 6-31+g(d,p) basis set. The results are similar for all the methods employed (Figure 5.18 and Table 5.5).

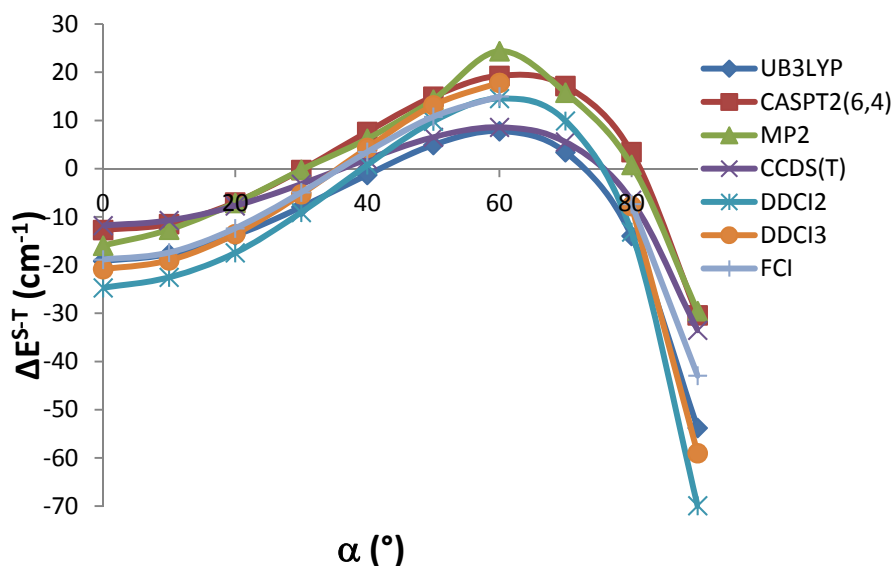


Figure 5.18 Energy gap ΔE^{S-T} (cm⁻¹) between singlet and triplet states for the interaction between two molecules H₂N-O...O-NH₂ along the XZ path. The calculations have been performed with B3LYP, CAS(6,4), MP2, CCSD, DDCI2, DDCI3 and FullCI. The basis set for all the calculations has been 6-31+g(d,p).

^{vi} CCSD(T): Coupled cluster method with a full treatment of single and double excitations and the connected triples estimated non-iteratively using Many-Body Perturbation Theory arguments.

^{vii} DDCI: Difference dedicated configuration Interaction.

In the interaction between the two H₂NO molecules along the **XZ** plane, it is observed that the ground state is a singlet ($\Delta E^{S-T} < 0$) at $\alpha = 0^\circ - 30^\circ$. However, at angles $40^\circ - 70^\circ$ the triplet state is more stable ($\Delta E^{S-T} > 0$), to become singlet again at $\alpha = 80^\circ - 90^\circ$ (Figure 5.18 and Table 5.5).

Table 5.5 Results of the energy gap ΔE^{S-T} (cm⁻¹) between the singlet and the triplet for the interaction of two molecules H₂N-O...O-NH₂ along the XZ orientation.

	UB3LYP	CASPT2 (6,4)	MP2	CCSD(T)	DDCI2	DDCI3	FullCI
0°	-19.16	-12.70	-15.96	-11.80	-24.71	-20.83	-18.84
10°	-17.72	-11.47	-12.64	-10.74	-22.54	-19.01	-17.39
20°	-13.88	-7.00	-7.11	-7.72	-17.46	-13.56	-12.36
30°	-7.93	-0.25	-0.22	-3.20	-9.07	-5.3	-4.91
40°	-1.28	7.65	6.21	1.97	0.78	4.34	3.49
50°	4.93	14.96	14.33	6.51	9.85	13.16	10.78
60°	7.79	19.28	24.38	8.59	14.55	17.81	14.98
70°	3.42	17.17	15.79	5.54	9.90	-	-
80°	-13.92	3.45	0.79	-6.52	-13.15	-7.77	-7.31
90°	-53.76	-30.41	-29.52	-33.51	-69.91	-59.01	-42.93

The ΔP_{ij}^{S-T} values were calculated at CASVB(6,6) level using the 6 active orbitals of the two H₂NO interacting molecules at the angles 0°- 30°- 40°- 50°- 80°- 90°. The i, j active orbitals for each H₂NO molecules were the ones shown in Figure 5.19. The matrix of ΔP_{ij} parameters obtained was practically the same for all the angles studied (Table 5.6). It is observed that the ΔP_{ij} value that is clearly different from zero is the one between the two π orbitals of both molecules, $\Delta P_{\pi_1-\pi_2} = 2.0$. This indicates that the unpaired electrons are located on the π orbitals and that these are the electrons that show different spin orientation in the singlet and triplet states. In the triplet both electrons have parallel spins ($P_{ij}^T = -1$) and in the singlet their spins are antiparallel ($P_{ij}^S = 1$).

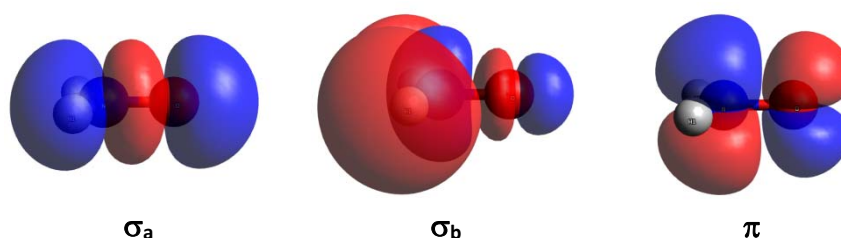


Figure 5.19 H₂NO orbitals considered to be the active space for the CAS(6,6) calculations. Each orbital was occupied by one electron in these calculations.

Table 5.6 Resulting ΔP_{ij}^{S-T} for the 6 active orbitals in the interaction between two H₂NO molecules.

ΔP_{ij}^{S-T}	π_1	σ_{1a}	σ_{1b}
π_2	1.997	0.034	-0.034
σ_{2a}	0.035	0.001	-0.001
σ_{2b}	-0.034	0	0

Comparative studies between CAS methodologies carried out using different active spaces [CAS(6,6), CAS (6,4) and CAS (2,2)] (Figure 5.20) showed that the results for the energy gap between the singlet and the triplet are equivalent. Therefore, the system can be sufficiently well described at CAS(2,2) level.

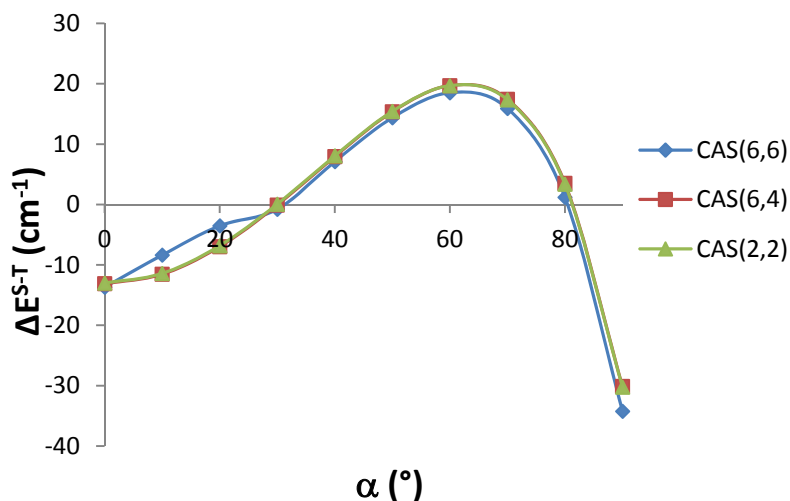


Figure 5.20 Energy gap, ΔE^{S-T} (cm^{-1}), for the angular variation in the interaction between two $\text{H}_2\text{N-O}\cdots\text{O-NH}_2$ units along the XZ plane. Calculations have been performed with CAS(6,6), CAS(6,4) and CAS(2,2).

A qualitative description of the interaction was done evaluating the LUMO and the HOMO orbitals of the dimer [Figure 5.21]. As anticipated, the preference for a low-spin state (singlet) at angles $\alpha = 0^\circ - 30^\circ$ and $\alpha = 80^\circ - 90^\circ$ is basically due to the stabilization of one of the combination of the SOMO orbitals vs the other. At $40^\circ - 70^\circ$ angles, each unpaired electron is located in the SOMO of each molecule $(\pi^*_A)^1(\pi^*_B)^1$ and the triplet is the preferred spin state.

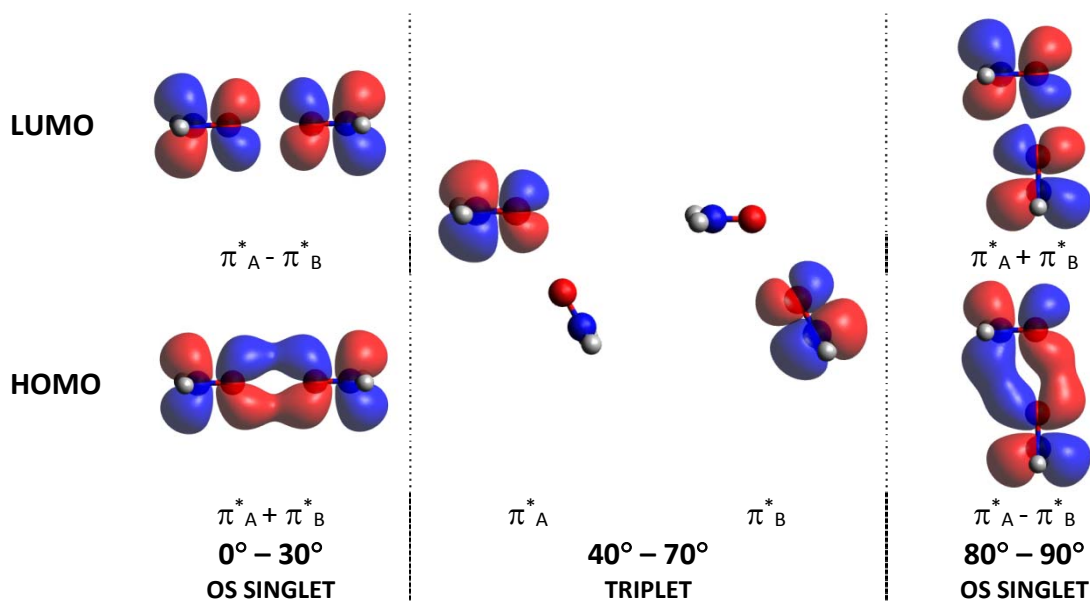


Figure 5.21 HOMO and LUMO of two H_2NO radicals interacting the XZ path.

As a consequence, when defining the spin multiplicity preference of the ground state of two H_2NO interacting radicals, one should pay attention to the spatial orientation between them. Depending on that orientation, the molecular orbitals interact in a different way and define the spin multiplicity for the ground state.

According to the results obtained, when designing molecular crystals based on molecules with NO radical groups, the positioning of these groups should be at angles $20^\circ - 40^\circ$ and 90° in an orientation SS-PP or at angles between $40^\circ - 70^\circ$ in the XZ plane to favor the FM interaction between the unpaired electrons.

5.2.3 Analysis of the interaction between methyl-allyl molecules

The interaction between methyl and allyl radicals was also studied. Each one of these radicals has one delocalized electron that can interact antiferromagnetically (AFM), in which case the ground state will have a low-spin multiplicity (singlet), or ferromagnetically (FM), which will stabilize the high-spin state (triplet). Likewise to H_2NO radicals, we analyzed whether the spatial orientation of these two radicals determine the multiplicity of the bimolecular system and which contributions are responsible for the spin multiplicity of the ground state.

The unpaired electron in the methyl radical is located in the p_z -orbital of the central C atom, *i.e.* perpendicular to the plane of the molecule (Figure 5.22a). The unpaired electron in the allyl is placed in a molecular orbital formed by the p_z orbitals of the lateral C atoms of the molecule, with a nodal center in the central C atom (Figure 5.22b). These two orbitals are the singly-occupied molecular orbitals (SOMOs) that constitute the active space of the system.

The calculations have been carried out at MMVB and CAS(4,4)/6-31g(d) level with the aim of analyzing the variations on energy as well as the values of P_{ij} and J_{ij} , being i,j the active orbitals.

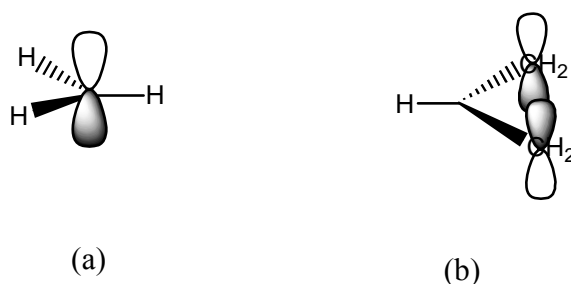


Figure 5.22 SOMO orbitals of the (a) methyl radical and (b) allyl radical.

The study has been performed at different orientations of both radicals placed on parallel planes (section 5.2.3.1) and at different angles between both radicals (section 5.2.3.2).

5.2.3.1 Methyl-allyl Interaction on parallel planes

As indicated before, according to McConnell-I theory¹⁴, the interaction of two electrons in two radicals placed on the π orbitals in parallel planes is expected to be AFM when the spin densities are of the same sign, and FM when they are of opposite sign.

Knowing that the spin densities are positive in the lateral carbons of the allyl and in the methyl carbon and negative in the central carbon of the allyl (Table 5.7), it is expected that the ground state will be a singlet when the methyl radical is located on one of the C side of the allyl (**Cs4vs1**, Figure 5.23) and a triplet when interaction occurs between the central carbon of the allyl and methyl (**Cs4vs2**, Figure 5.23). However, the prediction of the multiplicity of the system is not easy when the methyl radical is placed on intermediate positions regarding the allyl such as located on the central point between the two lateral allyl carbon atoms (**Cs4vsmid2**, Figure 5.23), placed on the middle point of the triangle formed by the three allyl carbon atoms (**Cs4vsmid**, Figure 5.23) or positioned on the hydrogen of the central allyl carbon atom (**Cs4vsmidH**, Figure 5.23).

Table 5.7 Average atomic spin density values on the methyl and allyl carbon atoms. Spin densities are positive on the methyl C atom and the allyl C_{lateral} atoms. Central C allyl atom has a negative spin density.

	Mulliken atomic spin densities
C _{lateral} (allyl)	1.0
C _{centerl} (allyl)	-0.8
C _{lateral} (allyl)	1.0
C (methyl)	1.3

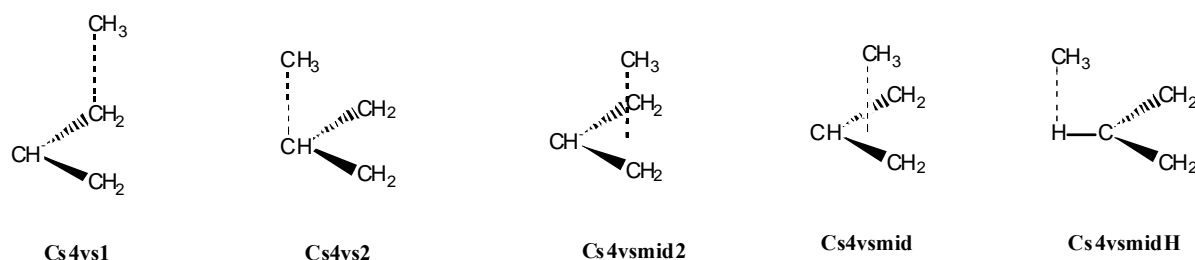


Figure 5.23 Graphical representation of the different orientations studied for methyl vs allyl.

As it has been discussed previously, the energy gap between the singlet and the triplet can be estimated from the J_{ij} and P_{ij} parameters [equation (5.6)].

$$\Delta E^{S-T} = \sum_{i,j} \Delta(J_{ij}P_{ij})^{S-T} \quad (5.6)$$

In these systems the methyl radical is placed in a plane parallel to the allyl. Consequently, it is expected that the main contributions to the energy gap will be the intermolecular interaction from the $\pi^{\text{methyl}}-\pi^{\text{allyl}}$ orbitals that constitute the active space.

The energy gap between the singlet and the triplet can be then partitioned into the different $\pi-\pi$ contributions [equation (5.7)], based on the interaction between the methyl

and the allyl carbon atoms ($i \in \pi^{\text{methyl}}$ and $j \in \pi^{\text{allyl}}$). Note that the C atoms belonging to the allyl radical are in turn partitioned into lateral (C_{lateral}) and central (C_{central}) atoms:

$$\Delta E^{S-T} = \sum_{\substack{i \in \text{methyl} \\ j \in \text{allyl}}} \Delta(J_{ij}P_{ij})^{S-T} = \Delta(J_{ij}P_{ij})^{C_{\text{methyl}}-C_{\text{lateral1}}} + \Delta(J_{ij}P_{ij})^{C_{\text{methyl}}-C_{\text{central}}} + \Delta(J_{ij}P_{ij})^{C_{\text{methyl}}-C_{\text{lateral2}}} \quad (5.7)$$

If we consider the same geometry for the singlet and the triplet, the J_{ij} parameter will be equivalent for both spin states and the energy gap can then be expressed as:

$$\Delta E^{S-T} = \sum_{\substack{i \in \text{methyl} \\ j \in \text{allyl}}} J_{ij} \Delta P_{ij}^{S-T} = J_{ij} \Delta P_{ij}^{C_{\text{methyl}}-C_{\text{lateral1}}} + J_{ij} \Delta P_{ij}^{C_{\text{methyl}}-C_{\text{central}}} + J_{ij} \Delta P_{ij}^{C_{\text{methyl}}-C_{\text{lateral2}}} \quad (5.8)$$

As it has been discussed previously²⁴, if there is a relationship between $\Delta P_{ij}^{S-T} \Leftrightarrow \rho_i \rho_j$, that connects equation (5.7) with Mc Connell-I theory [equation (5.4)]. Accordingly, the sign of ΔP_{ij}^{S-T} (Table 5.8) correlates with $\rho_i^{\text{methyl}} \rho_j^{\text{allyl}}$ (Table 5.7): the interaction of the methyl radical with the allyl lateral carbons (C_1 and C_3) has a positive ΔP_{ij}^{S-T} contribution (Table 5.8), while the ΔP_{ij}^{S-T} value for the interaction between the methyl and the central allyl atom (C_2) is negative.

Let us stress the fact that ΔP_{ij}^{S-T} values are equivalent for all the orientations studied (Table 5.8). Therefore, it is the J_{ij} parameter that will determine the predominant contributions to the energy gap, and the ground state preference for the high or low-spin multiplicity.

As expected, the multiplicity of the ground states for **Cs4vs1** is a singlet and for **Cs4vs2** a triplet (Table 5.8). The multiplicity of the ground states for these two systems agrees with what was predicted by McConnell's theory. In both cases, the respective preference for low and high-spin state coincides with the result obtained by the calculation $\sum J_{ij} \Delta P_{ij}^{S-T}$ (Table 5.8). In the case of the orientation **Cs4vsmidH** the preference for the triplet ground state is supported by the CASVB calculation ($\Delta E^{S-T} = 0.9$ Kcal/mol) and the $\sum J_{ij} \Delta P_{ij}^{S-T} = 1.1$ kcal/mol estimation.

Table 5.8 Values of J_{ij}^T , ΔP_{ij}^{S-T} and $\Delta(J_{ij}P_{ij})^{S-T}$ in kcal/mol calculated at CAS(4,4)/6-31g(d) level.

	J_{ij}^T kcal/mol			ΔP_{ij}^{S-T} kcal/mol			$J_{ij}^T \Delta P_{ij}^{S-T}$ kcal/mol			$\sum J_{ij}^T \Delta P_{ij}^{S-T}$ kcal/mol (1)	ΔE^{S-T} kcal/mol
	C_1	C_2	C_3	C_1	C_2	C_3	C_1	C_2	C_3		
Cs4vs1	-4.29	-0.09	-0.03	1.25	-0.33	1.04	-5.36	0.03	-0.03	-5.3	-5.1
Cs4vs2	-0.08	-4.00	-0.08	1.18	-0.38	1.18	-0.10	1.51	-0.10	1.3	1.6
Cs4vsmid2	-0.91	-0.30	-0.91	1.17	-0.35	1.17	-1.07	0.01	-1.07	-2.0	0.2
Cs4vsmid	-0.64	-1.87	-0.64	1.18	-0.37	1.18	-0.75	0.68	-0.75	-0.8	0.9
Cs4vsmidH	0.04	-2.85	0.04	1.18	-0.37	1.18	0.04	1.05	0.04	1.1	0.9

(1) Considering only the through-space interactions

For the orientations **Cs4vsmid2** and **Cs4vsmid** the multiplicity of the ground state estimated with CASVB is a triplet ($\Delta E^{S-T} > 0$, Table 5.8). However, the approximation $\sum J_{ij}\Delta P_{ij}^{S-T}$ estimates a preference for the singlet ($\sum J_{ij}\Delta P_{ij}^{S-T} < 0$, Table 5.8). This inconsistency can be due to the existence of other interactions not included in the active space selected, since we have considered only the intermolecular through-space π - π interactions in the $\sum J_{ij}\Delta P_{ij}^{S-T}$ calculations. Let us remind here that the interaction of methyl with the central allyl C atom (C_2) favors the high-spin state, while the contacts with the lateral C atoms (C_1, C_3) has preference for low-spin state.

The J_{ij} exchange coupling are mostly negative for the through-space ij interactions considered (Table 5.8) and highly dependent on the distance between the interacting atoms. In the **Cs4vs1**, the major contribution to the energy gap comes from the methyl and the lateral allyl C_1 atom on which the methyl is placed ($C_{\text{methyl}} - C_1$ in Table 5.8). This main interaction stabilizes the singlet. For **Cs4vs2** and **Cs4vsmidH** the main contribution comes from the methyl and the central allyl C atom ($C_{\text{methyl}} - C_2$ in Table 5.8). For this interaction, the product $J_{ij}\Delta P_{ij}$ ($i = \text{methyl}, j = C_2\text{-allyl}$) is positive, which implies the stabilization of the triplet. The most important contributions for **Cs4vsmid2** and **Cs4vsmid** orientations are the interactions of the methyl C atom with the lateral allyl C atoms and, as mentioned, these contributions stabilize the singlet state (Table 5.8). However, the energy CASVB calculations indicated that the triplet state is slightly lower in energy ($\Delta E^{S-T} > 0$ in Table 5.8), which, as mentioned, implies that there must be other ij interactions not taken into account in the selected π orbitals active space that contribute to the stabilization of the triplet state.

As a conclusion, it could be said that McConnell-I theory is valid only when there is a clear preferential interaction among all the possible ones. This method has to be applied carefully, taking into account the arrangement of the interacting molecules, because small variations in the geometrical distribution of two radicals can result in different ground state spin multiplicity.

5.2.3.2 Methyl-allyl interaction as a function of the intermolecular angle α

In the previous section, the methyl and allyl radicals were placed on parallel planes and the intermolecular interactions considered were the $\pi - \pi$ stacking interaction through the SOMO orbitals of each molecule. When the two radicals change their relative orientation as a function of an angle α , the orientation of the active orbitals varies. In this section we analyzed the interaction between methyl and allyl radicals vs the angle α , and how the preference for a high or low-spin state changes with the angle (Figure 5.24²⁵). Accordingly, within the $0^\circ - 20^\circ$ and $130^\circ - 150^\circ$ range, the ground state is a singlet; otherwise, the triplet is favored. The study was performed at CAS(4,4)/6-31g(d) level.

As it has been discussed before, the energy gap can be partitioned into the different contributions that represent the interaction between the ij active orbitals from methyl (i) and allyl (j) [equation (5.2)]. At 45° and 90° , the interaction between the methyl C atom and central allyl carbon atom (C_2) is the main contribution to the energy gap. This interaction, with $J_{ij} < 0$ and $\Delta P_{ij}^{S-T} < 0$, favors the stabilization of the high-spin state ($\sum J_{ij}^T \Delta P_{ij}^{S-T} > 0$ in Table 5.9). Contrarily, at 135° , the interactions of the methyl C atom with both lateral allyl C

atoms are the main contributions to the energy gap, with $J_{ij} < 0$ and $\Delta P_{ij}^{S-T} > 0$, which results in a ground state with low multiplicity ($\sum J_{ij}^T \Delta P_{ij}^{S-T} < 0$ in Table 5.9).

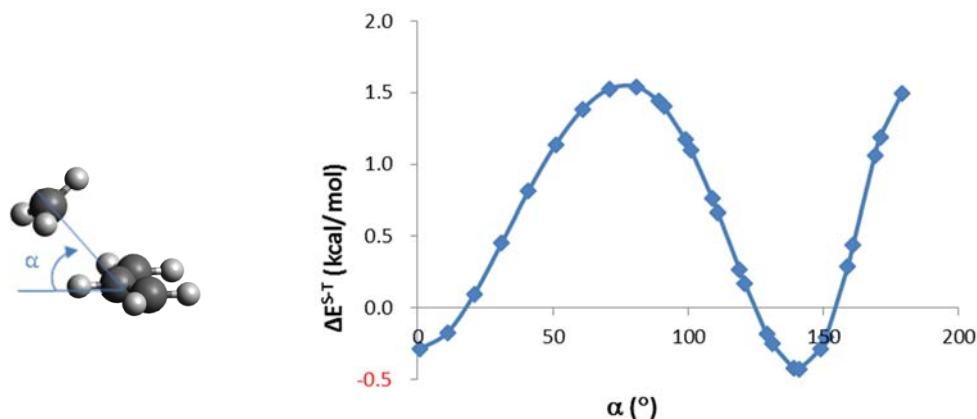


Figure 5.24 Values of the energy gap ΔE^{S-T} (in kcal/mol) with a methyl...allyl intermolecular distance of 3 Å calculated at CAS(4,4)/6-31g(d) level.

Table 5.9 Values of J_{ij}^T , ΔP_{ij}^{S-T} , $\sum J_{ij}^T \Delta P_{ij}^{S-T}$ and ΔE^{S-T} , calculated at CASSCF(4,4)/6-31g(d) level at a fixed intermolecular methyl...allyl distance $r = 3$ Å.

	J_{ij}^T kcal/mol			ΔP_{ij}^{S-T} kcal/mol			$\sum J_{ij}^T \Delta P_{ij}^{S-T}$ kcal/mol (1)	ΔE^{S-T} kcal/mol
	C_1	C_2	C_3	C_1	C_2	C_3		
0°	0.000	0.000	0.000	1.173	-0.345	1.173	0.0	-0.3
45°	-0.048	-3.853	-0.048	1.181	-0.369	1.181	1.3	1.0
90°	-0.085	-3.998	-0.085	1.184	-0.38	1.184	1.3	1.4
135°	-2.564	-0.106	-2.564	1.164	-0.347	1.164	-5.9	-0.4
180°	0.000	0.000	0.000	1.178	-0.356	1.178	0.0	1.4

(1) Only considering the through-space interactions

Similar results are obtained with MMVB calculations (Table 5.10). The preferred interaction at angles within the 10° - 90° range (20° - 120° in CAS calculations) is between the methyl carbon atom and the allyl central carbon C_2 atom, which stabilizes the triplet as a ground state ($\Delta E^{S-T} > 0$). The fundamental state at 100° - 170° angles (130° - 150° in CAS calculations) is a singlet ($\Delta E^{S-T} < 0$), and the main contributions are the interactions of the methyl carbon atom with the two lateral allyl carbon atoms (C_1 and C_3). There is no discrepancy between the energy gap calculated as ΔE^{S-T} and $\sum J_{ij}^T \Delta P_{ij}^{S-T}$ in MMVB since both are equivalent.

When compared to CASSCF, it is noticed that MMVB cannot evaluate properly some interactions. MMVB underestimates the interactions that cannot compute correctly, as the interaction involving orbitals that are perpendicular, and overestimates those involving the

orbitals that constitute the active space. That results in a discrepancy between the CASSCF and MMVB results when determining the spin multiplicity of the ground state in some cases.

Table 5.10 Values of J_{ij}^T , ΔP_{ij}^{S-T} , $\Sigma J_{ij}^T \Delta P_{ij}^{S-T}$ and ΔE^{S-T} calculated with MMVB at a fixed intermolecular distance $r = 3 \text{ \AA}$.

α	J_{ij}^T kcal/mol			ΔP_{ij}^{S-T} kcal/mol			$\Sigma J_{ij}^T \Delta P_{ij}^{S-T}$ kcal/mol	ΔE^{S-T} kcal/mol
	C_1	C_2	C_3	C_1	C_2	C_3		
0°	0.000	0.000	0.000	1.333	-0.667	1.333	0.0	0.0
11°	0.000	-0.282	0.000	1.335	-0.67	1.335	0.2	0.2
45°	-0.075	-2.297	-0.075	1.348	-0.697	1.348	1.4	1.4
61°	-0.207	-3.037	-0.207	1.352	-0.705	1.352	1.6	1.5
81°	-0.615	-3.545	-0.615	1.352	-0.705	1.352	0.8	0.8
90°	-0.935	-3.602	-0.935	1.352	-0.705	1.352	0.0	0.0
101°	-1.450	-3.520	-1.450	1.348	-0.697	1.348	-1.5	-1.5
131°	-3.075	-2.510	-3.075	1.329	-0.659	1.329	-6.5	-6.5
151°	-2.993	-1.343	-2.993	1.322	-0.644	1.322	-7.0	-7.1
171°	-0.809	-0.195	-0.809	1.329	-0.659	1.329	-2.0	-2.0
180°	0.000	0.000	0.000	1.333	-0.667	1.333	0.0	0.0

The preference for the singlet state at 0° calculated at CASSCF level ($\Delta E^{S-T} = -0.3 \text{ kcal/mol}$) is neither observed in the $\Sigma J_{ij}^T \Delta P_{ij}^{S-T}$ (0.0 kcal/mol) nor MMVB analysis. The plane that contains the methyl radical is perpendicular to the allyl plane at 0° and, accordingly the p_z -methyl active orbital is perpendicular to the p_z -allyl orbitals. Consequently, all J_{ij} parameters for $i \in p_z$ -methyl and $j \in p_z$ -allyl orbitals are zero. The main intermolecular interaction at 0° is expected to take place between the p_z -methyl orbital and a σ -like allyl orbital close to the methyl. We believe that this interaction can stabilize the singlet. However, it is neither considered in $\Sigma J_{ij}^T \Delta P_{ij}^{S-T}$ nor in MMVB calculations.

At 90° the triplet state is lower in energy in CASSCF calculations ($\Delta E^{S-T} = 1.4 \text{ kcal/mol}$ in Table 5.9). On the contrary, MMVB estimates that both states singlet and triplet are quasi-degenerated (Table 5.10). As for J_{ij} , the value of the exchange interaction between the methyl carbon atom and the allyl lateral carbon atoms (C_1 and C_3) is much higher at MMVB level than at CASSCF (-0.935 kcal/cal vs -0.085 kcal/cal). The larger value of J_{ij} at MMVB level gives more weight to these interactions, counterbalancing the through-space contribution of the central allyl carbon atom and establishing a quasi-degeneracy of the triplet and singlet states. In CASSCF calculations, the preferred interaction takes place between the methyl and the allyl central C atom that stabilizes the triplet.

At 180° the triplet is lower in energy in CASSCF calculations ($\Delta E^{S-T} = 1.4 \text{ kcal/mol}$). As for the 90° case, both singlet and triplet states have the same energy when estimated with $\Sigma J_{ij}^T \Delta P_{ij}^{S-T}$ and MMVB methods. At 180° , all intermolecular ij interactions have exchange integral values equal to zero ($i \in p_z$ -methyl and $j \in p_z$ -allyl orbitals) using either MMVB or

$\sum J_{ij}^T \Delta P_{ij}^{S-T}$ approaches. Consequently these two methods cannot describe correctly this intermolecular interaction and the multiplicity of the ground state is not described properly.

To sum up, the study of the methyl-allyl interaction on parallel planes uncovers that the preferred orientation of two radicals with unpaired electrons in π -orbitals should be **Cs4vs2** or **CsvsmidH** to show FM coupling. Besides, the study of this interaction as a function of the intermolecular angle shows that angles ranging from 20° to 120° ensure the FM interaction of the spins of the free electrons.

5.2.4 Analysis of the interaction between two allyl-allyl radicals





The study can be extended to more complex bimolecular systems, such as the interaction of two allyl radicals. We performed a similar analysis for the interaction of two allyl-allyl radicals: (1) coplanar, (2) placed on parallel planes, and (3) orienting them at different angles.

The calculations of the energy of the different states, and the P_{ij} and J_{ij} parameter, were carried out with MMVB and CAS(n,n)/6-31g(d), being i,j the active orbital where the unpaired electrons are located.

5.2.4.1 Allyl...allyl interaction. Spin multiplicity dependence on molecular arrangement: two coplanar allyls vs. allyl radicals on parallel planes

For the different orientation of two coplanar allyl radicals, namely **pIC**, **pIC2**, **pICC** and **pICC2**, the ground state was found to be a singlet or practically degenerated with the triplet (Table 5.11).

Table 5.11 ΔE^{S-T} calculated according at CASVB/6-31g(d) level for two coplanar allyl radicals using an intermolecular distance of 3 Å.

	ΔE^{S-T} kcal/mol
pIC 	-0.0
pIC2 	-0.9
pICC 	-0.9
pICC2 	-7.0

Another study included systems constituted by two allyl radicals placed on parallel planes with a fixed distance between planes of 3 Å at different orientations. The orientations studied were **FMa**, **FMb**, **AFMa**, **AFMb**, **AFM_1**, **AFM_2**, **Center-cis** and **Center-trans**, as shown in Figure 5.25. The intermolecular interactions were ferromagnetic (FM) only in two cases: **FMa** and **FMb** (Table 5.12, $\Delta E^{S-T} > 0$). The intermolecular interaction for all the other orientations (**AFMa**, **AFMb**, **AFM_1**, **AFM_2**, **Center-cis** and **Center-trans**) was preferably antiferromagnetic (AFM) and the singlet was more stable than the triplet (Table 5.12, $\Delta E^{S-T} < 0$). The systems found to be ferromagnetic, **FMa** and **FMb**, have been discussed previously in the literature²⁶.

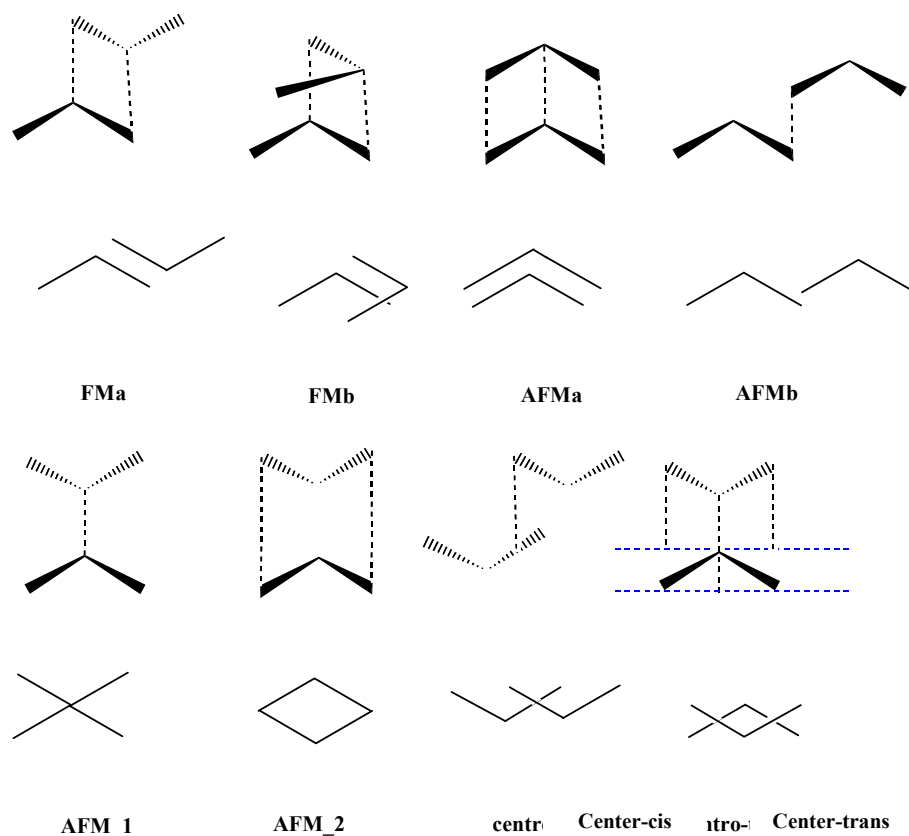


Figure 5.25 Several orientations between two allyl molecules on parallel planes.

Table 5.12 Energy gap ΔE^{S-T} calculated according to CASVB(6,6)/6-31g(d) for two allyl radicals placed on parallel planes with an intermolecular distance $r = 3$ Å.

	ΔE^{S-T} kcal/mol
FMa	0.6
FMb	1.0
AFMa	-11.5
AFMb	-2.0
AFM_1	-4.5
AFM_2	-11.4
centro_cis	-0.3
centro_trans	-9.1

As discussed previously, if we consider that the main contributions to the multiplicity of the ground states are the through-space intermolecular interactions between the two allyl molecules (assuming that the molecules and the intramolecular interactions do not vary significantly among the singlet and triplet states), the energy gap between the singlet and the triplet can be approximated as the sum of the interaction between the carbon p_z -orbitals of one allyl with the carbon p_z -orbitals of the other allyl molecule, being the carbon p_z -orbitals the ij active space [equation (5.9)].

$$\begin{aligned} \Delta E^{S-T} &= \sum_{\substack{i \in \text{allyl1} \\ j \in \text{allyl2}}} \Delta(J_{ij} P_{ij})^{S-T} = \\ &= \Delta(J_{ij} P_{ij})^{C_{lateral}^{allyl1} - C_{lateral}^{allyl2}} + \Delta(J_{ij} P_{ij})^{C_{lateral}^{allyl1} - C_{central}^{allyl2}} + \Delta(J_{ij} P_{ij})^{C_{lateral}^{allyl1} - C_{lateral}^{allyl2}} + \\ &+ \Delta(J_{ij} P_{ij})^{C_{central}^{allyl1} - C_{lateral}^{allyl2}} + \Delta(J_{ij} P_{ij})^{C_{central}^{allyl1} - C_{central}^{allyl2}} + \Delta(J_{ij} P_{ij})^{C_{central}^{allyl1} - C_{lateral}^{allyl2}} + \\ &+ \Delta(J_{ij} P_{ij})^{C_{lateral}^{allyl1} - C_{lateral}^{allyl2}} + \Delta(J_{ij} P_{ij})^{C_{lateral}^{allyl1} - C_{central}^{allyl2}} + \Delta(J_{ij} P_{ij})^{C_{lateral}^{allyl1} - C_{lateral}^{allyl2}} \end{aligned} \quad (5.9)$$

To exemplify McConnell-I theory, we selected two orientations **FMa** and **AFM_1**, which represent two types of interactions with different spin multiplicity preference. In both **FMa** and **AFM_1** the allyl molecules are placed on parallel planes and the intermolecular interaction takes place between the p_z orbitals of one radical with the p_z orbitals of the other, with negligible contributions from other crossed interactions.

As previously discussed, McConnell-I theory is expected to predict correctly the spin multiplicity of two radicals placed on parallel planes with well-defined intermolecular interactions. In such a case, we have concluded that McConnell-I model can be assessed by MMVB methodology. Therefore, we have used MMVB to describe the spin state preference for orientations **FMa** and **AFM_1** and evaluate the validity of McConnell-I model.

The matrix of ΔP_{ij} values is equivalent for both orientations (Table 5.13). Therefore, it is expected that the J_{ij} parameter will determine the predominant contributions to the energy gap, and, consequently, the preference for the high or low-spin ground state.

Table 5.13 ΔP_{ij}^{S-T} values between two allyl molecules calculated with MMVB for the orientations **FMa** and **AFM_1**.

		ΔP_{ij}^{S-T} MMVB		
		C_1^1	C_2^1	C_3^1
FMa	C_1^2	0.903	-0.471	0.908
	C_2^2	-0.471	0.234	-0.462
	C_3^2	0.908	-0.462	0.911
AFM_1	C_1^2	0.883	-0.438	0.882
	C_2^2	-0.438	0.222	-0.438
	C_3^2	0.882	-0.438	0.883

The J_{ij} values obtained for the two analyzed systems, namely **FMa** and **AFM_1** can be considered practically equivalent in both singlet and triplet states (Figure 5.26). The J_{ij}

values that are significantly different from zero in **FMa** are the exchange coupling between $C_2^1(\text{allyl1})-C_1^2(\text{allyl2})$ and $C_3^1(\text{allyl1})-C_2^2(\text{allyl2})$. Consequently, these will be the main contributors to the **FMa** energy gap (Figure 5.26). For **AFM_1** there is only one J_{ij} value to be considered, that is between the two central C atoms of both allyl molecules $C_2^1(\text{allyl1})-C_2^2(\text{allyl2})$ [**AFM_1** in Figure 5.26].

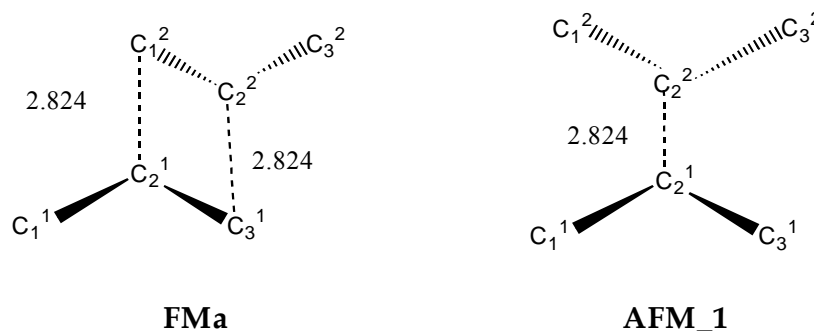


Figure 5.26 J_{ij} values in kcal/mol between the closest atoms in space for **FMa** and **AFM_1** allyl...allyl orientations.

The equation (5.9) can be simplified to the contributions of those interactions which have a parameter J_{ij} with values significantly different from zero [equation (5.10) for **FMa** and equation (5.11) for **AFM_1**]

$$\Delta E^{S-T}(\text{FMa}) = J_{ij}(\Delta P_{ij}^{C_{lateral}^{allyl1}-C_{central}^{allyl2}} + \Delta P_{ij}^{C_{central}^{allyl1}-C_{lateral}^{allyl2}}) \quad (5.10)$$

$$\Delta E^{S-T}(\text{AFM}_1) = J_{ij}\Delta P_{ij}^{C_{central}^{allyl1}-C_{central}^{allyl2}} \quad (5.11)$$

By means of the ΔP_{ij} values (Table 5.13) together with the values of the J_{ij} interaction between the C active centers (Figure 5.26), the energy gap can be estimated using equation (5.10) for **FMa** and equation (5.11) for **AFM_1**.

The results calculated as $\sum J_{ij}\Delta P_{ij}^{S-T}$, considering only the main ij intermolecular contributions, agree with those calculated as $\Delta E^{S-T}(\text{MMVB})$ [Table 5.14]. These values are of the same sign than the $\Delta E^{S-T}(\text{CAS})$ although slightly different in magnitude. The energy gap estimated as $\sum J_{ij}\Delta P_{ij}^{S-T}$ calculates correctly the spin multiplicity of the ground state. However, it does not consider other interactions that contribute to the final magnitude of the energy gap.

Table 5.14 Energy gap ΔE^{S-T} between the singlet and triplet states for the interaction between two allyl molecules with CAS, MMVB and $\sum J_{ij}\Delta P_{ij}^{S-T}$ for the orientations **FMa** and **AFM_1**.

	ΔE^{S-T} CAS kcal/mol	ΔE^{S-T} MMVB kcal/mol	$\sum J_{ij}\Delta P_{ij}^{S-T}$ MMVB kcal/mol
FMa	0.6	2.6	2.6
AFM_1	-4.5	-0.6	-0.6

5.2.4.2 Allyl...allyl interaction. Spin multiplicity dependence on the angular relative orientation

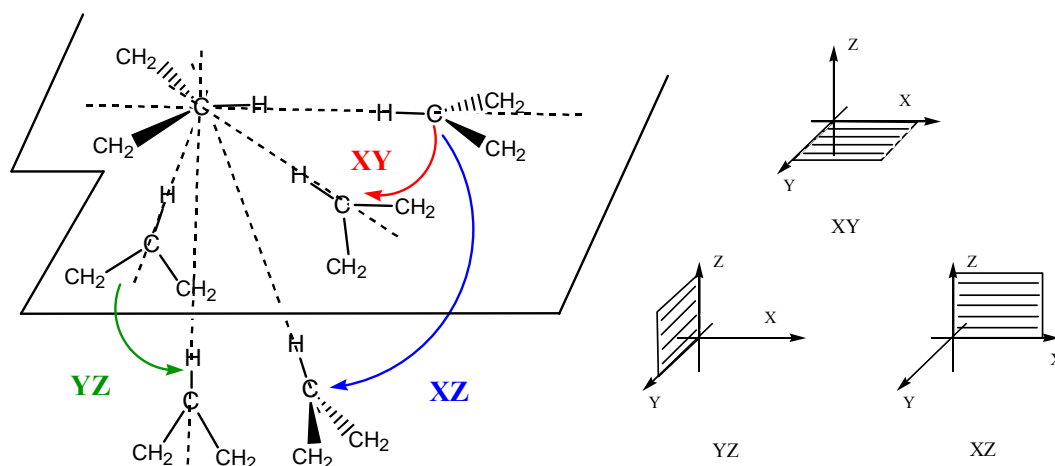


Figure 5.27 Orientation between two allyl molecules along the paths XY, XZ and YZ.

The analysis of the interaction between two allyl radicals at different angular orientations along the paths within planes XY, XZ and YZ (Figure 5.27) reveals several areas where the ferromagnetic interaction is preferred. The preference for the high-spin state in the **XY** orientations is observed at angles $> 60^\circ$ (Figure 5.28). Within **XZ**-plane, both states are practically degenerated at all the studied angles (Figure 5.28). Finally, for the **YZ**-plane, the intermolecular interaction is ferromagnetic at angles $< 20^\circ$ and $> 60^\circ$ (Figure 5.28).

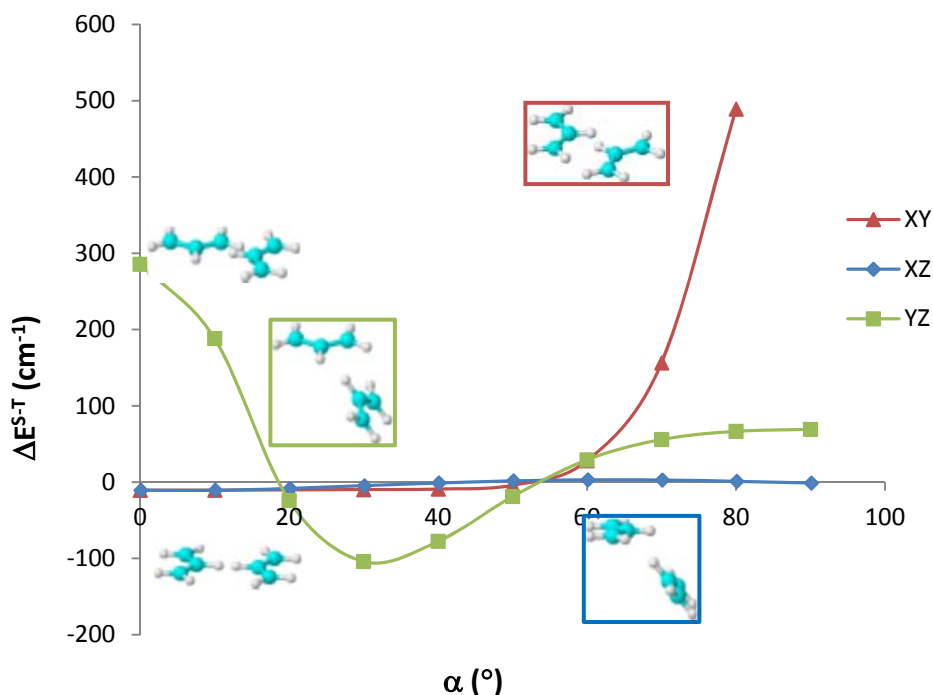


Figure 5.28 Energy gap ΔE^{S-T} (cm^{-1}) between the singlet and the triplet state calculated at CAS(6,6)/6-31g(d) level for the interaction between two allyl molecules along the paths XY, XZ and YZ.

The active space of the systems is constituted by the highest occupied molecular orbital (HOMO) and the singly-occupied molecular orbital (SOMO) of each allyl molecule (Figure 5.29).

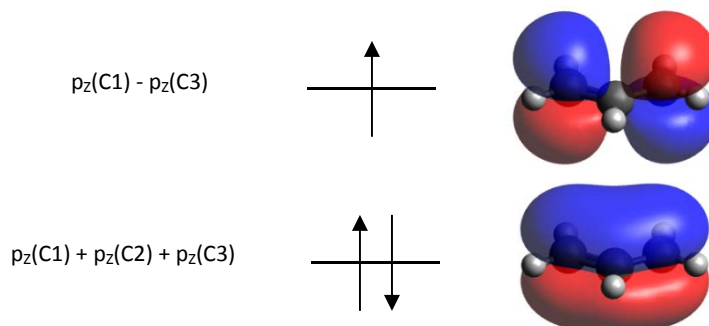


Figure 5.29 Allyl highest fully occupied orbital (HOMO) and SOMO orbitals.

Projecting the active MOs into a VB space where each carbon atom is an active center, the active space is constituted by all the p_z -orbitals of the carbon atoms of both molecules. The energy gap can be then partitioned as the contributions of all the ij intermolecular interactions [equation (5.12)] where ij are the active carbon p_z -orbitals of both allyl radicals.

$$\Delta E^{S-T} = \sum_{\substack{i \in \text{allyl1} \\ j \in \text{allyl2}}} J_{ij} \Delta P_{ij}^{S-T} \quad (5.12)$$

As discussed previously, the energy gap between the singlet and the triplet states, ΔE^{S-T} , can be estimated from the parameters J_{ij} and P_{ij} as $J_{ij}^T \Delta P_{ij}^{S-T}$ using MMVB and CASVB(6,6) methods. In all the orientations the matrix of ΔP_{ij} values is equivalent: $\Delta P_{C1^1-C1^2} \approx \Delta P_{C1^1-C3^2} \approx \Delta P_{C3^1-C1^2} \approx \Delta P_{C3^1-C3^2} \approx 0.9$, $\Delta P_{C2^1-C2^2} \approx 0.2$, $\Delta P_{C2^1-C1^2} \approx -0.5$ (Table 5.15). The multiplicity of the ground state will be then defined by the interaction with higher J_{ij} value.

Table 5.15 Values ΔP_{ij}^{S-T} for i and j the p_z orbitals of the carbon atoms of the two allyl molecules.

	ΔP_{ij}^{S-T} MMVB		
	C_1^1	C_2^1	C_3^1
C_1^2	0.9	-0.5	0.9
C_2^2	-0.5	0.2	-0.5
C_3^2	0.9	-0.5	0.9

In the orientations **XY** both states singlet and triplet are practically degenerated at angles $< 60^\circ$ (Figure 5.28). The triplet starts to be more stable at $\alpha > 60^\circ$. However, at 90° , the two molecules are too close. Thus, there is a stereochemical repulsion and, in turn, the CASSCF calculations do not converge (Table 5.16). Nevertheless, we performed single point MMVB and CASVB calculations to study the interaction in this forced orientation. It is observed that

the exchange integrals J_{ij} for the interactions between ij orbitals considered in the active space are practically zero at angles $< 60^\circ$, and consequently, both the low and high-spin states are virtually degenerated (Table 5.17). The value of the interaction integral $J_{C_2^1-C_1^2}$ between the central C atoms of both allyl radicals (C_2^1 - C_2^2) increases with the angle α , becoming the predominant interaction at $\alpha > 60^\circ$. The positive value of the contribution C_2^1 - C_1^2 , $J_{ij}^T \Delta P_{ij}^{S-T} > 0$, defines the triplet as a ground state for angles $\alpha > 60^\circ$.

Table 5.16 Values of ΔE^{S-T} and $\Sigma J_{ij}^T \Delta P_{ij}^{S-T}$ in cm^{-1} , calculated with MMVB and CASVB(6,6) for the angles 0° - 30° - 60° - 80° - 90° between two allyl molecules along the **XY**-plane.

	ΔE^{S-T} CAS cm^{-1}	ΔE^{S-T} MMVB cm^{-1}	$\Sigma J_{ij}^T \Delta P_{ij}^{S-T}$ MMVB cm^{-1}	ΔE^{S-T} CASVB cm^{-1}	$\Sigma J_{ij}^T \Delta P_{ij}^{S-T}$ CASVB cm^{-1}
0°	-10.6	-8.0	-3.9	-17.6	-12.8
30°	-9.7	-8.2	-2.4	-19.3	-9.3
60°	28.2	45.5	57.3	15.6	138.8
90°	489.2 (80°)	1333.6	1662.7	1366.9	1799.6

Table 5.17 Values of $J_{ij}^T \Delta P_{ij}^{S-T}$ in cm^{-1} , calculated with MMVB and CASVB(6,6) for the angles 0° - 30° - 60° - 90° between two allyl molecules along the **XY**-plane.

		$J_{ij}^T \Delta P_{ij}^{S-T}$ MMVB cm^{-1}			$J_{ij}^T \Delta P_{ij}^{S-T}$ CASVB cm^{-1}		
		C_1^1	C_2^1	C_3^1	C_1^1	C_2^1	C_3^1
0°	C_1^2	0.0	1.0	0.0	0.6	2.5	-0.9
	C_2^2	1.0	-7.8	1.0	2.5	-22.3	2.5
	C_3^2	0.0	1.0	0.0	-1.0	2.5	0.6
30°	C_1^2	-2.0	4.9	0.0	-8.9	4.3	3.4
	C_2^2	1.0	-8.3	1.0	1.5	-18.4	5.9
	C_3^2	0.0	1.0	0.0	0.0	3.1	-0.3
60°	C_1^2	-99.7	209.8	-42.9	-5.7	212.7	-75.2
	C_2^2	4.9	-18.8	2.0	19.6	-5.1	0.2
	C_3^2	0.0	2.0	0.0	-3.8	-2.1	-1.8
90°	C_1^2	-1071.6	3327.2	-482.6	-45.2	2209.7	-348.8
	C_2^2	28.2	-142.5	2.9	18.6	-39.7	16.6
	C_3^2	0.0	1.1	0.0	-12.2	10.7	-10.1

The angular variation of the two allyl radicals on the **XZ**-plane starts on the same point as the previous **XY** curve. At all studied angles between 0° – 90° the J_{ij} parameters are practically zero. Consequently, singlet and triplet states are essentially degenerate for all studied points (Figure 5.28).

The initial point on the **YZ**-plane ($\alpha = 0^\circ$) corresponds to a **XY** orientations at $\alpha = 75^\circ$. This structure has been seen to have a triplet ground state (Table 5.18). Along this path and similarly as in the previous case, the active orbitals interact varying not only their position,

but also their interaction angle. At the initial point, $\alpha = 0^\circ$, the main contribution between C_{central} of the allyl₁ and the C_{lateral} of the allyl₂ favors the triplet as ground state (Table 5.19). At 30° the ground state is the singlet, defined as a result of two negative contributions C_2^1 - C_2^2 and C_1^1 - C_1^2 that overcome the positive contribution C_2^1 - C_1^2 (Table 5.19). At 60° and 90° the positive contribution C_2^1 - C_1^2 determines the spin preference for the triplet in the ground state. At $\alpha = 90^\circ$, given the symmetry of the system, a similar value for the interaction C_2^1 - C_3^2 will contribute to the stabilization of the high-spin state.

Table 5.18 Values of ΔE^{S-T} and $\sum J_{ij}^T \Delta P_{ij}^{S-T}$ in cm^{-1} , calculated with MMVB and CASVB (6,6) for the angles 0° - 30° - 60° - 90° between two allyl molecules along the YZ-plane.

	ΔE^{S-T} CAS cm^{-1}	ΔE^{S-T} MMVB cm^{-1}	$\sum J_{ij}^T \Delta P_{ij}^{S-T}$ MMVB cm^{-1}	ΔE^{S-T} CASVB cm^{-1}	$\sum J_{ij}^T \Delta P_{ij}^{S-T}$ CASVB cm^{-1}
0°	285.7	271.4	305.8	314.6	599.1
30°	-104.0	-6.2	-9.3	-100.2	-26.0
60°	29.3	43.7	46.3	30.7	86.3
90°	69.1	25.4	12.7	75.5	39.7

Table 5.19 Values of $\sum J_{ij}^T \Delta P_{ij}^{S-T}$ in cm^{-1} , calculated with MMVB and CASVB(6,6) for the angles 0° - 30° - 60° - 90° between two allyl molecules along the YZ-plane.

		$\sum J_{ij}^T \Delta P_{ij}^{S-T}$ MMVB cm^{-1}			$\sum J_{ij}^T \Delta P_{ij}^{S-T}$ CASVB cm^{-1}		
		C_1^1	C_2^1	C_3^1	C_1^1	C_2^1	C_3^1
0°	C_1^2	-442.4	963.3	-179.2	-166.3	834.4	-72.0
	C_2^2	14.9	-54.8	2.0	3.6	-8.0	26.3
	C_3^2	0.0	2.0	0.0	-5.7	0.1	-13.2
30°	C_1^2	-9.8	3.9	0.0	1.4	9.3	-16.9
	C_2^2	1.0	-6.3	1.0	-0.6	-7.2	5.8
	C_3^2	0.0	1.0	0.0	0.2	0.7	-18.8
60°	C_1^2	-46.9	123.9	-25.3	-0.7	124.5	-24.4
	C_2^2	2.0	-8.3	0.0	0.7	-12.3	1.4
	C_3^2	0.0	1.0	0.0	-0.7	-0.7	-1.6
90°	C_1^2	-3.9	12.7	-2.0	-0.2	30.1	-10.1
	C_2^2	0.0	-1.0	0.0	0.4	-0.9	0.7
	C_3^2	-3.9	12.7	-2.0	-0.2	30.0	-10.1

After this analysis we can conclude that the relative orientation of the radicals is crucial in defining the nature, ferromagnetic or antiferromagnetic, of the interaction. Therefore, when designing magnetic molecular crystals, it would be advisable to make a preliminary study to describe the types of interaction at different orientations and define which one will favor a given magnetic behavior. When the interacting radicals are located in parallel planes, the orientation that favors the FM interaction between the radical centers with opposite spin densities is preferred, according to McConnell-I theory. On the other hand, if both radicals are placed so that there is an angular alignment between the planes that contain them, the

FM interaction is favored when the overlap is minimized and the exchange interaction $J_{ij} > 0$ is maximized between the molecular orbitals containing the unpaired electrons.

McConnell-I theory and MMVB should not be used to establish the spin multiplicity in systems where the radicals are not oriented on parallel planes and/or there are different possible interactions between the radical centers. These two methodologies underestimate contributions that are critical in the characterization of the spin multiplicity of the ground state in these cases.

5.3 Conclusions

Using Bader's Atoms In Molecules (AIM)⁴ methodology we assessed whether the only presence of intermolecular Bond Critical Points (BCP) could characterize the stabilization of intermolecular interactions. We observed that the topological features of the electronic density identify weak intermolecular interactions like hydrogen bonds or van der Waals interactions. However it has been seen that the presence of bond critical points (BCP) between two molecules is a necessary condition for the existence of intermolecular interactions but not sufficient to define whether it is attractive. An energetic study of the interactions must accompany the AIMs description of the intermolecular connections to be able to define the intermolecular stabilization.

Additionally, we evaluated Mc-Connell methodology in a systematic characterization of the interaction between two radicals at different spatial orientations. The results from these investigations illustrate that there are optimal spatial orientations that favor the ferromagnetic interaction between the molecules depending on their molecular characteristics. However, the frontier between the ferromagnetic and antiferromagnetic coupling is very subtle. Therefore, each case should be analyzed carefully to determine the ferromagnetic character of the interaction.

Bibliography

- (1) Rovira, C.; Veciana, J. *CrystEngComm* **2009**, *11* (10), 2031–2031.
- (2) Novoa, J. J.; Deumal, M.; Veciana, J. *Synth. Met.* **1999**, *103* (1), 2283–2286.
- (3) Veciana, J.; Cirujeda, J.; Hernández, E.; Rovira, C.; Molins, E.; Mas, M.; Stanger, J. L.; Turek, P. *Inst. Electr. Electron. Eng.* **1994**, 262–272.
- (4) Bader, R. F. W. *Atoms in Molecules*, Clarendon; Oxford, 1990.
- (5) Chen, W.; Wong, M. W.; Andres, J. L.; Head-Gordon, M.; Replogle, E. S.; Pople, J. A. *Inc Pittsburgh PA* **1998**.
- (6) Møller, C.; Plesset, M. S. *Phys. Rev.* **1934**, *46* (7), 618–622.
- (7) Head-Gordon, M.; Pople, J. A.; Frisch, M. J. *Chem. Phys. Lett.* **1988**, *153* (6), 503–506.
- (8) Sæbø, S.; Almlöf, J. *Chem. Phys. Lett.* **1989**, *154* (1), 83–89.
- (9) Frisch, M. J.; Head-Gordon, M.; Pople, J. A. *Chem. Phys. Lett.* **1990**, *166* (3), 281–289.
- (10) Head-Gordon, M.; Head-Gordon, T. *Chem. Phys. Lett.* **1994**, *220* (1), 122–128.
- (11) Matta, C. F.; Boyd, R. J. In *The Quantum Theory of Atoms in Molecules*; F. tta, C., Boyd, R. J., Eds.; Wiley-VCH Verlag GmbH & Co. KGaA, 2007; pp 1–34.
- (12) Espinosa, E.; Alkorta, I.; Elguero, J.; Molins, E. *J. Chem. Phys.* **2002**, *117* (12), 5529–5542.
- (13) Haaland, A.; Shorokhov, D. J.; Tverdova, N. V. *Chem. Weinh. Bergstr. Ger.* **2004**, *10* (18), 4416–4421.
- (14) McConnell, H. M. *J. Chem. Phys.* **1963**, *39* (7), 1910–1910.
- (15) Yamaguchi, K.; Fueno, T.; Nakasuji, K.; Murata, I. *Chem. Lett.* **1986**, *15* (4), 629–632.
- (16) Yamaguchi, K.; Toyoda, Y.; Fueno, T. *Chem. Phys. Lett.* **1989**, *159* (5), 459–464.
- (17) Tanaka, K.; Takeuchi, T.; Yoshizawa, K.; Toriumi, M.; Yamabe, T. *Synth. Met.* **1991**, *44* (1), 1–8.
- (18) Kahn, O. *Molecular Magnetism*; VCH Publishers, Inc. (USA), 1993.
- (19) Kollmar, C.; Kahn, O. *J. Am. Chem. Soc.* **1991**, *113* (21), 7987–7994.
- (20) Caneschi, A.; Gatteschi, D.; Sessoli, R.; Rey, P. *Acc. Chem. Res.* **1989**, *22* (11), 392–398.
- (21) Yoshizawa, K.; Hoffmann, R. *J. Am. Chem. Soc.* **1995**, *117* (26), 6921–6926.
- (22) Saito, T.; Ito, A.; Watanabe, T.; Kawakami, T.; Okumura, M.; Yamaguchi, K. *Chem. Phys. Lett.* **2012**, *542*, 19–25.
- (23) Yamaguchi, K.; Okumura, M.; Maki, J.; Noro, T.; Namimoto, H.; Nakano, M.; Fueno, T.; Nakasuji, K. *Chem. Phys. Lett.* **1992**, *190* (3–4), 353–360.
- (24) Deumal, M.; Novoa, J. J.; Bearpark, M. J.; Celani, P.; Olivucci, M.; Robb, M. A. *J. Phys. Chem. A* **1998**, *102* (43), 8404–8412.
- (25) Deumal i Solé, Mercè. *Estudi Teòric del magnetisme en cristalls moleculars: Mecanismes d'interacció i empaquetament.*, Universitat de Barcelona: Barcelona, 1999.
- (26) Lahti, P. M. *Magnetic Properties of Organic Materials*; CRC Press, 1999.

CHAPTER 6

CRYSTAL PACKING IN MOLECULAR MAGNETISM

6 Crystal packing in molecular magnetism

In the previous two chapters, we have described and evaluated the tools to understand how molecules stabilize high-spin ground states and which spatial orientations favor the ferromagnetic interaction between these molecules. In this chapter, these tools have been used to study the interactions between the molecules that constitute real crystals.

Using a fragment based analysis, we studied the intermolecular interactions within two real crystals (HNOBEN¹ and YIMWIA²) to identify the contacts that stabilize the structure of the macroscopic state.

Furthermore, we evaluated the possible magneto-structural relationships in a group of α -nitronyl nitroxide crystals analyzing the spatial orientation of the constitutive molecules versus the ground state spin multiplicity.

6.1 Crystal packing: study of HNOBEN and YIMWIA crystals

Molecular crystals so-called HNOBEN¹ and YIMWIA² are constituted by molecular units that are repeated in the space. The crystal HNOBEN is based on a single molecule, hexanitrobenzene, HNOBEN (Figure 6.1a). On the other hand, crystal YIMWIA structure is based on two different molecules: trimethyl isocyanurate, TMIC, and 1,3,5-trinitrobenzene, 1,3,5-TNB (Figure 6.1b and Figure 6.1c respectively). Each molecule forms a layer and the layers of two different molecules interact among them alternatively to form the crystal. In this study we have studied the interactions between the building units within (intra-) and between (inter-) layers in these two crystals to understand what kinds of interactions stabilize the system.

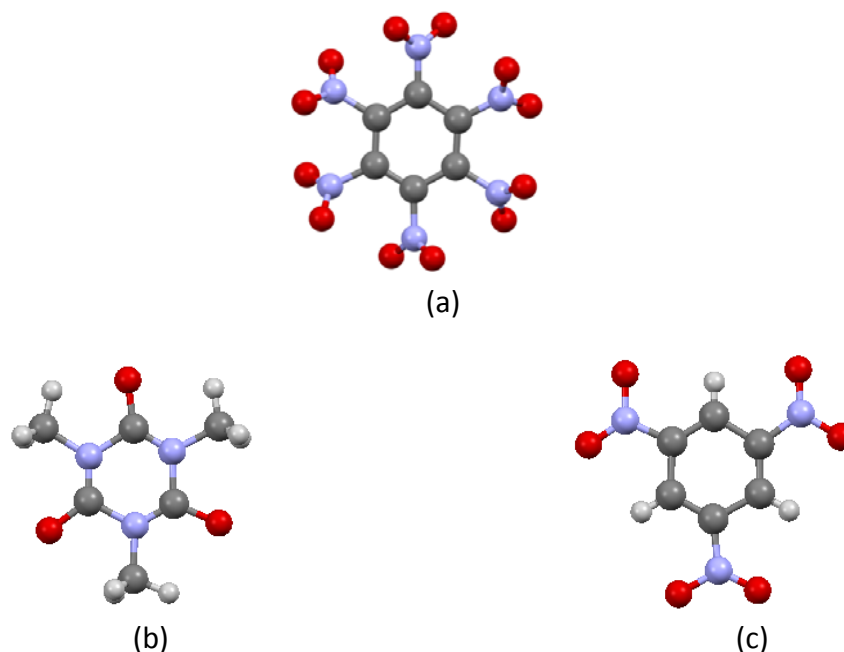


Figure 6.1 (a) Hexanitrobenzene (HNOBEN), constitutive molecule of the crystal HNOBEN; (b) trimethyl isocyanurate (TMIC) and (c) 1,3,5-trinitrobenzene (1,3,5-TNB) the two constitutive molecules of the crystal YIMWIA.

6.1.1 Methods

The geometry of the interacting molecules was extracted from the crystallographic data in the Cambridge Structural Database (CSD)³. It was considered that the forces that stabilize the crystal would be mainly between the closest spatial neighboring molecules. For that reason, the study performed consisted in establishing the most relevant interactions between the constitutive units (closer in space) and calculating the interaction energy of the considered interacting molecules or fragments, what is called a fragment based analysis.

The *ab-initio* calculations carried out determined whether the interactions studied were repulsive, *i.e.* destabilizing for the crystal, or, on the contrary, attractive, *i.e.* stabilizing for the crystalline structure.

The usual method was MP2 with basis set superposition error correction (BSSE). The basis sets used were 3-21g(d), 6-31g(d), 6-31g(2d,2p) for the complete dimers and 6-31g(d), 6-31g(2d,2p) and cc-pvtz for the small fragments.

6.1.2 HNOBEN

6.1.2.1 Description of the system

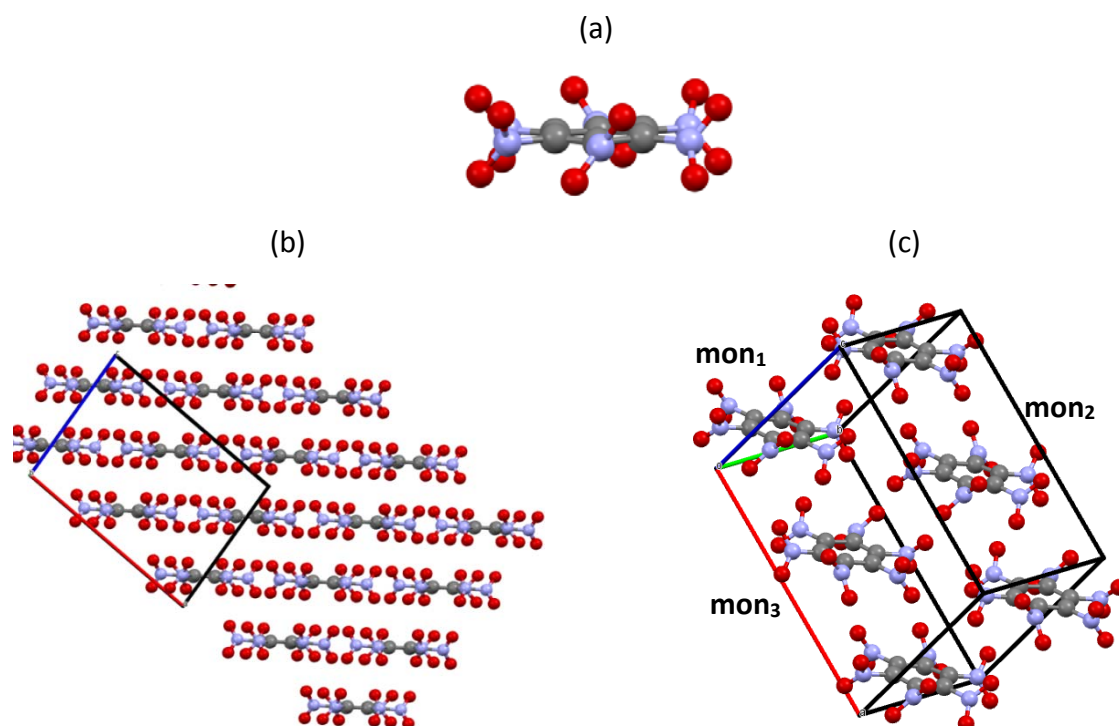


Figure 6.2 (a) Lateral view of the hexanitrobenzene (HNOBEN) molecule on the benzene plane, (b) hexanitrobenzene (HNOBEN) crystal and (b) unit cell of the HNOBEN crystal showing mon₁, mon₂ and mon₃ monomers.

HNOBEN¹ is a crystal formed by molecules of hexanitrobenzene, HNOBEN. In this molecule six nitro groups ($-\text{NO}_2$) are bound to a benzene ring. To minimize the large steric repulsion

existing between these groups the six nitro groups are placed such that there is a rotation angle regarding the plane of the benzene ring (Figure 6.2a). When analyzing the intermolecular interactions, it is important to characterize the interactions between the nitro groups among neighboring molecules.

The crystal is based in a unit cell that contains six HNOBEN molecules, whose centroids fit inside the unit cell (Figure 6.2b and c). After the analysis of the geometrical parameters between the molecules (namely distances and angles), three types of different interactions are identified (Figure 6.3b): the intra-layer (a) $\text{mon}_1\text{-mon}_2$, and the two inter-layer (b) $\text{mon}_1\text{-mon}_3$ and (c) $\text{mon}_2\text{-mon}_3$. The interactions between the three molecules mon_1 , mon_2 and mon_3 within the unit cell describe the totality of the primary coordination sphere interactions existing in the crystal. These three types of interactions are the ones that we analyzed to study the stabilization of the crystal.

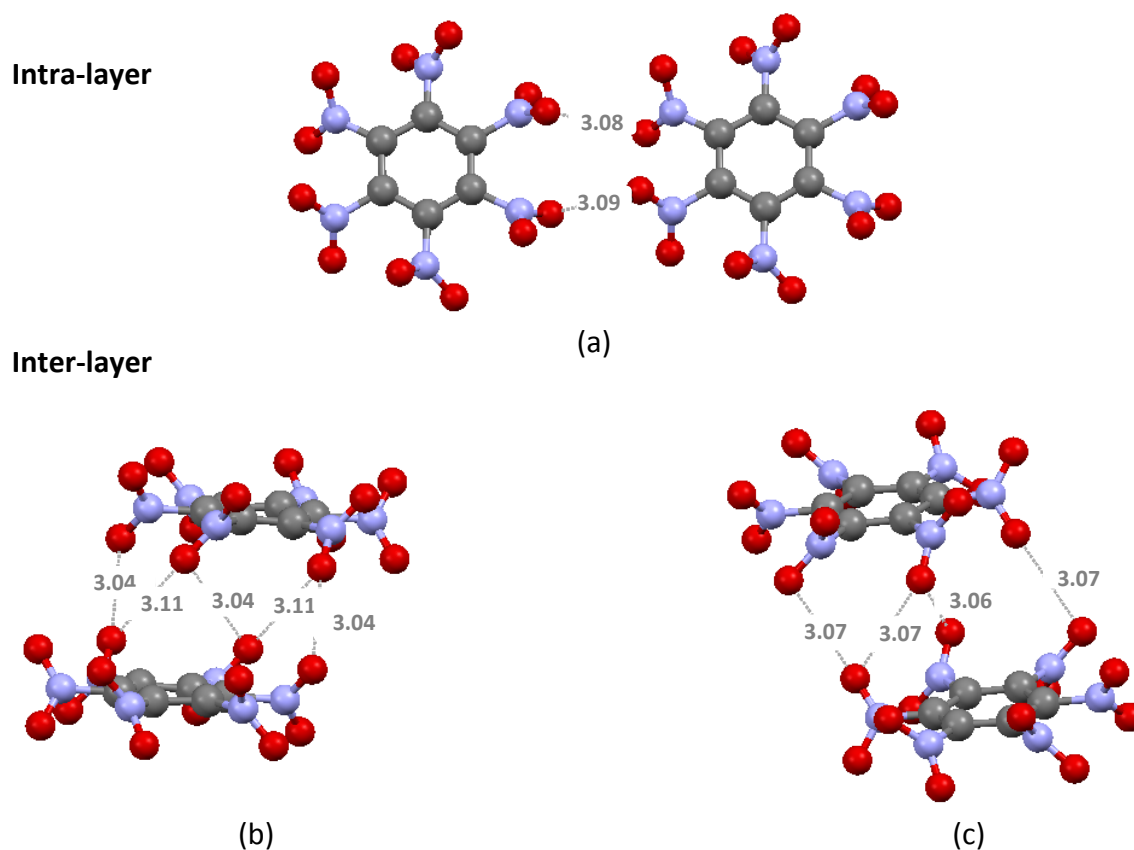


Figure 6.3 Molecules of hexanitrobenzene representing the intra-layer (a) $\text{mon}_1\text{-mon}_2$, and inter-layer (b) $\text{mon}_2\text{-mon}_3$ and (c) $\text{mon}_1\text{-mon}_3$ interactions within the HNOBEN crystal

6.1.2.2 Intermolecular interactions

The $\text{mon}_1\text{-mon}_2$ dimer in Figure 6.3a exemplifies the intra-layer interactions. Two nitro groups of one molecule are located in front of two nitro groups of the second molecule. The oxygen atoms of the NO_2 groups are placed at a short distance (~ 3.1 Å) one from the other. The results obtained from the MP2 calculations with 3-21g, 6-31g(d,p) and 6-31g(2d,2p) basis set once the basis set superposition error has been corrected indicate that the energy of the dimer is lower than the sum of the two monomers and, therefore, that this

interaction is stabilizing (Table 6.1). Additional studies were performed to analyze the role played by the two interacting nitro groups. In this approach, we considered only the $-\text{NO}_2$ closer in space and replaced the rest of the molecule by a methyl CH_3 group (Figure 6.4). The CH_3NO_2 molecules are placed at the same positions than $-\text{NO}_2$ groups of the HNOBEN interacting molecules. The calculations were performed using 6-31g(d,p), 6-31g(2d,2p) and cc-pvtz basis sets. The three results were very similar, being the 6-31g(2d,2p) and cc-pvtz the values in better agreement (Table 6.1). The results from the CH_3NO_2 fragments were also comparable to the results of the interaction between the full HNOBEN molecules.

Table 6.1 Values of interaction energy ($E_{\text{int}} = E_{\text{dim}} - E_{1+2}$) in kcal/mol for two interacting HNOBEN and CH_3NO_2 molecules representing the intra-layer (a) $\text{mon}_1\text{-mon}_2$ and inter-layer (b) $\text{mon}_2\text{-mon}_3$ and (c) $\text{mon}_1\text{-mon}_3$ interactions within the HNOBEN crystal.

HNOBEN			CH ₃ NO ₂ Fragments		
MP2/ 3-21g	MP2/ 6-31g(d,p)	MP2/ 6-31g(2d,2p)	MP2/ 6-31g(d,p)	MP2/ 6-31g(2d,2p)	MP2/ cc-pvtz
Intra-layer ($\text{mon}_1\text{-mon}_2$)					
-1.3	-1.9	-2.9	-1.5	-2.3	-2.1
Inter-layer ($\text{mon}_2\text{-mon}_3$)					
-3.5	-5.2	-6.7	Short: -9.1 Long: -3.8	-10.1 -4.4	-10.4 -4.4
Inter-layer ($\text{mon}_1\text{-mon}_3$)					
-4.0	-5.5	-6.8	Short: -0.9 Long: 1.4	-2.9 -0.6	-3.7 -1.1

Regarding the inter-layer structure, there are two type intermolecular interaction identified: the (1) interactions $\text{mon}_2\text{-mon}_3$ with a short 3.04 Å and a long 3.11 Å contacts between groups $-\text{NO}_2$ (Figure 6.3b) and the (2) interactions $\text{mon}_1\text{-mon}_3$ with two contacts between groups $-\text{NO}_2$ that are almost equivalent at 3.06 Å and 3.07 Å (Figure 6.3c). We will identify these latest contacts as “short” (3.06 Å) and “long” 3.07 Å to differentiate them.

The calculations performed between all dimers indicate that all the interactions are stabilizing (Table 6.1). The interaction $\text{mon}_2\text{-mon}_3$ is slightly more stabilizing than $\text{mon}_1\text{-mon}_3$. It is observed that short contacts have lower interaction energy (E_{int}) than the long ones.

B3LYP calculations with the same basis sets resulted in repulsive interactions, indicating that it is necessary to introduce perturbational methods to describe correctly the stability of these dimers.

A fragment analysis was performed to characterize the inter-layer connections between the nitro groups of both molecules. In this exploration, the benzene rings were replaced by methyl groups (Figure 6.4). The energy calculations indicated that those interactions were stabilizing. The long $\text{mon}_1\text{-mon}_3$ contact was wrongly described when the calculation was performed the smallest 6-31g(d,p) basis set. Indeed, one has to resort to either 6-31g(2d,2p) or cc-pvtz basis sets for a correct description of the $\text{mon}_1\text{-mon}_3$ interaction (Table 6.1).

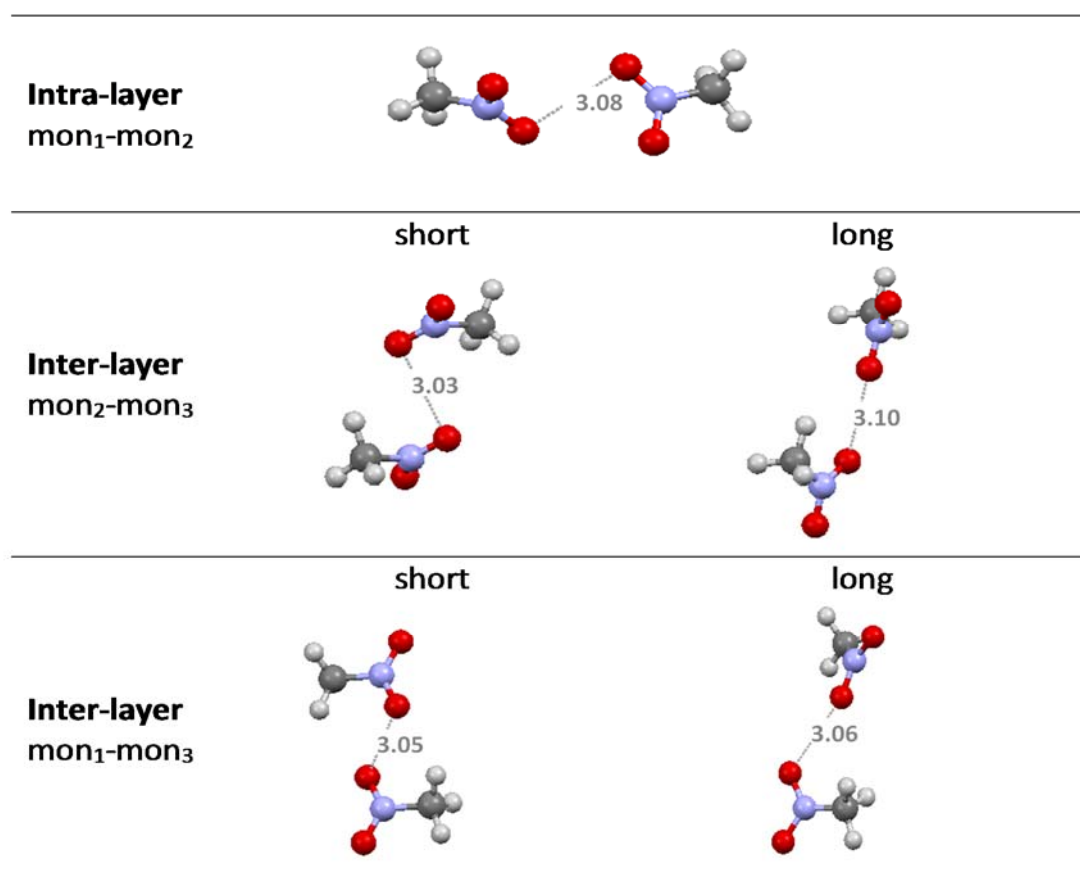


Figure 6.4 Graphical representation of two fragments CH_3NO that characterize the intermolecular interactions: (a) intra-layer $\text{mon}_1\text{-mon}_2$, (b) inter-layer $\text{mon}_2\text{-mon}_3$ and (c) inter-layer $\text{mon}_1\text{-mon}_3$.

We believe that this stabilization results from the interaction of the oxygen atoms of the nitro groups with the aromatic carbon atoms, which have some deficiency in electron density. Several bonds and ring critical points, BCP and RCP, have been found between two inter-layer HNOBEN molecules. Specifically, there are two BCP between the oxygen of one molecule and the aromatic carbon atoms of the other, with a density $\rho = 4 \cdot 10^{-3}$ a.u. and positive Laplacian. This contribution counteracts the repulsive interaction of the nitro groups with oxygen atoms at a short intermolecular distance. In the analysis done for the small model system $\text{CH}_3\text{NO}_2 \cdots \text{O}_2\text{NCH}_3$ the attractive interaction increases due to the possible formation of hydrogen bonds between the hydrogen atoms of the methyl group of one molecule and the oxygen of the nitro group of the other. In the case of the $\text{mon}_1\text{-mon}_3$ interaction, the oxygen atoms of the nitro groups of both molecules are close, which causes a large repulsion. As a result, the global interaction is less attractive than for the $\text{mon}_2\text{-mon}_3$ contact.

The magnitude of the interaction energy differs slightly between the HNOBEN dimer analysis and the CH_3NO_2 fragment analysis. This indicates that other intermolecular interactions different from the $\text{NO}_2\text{-NO}_2$ connections play a role in the inter-molecular stabilization. However, the overall stabilization has been described correctly in both analysis.

6.1.3 YIMWIA

6.1.3.1 Crystal structure

The crystal so-called YIMWIA is formed by the molecular complex 1:1 trimethyl isocyanurate: 1,3,5-trinitrobenzene². The crystal structure is described as alternate layers from each of the constituent molecules, that is, a structure ...-A-B-A-B-... where A and B are the trimethyl isocyanurate (TMIC) and 1,3,5-trinitrobenzene (1,3,5-TNB) respectively (Figure 6.5).

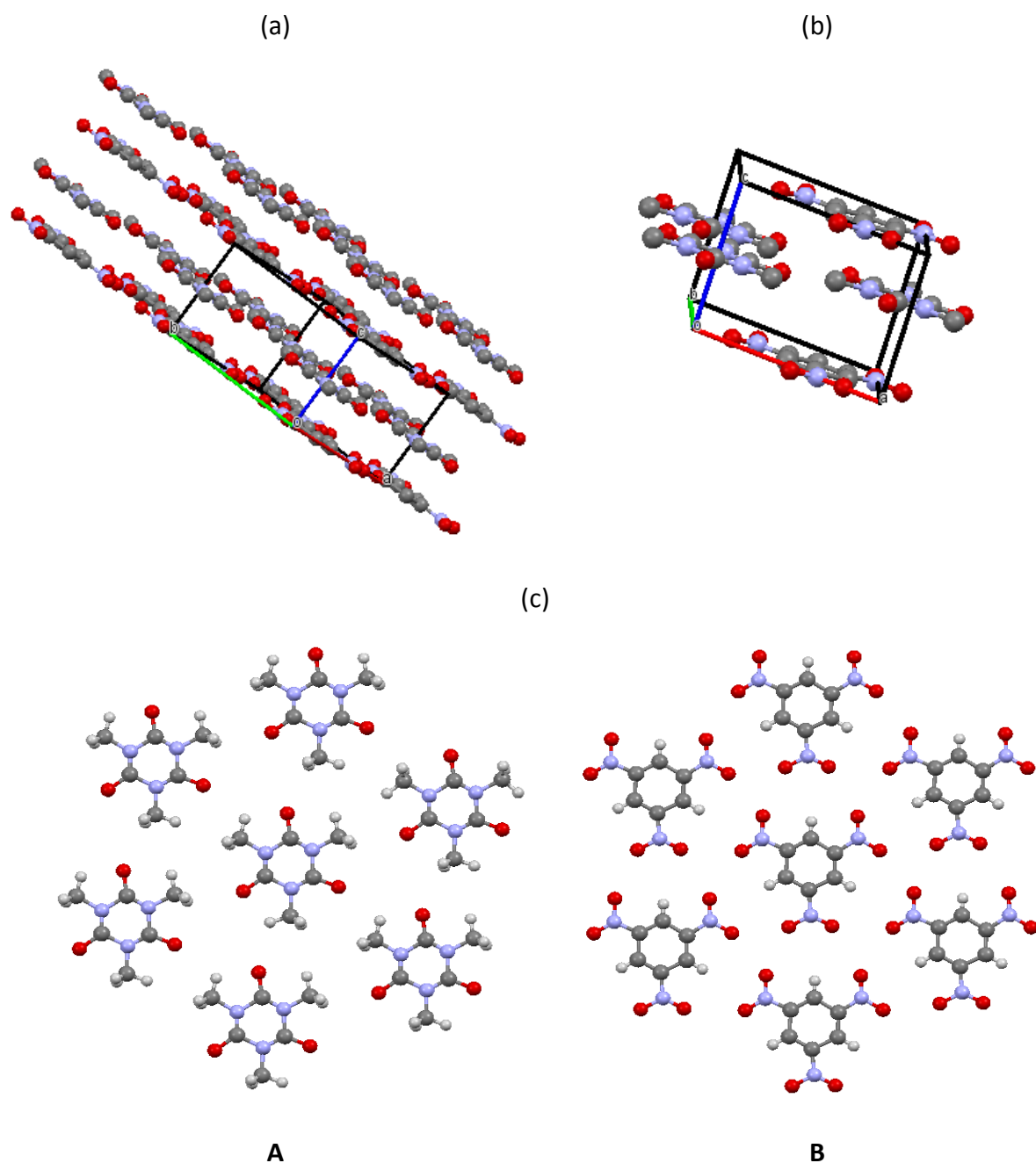


Figure 6.5 Representation of (a) the YIMWIA crystal, (b) the unit cell, and (c) the layers A TMIC and B 1,3,5-TNB.

Within the layers, each molecule is surrounded by six others in a hexagonal arrangement (Figure 6.5c). The interactions of the central molecule with its neighbors are all identical. Thus, we limited the study of intra-layer interactions to the evaluation of interactions between dimers, considering that the results could be extrapolated to the other interactions.

The inter-layer interaction between any two A-B layers presents a coordination number equal to six with three molecules below and three molecules above (Figure 6.6). Similarly to the intra-layer study, we restricted the study of inter-layer interactions to the first coordination sphere evaluating the interaction between one TMIC molecule and one 1,3,5-TNB molecule, since all the other interactions are identical.

Consequently, each molecule is surrounded by a total of 12 neighbors: six molecules in the same plane (intra-layer) and three above and three below the molecule (inter-layers). The analysis was limited to calculations of the dimers that represent the intra- and inter-layer interactions, as mentioned, extrapolating the results obtained for the equivalent neighbor molecules.

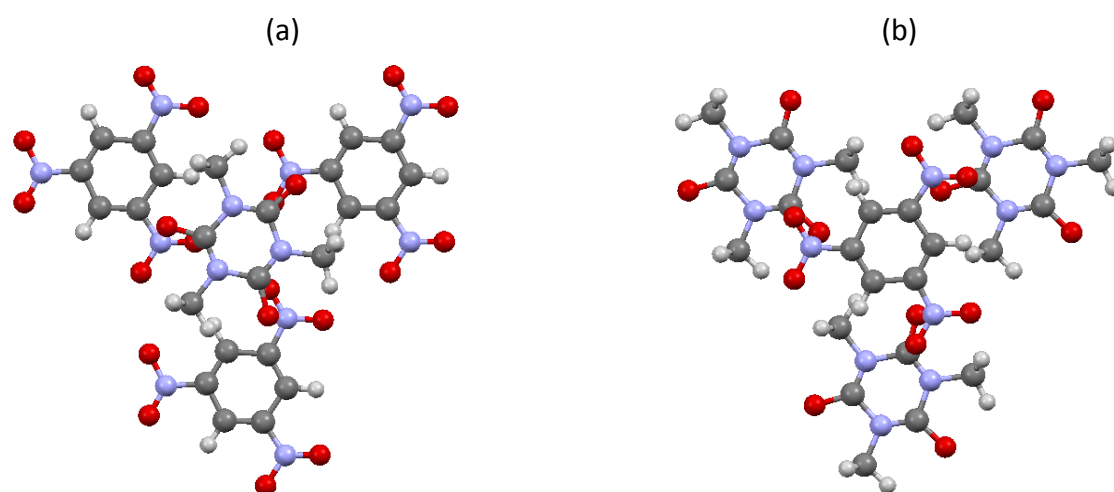


Figure 6.6 Bottom layer of the first sphere of coordination of a (a) TMIC and (b) 1,3,5-TNB molecule.

6.1.3.2 Intermolecular interactions

The MP2 calculations performed both with 6-31g(d,p) and 6-31g(2d,2p) basis sets determined that the dimers TMIC-TMIC (Figure 6.7a), TNB-TNB (Figure 6.7b) and TMIC-TNB (Figure 6.7c) are all attractive. Therefore, the formation of the bimolecular systems is stabilized with respect to the two separated molecules (Table 6.2). However, it is noticed that the inter-layer interaction TMIC-TNB is more stabilizing than the two intra-layer TMIC-TMIC and TNB-TNB.

We believe that the stabilization of the bimolecular system within the **TMIC** layer (Figure 6.7a) is possibly due to an attractive interaction between the oxygen atom of one molecule and the methyl group of the other. An AIMs analysis identified two low density

intermolecular *Bond Critical Points* (BCP) in this area that could be assigned to the stabilization of the system.

Table 6.2 Energy values for the dimers (E_{dim}), two separate monomers ($E_{\text{TMIC+TMIC}}$, $E_{\text{TNB+TNB}}$, $E_{\text{TMIC+TNB}}$) and the interaction energy (E_{int}) representing the intra-layer (a) TMIC-TMIC and (b) TNB-TNB and the inter-layer (c) TMIC-TNB interactions within the YIMWIA crystal.

	MP2/ 6-31g(d,p)	MP2/ 6-31g(2d,2p)
Intra-layer TMIC		
E_{int} (kcal/mol)	-1.3	-1.5
Intra-layer 1,3,5-TNB		
E_{int} (kcal/mol)	-0.5	-0.9
Inter-layer TMEC-TNB		
E_{int} (kcal/mol)	-5.7	-7.2

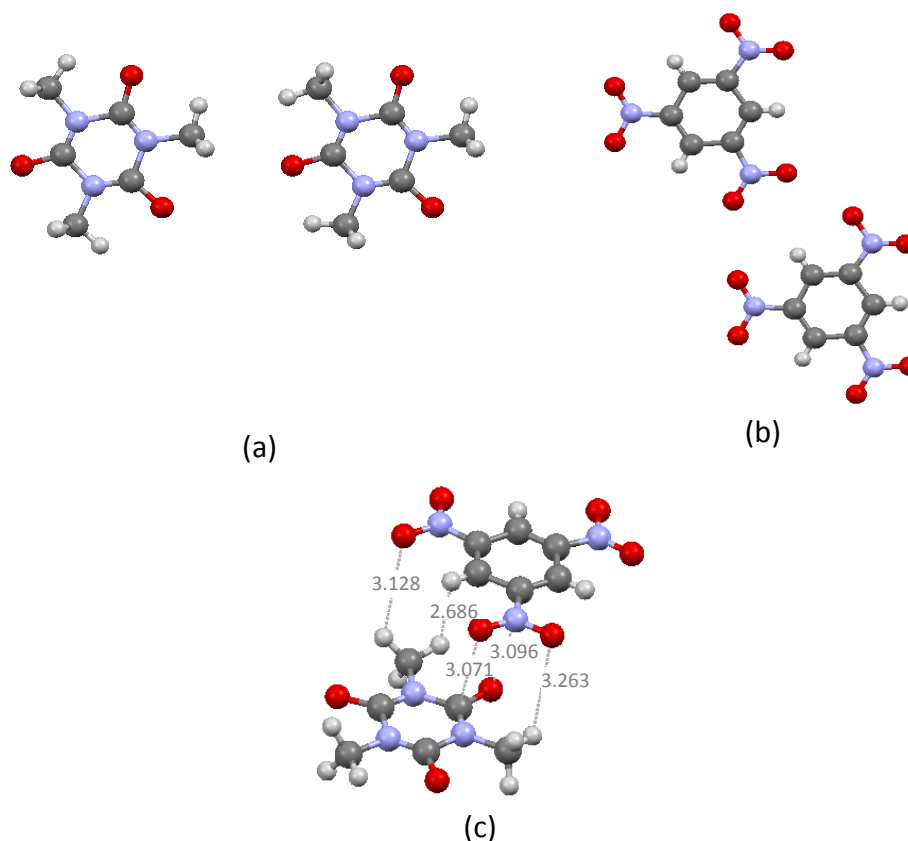


Figure 6.7 Representation of the intermolecular interactions between two molecules within the intra-layers (a) TMIC and (b) 1,3,5-TNB and the inter-layer (c) TMIC-TNB.

The **1,3,5-TNB** layer is formed by 1,3,5-trinitrobenzene molecules (Figure 6.7b). The nitro ($-\text{NO}_2$) groups of the molecules are placed in the same plane that the benzene ring. To evaluate if this is the optimum geometry of the molecule, we carried out a MP2/6-31g(2d,2p) calculation placing the nitro groups at different angles (10° - 90°) out of the benzene plane. All the optimizations lead to the flat structure as the more stable one. Optimizations of the geometry of the molecule fixing the angle of the nitro groups with respect to the benzene plane at 0° , 10° , 20° , 30° , showed that the energy is higher as the

angle increases (Table 6.3). These results confirm the observation that the most stable geometry is that one with the nitro groups in the plane of the benzene ring.

Table 6.3 Energy for the optimized 1,3,5-TNB molecules at different angles (α) of the nitro groups in reference to the benzene plane.

Angle (α)	Energy a.u.	$\Delta E(E_\alpha - E_{opt})$ kcal/mol
0° (<i>opt</i>)	-843.4955	0.0
10°	-843.4953	0.1
20°	-843.4947	0.5
30°	-843.4930	1.6

As mentioned before, MP2(BSSE) calculations with 6-31g(d,p) and 6-31g(2d,2p) basis sets showed that the dimer is more stable than the sum of the energy of two 1,3,5-TNB free molecules (Table 6.2).

The AIM analysis of the electronic densities of the dimer identified two *Bond Critical Points* (BCP) located between the oxygen atoms of the interacting nitro groups of the two monomers ($\delta_{BCP1} = 8.3 \cdot 10^{-3}$ a.u. and $\delta_{BCP2} = 5.3 \cdot 10^{-3}$ a.u.) and a *Ring Critical Point* (RCP) in the center of the three nitro groups ($\delta_{RCP} = 1.6 \cdot 10^{-3}$ a.u.) [Figure 6.8]. The first two BCP are located between the two oxygen atoms. We believe that they appeared as an overlap of the tails of the electronic densities of the oxygen atoms by spatial proximity. Therefore, if this were true, these two BCP would not be true bonding interactions and would not contribute to the stabilization of the structure. On the other hand, the so-called RCP could be a possible hydrogen bond masked by the electronic densities of the nitro groups that surround it.

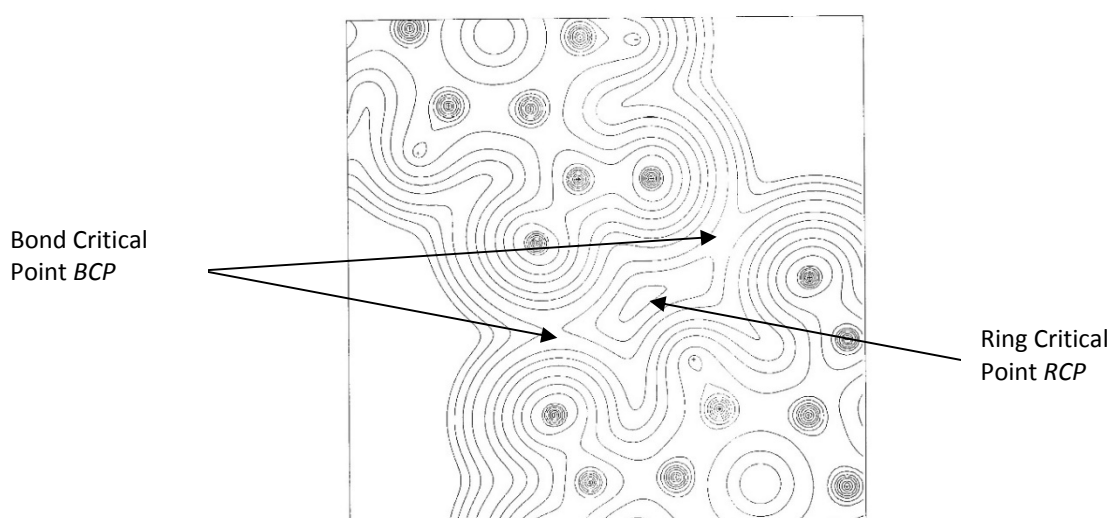


Figure 6.8 Bond Critical Points, *BCP*, and Ring Critical Point, *RCP*, between two constituent units of the layer 1,3,5-TNB.

To verify this hypothesis, we analyzed two different fragment based assays:

- I. We evaluated the interaction between monomer 1 (1,3,5-TNB molecule) and monomer 2 without the two nitro groups that interact with monomer 1 (nitrobenzene molecule) [Figure 6.9b]. With this approach we intended to study the interaction between both molecules neglecting both the repulsive component and the overlap of the electron density of the nitro groups. If a bond critical point exists between both molecules and the interaction is attractive, this will mean that a true intermolecular bond exists between the two molecules.
- II. Alternatively, we studied the interaction of the monomer 1 (1,3,5-TNB) with the two nitro groups (HNO_2 , without the nitrobenzene part) of monomer 2 (Figure 6.9b). In case the interaction is attractive, the BCP that appears between both molecules will suggest that there is a true intermolecular interaction. On the other hand, if the interaction is repulsive, the critical points that appear between the nitro groups will represent an overlap of densities.

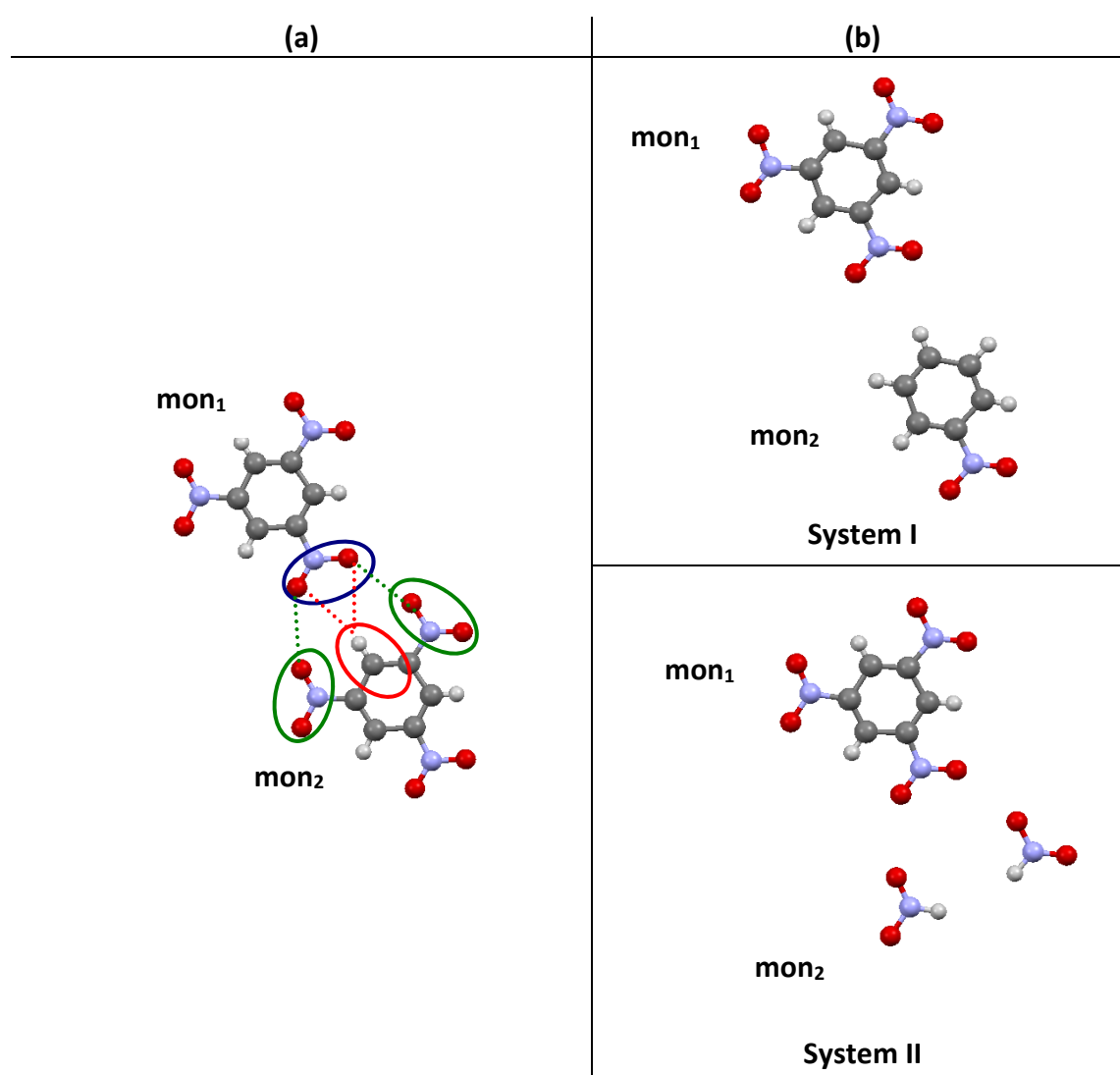


Figure 6.9 (a) Intermolecular interactions between two 1,3,5-TNB molecules. (b) System I and System II. System I represents the interactions of a 1,3,5-TNB molecule with a nitrobenzene that replaces monomer 2 to suppress the contribution of the closest interacting nitro ($-\text{NO}_2$) groups. System II represents the interaction between monomer 1 (1,3,5-TNB) and the two closest nitro (HNO_2) groups of monomer 2.

MP2 calculations with both 6-31g(d,p) and 6-31g(2d,2p) basis sets indicate that System I is stabilized with respect to two individual molecules by -1.4 kcal/mol and -1.5 Kcal/mol, respectively (Table 6.4). The AIM analysis showed a BCP ($\delta_{\text{BCP}} = 3.2 \cdot 10^{-3}$ a.u.) that appears between the hydrogen of the nitrobenzene molecule and one nitro group of the other (Figure 6.10). The BCP is assigned to a weak bond that stabilizes the interaction between both molecules.

Table 6.4 Interaction energy E_{int} (kcal/mol) for two 1,3,5-TNB molecules and systems I and II.

	E_{int} (kcal/mol)	
	MP2/ 6-31g(d,p)	MP2/ 6-31g(2d,2p)
1,3,5-TNB dimers	-0.5	-0.9
Fragments System I	-1.4	-1.5
Fragments System II	1.5	1.0

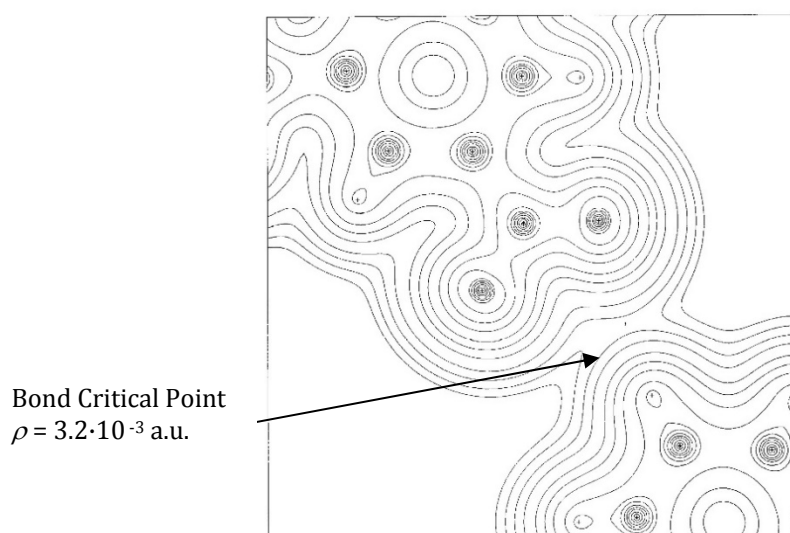


Figure 6.10 Bond Critical Point BCP for the interaction of the fragments in Figure 6.9a.

The attractive contribution calculated from System I counteracts the repulsive contribution from the interaction of the nitro groups in System II. The global outcome is that the interaction between two 1,3,5-TNB molecules is slightly stabilizing. To understand the stabilization of the interaction between two 1,3,5-TNB molecules is crucial to take into consideration the role played by the intermolecular interaction between the $-\text{NO}_2$ group of one molecule and the benzene's hydrogen of the other, since without them such stabilization would not be feasible.

For the inter-layer **TMIC-TNB** interactions (Figure 6.7c), calculations were performed at MP2 level with both 6-31g(d,p) and 6-31g(2d,2p) basis sets. The results indicated that this interaction is attractive, being -5.7 kcal/mol and -7.2 kcal/mol at MP2/6-31g(d,p) and MP2/6-31g(2d,2p), respectively.

It is argued that the stabilization of the energy in this system could be due to two factors: (a) the existence of hydrogen bonds between the hydrogens of TMIC methyl groups and the oxygen of the TNB nitro groups, and (b) a possible interaction between the oxygen atoms, with high electron density, and the benzene rings depleted in electron density. According to the AIM analysis, three intermolecular bond critical points (BCP) and three ring critical points (RCP) are found between the TMIC and TNB molecules.

In the analysis of the YIMWIA crystal, we observed that all the intermolecular interactions of the dimers that represent the intra-layer TMIC-TMIC and TNB-TNB and the inter-layer TMIC-TNB interactions are stabilizing. It is believed that the stabilization in the interaction between TMIC molecules is due to the attractive interactions between the methyl groups of a molecule and the oxygen atom from the nitro groups of the neighboring molecule. In the case of the 1,3,5-TNB layer, the interaction is also stabilizing. It has been deduced that, despite the repulsive interaction between the nitro groups, there is an attractive contribution between the NO₂ group of one of the 1,3,5-TNB molecules and a hydrogen with depleted electron density of the other 1,3,5-TNB molecule that stabilizes the layer. The inter-layers interaction between TMIC and is the most attractive interaction, which stabilizes the global crystal structure.

6.2 Magneto structural study on the molecular α -nitronyl nitroxide crystals.

Within the molecular materials with magnetic properties, one of the most used and studied crystal family is the one constituted by the so-called α -nitronyl nitroxides^{viii} (α -NN). The molecular components of these crystals are characterized by the presence of a five atom ring (Figure 6.11a) with an organic group **R** that can vary in the different crystals⁴⁻¹⁷. Note that the carbons in the ring may have different substituents that are not represented in the figure. This monomer is a radical containing one unpaired electron. According to studies on the distribution of spin densities¹⁸⁻²⁰, this unpaired electron is basically delocalized over the ONCNO group of atoms (Figure 6.11b). The delocalization of the unpaired electron over the ONCNO indicates that there is a resonance between two different possible configurations (Figure 6.11c).

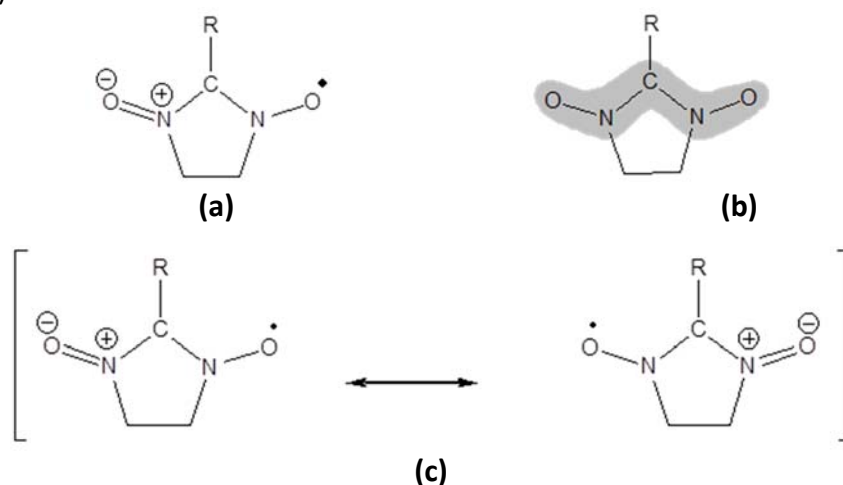


Figure 6.11 (a) α -Nitronyl nitroxide monomer, where **R** represents different organic groups. (b) Spin density distribution in the α -nitronyl nitroxide monomer. (c) Resonance between possible configurations of α -nitronyl nitroxide systems.

^{viii} Family of the 4,5-dihydro-4,4,5,5-tetramethyl-3-oxido-1H-imidazol-3-ium-1-oxyl.

Table 6.5 Atomic spin population (in a.u.) on the regions of the α -nitronyl nitroxide molecules in the systems studied (Figure 6.12). Contributions from the C(sp²) atom in the ONCNO group, the ONCNO group (sum of the absolute values), the remaining atoms in the nitronyl nitroxide ring [r(5)-ONCNO] and the substituent group R.

Refcode	C(sp ²)	ONCNO	r(5)-ONCNO	R
000M PY ²¹³	-0.21	1.43	0.10	0.10
000PPY ²¹⁴	-0.20	1.41	0.10	0.13
00DPNP ²¹⁵	-0.22	1.46	0.09	0.21
00GPNP ²¹⁶	^a	^a	^a	^a
0PBRPH ²¹⁷	-0.21	1.42	0.10	0.15
HAFXOB ²¹⁸	-0.21	1.43	0.08	0.17
LICM IT ²⁰³	-0.19	1.37	0.08	0.13
M ACO PY ²¹⁹	-0.23	1.45	0.08	0.08
M M EPYC ²²⁰	-0.21	1.45	0.10	0.17
PEFM ES ²²¹	-0.22	1.51	0.10	0.45
PEYPUA ²²²	-0.20	1.42	0.10	0.13
YISCEI ²²³	-0.19	1.40	0.10	0.15
YISCOS ²²³	-0.23	1.46	0.08	0.05
YISNIX ²²⁴	-0.20	1.41	0.10	0.11
YIW SEC ²²⁵	-0.19	1.44	0.08	0.15
YOM YII ²⁰⁴	-0.17	1.34	0.08	0.09
YUJNEW ²²⁶	-0.20	1.43	0.08	0.17
YULPOK ²²⁷	-0.19	1.44	0.09	0.33
ZORHIX ²²⁸	-0.21	1.43	0.08	0.11
<i>Minimum</i>	-0.23	1.34	0.08	0.05
<i>Maximum</i>	-0.17	1.51	0.10	0.45
<i>Mean</i> (\bar{d}_j)	-0.20	1.43	0.09	0.16
<i>Variance</i> (s_j^2)	0.000	0.001	0.000	0.009

^a No data available

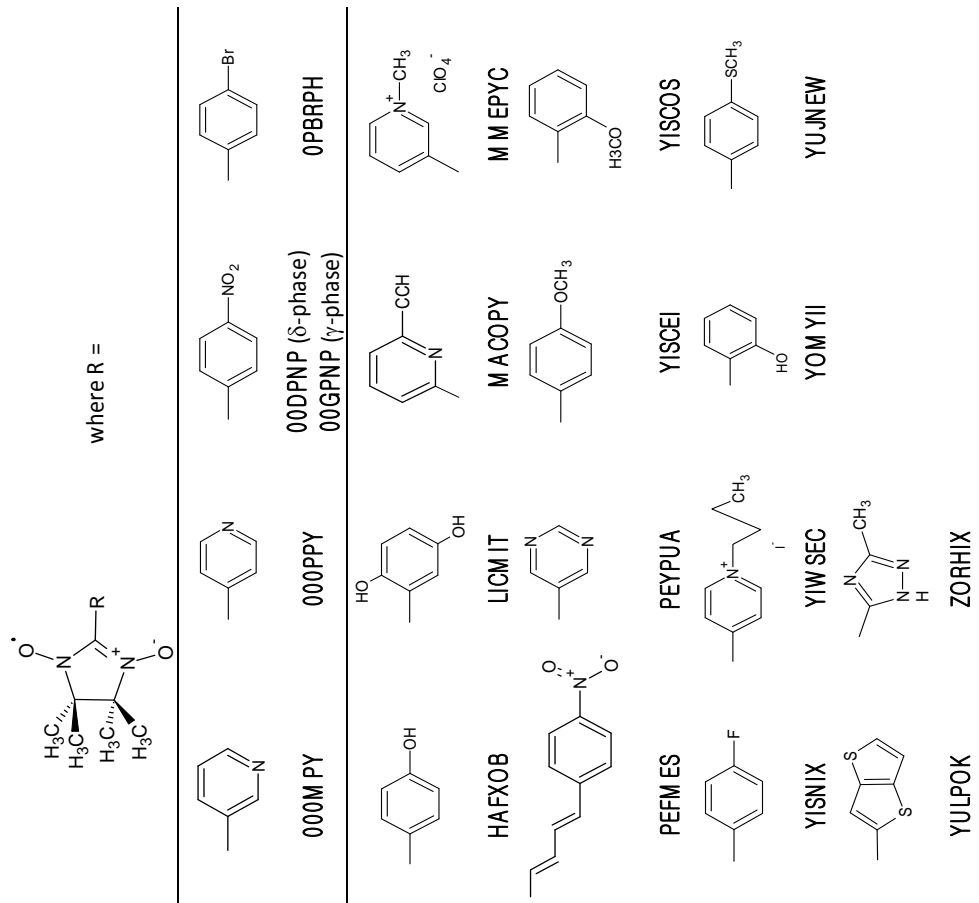


Figure 6.12 α -Nitronyl nitroxides monomers that constitute crystals with ferromagnetic properties⁸.

Table 6.6 Values of the position vector for close ONCNO contacts in crystals composed of molecular α -NN shown in Figure 6.13, where D distance is given in Å and angles and dihedrals in degrees.

	D (Å)	A ₁ (°)	A ₂ (°)	T ₁ (°)	T ₂ (°)	T ₃ (°)
000MPY ²¹³	3.499	76.365	127.455	-162.129	-92.066	104.269
000PPY ²¹⁴	3.903	136.484	136.484	-180.000	-7.185	7.185
00DPNP ²¹⁵	4.275	104.682	134.037	90.464	60.541	172.841
00GPNP1 ²¹⁶	3.997	127.976	127.976	-179.98	42.622	-42.622
00GPNP2 ²¹⁶	4.296	126.576	126.576	-180.000	30.266	-30.266
0PBRPH1 ²¹⁷	4.221	136.114	136.114	180.000	49.278	-49.278
0PBRPH2 ²¹⁷	4.290	59.719	109.975	-106.074	83.964	-52.818
HAFXOB ²¹⁸	4.912	75.681	114.361	-72.588	72.142	-85.699
LICMIT1 ²⁰³	3.158	146.855	146.855	180.000	-0.048	0.048
LICMIT2 ²⁰³	4.594	96.254	105.830	-144.552	-111.857	-80.037
MACOPY1 ²¹⁹	4.324	103.567	114.166	56.310	-87.876	-158.443
MACOPY2 ²¹⁹	4.720	77.374	93.922	147.211	116.528	62.422
MMEPYC1 ²²⁹	3.429	67.952	153.184	173.295	70.122	-40.081
MMEPYC2 ²²⁹	3.453	70.640	154.16	-166.325	-68.405	30.817
PEFMES ²²¹	4.328	83.379	113.837	148.887	81.584	-5.740
PEYPUA ²²²	3.719	58.945	114.625	172.944	-66.474	-113.975
YIWSEC	4.685	98.736	118.948	159.473	132.595	-114.518
YISCEI ²²³	4.705	62.072	104.465	-105.279	81.031	-57.766
YISCOS ²²³	4.768	96.725	142.896	61.439	-174.778	-77.065
YISNIX ²²⁴	4.130	65.375	142.49	-122.206	69.348	-33.356
YOMYII ²⁰⁴	3.966	105.705	128.121	87.421	-135.685	-145.276
YUJNEW ²²⁶	4.709	63.156	98.765	103.827	-85.230	60.537
YULPOK1 ²²⁷	4.465	94.377	129.309	164.761	97.144	18.858
YULPOK2 ²²⁷	4.509	71.758	71.758	-179.980	100.129	-100.129
ZORHIX1 ²²⁸	3.168	71.514	126.905	119.006	-76.211	46.489
ZORHIX2 ²²⁸	4.674	100.994	100.994	-180.000	176.748	-176.749

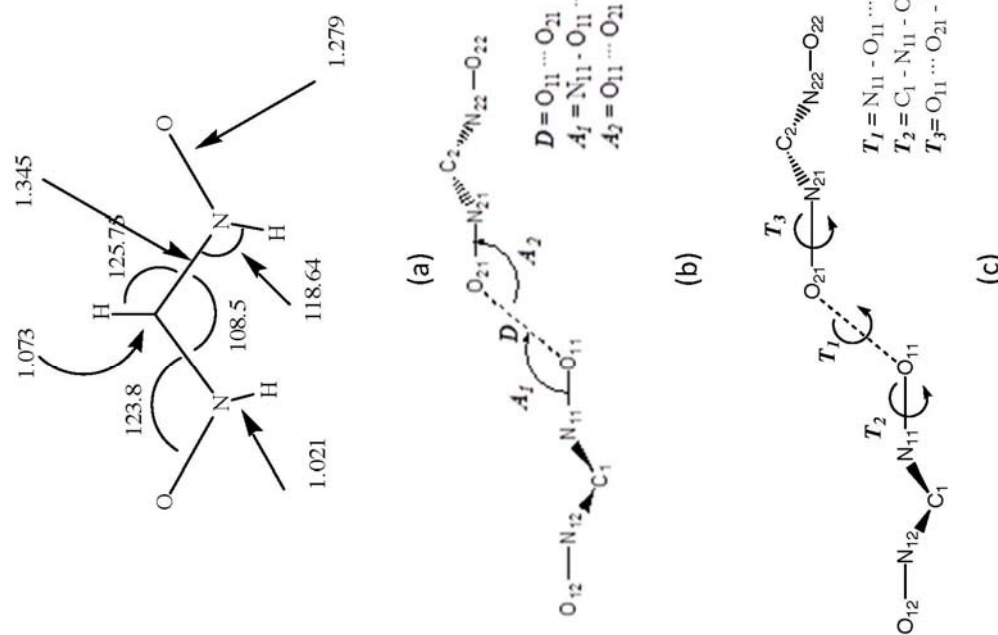


Figure 6.13 (a) ONCNO model system and average values for intramolecular distances and angles (in Å and degrees, respectively). (b) Parameters D, A₁, A₂ and (c) T₁, T₂, T₃ that define the orientation of the two ONCNO molecules in the space.

In order to investigate possible magneto-structural relationships between the spin-containing atoms, we analyzed the nature of the interaction within the family of α -nitronyl nitroxide crystals. The crystallographic data of these crystals has been obtained from the Cambridge Structural Database (CSD)³. The α -nitronyl nitroxide crystals can be classified according to being macroscopically ferromagnetic (FM) or antiferromagnetic (AFM)^{38,39}. In previous studies, it was demonstrated that no conclusion could be drawn about a general relationship between magnetism and orientation of the radicals^{38,39}. We wondered if there was a direct relationship between the macroscopic magnetic character of the crystals and the microscopic energetic spin preference considering only the ONCNO spin-containing atoms. In this thesis, we focused on the FM subset of crystals^{38,39}. Specifically, for each FM crystal studied (Figure 6.12) we calculated if the interactions between the ONCNO groups, whose geometry was extracted from the crystal itself, were ferromagnetic (FM, $\Delta E^{S-T} > 0$) or antiferromagnetic (AFM, $\Delta E^{S-T} < 0$).

It is supposed that the macroscopic magnetic behavior of a given crystal will be determined by the spin preference of the intermolecular interaction between its constitutive molecules. As discussed previously, the spin preference of two interacting molecules is allegedly characterized by the interaction of the spin containing atoms that are closer in space. In the crystals studied, the spin density is located mainly on the ONCNO atoms of the α -nitronyl nitroxide molecules (Table 6.5). Therefore, the spin preference of the interacting molecules is supposed to be defined by the ONCNO atoms of the constitutive molecules of the crystals shown in Figure 6.12.

Since the main contribution to the spin densities is within the ONCNO groups (Table 6.5), the calculations performed were carried out on simplified molecules constituted basically by the ONCNO group (Figure 6.13a). To simplify, these molecules will be referred as ONCNO. The intramolecular parameters of distances and angles in Figure 6.13 are average values of the α -nitronyl nitroxide systems studied⁴⁰. The intermolecular spatial distribution of the dimers is characterized by a vector of 6 components (see D , A_1 , A_2 , T_1 , T_2 , T_3 in Figure 6.13b and c).

The experimental measurements of the intermolecular parameters that describe the α -nitronyl nitroxide arrangement within the selected set of FM crystals (Figure 6.12) were used to construct the vectors (D , A_1 , A_2 , T_1 , T_2 and T_3) that define the location of two ONCNO groups within each studied crystal (Table 6.6).

6.2.1 Methods

The study was performed on dimeric systems built from the intramolecular (Figure 6.13) and the intermolecular geometrical parameters obtained from the experimental data (Table 6.6).

Initially the energy gap between the low (singlet) and high (triplet) spin states were calculated (ΔE^{S-T}). This spin preference was described studying the contributions of the exchange integral (J_{ij}) and exchange density matrix elements (P_{ij}) between the spin containing atoms. Additionally, a statistical analysis of the orientation of the two molecules

was performed trying to correlate the spatial orientation of the interacting molecules with the preference for the high or low-spin state of the studied crystals.

The methods used in these calculations were CAS(6,6), CASPT2(6,6), B3LYP and MP2 with 6-31+g(d,p) basis set.

6.2.2 McConnell theory applied to α -nitronyl nitroxide crystals.

As described previously (see Chapter 5, Section 5.2), according to McConnell's theory⁴¹, there is a magneto-structural relationship between the spin multiplicity of a given system and the spatial arrangement of the electron densities of the two radicals constituting the system. McConnell proposed the effective Hamiltonian \hat{H}^{AB} in equation (6.1) to study the interaction between A and B radical units. In this expression \hat{S}_i^A, \hat{S}_j^B are the spin operators and J_{ij}^{AB} the exchange integral of atoms $i \in A$ and $j \in B$.

$$\hat{H}^{AB} = -\sum_{\substack{i \in A \\ j \in B}} J_{ij}^{AB} \hat{S}_i^A \cdot \hat{S}_j^B \quad (6.1)$$

Assuming that the spin operators \hat{S}_i^A, \hat{S}_j^B operating on i, j orbitals of A and B molecules, respectively, can be expressed as the product between the total spin operator on A, \hat{S}^A , and B, \hat{S}^B , and the electron density on $i \in A$ (ρ_i) and $j \in B$ (ρ_j) [equations (6.2) and (6.3)], the eigenvalue of this effective Hamiltonian (6.1) can be expressed as in equation (6.4).

$$\hat{S}_i^A = \hat{S}^A \rho_i \quad (6.2)$$

$$\hat{S}_j^B = \hat{S}^B \rho_j \quad (6.3)$$

$$\langle \hat{H}^{AB} \rangle = -\sum_{\substack{i \in A \\ j \in B}} J_{ij}^{AB} \langle \hat{S}_i^A \cdot \hat{S}_j^B \rangle = -\langle \hat{S}^A \cdot \hat{S}^B \rangle \sum_{\substack{i \in A \\ j \in B}} J_{ij}^{AB} (\rho_i^A \rho_j^B) \quad (6.4)$$

The energy difference between the low-spin (LS) and high-spin (HS) states can then be estimated using equation (6.5):

$$\begin{aligned} \langle \hat{H}^{AB} \rangle^{LS} - \langle \hat{H}^{AB} \rangle^{HS} &= -\sum_{\substack{i \in A \\ j \in B}} J_{ij}^{AB} \left[\langle \hat{S}_i^A \cdot \hat{S}_j^B \rangle^{LS} - \langle \hat{S}_i^A \cdot \hat{S}_j^B \rangle^{HS} \right] = \\ &= -\left[\langle \hat{S}^A \cdot \hat{S}^B \rangle^{LS} - \langle \hat{S}^A \cdot \hat{S}^B \rangle^{HS} \right] \sum_{\substack{i \in A \\ j \in B}} J_{ij}^{AB} (\rho_i^A \rho_j^B) \end{aligned} \quad (6.5)$$

where

$$\langle \hat{S}^A \cdot \hat{S}^B \rangle = \frac{1}{2} [S(S+1) - S_A(S_A+1) - S_B(S_B+1)] \quad (6.6)$$

If we consider a two free-electron system (biradical), where $i \in A$ and $j \in B$, the LS and HS states are the singlet (S) and triplet (T), respectively, depending on whether the two electrons interact antiferromagnetically or ferromagnetically. Considering $\langle \hat{S}^A \cdot \hat{S}^B \rangle^S = -3/4$ and $\langle \hat{S}^A \cdot \hat{S}^B \rangle^T = 1/4$, the $\left[\langle \hat{S}^A \cdot \hat{S}^B \rangle^{LS} - \langle \hat{S}^A \cdot \hat{S}^B \rangle^{HS} \right]$ term in equation (6.5) becomes a negative number $\left[\langle \hat{S}^A \cdot \hat{S}^B \rangle^S - \langle \hat{S}^A \cdot \hat{S}^B \rangle^T \right] = -1$ and the expression of the energy gap between the singlet and the triplet is approximated as equation (6.7). Usually, the value of the exchange integral J_{ij}^{AB} between two electrons is negative. Consequently, if the spin density product of the two i, j electrons is positive ($\rho_i^A \rho_j^B > 0$), the low-spin state is lower in energy ($\Delta E^{LS-HS} = \langle \hat{H}^{AB} \rangle^{LS} - \langle \hat{H}^{AB} \rangle^{HS} < 0$). On the other hand, when the spin density product the two interacting electrons is negative ($\rho_i^A \rho_j^B < 0$) the state lower in energy is the one with high-spin multiplicity $\Delta E^{LS-HS} = \langle \hat{H}^{AB} \rangle^{LS} - \langle \hat{H}^{AB} \rangle^{HS} > 0$.

$$\langle \hat{H}^{AB} \rangle^S - \langle \hat{H}^{AB} \rangle^T = \sum_{\substack{i \in A \\ j \in B}} J_{ij}^{AB} (\rho_i^A \rho_j^B) \quad (6.7)$$

Accordingly, in systems with many electrons within the active space, such as the α -NN, the high-spin multiplicity systems will be energetically favored when the main intermolecular interactions take place between atoms with spin density of opposed sign.

Spin densities of the α -nitronyl nitroxides are mainly located in the ONCNO atoms, being positive in the NO groups and negative in the central C₅ (Table 6.5). Using McConnell's theory, it is predicted that, considering both ONCNO groups placed on parallel planes, the interaction will be preferably antiferromagnetic (AFM) when it is between the NO group of one molecule and the NO of the other (Figure 6.14a) and ferromagnetic (FM) when the it is between the NO group of one molecule and the central C atom of the other (Figure 6.14b).

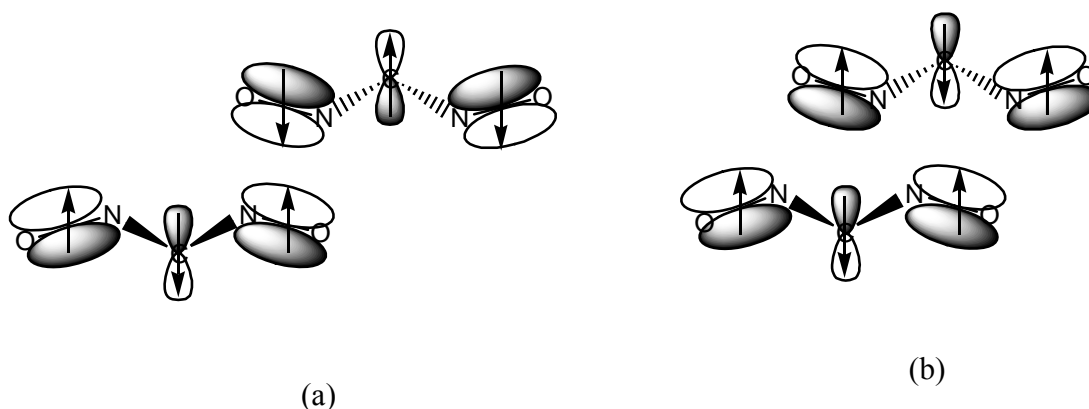


Figure 6.14 Interaction between two ONCNO units: (a) AFM interaction (ground state singlet) and (b) FM interaction (ground state triplet)

The spin Hamiltonian⁴² in equation (6.8) represents an approximation for the interaction between two A and B fragments, where only the terms between the fragments are considered and the intramolecular terms are neglected. The eigenvalue of this Hamiltonian [equation (6.10)] is expressed as a Q term that characterizes the Coulomb repulsion, a sum of the exchange integrals J_{ij} , and the exchange density matrix elements P_{ij} among all the interacting orbitals $i \in A$ and $j \in B$. The P_{ij} is expressed as the eigenvalue of twice the product of the atomic spin operators on i and j , plus half the eigenvalue of the identity operator on i and j [equation (6.9)].

$$\hat{H}_S^{AB} = Q - \sum_{\substack{i \in A \\ j \in B}} J_{ij}^{AB} \left(2\hat{S}_i^A \cdot \hat{S}_j^B + \frac{1}{2} \hat{I}_{ij}^{AB} \right) \quad (6.8)$$

$$P_S^{AB} = \left\langle - \left(2\hat{S}_i^A \cdot \hat{S}_j^B + \frac{1}{2} \hat{I}_{ij}^{AB} \right) \right\rangle \quad (6.9)$$

$$\hat{H}_S^{AB} = Q + \sum_{\substack{i \in A \\ j \in B}} J_{ij}^{AB} P_{ij}^{AB} \quad (6.10)$$

Considering that both Q and J_{ij} parameters are the same for both the low-spin (LS) and the high-spin (HS) states, the energy gap for both spin states according to the spin Hamiltonian in equation (6.8) can be expressed as the sum of the J_{ij} and ΔP_{ij}^{S-T} parameters [equation (6.11)].

$$\Delta E^{LS-HS} = \langle \hat{H}^{AB} \rangle^{LS} - \langle \hat{H}^{AB} \rangle^{HS} = \sum_{\substack{i \in A \\ j \in B}} J_{ij}^{AB} \Delta P_{ij}^{AB} \quad (6.11)$$

Assuming that the approximation made in equations (6.2) and (6.3) is valid to define \hat{S}_i^A, \hat{S}_j^B , according to equation (6.9)⁴³, a clear relationship is found between the electron density $\rho_i^A \rho_j^B$ product and the P_{ij} parameters [equation (6.12)].

$$P_{ij}^{AB} = -\hat{S}^A \cdot \hat{S}^B \left\langle \left(2\rho_i^A \rho_j^B + \frac{1}{2} \hat{I}_{ij}^{AB} \right) \right\rangle \quad (6.12)$$

ΔP_{ij}^{S-T} and ΔE^{S-T} can be thus expressed as equations (6.13) and (6.14), respectively.

$$\begin{aligned} \Delta P_{ij}^{AB} &= \left\langle - \left(2\hat{S}_i^A \hat{S}_j^B + \frac{1}{2} \hat{I}_{ij}^{AB} \right) \right\rangle^{LS} - \left\langle - \left(2\hat{S}_i^A \hat{S}_j^B + \frac{1}{2} \hat{I}_{ij}^{AB} \right) \right\rangle^{HS} = \\ &= -2 \left(\langle \hat{S}_i^A \hat{S}_j^B \rangle^{LS} - \langle \hat{S}_i^A \hat{S}_j^B \rangle^{HS} \right) = -2 \left[\langle \hat{S}^A \cdot \hat{S}^B \rangle^{LS} - \langle \hat{S}^A \cdot \hat{S}^B \rangle^{HS} \right] \rho_i^A \rho_j^B \end{aligned} \quad (6.13)$$

$$\begin{aligned} \Delta E^{LS-HS} &= \langle \hat{H}^{AB} \rangle^{LS} - \langle \hat{H}^{AB} \rangle^{HS} = \sum_{\substack{i \in A \\ j \in B}} J_{ij}^{AB} \Delta P_{ij}^{AB} = \\ &= -2 \left[\langle \hat{S}^A \cdot \hat{S}^B \rangle^{LS} - \langle \hat{S}^A \cdot \hat{S}^B \rangle^{HS} \right] \sum_{\substack{i \in A \\ j \in B}} J_{ij}^{AB} (\rho_i^A \rho_j^B) \end{aligned} \quad (6.14)$$

We must stress the fact that equations (6.5) and (6.14) only differ by a numerical factor. Therefore, they are fundamentally equivalent. Consequently, it can be assumed that the analysis of the energy gap between two spin states according to McConnell-I model can be evaluated using the parameters J_{ij} and ΔP_{ij} in equation (6.11).

6.2.3 Analysis of the energy gap between spin states for different ONCNO dimers

In order to analyze whether there is a magneto-structural relationship between the spatial orientation of the constituent molecules of the crystals in Figure 6.12 and their magnetic behavior, we studied the interactions between ONCNO dimers maintaining the geometrical parameters found in the actual crystals.

Table 6.7 Values of interaction energy $E_{\text{int}} = E_{\text{dimer}}^T - 2E_{\text{mon}}$ (in kcal/mol) calculated with HF, MP2, B3LYP, CAS(6,6) and CASPT2(6,6) methods with 6-31+g(d,p) basis set.

	$E_{\text{int}}[\text{HF}]$ (kcal/mol)	$E_{\text{int}}[\text{MP2}]$ (kcal/mol)	$E_{\text{int}}[\text{B3LYP}]$ (kcal/mol)	$E_{\text{int}}[\text{CAS}(6,6)]$ (kcal/mol)	$E_{\text{int}}[\text{CASPT2}]$ (kcal/mol)
000MPY	-0.771	-2.714	-0.755	-1.146	-3.460
000PPY	0.485	0.077	0.654	0.055	-
00DPNP	0.611	0.235	0.686	0.223	-
00GPNP1	0.378	-0.084	0.490	-0.038	-0.150
00GPNP2	0.127	-0.335	0.182	-0.277	-0.546
0PBRPH1	0.657	0.411	0.773	0.241	-
0PBRPH2	-1.813	-4.171	-1.673	-2.234	-4.988
HAFXOB	-0.392	-1.238	-0.261	-0.798	-
LICMIT1	1.584	1.056	1.754	1.063	1.639
LICMIT2	-0.017	-0.629	-0.035	-0.382	-
MACOPY1	0.936	0.757	1.085	0.574	-
MACOPY2	-0.666	-1.676	-0.630	-1.059	-
MMEPYC1	-0.958	-4.127	-1.116	-1.491	-4.734
MMEPYC2	-0.922	-3.801	-1.015	-1.440	-4.366
PEFMES	-0.908	-2.082	-0.824	-1.324	-
PEYPUA	-1.217	-5.064	-1.737	-1.696	-5.626
YIWSEC	-0.239	-0.703	-0.251	-0.603	-
YISCEI	-1.273	-2.926	-1.113	-1.656	-
YISCOS	0.553	0.375	0.618	0.204	-
YISNIX	-1.182	-3.242	-1.147	-1.593	-3.986
YOMYII	0.519	0.165	0.648	0.140	-
YUJNEW	-1.268	-2.873	-1.093	-1.649	-
YULPOK1	-0.225	-0.880	-0.194	-0.602	-
YULPOK2	-1.468	-3.074	-1.356	-1.943	-
ZORHIX1	-0.406	-3.986	-0.718	-0.897	-4.238
ZORHIX2	-1.333	-1.975	-1.244	-1.732	-

The 26 ONCNO dimers studied (Table 6.7) have macroscopic ferromagnetic properties. Therefore, it was initially supposed that the high-spin state (triplet) was the energetically preferred state for the two interacting ONCNO radicals. We computed the interaction energy, defined as $E_{\text{int}} = E^{\text{T}}_{\text{dimer}} - 2E_{\text{mon}}$, with HF, MP2, B3LYP, CAS(6,6) and CASPT2(6,6) methods using the 6-31+g(d,p) basis set. CASPT2 was performed only with selected systems to verify if the results were comparable to MP2 and/or CAS methods. At CAS(6,6) level, the results showed that in most of the interactions the dimer was more stable than the two separated monomers. However, there were some ONCNO systems (namely **000PPY**, **00DPNP**, **0PBRPH1**, **LICMIT1**, **MACOPY1**, **YISCOS**, **YOMYII**) whose triplet was not favored energetically compared to two independent molecules (Table 6.7). For **00GPNP1** and **00GPNP2** the HF and B3LYP calculations indicated a positive value of E_{int} , but MP2, CAS(6,6) and CASPT2(6,6) calculations estimated that the triplet was slightly favored in energy, $E_{\text{int}} < 0$. Generally speaking, MP2 and CASPT2(6,6) calculations showed larger values of E_{int} than HF, B3LYP and CAS(6,6).

MP2 and B3LYP calculations on the singlet state showed a significant spin contamination, indicating that these are systems that exhibit an important multiconfigurational character. Therefore, CASSCF(6,6) and CASPT2(6,6) methods are preferred to calculate properly the energy of the different spin states. It was observed that in the singlet state the supposedly doubly occupied orbital (HOMO) showed an occupation number of 1.8 while the virtual orbitals (LUMO) had an occupation number of 0.2, which clearly indicates the need of including configuration interaction when describing these systems. CASPT2 energies were comparable to the MP2 results.

Table 6.8 Values of $\Delta E^{\text{S-T}}$ (in cm^{-1}) calculated at CAS(6,6) using 6-31+g(d,p) basis set.

	$\Delta E^{\text{S-T}}$ CAS(6,6) (cm^{-1})		$\Delta E^{\text{S-T}}$ CAS(6,6) (cm^{-1})
000MPY	9.15	PEFMES	-0.07
000PPY	-0.09	PEYPUA	35.33
00DPNP	0.08	YISCEI	0.06
00GPNP1	0.10	YISCOS	-0.68
00GPNP2	0.05	YISNIX	0.01
0PBRPH1	0.04	YIWSEC	6.75
0PBRPH2	-1.54	YOMYII	0.31
HAFXOB	-0.20	YUJNEW	-0.46
LICMIT1 ^{44,45}	-2.64	YULPOK1	0.06
LICMIT2	0.14	YULPOK2	-0.49
MACOPY1	0.12	ZORHIX1	12.06
MACOPY2	0.12	ZORHIX2	0.00
MMEPYC1	-4.85		
MMEPYC2	-5.12		

The energy gap between the singlet and the triplet states, ΔE^{S-T} , were calculated with CAS(6,6) and B3LYP-*broken symmetry* methods. However the results from B3LYP did not describe correctly most of the singlet states and we could not use these results. The CAS calculations identified three kinds of intermolecular interactions based on the spin multiplicity preference obtained (Table 6.8): Five **FM** ($\Delta E^{S-T} > 0.1 \text{ cm}^{-1}$: **000MPY**, **PEYPUA**, **YISNIX**, **YOMYII**, **ZORHIX1**), eight **AFM** ($\Delta E^{S-T} < -0.1 \text{ cm}^{-1}$: **OPBRPH2**, **HAFXOB**, **LICMIT1**, **MMEPYC1**, **MMEPYC2**, **YISCEI**, **YUJNEW**, **YULPOK2**) and thirteen non-defined or magnetically silent ($|\Delta E^{S-T}| \leq 0.1 \text{ cm}^{-1}$: **000PPY**, **00DPNP**, **00GPNP1**, **00GPNP2**, **OPBRPH1**, **LICMIT2**, **MACOPY1**, **MACOPY2**, **PEFMES**, **YISCOS**, **YIWSEC**, **YULPOK1**, **ZORHIX2**). Therefore, no clear preference for the high-spin state was observed in the analyzed ONCNO systems. Bearing in mind that the studied systems have been selected from crystals characterized by displaying FM properties macroscopically, the results obtained lead to the conclusion that another type of interaction must exist apart from the intermolecular interaction between ONCNO-ONCNO groups that helps to stabilize the high-spin state, since these dimers have not been shown to be conclusive in defining the magnetic properties of the crystals. When all the molecule is included in the calculation (and not only the ONCNO group), the results for LICMIT, YOMYII, KAKHAS and YUJNEW show that the triplet state is the lowest in energy^{44,45}.

Several systems displaying **FM-FM** (FM crystal – FM intermolecular interaction: **000MPY**, **PEYPUA**, **YISNIX**, **ZORHIX1**) and **FM-AFM** (FM crystal – AFM intermolecular interaction: **OPBRPH2**, **MMEPYC1**, **MMEPYC2**,) behavior were selected for a deeper analysis of the intermolecular interactions. Considering the possible need of including configuration interaction and correlation, CASPT2(6,6)/6-31+g(d,p) calculations were compared to CASSCF using the same basis set. The results indicated that both methods are equivalent (Table 6.9).

Table 6.9 Values of ΔE^{S-T} (in cm^{-1}) calculated with CAS(6,6), CASPT2(6,6) and as $\sum J_{ij}^T \Delta P_{ij}$, using a 6-31+g(d,p) basis set for the dimers formed by ONCNO molecules within FM-FM (**ZORHIX1**, **000MPY**, **PEYPUA** and **YISNIX**) and FM-AFM (**MMEPYC1**, **MMEPYC2** and **OPBRPH**) crystals.

<i>FM-FM</i>	ΔE^{S-T} CAS(6,6) (cm^{-1})	ΔE^{S-T} CASPT2(6,6) (cm^{-1})	$\sum J_{ij}^T \Delta P_{ij}$ (cm^{-1})
000MPY	9.2	9.9	1.2
PEYPUA	36.9	49.8	58.2
YISNIX	6.8	6.8	9.5
ZORHIX1	12.0	11.5	4.8
<i>FM-AFM</i>	ΔE^{S-T} CAS(6,6) (cm^{-1})	ΔE^{S-T} CASPT2(6,6) (cm^{-1})	$\sum J_{ij}^T \Delta P_{ij}$ (cm^{-1})
OPBRPH2	-1.5	-1.4	-4.1
MMEPYC1	-4.8	-6.4	-4.2
MMEPYC2	-5.1	-6.3	-4.2

As seen before, the energy gap ΔE^{S-T} can be approximated as $\sum J_{ij} \Delta P_{ij}$, where ij are the active orbitals, and the parameters P_{ij} and J_{ij} can be used to identify the intermolecular interactions that define the multiplicity of the system. The P_{ij} and J_{ij} parameters were

estimated by projecting the CASSCF calculations into a valence bond space with an active space constituted by the π orbitals of the ONCNO groups. Usually, it is considered that the J_{ij} parameter is similar in the singlet and triplet states. The J_{ij} parameter of the triplet state (J_{ij}^T) is used in these calculations. The ij orbitals are the two $p_z(\text{N})+p_z(\text{O})$ [ON_1 and ON_2] and the $p_z(\text{C})$ [C] orbitals located on the active centers with occupations close to 1.0.

Table 6.10 Contributions to the energy gap ΔE^{S-T} (in cm^{-1}) of ΔP_{ij} and J_{ij} (in cm^{-1}) parameters calculated at CASVB(6,6)/6-31+g(d,p) level for the ONCNO α -nitronyl nitroxide fragments within FM-FM (**ZORHIX1**, **000MPY**, **PEYPUA** and **YISNIX**) and FM-AFM (**MMEPYC1**, **MMEPYC2** and **OPBRPH**) crystals. Note that the most important contributions to the intermolecular interaction for each studied dimer are in *cursive*.

FM-FM		ΔP_{ij}			J_{ij}			$J_{ij}\Delta P_{ij}$		
		<i>ON₁</i>	<i>C</i>	<i>ON₂</i>	<i>ON₁</i>	<i>C</i>	<i>ON₂</i>	<i>ON₁</i>	<i>C</i>	<i>ON₂</i>
000MPY	<i>ON₁</i>	0.758	-0.269	0.786	-0.786	-6.148	0	-0.596	1.654	0
	<i>C</i>	-0.256	0.089	-0.257	-0.41	0	0	0.105	0	0
	<i>ON₂</i>	0.682	-0.242	0.709	0	0	0	0	0	0
PEYPUA	<i>ON₁</i>	0.632	-0.266	0.749	4.063	-212.701	-1.2	2.568	56.578	-0.899
	<i>C</i>	-0.232	0.088	-0.276	-0.569	-5.327	-0.656	0.132	-0.469	0.181
	<i>ON₂</i>	0.707	-0.264	0.837	0	-0.517	0	0	0.137	0
YISNIX	<i>ON₁</i>	0.693	-0.256	0.78	0.503	-35.168	0.368	0.349	9.003	0.287
	<i>C</i>	-0.241	0.089	-0.271	0	-1.056	0	0	-0.094	0
	<i>ON₂</i>	0.687	-0.253	0.773	0	0	0	0	0	0
ZORHIX1	<i>ON₁</i>	0.815	-0.251	0.641	-7.715	-45.714	0	-6.288	11.474	0
	<i>C</i>	-0.286	0.088	-0.224	0	-7.353	-0.687	0	-0.647	0.154
	<i>ON₂</i>	0.824	-0.251	0.645	0	-0.471	0	0	0.118	0

FM-AFM		ΔP_{ij}			J_{ij}			$J_{ij}\Delta P_{ij}$		
		<i>ON₁</i>	<i>C</i>	<i>ON₂</i>	<i>ON₁</i>	<i>C</i>	<i>ON₂</i>	<i>ON₁</i>	<i>C</i>	<i>ON₂</i>
OPBRPH2	<i>ON₁</i>	0.683	-0.243	0.717	-2.318	0	-3.602	-1.583	0	-2.583
	<i>C</i>	-0.25	0.089	-0.264	-0.337	-0.595	0	0.084	-0.053	0
	<i>ON₂</i>	0.747	-0.266	0.784	0	0	0	0	0	0
MMEPYC1	<i>ON₁</i>	0.761	-0.245	0.665	-3.655	-7.832	-5.059	-2.782	1.919	-3.365
	<i>C</i>	-0.257	0.088	-0.252	-0.356	-1.112	0	0.091	-0.098	0
	<i>ON₂</i>	0.799	-0.257	0.699	0	0	0	0	0	0
MMEPYC2	<i>ON₁</i>	0.794	-0.25	0.661	-4.762	-3.682	-1.957	-3.781	0.92	-1.294
	<i>C</i>	-0.278	0.087	-0.232	0	-0.647	-0.228	0	-0.056	0.053
	<i>ON₂</i>	0.805	-0.253	0.666	0	0	0	0	0	0

When comparing the results obtained for the energy gap ΔE^{S-T} calculated with CASSCF, CASPT2 and $\sum J_{ij}\Delta P_{ij}$, it must be stressed that the $\sum J_{ij}\Delta P_{ij}$ results show the same trend and establish the same spin multiplicity preference than CASSCF and CASPT2 (Table 6.9). Although the magnitude of ΔE^{S-T} at CASSCF and CASPT2 level is slightly different than the results

computed as $\sum J_{ij}\Delta P_{ij}$, the analysis based on the P_{ij} and J_{ij} parameters is adequate to characterize the main contributions that stabilize the spin preference in the system (Table 6.10).

The calculated ΔP_{ij} matrix is very similar for all the systems studied, irrespective of showing either **FM** or **AFM** intermolecular interaction preference, both in magnitude and sign (Table 6.10). Subsequently, it is the J_{ij} parameter which determines the final spin multiplicity of the ground state of the interacting molecules. Note that the active sites are identified within each monomer as ON₁-C-ON₂.

From the results obtained, it is observed that in all FM-FM systems the main contribution to the energy gap between the low and high-spin states is the interaction between the NO group of one fragment and the C atom of the other (for example, PEYPUA $J_{ij}\Delta P_{ij}(\text{ON}_1\text{-C}) = 56.6 \text{ cm}^{-1}$, Table 6.10 FM-FM). Therefore, when the interaction is mainly between centers with opposite spin densities ($\rho_i\rho_j < 0 \Leftrightarrow \Delta P_{ij} < 0$), the interaction will show a preference for the high-spin state. On the other hand, within the FM-AFM subset, it is the interaction between the groups ON (mon1) - ON (mon2) which determines the low-spin state of the dimers (see MMEPYC2 $J_{ij}\Delta P_{ij}(\text{ON}_1\text{-ON}_1) = -3.8 \text{ cm}^{-1}$ and $J_{ij}\Delta P_{ij}(\text{ON}_1\text{-ON}_2) = -1.3 \text{ cm}^{-1}$, Table 6.10, FM-AFM).

We can thus conclude that it appears to exist a relationship between the spatial distribution of the active centers of the interacting molecules and the spin preference of the ground state. We should remark, however, that the study performed on the ONCNO group, which mainly contains the spin density, does not reproduce the ferromagnetic properties observed experimentally. It thus follows that other interactions, that are not contemplated in the simplified ONCNO system, play a significant role stabilizing the high-spin state.

6.2.4 Statistical treatment

As mentioned before, McConnell I theory⁴¹ postulates that the magnetic coupling between radical units has a direct relationship with the interaction between their spin densities. It has been seen that the distance (D) by itself is not sufficient criterion to establish the type of interaction between molecules. Therefore, we evaluated a possible relationship between the singlet-triplet energy gap ΔE^{S-T} and the spatial orientation of the interacting molecules. For that, we analyzed the set of 6 geometrical parameters (D, A₁, A₂, T₁, T₂ and T₃) that define the relative spatial location of any two ONCNO interacting molecules and we tried to find a correlation between these parameters and the spin preference of the interaction.

Let us define **D** ($m \times n$) as the matrix of the position vectors, where m represents the number of ONCNO dimers analyzed ($m = 26$) and n the coordinates ($n = 6$) that describe each one of them. Position vectors were constructed from the geometrical parameters that describe the closest ONCNO interactions in the selected pairs of NN radicals (see A angles and T dihedrals in degrees in Table 6.6, and in radians in Table 6.11; note that lower case a and t refers to radians).

The mean d_j [equation (6.15)] and the variance s_j^2 [equation (6.16), where s_j is the standard deviation of the samples] were calculated for each geometrical parameter j of the

set of crystals studied (Table 6.11). Unfortunately, it is not possible to distinguish easily FM from AFM interactions based simply on the statistical descriptive parameters or the position vectors.

$$d_j = \frac{1}{m} \sum_{i=1}^m d_{ij} \quad (6.15)$$

$$s_j^2 = \frac{1}{m-1} \sum_{i=1}^m (d_{ij} - d_j)^2 \quad (6.16)$$

Table 6.11 D (26×6) matrix representing the position vectors for the closest contacts found in the studied crystals (distance in Angstroms, angles and dihedrals in radians).

	D (Å)	a ₁ (rad)	a ₂ (rad)	t ₁ (rad)	t ₂ (rad)	t ₃ (rad)
000MPY	3.499	1333	2.225	3.454	4.676	1.820
000PPY	3.903	2.382	2.382	3.142	6.158	0.125
00DPNP	4.275	1.827	2.339	1.579	1.057	3.017
00GPNP1	3.997	2.234	2.234	3.142	0.744	5.539
00GPNP2	4.296	2.209	2.209	3.142	0.528	5.755
0PBRPH1	4.221	2.376	2.376	3.142	0.860	5.423
0PBRPH2	4.290	1.042	1919	4.432	1.465	5.361
HAFXOB	4.912	1.321	1996	5.016	1.259	4.787
LICMIT1	3.158	2.563	2.563	3.142	6.282	0.001
LICMIT2	4.594	1680	1847	3.760	4.331	4.886
MMEPYC1	3.429	1.186	2.674	3.025	1.224	5.584
MMEPYC2	3.453	1.233	2.691	3.380	5.089	0.538
MACOPY1	4.324	1.808	1993	0.983	4.749	3.518
MACOPY2	4.720	1.350	1639	2.569	2.034	1.089
PEFMES	4.328	1.455	1987	2.599	1.424	6.183
PEYPUA	3.719	1.029	2001	3.018	5.123	4.294
YIWSEC	4.685	1.723	2.076	2.783	2.314	4.284
YISCEI	4.705	1.083	1823	4.446	1.414	5.275
YISCOS	4.768	1.688	2.494	1.072	3.233	4.938
YISNIX	4.130	1.141	2.487	4.150	1.210	5.701
YOMYII	3.966	1.845	2.236	1.526	3.915	3.748
YUJNEW	4.709	1.102	1.724	1812	4.796	1.057
YULPOK1	4.465	1.647	2.257	2.876	1.695	0.329
YULPOK2	4.509	1.252	1.252	3.142	1.748	4.536
ZORHIX1	3.168	1248	2.215	2.077	4.953	0.811
ZORHIX2	4674	1.763	1.763	3.142	3.085	3.198
Mean (\bar{d}_j)	4.188	1.597	2.131	2.944	2.899	3.531
Variance (s_j^2)	0.266	0.211	0.116	1.007	3.436	4.342

In order to elucidate if there is any relationship between the spin multiplicity preference and the spatial orientation of the interacting units, two statistical analyses were performed.

In a first approach, a factor analysis (based on a principal component analysis) was done as described in ref⁴⁶ to try to identify the factor that is the main contributor to the variance between the geometrical parameters for all the studied systems. Secondly, we evaluated the possible grouping of the system as AFM or FM performing a cluster analysis in terms of Euclidean and Mahalanobis distances. All the the statistical treatments were carried out with Fortran90.

To perform these statistical analyses, first we calculated the covariance **C** matrix (Table 6.12) for the original data set according to equation (6.17):

$$c_{kl} = \frac{1}{m-1} \sum_{i=1}^m (d_{ik} - \bar{d}_k)(d_{il} - \bar{d}_l) \quad (6.17)$$

The covariance **C** matrix has the following properties¹³:

- The c_{kl} elements of the **C** matrix measure the association between the parameters k, l (being k and l the geometrical parameters D, a_1, a_2, t_1, t_2 and t_3)
- The diagonal elements represent the variance $c_{kk} = s_k^2$.
- **C** is a symmetric matrix.
- The trace of the **C** matrix, $\text{Tr}(\mathbf{C})$, is the total variance.
- A positive and large c_{kl} value indicates that the majority of values for the variables k, l deviate in the same direction.

Table 6.12 Covariance matrix for the considered data sample.

	D	a₁	a₂	t₁	t₂	t₃
D	0.266	-0.026	-0.104	0.024	-0.439	0.374
a₁	-0.026	0.211	0.052	-0.103	0.071	-0.114
a₂	-0.104	0.052	0.116	-0.031	0.080	-0.090
t₁	0.024	-0.103	-0.031	1.007	-0.520	0.509
t₂	-0.439	0.071	0.080	-0.520	3.436	-2.604
t₃	0.374	-0.114	-0.090	0.509	-2.604	4.342

Table 6.13 Correlation coefficients r_{kl} corresponding to vectors of position matrix.

	D	a₁	a₂	t₁	t₂	t₃
D	1.000	-0.108	-0.594	0.047	-0.459	0.347
a₁	-0.108	1.000	0.333	-0.224	0.084	-0.119
a₂	-0.594	0.333	1.000	-0.091	0.126	-0.127
t₁	0.047	-0.224	-0.091	1.000	-0.280	0.244
t₂	-0.459	0.084	0.126	-0.280	1.000	-0.674
t₃	0.347	-0.119	-0.127	0.244	-0.674	1.000

The covariance matrix is a triangular matrix where the diagonal elements represent the variance of the parameter. Considering only the non-diagonal $c_{ij} = c_{ji}$ elements in Table

6.12, one realizes that the largest value (**-2.604**) takes place between t_2 and t_3 dihedrals, which indicates that there is a significant association between these two parameters.

From the covariance matrix c_{kl} elements and the standard deviation of each s_k and s_l parameter, the correlation coefficients $-1 < r_{kl} < 1$ can be calculated using equation (6.18). Again, it can be seen that the largest coefficient in absolute value corresponds to the correlation between the two dihedrals t_2 and t_3 (Table 6.13).

$$r_{kl} = \frac{c_{kl}}{s_k \cdot s_l} \quad (6.18)$$

6.2.4.1 Factor analysis

The factor analysis⁴⁶ consists in a conversion of the n orthogonal axes of reference in new axes placed in the direction of the maximum variance. While one of the axes represents the direction of the maximum variance, it is expected that its orthogonal axes represent a minimum variation. The minimum number of factors (usually 1 or 2) that describe the maximum variability are selected to define the distribution of data in a new space which results from the combination of the initial axes. In that way, it is possible to describe the distribution of the data in a space of reduced dimensionality⁴⁷.

Therefore, the factor analysis is a statistical tool that allows us to convert the n -dimensional space multivariate data matrix in a matrix of factors where the one/ones that represent the direction of maximum variance is/are suitable to describe the distribution of the data. The analysis of the obtained factors will also reveal which combination of variables has the higher influence on the variation.

The mathematical foundation of the factor analysis is based on the eigenvalues λ_i (Λ , eigenvalues matrix) and the eigenvectors \mathbf{e}_i (\mathbf{E} , eigenvectors matrix) of the covariance \mathbf{C} matrix, where \mathbf{I} is the identity matrix [equation (6.19)]:

$$\mathbf{C} \cdot \mathbf{e}_i = \lambda_i \cdot \mathbf{I} \cdot \mathbf{e}_i \quad (6.19)$$

and, consequently,

$$(\mathbf{C} - \lambda \mathbf{I}) \cdot \mathbf{e} = 0$$

$$|\mathbf{C} - \lambda \mathbf{I}| = 0 \quad (6.21)$$

We will use equations (6.20) and (6.21) to calculate λ_i and \mathbf{e}_i , respectively. Since the covariance \mathbf{C} matrix is symmetrical, it will not have negative eigenvalues λ_i . The n factors f_i of the \mathbf{F} matrix (matrix $n \times n$ of the calculated factors) are defined as the product between

the matrix of the normalized eigenvectors \mathbf{E} and the $n \times n$ diagonal matrix of eigenvalues $\mathbf{\Lambda}^{1/2}$ [equation (6.22)].

$$\mathbf{F} = \mathbf{E} \cdot \mathbf{\Lambda}^{1/2} \quad (6.22)$$

The product of the factor matrix and its transpose gives as a result the covariance matrix [equation (6.23)].

$$\mathbf{C} = \mathbf{F} \cdot \mathbf{F}^T \quad (6.23)$$

The factors are a linear combination of the original parameters ($\mathbf{x}_i = \mathbf{D}, \mathbf{a}_1, \mathbf{a}_2, \mathbf{t}_1, \mathbf{t}_2, \mathbf{t}_3$) weighted by the $f_{i,j}$ coefficients that indicate the contribution of the variable j into the factor \mathbf{f}_i [equation (6.24)].

$$\mathbf{f}_i = f_{i,1}x_1 + f_{i,2}x_2 + \dots + f_{i,n}x_n \quad (6.24)$$

The eigenvalues λ_i represent the contribution of the corresponding eigenvector to the total of the variance. Therefore, the factors with the largest eigenvalues are the ones that represent the axis of maximum variance and they are considered the main factors.

Finally, the original data matrix \mathbf{D} (Table 6.11) needs to be converted to a new data matrix \mathbf{S} [equation (6.25)] using the calculated factors \mathbf{F} . This new matrix \mathbf{S} represents the data in a n -dimensional space defined by the n calculated factors.

$$\mathbf{S} = \mathbf{D} \cdot \mathbf{F} \quad (6.25)$$

For the position vectors defined for the systems studied (Table 6.11), the corresponding eigenvalues are $\lambda_1 = 0.048$ (0.5%), $\lambda_2 = 0.916$ (9.8%), $\lambda_3 = \mathbf{6.682}$ (71.3%), $\lambda_4 = 1.267$ (13.1%), $\lambda_5 = 0.181$ (1.9%) and $\lambda_6 = 0.284$ (3.0%). The sum of all the eigenvalues $\lambda_1 + \lambda_2 + \lambda_3 + \lambda_4 + \lambda_5 + \lambda_6 = 9.378$ is equivalent to the sum of the variances of the original data ($0.266 + 0.211 + 0.116 + 1.007 + 3.436 + 4.342 = 9.378$).

$$\mathbf{E} = \begin{pmatrix} 0.481 & -0.087 & 0.088 & -0.080 & 0.485 & -0.716 \\ -0.206 & -0.121 & -0.023 & -0.002 & 0.858 & 0.454 \\ 0.851 & -0.016 & -0.020 & 0.011 & -0.074 & 0.519 \\ 0.021 & 0.966 & 0.127 & -0.180 & 0.133 & 0.023 \\ 0.047 & 0.210 & -0.638 & 0.728 & 0.079 & -0.101 \\ -0.003 & 0.021 & 0.754 & 0.656 & 0.011 & 0.023 \end{pmatrix}$$

and the square root diagonal matrix of the eigenvalues $\mathbf{\Lambda}^{1/2}$

$$\Lambda^{1/2} = \begin{pmatrix} 0.220 & 0 & 0 & 0 & 0 & 0 \\ 0 & 0.957 & 0 & 0 & 0 & 0 \\ 0 & 0 & 2.585 & 0 & 0 & 0 \\ 0 & 0 & 0 & 1.125 & 0 & 0 \\ 0 & 0 & 0 & 0 & 0.425 & 0 \\ 0 & 0 & 0 & 0 & 0 & 0.533 \end{pmatrix},$$

The factors **F** coefficients are calculated according to the equation (6.22).

$$\mathbf{F} = \begin{pmatrix} 0.105 & -0.083 & 0.229 & -0.090 & 0.206 & -0.382 \\ -0.045 & -0.116 & -0.059 & -0.002 & 0.365 & 0.242 \\ 0.187 & -0.015 & -0.052 & 0.013 & -0.031 & 0.277 \\ 0.005 & 0.924 & 0.328 & -0.203 & 0.056 & 0.012 \\ 0.010 & 0.201 & -1.649 & 0.819 & 0.033 & -0.054 \\ -0.001 & 0.020 & 1.948 & 0.739 & 0.005 & 0.012 \end{pmatrix}$$

The six new factors are represented as a linear combination of the initial coordinates **D**, **a**₁, **a**₂, **t**₁, **t**₂, **t**₃. The factor **F** matrix can be expressed as follows:

$$\begin{aligned} \mathbf{f}_1 &= 0.105 \mathbf{D} - 0.045 \mathbf{a}_1 + 0.187 \mathbf{a}_2 + 0.005 \mathbf{t}_1 + 0.010 \mathbf{t}_2 - 0.001 \mathbf{t}_3 \\ \mathbf{f}_2 &= -0.083 \mathbf{D} - 0.116 \mathbf{a}_1 - 0.015 \mathbf{a}_2 + 0.924 \mathbf{t}_1 + 0.201 \mathbf{t}_2 + 0.020 \mathbf{t}_3 \\ \mathbf{f}_3 &= 0.229 \mathbf{D} - 0.059 \mathbf{a}_1 - 0.052 \mathbf{a}_2 + 0.328 \mathbf{t}_1 - 1.649 \mathbf{t}_2 + 1.948 \mathbf{t}_3 \\ \mathbf{f}_4 &= -0.090 \mathbf{D} - 0.002 \mathbf{a}_1 + 0.013 \mathbf{a}_2 - 0.203 \mathbf{t}_1 + 0.819 \mathbf{t}_2 + 0.739 \mathbf{t}_3 \\ \mathbf{f}_5 &= 0.206 \mathbf{D} + 0.365 \mathbf{a}_1 - 0.031 \mathbf{a}_2 + 0.056 \mathbf{t}_1 + 0.033 \mathbf{t}_2 + 0.005 \mathbf{t}_3 \\ \mathbf{f}_6 &= -0.382 \mathbf{D} + 0.242 \mathbf{a}_1 + 0.277 \mathbf{a}_2 + 0.012 \mathbf{t}_1 - 0.054 \mathbf{t}_2 + 0.012 \mathbf{t}_3 \end{aligned}$$

and the product of the factor matrix by its transpose $\mathbf{F} \cdot \mathbf{F}^T$ gives as a result the covariance matrix if the eigenvalue have been normalized, as it is in this case.

The specific weight of each factor is determined by the value of the corresponding eigenvalue. The main factor in this case is the factor **f**₃ since its corresponding eigenvalue ($\lambda_3 = 6.682$) represents the 71.3% of the total variance. Accordingly, **f**₁, **f**₂, **f**₃, **f**₄, **f**₅, **f**₆ describe the 0.5%, 9.8%, 71.3%, 13.5%, 1.9% and 3.0% of the variance. The three most important factors (**f**₂, **f**₃, **f**₄) represent the 94.5% of the total variance. We must remark that the main contributors to these three factors are the three dihedral angles **t**₁, **t**₂, **t**₃, which in turn are the parameters with the higher standard deviations. The three dihedral angles establish the relative orientation of planes that contain the active atoms in each molecule

For a comprehensive study on the new axes of the factors **f**_{*i*}, we must calculate the matrix **S** from the original data within the new space. The elements of the **s**_{*i*} vectors are calculated as $\mathbf{s}_i = \mathbf{d}_k \cdot \mathbf{f}_i$, being **k** each one of the studied systems and **i** each one of the new factors (Table 6.14). It is observed that **s**₃ has now the higher standard deviation when compared to

the other factors. Therefore, this is the parameter that shows the highest variability between the systems studied.

Table 6.14 New matrix **S** resulting from the product between the original position vector **D** matrix and the new factor **F** matrix.

	$s_1 = \mathbf{d}_k \cdot \mathbf{f}_1$	$s_2 = \mathbf{d}_k \cdot \mathbf{f}_2$	$s_3 = \mathbf{d}_k \cdot \mathbf{f}_3$	$s_4 = \mathbf{d}_k \cdot \mathbf{f}_4$	$s_5 = \mathbf{d}_k \cdot \mathbf{f}_5$	$s_6 = \mathbf{d}_k \cdot \mathbf{f}_6$
000MPY	0.787	3.692	-2.428	4.187	1.498	-0.584
000PPY	0.827	3.510	-8.253	4.177	1.983	-0.545
00DPNP	0.821	1.132	5.400	2.416	1.614	-0.543
00GPNP1	0.756	2.543	11.263	3.729	1.798	-0.302
00GPNP2	0.782	2.482	12.109	3.685	1.846	-0.414
0PBRPH1	0.801	2.526	10.880	3.720	1.895	-0.321
0PBRPH2	0.795	3.995	10.303	3.899	1.530	-0.814
HAFXOB	0.864	4.397	9.839	3.132	1.781	-0.952
LICMIT1	0.775	3.571	-8.891	4.256	1.894	-0.174
LICMIT2	0.812	3.844	4.467	6.003	1.883	-0.963
MACOPY1	0.798	1.338	0.121	5.925	1.720	-0.862
MACOPY2	0.775	2.234	0.526	1.544	1.633	-1.086
MMEPYC1	0.830	2.694	10.428	4.237	1.295	-0.243
MMEPYC2	0.879	3.690	-5.660	3.604	1.441	-0.500
PEFMES	0.784	2.257	11.351	4.841	1.586	-0.720
PEYPUA	0.783	3.451	1.593	6.447	1.442	-0.803
YIWSEC	0.838	2.506	6.306	4.099	1.785	-0.835
YISCEI	0.819	3.958	10.321	3.752	1.632	-0.987
YISCOS	0.927	1.114	5.502	5.680	1.714	-0.822
YISNIX	0.876	3.684	11.221	4.019	1.493	-0.557
YOMYII	0.797	1.698	2.027	5.336	1.656	-0.594
YUJNEW	0.826	2.118	-4.334	3.940	1.587	-1.276
YULPOK1	0.849	2.411	-0.405	0.674	1.672	-0.733
YULPOK2	0.682	2.811	7.878	3.753	1.605	-1.072
ZORHIX1	0.752	2.493	-5.371	3.978	1.326	-0.525
ZORHIX2	0.787	2.972	3.048	3.852	1.848	-0.958
Mean	0.809	2.812	3.817	4.034	1.660	-0.699
Variance	0.002	0.839	44.654	1.604	0.033	0.081

If the s_3 values (corresponding to the main factor \mathbf{f}_3) are represented as a function of the energy gap ΔE^{S-T} (considering only the systems with $|\Delta E^{S-T}| > 0.1 \text{ cm}^{-1}$, see Table 6.8), the formation of certain groups is appreciated (Figure 6.15) that seems to indicate the existence of "some" relationship between geometry and spin multiplicity preference. It is noticed that at $5 < |s_3| < 10$ the studied ONCNO dimers are mostly AFM ($\Delta E^{S-T} < 0$). On the contrary, for $|s_3| < 5$ or $|s_3| > 10$ the systems show mainly FM behavior. The s_3 basically results from the t_2 and the t_3 contributions. It follows that, at certain t_2 and the t_3 orientations, it appears to be a specific preference for the ferromagnetic interaction between the two ONCNO units.

AFM ($5 < |s_3| < 10$):

- YUJNEW ($s_3 = -4$), LICMIT1 ($s_3 = -9$), MMPEYC2 ($s_3 = -6$)
- YULPOK2 ($s_3 = 8$), HAFXOB ($s_3 = 10$), YISCEI ($s_3 = 10$), OPBRPH2 ($s_3 = 10$), MMPEYC1 ($s_3 = 10$)

FM ($|s_3| < 5$ or $|s_3| > 10$):

- ZORHIX1 ($s_3 = -5$), 000MPY ($s_3 = -2$)
- MACOPY1 ($s_3 = 0$), MACOPY2 ($s_3 = 1$), YOMYII ($s_3 = 2$), LICMIT2 ($s_3 = 4$)
- YISNIX ($s_3 = 11$), 00GPNP1 ($s_3 = 11$)

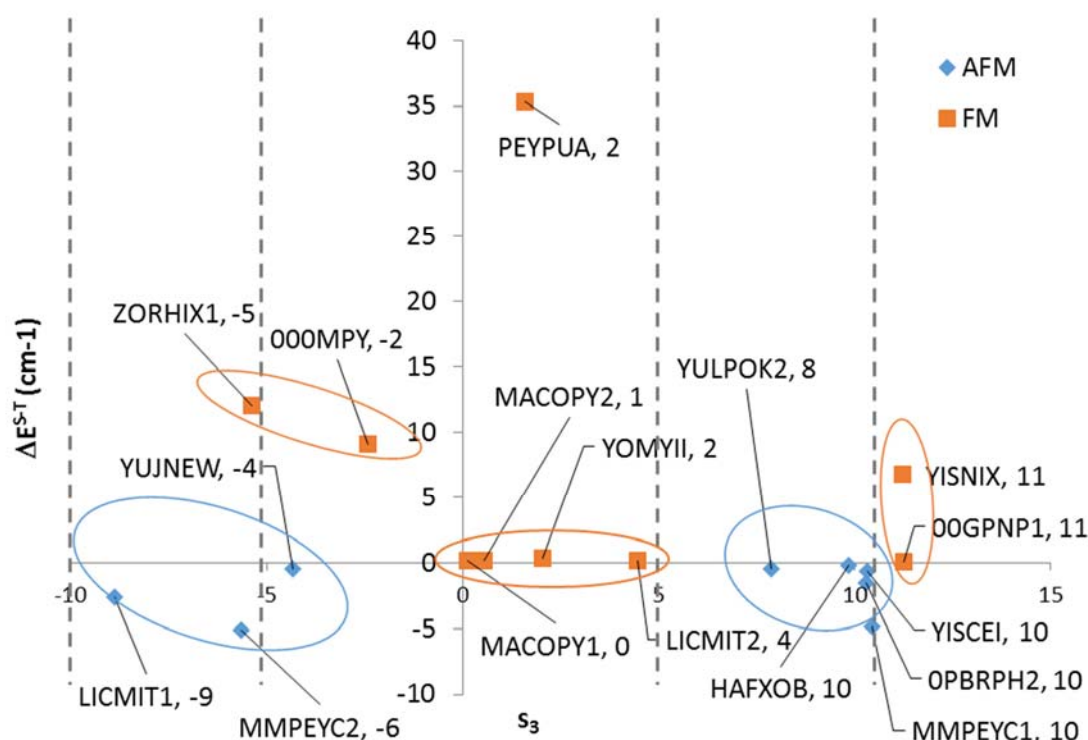


Figure 6.15 Graph that represents the energy gap ΔE^{S-T} as a function of the contributions from main factor s_3 . There is certain clustering of FM and AFM systems. Labels indicate systems code and s_3 value.

However, it is observed in Figure 6.15 that, despite the possible clustering, there are one AFM (YUJNEW) dimer that is out of this grouping scheme. Additionally, there are several systems that are in the borderline (ZORHIX with $s_3 = 5$ and HAFXOB, YISCEI, OPBRPH2, MMPEYC1 with $s_3 = 10$). Consequently, it can be said that the frontier between AFM and FM system is very difficult to establish and a slight variation of the orientation of the NN radicals may vary the multiplicity of the ground state.

6.2.4.2 Cluster analysis on the initial geometrical coordinates

The cluster analysis methodology^{46,48} used has been the single linkage or nearest neighbor clustering. According to this technique, the relationship of closeness within a group of data is represented calculating the "distance" d_{ij} between the elements of the group. The cluster analysis is a hierarchical methodology based on the shortest distance ϵ between the

elements of the cluster. New clusters are merged considering the shortest distance ε between the two clusters, which define the level of proximity between two clusters and represents the threshold distance for that clustering. Ideally, we would expect the formation of two clusters, one AFM and another FM, that would correlate the spin preference of the interaction (AFM : $\Delta E^{S-T} < 0$; FM: $\Delta E^{S-T} > 0$) with the geometrical distances between the systems. Three different situations can be expected³⁹ (see, Figure 6.16): (a) AFM and FM clusters are disjoint ($\varepsilon_{AFM}, \varepsilon_{FM} < \varepsilon_{AFM+FM}$) and form completely separated groups; (b) two clusters AFM and FM form two distinguished clusters but there are common elements shared by both clusters ($\varepsilon_{AFM}, \varepsilon_{FM} \sim \varepsilon_{AFM+FM}$); and (c) the AFM and FM clusters are undistinguishable ($\varepsilon_{AFM+FM} \leq \varepsilon_{AFM}, \varepsilon_{FM}$).

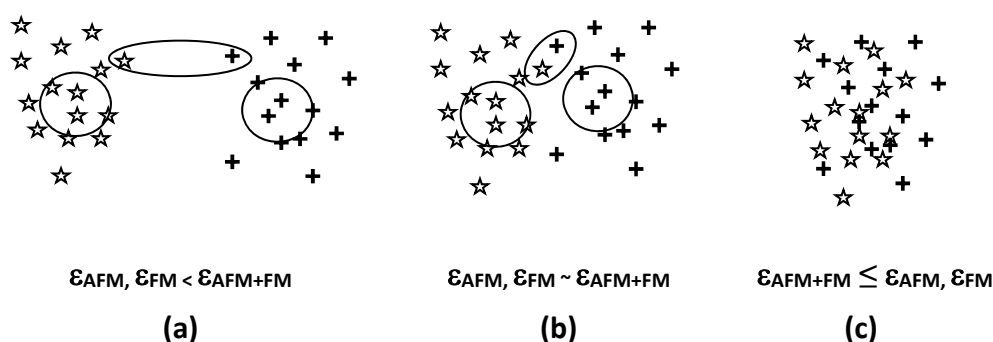


Figure 6.16 Graphical representation of the type of clusters expected³⁹: (a) disjoint ($\varepsilon_{AFM}, \varepsilon_{FM} < \varepsilon_{AFM+FM}$) forming completely separated groups; (b) two distinguished clusters but with common elements shared by both clusters ($\varepsilon_{AFM}, \varepsilon_{FM} \sim \varepsilon_{AFM+FM}$); and (c) the clusters are undistinguishable ($\varepsilon_{AFM+FM} \leq \varepsilon_{AFM}, \varepsilon_{FM}$).

The cluster analysis was performed based in two possible distances: the *Euclidean distance* (Table 6.16) and the *Mahalanobis distance* (Table 6.17). The Euclidean distance X_{kl} between two points k and l is defined as in equation (6.26), where $(\bar{d}_k - \bar{d}_l)$ is the vector difference between the vectors \bar{d}_k, \bar{d}_l , k and l represent the studied systems and j the coordinate within each system. Massart and Kaufman⁴⁸ showed that the Euclidean distance may represent a distortion and it would be necessary to compensate this effect by introducing the inverse of the correlation matrix, as is done in the calculation of the distances according to Mahalanobis [equation (6.27)]. Mahalanobis distances, therefore, study the distance between two objects considering the variation and correlation inherent to the data.

$$\left(\chi_{kl}^E\right)^2 = \sum_j (d_{kj} - d_{lj})^2 = (\bar{d}_k - \bar{d}_l) \times (\bar{d}_k - \bar{d}_l)^T \quad (6.26)$$

$$\left(\chi_{kl}^M\right)^2 = (\bar{d}_k - \bar{d}_l) \times C^{-1} \times (\bar{d}_k - \bar{d}_l)^T \quad (6.27)$$

Euclidian distances range from 0.3 to 8.2 and Mahalanobis from 0.6 to 5.7 (Table 6.15). It is observed that Mahalanobis distances are slightly shorter than the Euclidian ones and the range of values is smaller. Looking separately at the distances within the connections with $\Delta E^{S-T} < 0$ (AFM), $\Delta E^{S-T} > 0$ (FM), and in between both groups (AFM/FM), it is seen that the minimum, maximum and average distances within each AFM and FM group are very similar both in the Euclidean and the Mahalanobis and comparable to the distances between the AFM and FM groups. The application of the nearest neighbor algorithm resulted in AFM and

FM threshold distances (ϵ_{AFM} and ϵ_{FM}) higher than ϵ_{AFM+FM} (2.5 and 2.7 for Euclidean and Mahlanobis distances, respectively).

Table 6.15 Clusters identified considering Euclidean and Mahlanobis distances

	Euclidean Distances				Mahlanobis distances			
	Max	Min	Average	ϵ	Max	Min	Average	ϵ
AFM	8.1	0.4	3.9	3.1	5.2	1.0	3.2	3.1
FM	6.9	0.3	3.5	2.6	5.2	0.6	3.1	2.7
AFM/FM	8.2	0.8	4.0	<i>n.a.</i>	5.7	1.4	3.3	<i>n.a.</i>

It can be concluded that there is not a clear clustering that differentiates the nature of the magnetic intermolecular interaction based only on the geometrical distributions of the spin containing atoms within the α -NN crystals studied. If some relationship exists between the geometrical parameters that define the position of the ONCNO groups and the magnetic type of interaction between them, this type of correlation is so subtle that a slight variation in the position or orientation produces a change in the nature of the magnetic interaction between the fragments.

It could be said that McConnell I theory is valid when the molecules are placed on parallel planes and there is a clear intermolecular interaction of the spin containing atoms. However, slight modifications in the orientation angle between the orbitals or additional contributions from other through-space interactions could change the spin preference of the interactions. Thus, these factors should be considered when stablishing the overall spin multiplicity.

6.2.5 Conclusions

Our study has shown that there is not a direct correlation between the magnetic property experimentally observed for the α -NN crystals and the spin preference of the simplified ONCNO dimers. This observation indicates that there must be other through-space interactions not considered when evaluating only the intermolecular ONCNO interactions that must be important in the definition of the magnetic properties³⁹. It has been seen in other works that, in some of these cases, the right spin state is described when the calculation is performed with the whole molecules^{44,45}.

Accordingly, we can say that the magneto-structural correlation is very subtle and a slight variation in the position or orientation produces a change in the nature of the magnetic interaction between the fragments. As seen before, McConnell I theory is basically valid when the molecules are placed on parallel planes and there is a clear intermolecular interaction of the spin containing atoms. However, the magneto-structural relationship is more complicated when several through-space interactions must be considered.

Table 6.16 Euclidean distances

000MPY	0.0	2.5	4.3	5.5	5.8	5.4	5.0	2.8	3.3	3.2	3.2	5.1	1.4	5.6	2.6	3.7	5.0	4.4	5.3	2.9	2.2	3.5	4.2	1.8	2.5
000PPY	2.5	0.0	6.1	7.7	8.0	7.5	7.2	0.8	5.3	4.3	4.5	7.5	1.7	7.8	4.5	5.8	7.3	6.1	7.6	4.6	2.7	4.6	6.5	2.2	4.5
00DPNP	4.3	6.1	0.0	3.0	3.2	2.9	3.8	6.4	4.4	3.8	2.6	3.2	5.2	3.4	4.6	2.2	3.8	3.0	3.8	3.0	4.4	3.1	2.6	4.7	2.7
00GPNP1	5.5	7.7	3.0	0.0	0.4	0.3	2.0	7.9	3.8	5.0	4.8	1.4	6.7	1.4	4.7	2.2	2.1	3.4	1.6	4.0	6.4	5.4	2.0	6.5	3.4
00GPNP2	5.8	8.0	3.2	0.4	0.0	0.5	2.0	8.2	4.0	5.3	5.1	1.6	7.1	1.4	5.0	2.4	2.1	3.6	1.7	4.3	6.6	5.6	2.2	6.9	3.7
0PBRPH1	5.4	7.5	2.9	0.3	0.5	0.0	2.0	7.7	3.7	4.9	4.7	1.5	6.6	1.5	4.7	2.1	2.1	3.3	1.7	3.9	6.2	5.2	2.0	6.4	3.3
0PBRPH2	5.0	7.3	3.8	2.0	2.0	0.0	0.0	7.6	3.1	5.2	4.7	1.8	6.2	2.1	4.1	2.3	0.4	3.9	0.8	4.2	6.1	5.3	1.7	6.3	3.1
HAFXOB	5.0	7.2	4.0	0.5	2.5	2.4	1.1	0.0	7.5	5.5	4.5	2.7	6.2	2.9	4.5	2.6	0.8	4.5	1.6	4.6	6.1	5.0	2.1	6.4	3.1
LICMIT1	2.8	0.8	6.4	7.6	7.5	7.7	0.0	5.6	4.6	4.7	4.9	7.7	1.9	8.1	4.8	6.1	7.6	6.4	7.9	4.9	3.2	4.9	6.8	2.3	4.9
LICMIT2	3.3	5.3	4.4	3.1	3.4	3.7	3.1	5.6	0.0	3.1	4.6	3.6	4.7	3.4	1.7	2.3	3.1	3.0	3.4	2.7	4.4	5.4	2.8	4.7	2.2
MACOPY1	3.2	4.3	4.0	4.7	4.7	4.7	4.7	4.7	3.1	0.0	4.0	4.7	4.0	4.6	2.4	3.1	5.2	2.2	5.3	1.1	2.7	4.8	3.9	3.2	2.8
MACOPY2	3.2	4.5	4.5	4.7	4.5	4.7	4.5	4.9	4.6	4.0	0.0	4.9	3.6	5.2	4.6	3.3	4.6	4.4	5.1	3.6	2.9	1.1	3.5	3.4	2.5
MMEPYC1	5.1	7.5	3.2	1.4	1.6	1.5	1.8	7.7	3.6	4.7	4.9	0.0	6.4	1.4	4.2	2.3	2.1	3.2	1.3	3.7	6.1	5.4	2.1	6.2	3.4
MMEPYC2	1.4	1.7	5.2	6.7	7.1	6.6	6.2	1.9	4.7	4.0	3.6	6.4	0.0	6.9	3.9	4.9	6.3	5.5	6.5	4.0	2.3	3.6	5.5	1.4	3.7
PEFMES	5.6	7.8	3.4	1.4	1.4	1.5	2.1	8.1	3.4	4.6	5.2	1.4	6.9	0.0	4.2	2.2	2.1	2.8	1.8	3.7	6.2	5.9	1.9	6.6	3.5
PEYPUA	2.6	4.5	4.6	4.7	5.0	4.7	4.1	4.5	4.8	2.4	4.6	4.2	3.9	4.2	0.0	3.1	4.2	3.1	4.4	2.2	3.6	5.3	3.6	3.7	2.6
YIWSEC	3.7	5.8	2.2	2.2	2.4	2.1	2.3	6.1	2.3	3.1	3.3	2.3	4.9	2.2	3.1	0.0	2.2	2.1	2.4	2.2	4.2	4.0	1.2	4.7	1.4
YISCEI	5.0	7.3	3.8	2.1	2.1	2.1	0.4	7.6	3.1	5.2	4.6	2.1	6.3	2.1	4.2	2.2	0.0	4.0	1.0	4.3	6.0	5.3	1.7	6.4	3.0
YISCOS	4.4	6.1	3.0	3.4	3.6	3.3	3.9	6.4	3.0	2.2	4.4	3.2	5.5	2.8	3.1	2.1	4.0	0.0	3.9	1.7	4.4	5.2	2.9	4.9	2.8
YISNIX	5.3	7.6	3.8	1.6	1.7	1.7	0.8	7.9	3.4	5.3	5.1	1.3	6.5	1.8	4.4	2.4	1.0	3.9	0.0	4.3	6.4	5.6	2.1	6.6	3.5
YOMYII	2.9	4.6	3.0	4.0	4.3	3.9	4.2	4.6	2.7	1.1	3.6	3.7	4.0	3.7	2.2	2.2	4.3	1.7	4.3	0.0	3.1	4.3	3.1	3.3	2.1
YUJINEW	2.2	2.7	4.4	6.4	6.6	6.2	6.1	3.2	4.4	2.7	2.9	6.1	2.3	6.2	3.6	4.2	6.0	4.4	6.4	3.1	0.0	3.5	4.8	1.7	3.1
YULPOK1	3.5	4.6	3.1	5.4	5.6	5.2	5.3	4.9	5.4	4.8	1.1	5.4	3.6	5.9	5.3	4.0	5.3	5.2	5.6	4.3	3.5	0.0	4.4	3.7	3.2
YULPOK2	4.2	6.5	2.6	2.0	2.2	2.0	1.7	6.8	2.8	3.9	3.5	2.1	5.5	1.9	3.6	1.2	1.7	2.9	2.1	3.1	4.8	4.4	0.0	5.3	2.0
ZORHIX1	1.8	2.2	4.7	6.5	6.9	6.4	6.3	2.3	4.7	3.2	3.4	6.2	1.4	6.6	3.7	4.7	6.4	4.9	6.6	3.3	1.7	3.7	5.3	0.0	3.6
ZORHIX2	2.5	4.5	2.7	3.4	3.7	3.3	3.1	4.9	2.2	2.8	2.5	3.4	3.7	3.5	2.6	1.4	3.0	2.8	3.5	2.1	3.1	3.2	2.0	3.6	0.0

Table 6.17 Mahlanobis distances

000MPY	0.0	2.9	3.5	3.2	3.3	3.4	2.1	3.4	2.8	3.1	3.3	3.3	3.3	2.9	2.1	2.7	2.1	2.8	2.6	4.6	2.8	2.6	3.1	3.5	3.4	1.9	2.6
000PPY	2.9	0.0	4.1	3.7	3.5	3.3	4.0	3.6	1.8	2.9	3.6	4.1	4.9	3.2	4.1	4.0	4.0	2.9	3.8	4.5	4.1	3.3	3.8	3.8	4.8	4.1	2.6
00DPNP	3.5	4.1	0.0	2.8	2.6	2.7	3.6	4.1	4.3	4.6	3.2	2.7	3.1	3.7	2.6	4.4	2.5	3.7	3.6	3.4	2.5	3.4	2.3	4.1	3.3	3.1	3.1
00GNP1	3.2	3.7	2.8	0.0	0.7	1.1	2.9	3.8	3.3	3.6	3.5	3.8	3.2	4.3	2.2	3.9	2.7	3.3	4.7	3.4	2.6	4.6	3.9	3.3	3.7	2.7	2.7
00GNP2	3.3	3.5	2.6	0.7	0.0	0.6	2.8	3.4	3.5	3.3	3.3	3.6	3.3	4.2	2.0	3.9	2.1	3.0	4.2	3.1	2.5	4.3	3.6	3.5	4.0	2.4	2.4
0PBRPH1	3.4	3.3	2.7	1.1	0.6	0.0	3.1	3.4	3.3	3.4	3.4	3.9	3.4	4.1	2.4	4.1	2.2	3.2	4.1	3.1	2.6	4.5	3.6	4.0	4.2	2.6	2.6
0PBRPH2	2.1	4.0	3.6	2.9	2.8	3.1	0.0	2.2	4.2	2.8	3.8	3.3	2.9	3.2	2.1	2.5	2.4	1.0	4.6	1.9	3.2	3.5	3.7	2.9	3.4	2.4	2.4
HAFXOB	3.4	3.6	4.1	3.8	3.4	3.4	2.2	0.0	4.5	2.8	4.5	3.7	4.3	3.5	3.4	4.0	2.4	1.4	4.4	2.4	4.1	3.8	3.4	4.3	4.9	2.5	2.5
LICMIT1	2.8	1.8	4.3	3.3	3.5	3.3	4.2	4.5	0.0	3.8	4.1	4.6	4.6	3.1	2.6	4.3	4.1	3.7	4.4	5.4	4.5	3.4	4.7	4.3	4.8	3.6	3.4
LICMIT2	3.1	2.9	4.6	3.6	3.3	3.4	2.8	2.8	3.8	0.0	3.0	4.3	4.6	4.1	2.9	2.7	2.3	2.4	4.0	3.5	3.0	3.5	3.5	4.8	3.8	4.5	2.0
MACOPY1	3.3	3.6	3.2	3.5	3.3	3.4	3.8	4.5	4.1	3.0	0.0	3.7	4.1	4.2	2.3	2.8	2.3	3.8	2.8	4.1	1.2	2.6	4.5	3.7	3.4	2.6	2.6
MACOPY2	3.3	4.1	2.7	3.8	3.6	3.9	3.3	3.7	4.6	4.3	3.7	0.0	4.5	4.0	3.3	4.3	2.8	3.1	4.9	4.2	3.5	2.4	2.1	2.9	3.4	2.4	2.4
MMEPYC1	2.9	4.9	3.1	3.2	3.3	3.4	2.9	4.3	4.6	4.6	4.1	4.5	0.0	3.1	2.6	3.3	3.5	3.5	4.3	2.1	3.1	4.6	4.3	4.6	3.1	4.2	4.2
MMEPYC2	2.1	3.2	3.7	4.3	4.2	4.1	3.2	3.5	3.6	4.1	4.2	4.0	3.1	0.0	3.9	3.4	3.3	3.4	4.2	2.6	3.5	3.5	3.3	5.2	3.0	3.7	3.7
PEFMES	2.7	4.1	2.6	2.2	2.0	2.4	2.1	3.4	4.3	2.9	2.3	3.3	2.6	3.9	0.0	2.5	1.9	2.4	3.5	2.7	1.7	3.3	4.0	2.7	3.1	2.4	2.4
PEYPUA	2.1	4.0	4.4	3.9	3.9	4.1	2.5	4.0	4.1	2.7	2.8	4.3	3.3	3.4	2.5	0.0	1.9	2.4	3.5	2.7	1.7	3.3	4.0	2.7	3.1	2.4	2.4
YIWSEC	2.8	2.9	2.5	2.7	2.1	2.2	2.4	2.4	3.7	2.3	2.3	2.8	3.5	3.3	1.9	1.9	0.0	2.0	2.7	2.5	2.0	2.5	3.0	3.5	3.7	1.4	1.4
YISCEI	2.6	3.8	3.7	3.3	3.0	3.2	1.0	1.4	4.4	2.4	3.8	3.1	3.5	3.4	2.4	2.4	2.0	0.0	4.3	2.1	3.4	3.2	3.5	3.1	3.9	2.1	2.1
YISCOS	4.6	4.5	3.6	4.7	4.2	4.1	4.6	4.4	5.4	4.0	2.8	4.9	4.3	4.2	3.5	3.5	2.7	4.3	0.0	3.7	3.0	3.6	4.6	5.7	5.1	4.0	4.0
YISNIX	2.8	4.1	3.4	3.4	3.1	3.1	1.9	2.4	4.5	3.5	4.1	4.2	2.1	2.6	2.7	2.7	2.5	2.1	3.7	0.0	3.3	4.0	3.7	4.6	3.9	3.4	3.4
YOMYII	2.6	3.3	2.5	2.6	2.5	2.6	3.2	4.1	3.4	3.0	1.2	3.5	3.1	3.5	1.7	1.7	2.0	3.4	3.0	3.3	0.0	2.9	4.0	3.5	2.7	2.5	2.5
YUJNEW	3.1	3.8	3.4	4.6	4.3	4.5	3.5	3.8	4.7	3.5	2.6	2.4	4.6	3.5	3.3	3.3	2.5	3.2	3.6	4.0	2.9	0.0	3.3	3.7	3.4	2.5	2.5
YULPOK1	3.5	3.8	2.3	3.9	3.6	3.6	3.7	3.4	4.3	4.8	4.5	2.1	4.3	3.3	4.0	4.0	3.0	3.5	4.6	3.7	4.0	3.3	0.0	4.6	3.9	3.2	3.2
YULPOK2	3.4	4.8	4.1	3.3	3.5	4.0	2.9	4.3	4.8	3.8	3.7	2.9	4.6	5.2	2.7	2.7	3.5	3.1	5.7	4.6	3.5	3.7	4.6	0.0	3.5	2.7	2.7
ZORHIX1	1.9	4.1	3.3	3.7	4.0	4.2	3.4	4.9	3.6	4.5	3.4	3.4	3.1	3.0	3.1	3.1	3.7	3.9	5.1	3.9	2.7	3.4	3.9	3.5	0.0	3.6	3.6
ZORHIX2	2.6	2.6	3.1	2.7	2.4	2.6	2.4	2.5	3.4	2.0	2.6	2.4	4.2	3.7	2.4	2.4	1.4	2.1	4.0	3.4	2.5	2.5	3.2	2.7	3.6	0.0	0.0

Bibliography

- (1) Akopyan, Z. A.; Struchkov, Y. T.; Dashevskii, V. G. *J. Struct. Chem.* **1966**, 7 (3), 385–392.
- (2) Thalladi, V. R.; Panneerselvam, K.; Carrell, C. J.; Carrell, H. L.; Desiraju, G. R. *J. Chem. Soc. Chem. Commun.* **1995**, No. 3, 341–342.
- (3) Allen, F. H.; Bellard, S.; Brice, M. D.; Cartwright, B. A.; Doubleday, A.; Higgs, H.; Hummelink, T.; Hummelink-Peters, B. G.; Kennard, O.; Motherwell, W. D. S.; Rodgers, J. R.; Watson, D. G. *Acta Crystallogr. B* **1979**, 35 (10), 2331–2339.
- (4) Tamura, M.; Nakazawa, Y.; Shiomi, D.; Nozawa, K.; Hosokoshi, Y.; Ishikawa, M.; Takahashi, M.; Kinoshita, M. *Chem. Phys. Lett.* **1991**, 186 (4–5), 401–404.
- (5) Allemand, P. M.; Khemani, K. C.; Koch, A.; Wudl, F.; Holczer, K.; Donovan, S.; Grüner, G.; Thompson, J. D. *Science* **1991**, 253 (5017), 301–302.
- (6) Chiarelli, R.; Novak, M. A.; Rassat, A.; Tholence, J. L. *Nature* **1993**, 363, 147–149.
- (7) Sugawara, T.; Matsushita, M. M.; Izuoka, A.; Wada, N.; Takeda, N.; Ishikawa, M. *J. Chem. Soc. Chem. Commun.* **1994**, No. 14, 1723–1724.
- (8) Cirujeda, J.; Mas, M.; Molins, E.; Panthou, F. L. de; Laugier, J.; Park, J. G.; Paulsen, C.; Rey, P.; Rovira, C.; Veciana, J. *J. Chem. Soc. Chem. Commun.* **1995**, No. 7, 709–710.
- (9) Caneschi, A.; Ferraro, F.; Gatteschi, D.; le Lirzin, A.; Novak, M. A.; Rentschler, E.; Sessoli, R. *Adv. Mater.* **1995**, 7 (5), 476–478.
- (10) Pei, Y.; Kahn, O.; Aebersold, M. A.; Ouahab, L.; Le Berre, F.; Pardi, L.; Tholence, J. L. *Adv. Mater.* **1994**, 6 (9), 681–683.
- (11) Togashi, K.; Imachi, R.; Tomioka, K.; Tsuboi, H.; Ishida, T.; Nogami, T.; Takeda, N.; Ishikawa, M. *Bull. Chem. Soc. Jpn.* **1996**, 69 (10), 2821–2830.
- (12) Kahn, O. *Molecular Magnetism*; VCH Publishers, Inc. (USA), 1993.
- (13) Miller, J. S.; Epstein, A. J. *Angew. Chem. Int. Ed. Engl.* **1994**, 33 (4), 385–415.
- (14) Kinoshita, M. *Jpn. J. Appl. Phys.* **1994**, 33 (Part 1, No. 10), 5718–5733.
- (15) Coronado, E.; Delhaès, P.; Gatteschi, D.; Miller, J. *Molecular Magnetism: From Molecular Assemblies to the Devices*; Springer Science & Business Media, 2013.
- (16) Kahn, O. *Magnetism: A Supramolecular Function*; Springer Science & Business Media, 1996.
- (17) Novoa, J. J.; Deumal, M.; Kinoshita, M.; Hosokoshi, Y.; Veciana, J.; Cirujeda, J. *Mol. Cryst. Liq. Cryst. Sci. Technol. Sect. Mol. Cryst. Liq. Cryst.* **1997**, 305 (1), 129–141.
- (18) Veciana, J.; Cirujeda, J.; Rovira, C.; Vidal-Gancedo, J. *Adv. Mater.* **1995**, 7 (2), 221–225.
- (19) Zheludev, A.; Barone, V.; Bonnet, M.; Delley, B.; Grand, A.; Ressouche, E.; Rey, P.; Subra, R.; Schweizer, J. *J. Am. Chem. Soc.* **1994**, 116 (5), 2019–2027.
- (20) Novoa, J. J.; Mota, F.; Veciana, J.; Cirujeda, J. *Mol. Cryst. Liq. Cryst. Sci. Technol. Sect. Mol. Cryst. Liq. Cryst.* **1995**, 271 (1), 79–90.
- (21) Lanfranc of Panthou. 000MPY, University J. Fourier Grenoble I: Grenoble, 1994.
- (22) Awaga, K.; Inabe, T.; Maruyama, Y. *Chem. Phys. Lett.* **1992**, 190 (3), 349–352.
- (23) Prof. M Kinoshita. .
- (24) Turek, P.; Nozawa, K.; Shiomi, D.; Awaga, K.; Inabe, T.; Maruyama, Y.; Kinoshita, M. *Chem. Phys. Lett.* **1991**, 180 (4), 327–331.
- (25) Y Hosokoshi. OPBRPH, University of Tokyo: Tokyo, 1995.
- (26) Hernández, E.; Mas, M.; Molins, E.; Rovira, C.; Veciana, J. *Angew. Chem. Int. Ed. Engl.* **1993**, 32 (6), 882–884.
- (27) Romero, F. M.; Ziesel, R.; De Cian, A.; Fischer, J.; Turek, P. *New J. Chem.* **1996**, 20 (9), 919–924.

- (28) Awaga, K.; Inabe, T.; Maruyama, Y.; Nakamura, T.; Matsumoto, M. *Chem. Phys. Lett.* **1992**, *195* (1), 21–24.
- (29) Wang, H.; Zhang, D.; Wan, M.; Zhu, D. *Solid State Commun.* **1993**, *85* (8), 685–690.
- (30) De Panthou, F. L.; Luneau, D.; Laugier, J.; Rey, P. *J. Am. Chem. Soc.* **1993**, *115* (20), 9095–9100.
- (31) Angeloni, L.; Caneschi, A.; David, L.; Fabretti, A.; Ferraro, F.; Gatteschi, D.; Lirzin, A. le; Sessoli, R. *J. Mater. Chem.* **1994**, *4* (7), 1047–1053.
- (32) Hosokoshi, Y.; Tamura, M.; Kinoshita, M.; Sawa, H.; Kato, R.; Fujiwara, Y.; Ueda, Y. *J. Mater. Chem.* **1994**, *4* (8), 1219–1226.
- (33) Awaga, K.; Yamaguchi, A.; Okuno, T.; Inabe, T.; Nakamura, T.; Matsumoto, M.; Maruyama, Y. *J. Mater. Chem.* **1994**, *4* (9), 1377–1385.
- (34) Caneschi, A.; Ferraro, F.; Gatteschi, D.; le Lirzin, A.; Rentschler, E. *Inorganica Chim. Acta* **1995**, *235* (1–2), 159–164.
- (35) Akita, T.; Mazaki, Y.; Kobayashi, K.; Koga, N.; Iwamura, H. *J. Org. Chem.* **1995**, *60* (7), 2092–2098.
- (36) Kahn, O.; Lang, A.; Pei, Y.; Ouahab, L. *Adv. Mater.* **1996**, *8* (1), 60–62.
- (37) Awaga, K.; Okuno, T.; Yamaguchi, A.; Hasegawa, M.; Inabe, T.; Maruyama, Y.; Wada, N. *Phys. Rev. B* **1994**, *49* (6), 3975–3981.
- (38) Deumal i Solé, Mercè. *Estudi Teòric del magnetisme en cristalls moleculars: Mecanismes d'interacció i empaquetament.*, Universitat de Barcelona: Barcelona, 1999.
- (39) Deumal, M.; Cirujeda, J.; Veciana, J.; Novoa, J. J. *Chem. – Eur. J.* **1999**, *5* (5), 1631–1642.
- (40) Cirujeda, J. Thesis J Cirujeda, Universitat Ramon Llull: Barcelona, 1997.
- (41) McConnell, H. M. *J. Chem. Phys.* **1963**, *39* (7), 1910–1910.
- (42) McWeeny, R.; Sutcliffe, B. T. *Methods of Molecular Quantum Mechanics*; Academic Press, 1976.
- (43) Deumal, M.; Novoa, J. J.; Bearpark, M. J.; Celani, P.; Olivucci, M.; Robb, M. A. *J. Phys. Chem. A* **1998**, *102* (43), 8404–8412.
- (44) Deumal, M.; Bearpark, M. J.; Robb, M. A.; Pontillon, Y.; Novoa, J. J. *Chem. - Eur. J.* **2004**, *10* (24), 6422–6432.
- (45) Deumal, M.; Mota, F.; Bearpark, M. J.; Robb, M. A.; Novoa, J. J. *Mol. Phys.* **2006**, *104* (5–7), 857–873.
- (46) Auf der Heyde, T. P. E. *J. Chem. Educ.* **1990**, *67* (6), 461.
- (47) Malinowski, E. R.; Howery, D. G. *Factor analysis in chemistry*; John Wiley & Sons, New York, 1980.
- (48) Massart, D. L.; Kaufman, L. *The interpretation of analytical chemical data by the use of cluster analysis.*; Wiley, 1983.

CHAPTER 7

STUDY OF π -[TCNE]₂²⁻ DIMERS IN MOLECULAR CRYSTALS

7 Study of π -[TCNE] $_2^{2-}$ dimers in molecular crystals

7.1 Introduction

Charge transfer crystals¹ are the most successful compounds in the design of molecular materials with magnetic properties. In these compounds, there is a transfer of charge (electrons) between a donor (D) and an acceptor (A) species². During their synthesis, the donor gives an electron, becoming a radical cation ($[D]^+$), and the unit that accepts it becomes a radical anion ($[A]^-$): $[\cdots[D]^+[A]^- [D]^+[A]^- [D]^+[A]^- \cdots]$. Both radical units have unpaired electrons that, if they interact ferromagnetically and the interaction extends all along the space, result is a crystal with magnetic properties. These systems have been designed and synthesized with success³⁻¹⁵. For instance, strong organic electronic acceptors (A), such as tetracyanoethylene (TCNE), 7,7,8,8-tetracyano-p-quinodimethane (TCNQ), perfluoro-7,7,8,8-tetracyano-p-quinodimethane (TCNQF₄), 2,3-dichloro-5,6-dicyanobenzoquinone (DDQ), and hexacyanobutadiene, form stable electronic transfer salts that contain the radical anions of the acceptor molecule $[A]^-$. Studies of these salts have been essential for the discovery and development of molecular crystals¹⁶⁻²⁰ (e.g. [TTF][TCNQ], TTF = tetrathiafulvalene), which, as a result, lead to the discovery of molecular superconductors^{21,22}, as well as molecular magnets^{7-15,23} (e.g., $[\text{Fe}(\text{C}_5\text{Me}_5)_2][\text{TCNE}]$).

Table 7.1 Unielectronic reversible reduction potentials^[a] for strong acceptors **A**.

Acceptor	$E^{0/-}$ [V]	$E^{-/2-}$ [V]
TCNE	0.15	-0.57 ^[b]
TCNQ	0.17	-0.37 ^[b]
TCNQF ₄	0.53	0.02 ^[b]
DDQ	0.59	-0.25 ²⁴
C ₄ (CN) ₆	0.60	0.02 ²³
Cyanil	0.90	0.09 ^[b]
C ₃ [C(CN) ₂] ₃	1.13 ^[c]	0.34 ^[b]

[a] V vs. SCE in MeCN {Pt electrode; 0.1 M [*n*-Bu₄N][ClO₄]}}

[b] M. D. Ward, *Electroanal. Chem.* **1989**, 16, 182.

[c] The neutral form of the acceptor has not been isolated.

These strong acceptors have common characteristics of being planar, to present two reversible one-electron reductions (Table 7.1) and that both the radical anions and the diamagnetic dianions are stable species²⁵. Indeed, the magnetism in these charge-transfer complexes vanishes whenever the donor or the acceptor radicals interact forming diamagnetic dimers: $[D]_2^{2+}$ or $[A]_2^{2-}$ (e.g. systems that contain TCNE unit as acceptor, which becomes $[\text{TCNE}]_2^{2-}$)²⁶⁻²⁹. Therefore, it is exceedingly important to carry out a detailed study of the dimerization to understand which factors govern the interaction between equal units that results in the formation of homologous σ - or π -dimers. To perform such study, we selected the π -[TCNE] $_2^{2-}$ dimers because of its simplicity compared to π -[TCNQ] $_2^{2-}$ or other π -[A] $_2^{2-}$ dimers (see Table 7.1). Let us mention that the first spectroscopic evidence of the existence $[\text{TCNE}]_2^{2-}$ dimer formation appeared in the literature in 1960²⁶⁻²⁹. However, it was not until 1981 that the first $[\text{TCNE}]_2^{2-}$ dimer was structurally characterized in the $[\text{Fe}(\text{C}_5\text{H}_4)_2\text{C}_3\text{H}_6]_2[\text{TCNE}]_2$ crystal³⁰.

The structures of A^0 diamagnetic and A^{2-} dianion form few conformers, while the anion $[A]^-$ can form multitude of structures. The anion of TCNE $^-$ has been structurally isolated as [TCNE] $^-$ (**1**^{31–37} in Figure 7.1), its σ -dimer, octacyanobutanediide, [C $_4$ (CN) $_8$] $^{2-}$ (**2**³⁸ in Figure 7.1), and its π -dimer, π -[TCNE] $_2^{2-}$, (**3**^{30,39–51} in Figure 7.1). While **1** and **3** do not need to be N -metal coordinated to be stable, the **2** dimers only have been isolated as μ_4 - N -metal coordinated. The anion [TCNQ] $^-$ has the same structural diversity that [TCNE] $^-$ and the formation of π -dimers include uniform 1-D extended chains, that are the base of many molecular metals. Although [TCNE] $^-$ and [TCNQ] $^-$ have a great structural variability, other $[A]^-$ have also been characterized forming π -[A] $_2^{2-}$ structures, sometimes exclusively, as the case of cyanil²⁴.

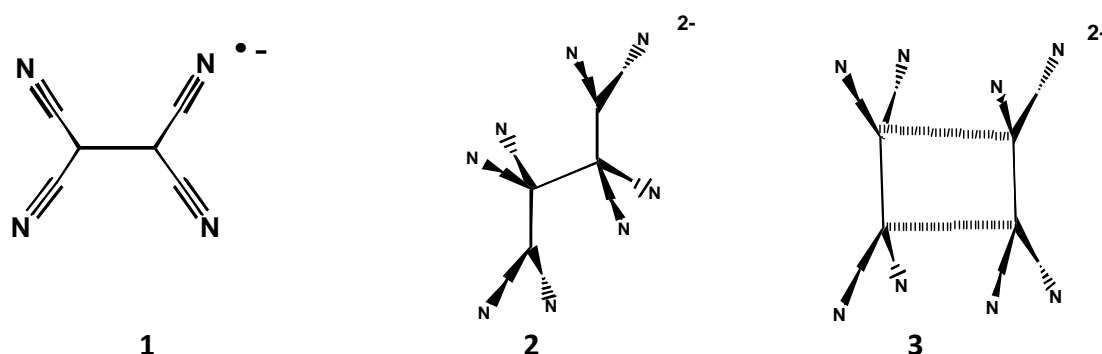


Figure 7.1 Graphical representation of **1** TCNE $^-$ monomer, **2** σ -[TCNE] $_2^{2-}$ dimer and **3** π -[TCNE] $_2^{2-}$ dimer.

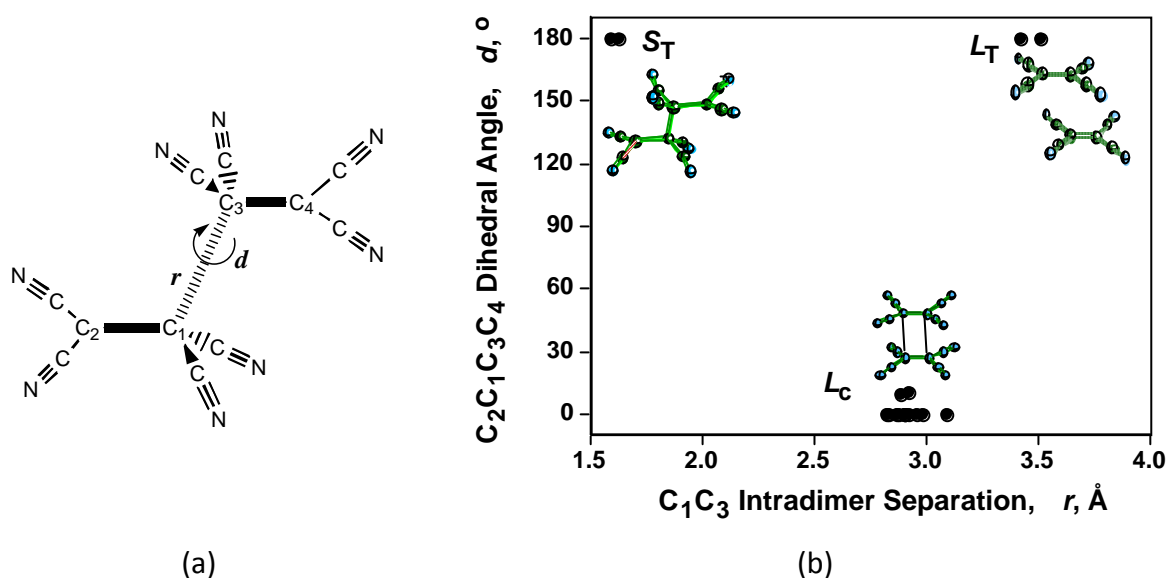


Figure 7.2 (a) Graphical representation of the inter-monomer C...C distance, r , and the dihedral d angle. (b) Representation of d as a function of r for the [TCNE] $_2^{2-}$ dimers structurally characterized (Table 7.2).

Structure **3** represents a rare class of organic compounds with exceptionally long bonding carbon-carbon (CC) interactions: from 2.83 Å⁴⁶ to 3.51 Å⁴³ (Table 7.2). These CC distances are twice the typical sp^3 - sp^3 CC bond distance (1.54 Å), and also substantially longer than the elongated CC bond, reported to be *ca.* 1.73 Å^{52,53}. Thus, these dimers have intermolecular π - π bonding interactions, which are a subclass of the van der Waals interactions since the distances in these π - π dimers are significantly shorter than the sum of

the van der Waals radii of the two atoms involved in the shortest contact distances. In addition, for each structure A = TCNE (1 - 3) there are characteristic ν_{CN} absorption bands in the IR spectra (Table 7.2): two bands for structure **1** and three bands for structures **2** and **3** that are $> 100 \text{ cm}^{-1}$ for 2, and $\sim 30 \text{ cm}^{-1}$ for 3.

[TCNE] $_2^{2-}$ dimers are classified according to the inter-monomer C \cdots C (CC) separation, r , and dihedral angles, d (see Figure 7.2). Experimentally three classes of [TCNE] $_2^{2-}$ dimers with singlet ground state have been characterized (namely, S_t , L_c and L_t , where S/L stands for short/long r distance and t/c for trans-/cis- orientation of the [TCNE] $^-$ radicals, corresponding to $d = 180^\circ/0^\circ$, respectively, see Figure 7.2). The S_t class ($r \approx 1.6 \text{ \AA}$, $d = 180^\circ$) corresponds to σ -dimers of [TCNE] $^-$ (octacyanobutanodieno, [C $_4$ (CN) $_8$] $^{2-}$) that have a typical, although long, sp^3 - sp^3 σ -bond between the two [TCNE] $^-$ radicals. The two classes defined as L are π -dimers of [TCNE] $^-$ radicals. L_c ($r \approx 2.9 \text{ \AA}$, $d = 0^\circ$) has the two monomer units arranged eclipsed with the nitrile groups bent *ca.* 5.0° ($sp^{2.17}$) outside the plane formed by the dimer. Contrarily, the monomers in L_t ($r \approx 3.5 \text{ \AA}$, $d \approx 180^\circ$) form a non-eclipsed structure with the nitrile groups bent toward the center of the dimer about 1.9° ($\sim sp^{2.06}$).

Ab initio studies were carried out on isolated [TCNE] $_2^{2-}$ dimers to investigate the formation and stability of dimers with exceptionally long C \cdots C bonds ($\geq 2.9 \text{ \AA}$). Additionally, the process of formation of the L_c and L_t π -[TCNE] $_2^{2-}$ dimers has been examined. The results of these computational studies showed a potential energy curve where the singlet ground state of the system changed from being closed-shell singlet to open-shell singlet, depending on the inter-molecular distance. All three classes (S_t , L_t and L_c) of dimers are metastable states in reference to the dissociation of the dimer in the isolated units [TCNE] $^-$. Consequently, the existence of dianion dimers in crystals is favored by the interaction (cation) $^+ \cdots$ [TCNE] $^-$ which provides the electrostatic stabilization necessary to overcome the intermolecular electrostatic repulsion of the dimer. The cation-mediated $\pi^*-\pi^*$ [TCNE] $^- \cdots$ [TCNE] $^-$ interaction complies with the definition of bond proposed by Pauling. This bonding interaction involves the π^* orbital of each interacting fragment, and implies the overlap of the b_{2g} SOMO orbitals of each [TCNE] $^-$ radical to form a filled b_{2u} orbital in the dimer [TCNE] $_2^{2-}$. Although a π -dimer is typically formed, if the fragments are close enough the σ -dimer can form. L dimers are also stabilized in a polar solvent that minimize the Coulomb repulsion between the anions.

Experimentally, the three classes of dimers have distinctive IR absorption spectra features ν_{CN} , ν_{CC} and δ_{CCN} . Due to the presence of the intermolecular C \cdots C bonds, the L_c π -[TCNE] $_2^{2-}$ dimers have ν_{CN} bands observed at 2191 ± 2 (m), 2173 ± 3 (s), and 2162 ± 3 (s) cm^{-1} and ν_{CC} at 1364 ± 3 (s) cm^{-1} . Additionally, a new band is observed in the UV-Vis range from 15000 to 18200 cm^{-1} ($549 - 667 \text{ nm}$), which has an average value of $16825 \pm 1180 \text{ cm}^{-1}$ (594 nm) and is assigned to the predicted new intradimer transition $^1A_{1g} \rightarrow ^1B_{1u}$. When decreasing the temperature to 77 K in 2-methyl tetrahydrofuran, this new band is observed at 18940 cm^{-1} (528 nm) for $\{[\text{Et}_4\text{N}]^+\}_2[\text{TCNE}]_2^{2-}$, and the yellow solution turns deep red. The L_t class is characterized by ν_{CN} absorption bands at 2215 ± 2 , 2197 ± 3 , and $2180 \pm 4 \text{ cm}^{-1}$ and ν_{CC} at 1209 ± 9 (w) cm^{-1} . Finally, the S_t class has the ν_{CN} bands at 2215 ± 4 , 2157 ± 3 , and $2107 \pm 4 \text{ cm}^{-1}$ and ν_{CC} at 1385 ± 1 (vs) cm^{-1} .

Table 7.2. Summary of the intermolecular dihedral (d , °) and distance (r , Å), intramolecular CC distance (C-C, Å), deviation from planarity (Desv., °) and frequencies ν_{CN} , ν_{CC} and $\delta_{\text{C-N}}$ for groups \mathcal{S} , L_c , and L_t of [TCNE] $_2^{2-}$ dimers characterized structurally.

Compound	Group	Form	d [°]	r [Å]	C-C [Å]	Desv. [°] ^[a]	ν_{CN} [cm ⁻¹]	ν_{CC} [cm ⁻¹]	$\delta_{\text{C-N}}$ [cm ⁻¹]	ω_{Max} [cm ⁻¹]	
Fe ^{II} [C ₄ (CN) ₈](NCMe) ₂ ·MeC ²⁶⁷	\mathcal{S}	μ_4 -N-[C ₄ (CN) ₈] ²⁻	179.91	1.627	1.627		2213 (w)	2109 (w)	558	537	509 ^[i]
Mn ^{II} [C ₄ (CN) ₈](NCMe) ₂ ·CH ₂ Cl ₂ ²⁶⁷	\mathcal{S}	μ_4 -N-[C ₄ (CN) ₈] ²⁻	179.96	1.59	1.59		2212 (w)	2100 (w)	556	530	504 ^[i]
Co ^{II} [C ₄ (CN) ₈](NCMe) ₂ ·CH ₂ Cl ₂	\mathcal{S}	μ_4 -N-[C ₄ (CN) ₈] ²⁻		[c]	[c]		2223 (m)	2159 (s)	556	539	510
Average values	\mathcal{S}	μ_4 -N-[C ₄ (CN) ₈] ²⁻	179.94	1.61	1.61		2215 (w)	2157 (s)	557	535	508
Standard deviation			0.02	0.01	0.01		4	3	1	5	3
[Cu(PPh ₃) ₃ (TCNE)] ₂ ²⁶⁸	L_c	π -[σ -TCNE] ₂ ²⁻	0.136	2.92	1.397	4.9	2193	2173	511	511	17 100
[Cr(C ₆ H ₆) ₂] ₂ [TCNE] ₂ ²⁶⁹	L_c	π -[TCNE] ₂ ²⁻	0.045	2.904	1.436	6.2	2189	2170	553	528	514
[Cr(C ₆ Me ₃ H ₃) ₂] ₂ [TCNE] ₂ ²⁶⁹	L_c	π -[TCNE] ₂ ²⁻	0.084	3.09 ^[b,c]	1.45 ^[b,c]	[c]	[c]	[c]	[c]	[c]	[c]
[Fe(C ₅ H ₄) ₂ C ₃ H ₆] ₂ [TCNE] ₂ ^{260,269}	L_c	π -[TCNE] ₂ ²⁻	0.030	2.90	1.350	5	2191	2169	548	526	513
Na ₂ [TCNE] ₂ (glyme) ₂ ²⁷⁰	L_c	μ_4 - π -[TCNE] ₂ ²⁻	0.000	2.961	1.423	2.3	[c]	[c]	[c]	[c]	[c]
K ₂ [TCNE] ₂ (glyme) ₂ ²⁷⁰	L_c	μ_4 - π -[TCNE] ₂ ²⁻	0.062	2.987	1.420	3.6	[c]	[c]	[c]	[c]	[c]
CS ₂ [TCNE] ₂ (glyme) ₂ ²⁷⁸	L_c	μ_{15} - π -[TCNE] ₂ ²⁻	10.000	2.89	1.430	5.4	2197	2179	551	539	521
[Fe(C ₅ H ₅)(C ₅ Me ₅) ₂] ₂ [TCNE] ₃ (THF) ²⁷¹	L_c	π -[TCNE] ₂ ²⁻	0.061	2.903	1.372	5.8	2190	2173	547	514	514
[Fe(C ₅ H ₅)(C ₅ Me ₅) ₂] ₂ [TCNE] ₃ (CH ₂ Cl ₂) ²⁷¹	L_c	π -[TCNE] ₂ ²⁻	0.047	2.833	1.459	6.4	2190	2174	549	530	517
[Et ₄ N] ₂ [TCNE] ₂ ²⁷⁵	L_c	π -[TCNE] ₂ ²⁻	0.000	2.827	1.418	6.6	2191	2170	545	526	516
[Pr ₄ N] ₂ [TCNE] ₂ ²⁷⁵	L_c	π -[TCNE] ₂ ²⁻	0.049	2.870	1.408	5.2	2191	2175	551	528	513
[(Me ₂ N) ₂ CC(NMe ₂) ₂] ₂ [TCNE] ₂ ^{42,43}	L_c	π -[TCNE] ₂ ²⁻	10.94	2.922	1.400	4.0	2193	2173	547	528	515
Tl ₂ [TCNE] ₂ ²⁷³	L_c	μ_{16} - π -TCNE ₂ ²⁻	0.087	2.874	1.51	4.4	2190	2173	550	534	518
[HAOC][TCNE] ₂ ^{277, [k]}	L_c	π -[TCNE] ₂ ²⁻		[c]	[c]	[c]	2190	2174	528	513	513
Average values	L_c	π -[TCNE] ₂ ²⁻	1.65	2.90	1.405	5.0	2191	2173	549	530	516
Standard deviation			4.1	0.05	0.03	1.3	2	3	2	4	3
α -[TfF] ₂ [TCNE] ₂ ²⁷²	L_t	π -[TCNE] ₂ ²⁻	178.81	3.426 ^[d,e]	1.40	-2.8 ^[e]	2218 (m)	2200 (s)	593	536	520
β -[TfF] ₂ [TCNE] ₂ ²⁷²	L_t	π -[TCNE] ₂ ²⁻	178.93	3.508 ^[d,f]	1.397	-1.0 ^[e]	2214 (m)	2198 (s)	585	534	520
Average values	L_t	π -[TCNE] ₂ ²⁻	178.87	3.47	1.399	-1.9 ^[e]	2216 ^[h]	2197 ^[h]	586	535	520
Standard deviation			0.06	0.04	0.002	0.9	2	3	1	3	1

[a] Average dihedral angle NC-C-C...C (CrystalMaker5). [b] Disordered - excluded from the average. [c] Not reported. [d] Nonclipsed. [e] Shortest intradimer CC distance = 3.48 Å. [f] Shortest intradimer CC distance = 3.52 Å. [g] Negative values indicate a bending towards the center of the dimer. [h] The values previously reported 2215, 2194, 2178 cm⁻¹ are included in the average calculation. [i] Spectrum not observed due to formation of M[TCNE]₂ under the conditions of the experiment. [j] Non-assignable absorption from the cation in this region. [k] Hexaazaoctadecahydrocoronene. [l] Some or all of the spectroscopic data as reported in ref. ²³⁵.

To sum up, in this chapter, we performed *ab initio* calculations to understand and explain the unusual intermolecular interaction associated with the formation of π -[TCNE] $_2^{2-}$ dimers, and, in particular, the appearance of the exceptionally long CC bond ($> 2.9 \text{ \AA}$) observed in some electronic transfer salts with TCNE as acceptor A unit. Based on the results of that investigation, we will discuss the factors that govern the process of dimerization of the [TCNE] $^-$ units, as a prototype of the π dimers formation observed in other strong electronic acceptors. We performed a detailed study of the geometries of these dimers and carried out a comprehensive analysis of electronic structures of these compounds, which made possible to understand their spectroscopic features. We also analyzed the energy process of the dimer formation, and sought and described the structures that are the energy minima of the potential surface, as well as analyzed the relative stability of the singlet and triplet states. Finally, we present experimental spectroscopic evidence (UV-Vis and IR spectra), measured in Prof. Joel Miller's group, that validate the theoretical study.

7.2 Geometry of the [TCNE] $_2^{2-}$ dimer

The known structures of the TCNE dianions [TCNE] $_2^{2-}$ (Table 7.2) can be represented by the parameters r , as the intermolecular C $_1$ -C $_3$ distance, and d , the dihedral angle between each [TCNE] $^-$ unit, *i.e.*, C $_2$ -C $_1$ -C $_3$ -C $_4$ (see Figure 7.2a). As briefly mentioned in the introduction, a representation of the experimental values of d vs r reveals three different classes (Figure 7.2b): S_t , L_c and L_t (S/L for short/long distance defined by r and t/c for *trans*-/*cis*- orientation of the TCNE molecules, corresponding to dihedral angles d of $180^\circ/0^\circ$ respectively). The S_t class corresponds to dimers with $r < 1.7 \text{ \AA}$ and with *trans* orientation of both [TCNE] $^-$ units ($d \sim 180^\circ$). L_c and L_t classes have $r > 2.8 \text{ \AA}$, but have opposite dihedral angles: in structures that are grouped as L_c both [TCNE] $^-$ units are *cis* oriented ($d \sim 0^\circ$) while the structures within the L_t class have a *trans* orientation ($d \sim 180^\circ$). Table 7.2 also details the intermolecular CC distances, the deviation from planarity of each nitrile group, and the *stretching* band ν_{CN} in the IR spectra for these dimers.

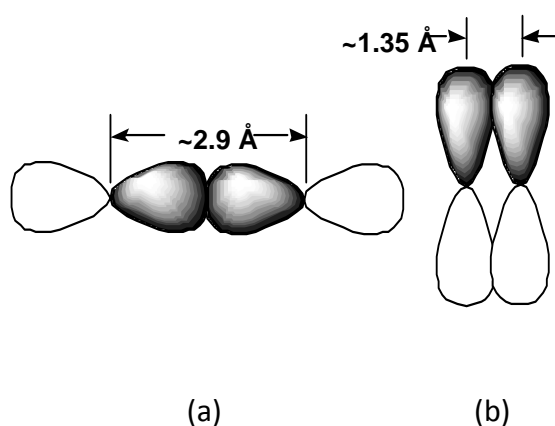


Figure 7.3 Graphical representation of (a) σ -like overlap and (b) lateral π -overlap of two p orbitals.

$M^{II}(\text{NCMe})_2[\text{C}_4(\text{CN})_8]$ ($M = \text{Mn}, \text{Fe}$) are examples of systems observed experimentally that belong to the S_t group. These compounds have a structure $\mu_4\text{-N-}[\text{C}_4(\text{CN})_8]^{2-}$ (**2** in Figure 7.1) with $r \sim 1.6 \text{ \AA}$ whose central C atoms present a clear sp^3 hybridization³⁸. Therefore, the [TCNE] $^-$ fragments are connected by a typical, although long³¹, σ -bond, and the dimer

corresponds to the octacyanobutanediide, $[C_4(CN)_8]^{2-}$ dianion³⁸ (**2**, Figure 7.1). Similarly, σ -[TCNQ] $_2^{2-}$ dimers have also been observed experimentally^{54–58}. The L_c and L_t dimers, with $r > 2.8$ Å, typically consist of two [TCNE] $^-$ units almost planar, whose central C atoms have a hybridization $\sim sp^2$. The intermolecular CC bond in the π -dimers (**3**, Figure 7.1) is mainly via the σ -like overlap between the p orbitals of the two interacting [TCNE] $^-$ units (Figure 7.3a), in contrast to the conventional π -bond (Figure 7.3b) observed in alkenes and alkynes, which implies a lateral overlap of the p orbitals.

7.3 The potential energy curve of the [TCNE] $_2^{2-}$ dimer

An initial potential energy surface of the [TCNE] $_2^{2-}$ dimers can be obtained by testing if the experimental energy structures are a minima on the potential energy surface. Thus, starting from the experimental structures of the [TCNE] $_2^{2-}$ dimers, a preliminary optimization of the potential energy surface was performed at UHF and closed-shell singlet B3LYP levels using STO-3g, 6-31+g and 6-31+g(d) basis sets. The geometry of the optimized minima was similar to the experimental geometries for each of the S_t , L_c , and L_t groups of conformers. The interaction energies and optimum values of the optimized parameter r were very close, irrespective of the method and basis set used (see Table 7.3). A vibrational analysis of the optimized geometries of the [TCNE] $_2^{2-}$ dimers verified the nature of energy minimum of these structures, since there was no imaginary frequency. It is worth mentioning that these minima are all higher in energy than the dissociated products by 72.8, 60.3 and 58.7 kcal/mol for S_t , L_c , and L_t , classes, respectively, *i.e.* the [TCNE] $_2^{2-}$ dimers are metastable at B3LYP/6-31+g level.

Table 7.3 Interaction energies E_{int} (in kcal/mol) referred to two TCNE $^-$ isolated monomers and the value of r (in Å) and d (in °) parameters for each optimized structures of the S_t , L_c , and L_t conformers of the dimers [TCNE] $_2^{2-}$ dimers, using different methods and basis sets.

Conformer	Parameter	E_{int} (kcal/mol)	r (Å)	d (°)
S_t	UHF/6-31+g(d)	72.1	1.62	180.0
	B3LYP/6-31+g	72.8	1.71	180.0
	B3LYP/6-31+g(d)	69.5	1.70	180.0
L_c	UHF/6-31+g(d)	94.9	2.74	0.0
	B3LYP/6-31+g	60.3	3.13	0.0
	B3LYP/6-31+g(d)	60.4	3.04	0.0
L_t	UHF/6-31+g(d)	[a]	[a]	[a]
	B3LYP/6-31+g	58.7	3.24	112.8
	B3LYP/6-31+g(d)	59.1	3.19	112.1

[a] no minimum found

The shape of the potential energy curve for the [TCNE] $_2^{2-}$ dimers was evaluated starting from configurations far away from the minimum energy points. The change of the interaction energy vs r was analyzed, allowing the optimization of all the other geometric parameters of the dimer. Initially, a calculation of E_{int} within the $1 < r < 5$ Å range was performed for the closed-shell singlet (S_0) at RB3LYP/6-31+g level for both L_c and L_t conformers, forcing the double occupation of the HOMO orbital (see Figure 7.4). At short distances, both energy profiles led to S_t minima. Consequently, three energy minima were

found, which corresponded to S_t , L_c and L_t conformers and are similar to those observed experimentally (Figure 7.2b, Table 7.2).

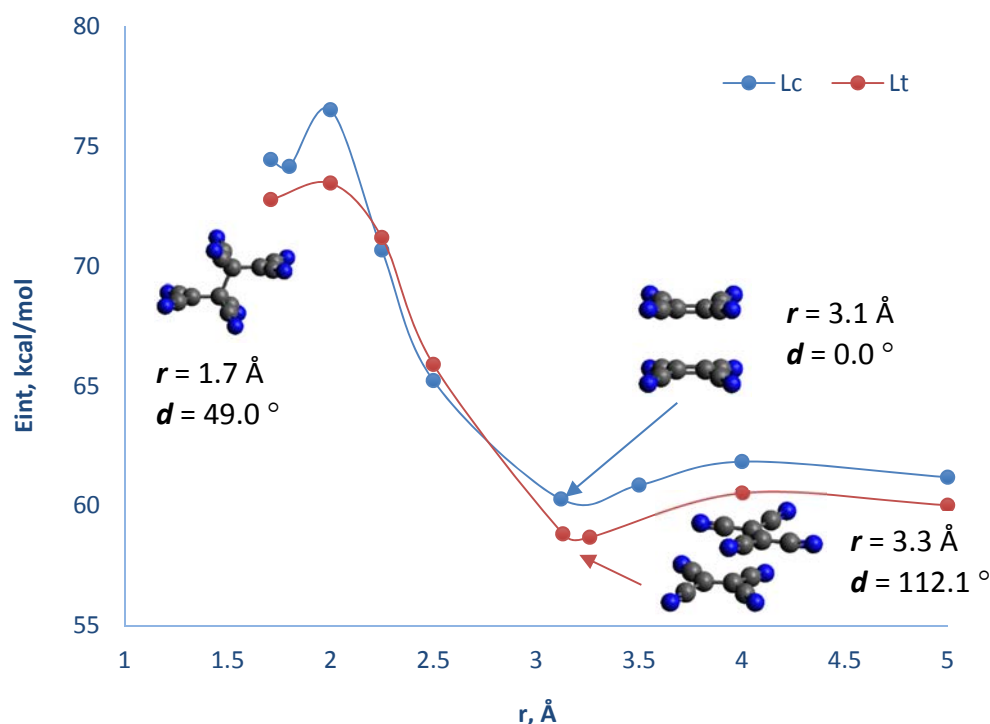


Figure 7.4 Adiabatic potential energy surface calculated as a function of r (Å) for L_c (in blue) and L_t (in red) conformers at RB3LYP/6-31+g level.

The change in the geometry of the [TCNE] $^-$ fragments when the inter-monomer separation, r , decreases, implies a change in the hybridization of the central carbon atoms of the [TCNE] $_2^{2-}$ dimers in the L_c and L_t arrangement. The central CC distance within each monomer unit increases when r decreases and, simultaneously, the C_1 - C_3 - C_4 -CN dihedral angle increases from 90° to 120° . This corresponds to a change of hybridization from sp^2 to sp^3 in the two central carbons of each [TCNE] $^-$ fragment. The change in hybridization of the central carbon atoms as the intradimer distance decreases implies a change in the C_1 - C_3 - C_4 -CN dihedral angle that ranges from 2.3° to 6.6° (average = $5.0^\circ \pm 1.3^\circ$, see Table 7.2). Therefore, the CN groups move out of the nominal [TCNE] $^-$ plane and away from the center of symmetry of the [TCNE] $_2^{2-}$ dimer. The displacement of the nitrile groups away from the center of the [TCNE] $_2^{2-}$ dimer in the L_c arrangement is shown in Figure 7.5. The average value of this curvature is about 5.0° , so the average of the C_1 - C_3 - C_4 -CN dihedral angle, whose value would be 90° if there were no curvature, is 95° . Assuming a linear relationship between the C_1 - C_3 - C_4 -CN dihedral angle and the carbon hybridization (at 90° / 120° there is a sp^2 / sp^3 hybridization, respectively^{43b}), the hybridization of the central carbon atoms in L_c is estimated to be 2.17 ($sp^{2.17}$). This change is expected when a CC bond is formed between C- sp^2 atoms. On the contrary, the nitriles are bent toward the center of symmetry of the [TCNE] $_2^{2-}$ dimer in the L_t class (Figure 7.5b) from 1.0° to 2.8° (average = $-1.9^\circ \pm 0.9^\circ$, see Table 7.2). The average of the deviation from planarity is -1.9° , which corresponds to a C_1 - C_3 - C_4 -CN dihedral angle of 91.9° . Therefore, the hybridization of the central carbon atoms of

the [TCNE] $_2^{2-}$ dimers in the L_t class is estimated to be 2.06 ($sp^{2.06}$)⁵⁹. This curvature towards the center of the dimer is not fully understood and will be the subject of further studies.

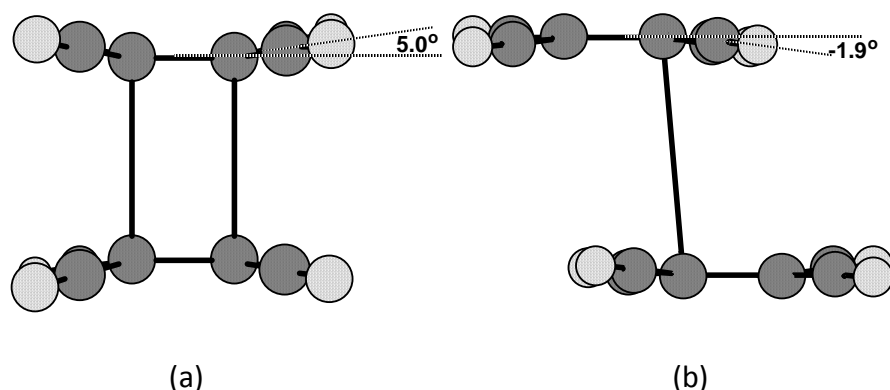


Figure 7.5 (a) Structure of $[Et_4N]_2[TCNE]_2$ exhibiting that the nitriles bend away the center of the dimer for the L_c class of [TCNE] $_2^{2-}$ dimers by an average of 5° (corresponding to a hybridization of 2.17), and (b) α -[TTF][TCNE] exhibiting that the nitriles bend toward the center of the dimer for the L_t class of [TCNE] $_2^{2-}$ dimers by an average of -1.9° (corresponding to a hybridization of 2.06).

For topological reasons, the existence of several minima on the potential energy surface requires the presence of transition states (TS) connecting each of these minima. The TS that connects S_t and L_t minima is around the maximum of energy in the surface (Figure 7.4), as it is the TS that connects the S_t and L_c minima. The TS between the conformers L_t and L_c is localized by calculating the variation of energy according to the dihedral angle d , between 0° - 180° , and permitting the optimization of all the other parameters. The resulting curve connects the optimum geometry of the conformer L_c ($r = 3.12 \text{ \AA}$, $d = 0^\circ$) with L_t ($r = 3.26 \text{ \AA}$, $d = 120^\circ$) through a TS that has low energy barrier ($\sim 3 \text{ kcal/mol}$, see Figure 7.6).

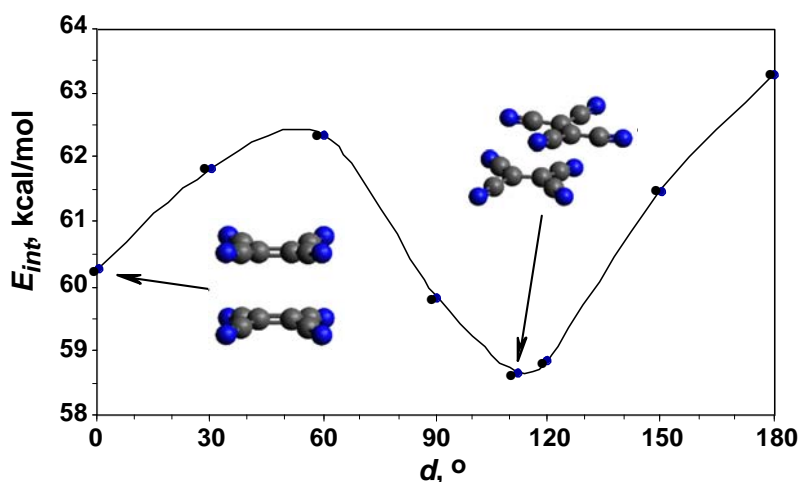


Figure 7.6 Potential energy curve for the L_c to L_t transformation along the dihedral angle d .

The existence of a transition state implies a process of formation and rupture of the intermolecular bonds to go from one conformer to the other. This process can only be understood in its entirety once the intermolecular bonds in each conformer have been properly established. The presence of intermolecular bonds in the conformers L_c ($d = 0^\circ$) and L_t ($d \approx 120^\circ$) can be evaluated with Bader's *atoms in molecules* (AIM)⁶⁰ methodology. This method identifies the presence of bonds analyzing the electron density and looking for the existence of bond critical points (3,-1). Mathematically, bond critical points (BCPs) are

regions in the electron density space, with coordinates r_c , where the gradient of the electron density is zero and the Hessian of the electron density has two negative and one positive eigenvalues (each eigenvalue identified as λ_i). Critical points associated with chemical molecular bonds (covalent or ionic) can be distinguished from those associated with the intermolecular bonds (hydrogen bonds or van der Waals)⁶¹. Intramolecular chemical bonds have a negative Laplacian [$\nabla^2\rho(r_c)$, defined as the sum of the eigenvalues of the Hessian], large values of density at the critical point $\rho(r_c)$ and large $|\lambda_1|/\lambda_3$ ratios (*i.e.*, the ratio between lowest and highest curvature of the electron density at the critical point). In contrast, the intermolecular bonds have a positive Laplacian, small values of the electron density at the critical point and small $|\lambda_1|/\lambda_3$ ratios. When the intermolecular critical point connects atoms A and B, then the contact $A\cdots B$ is considered to be a van der Waals bond³⁸. There is some controversy about whether the existence of a bond critical point (3,-1) is sufficient condition or simply a necessary condition for the existence of a bond, as we have seen in previous sections [some authors discuss whether the mere presence of these critical points (3,-1) associated with interactions strongly stable can be considered as bonds⁶²].

The BCPs (3,-1) existing between two [TCNE] $^-$ units were identified at RB3LYP level for each of the energy minima structures S_t , L_c and L_t (Figure 7.7, Table 7.4). Bond pathway lines in these structures connect bond critical points with the atoms of each [TCNE] $^-$ fragment that are involved in the bond. It is noted that bond pathways in the L_c and L_t conformers are not the same. That implies the existence of a transition state to go from one conformer to the other which involves the rupture and formation of intermolecular bonds.

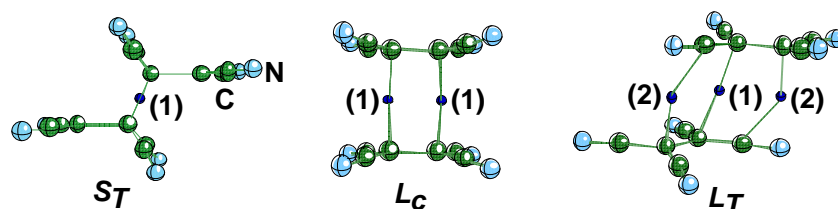


Figure 7.7 Position of the intermolecular bond critical points in the S_t , L_c and L_t arrangements of the [TCNE] $_2^{2-}$ dimers.

Table 7.4 Density at the point [$\rho(r_c)$], Laplacian value [$\nabla^2\rho(r_c)$] and ratio $|\lambda_1|/\lambda_3$ (see text for definitions) of the bond critical points BCP found in the S_t , L_c and L_t arrangements. When more than one BCP appears in a complex, they have been identified with different numbers (Figure 7.7).

Conformer	#BCP	$\rho(r_c)$	$\nabla^2\rho(r_c)$	$ \lambda_1 /\lambda_3$
S_t	1	0.167	-0.178	764
L_c	1	0.012	0.023	0.201
L_t	1	0.011	0.021	0.200
	2	0.009	0.021	0.184

There are two equivalent bond critical points connecting the central carbon atoms of each TCNE unit in the L_c structure (Figure 7.7). These bonds are expected for the structure **3** (Figure 7.1). However, in the L_t conformer ($d \approx 113^\circ$), in addition to the bond critical point CC between the central C atoms [type (1) in Figure 7.7], there are two equivalent intermolecular N-C bonds that connect the C atom of the ciano group of one fragment with

the central C atom of the other fragment [type (2) in Figure 7.7]. As a consequence, to convert L_c to L_t (or the other way around), the central intermolecular CC bond [type (1)] will break and two new N-C bonds [type (2)] will form. This bonds breaking/formation process requires the presence of energy barriers. Similarly, the formation of the S_t conformer from the L_t or L_c conformers requires the rupture of $C(sp^2)$ - $C(sp^2)$ or $C(sp^2)$ -N bonds while forming a $C(sp^3)$ - $C(sp^3)$ bond. Consequently, an energy barrier that separates the conformers S and L must exist, as discussed above and shown in Figure 7.4. The existence of a minimum in the potential energy surface for the σ -dimer at short distances (**2**, Figure 7.1) may be associated with the overlap between the sp^3 orbital in the $C(sp^3)$ - $C(sp^3)$ bond, in contrast to the p-p overlapping found in the intermolecular $C(sp^2)$ - $C(sp^2)$ bond. Due to the increase of the Coulomb repulsion effect between monomers in S_t , due to the short intermonomer distance, the net effect is a destabilization of the S_t conformer against the L conformers.

Quantitative features (electron density, Laplacian and ratio $|\lambda_1|/\lambda_3$) for each intermolecular critical point for the S_t , L_c and L_t conformers are summarized in Table 7.4. The value of the Laplacian in the critical point is negative in S_t , but positive in both conformers L . The magnitude of the $|\lambda_1|/\lambda_3$ ratio is large for the S_t conformer (764), but small for the L conformers (≈ 0.2). These results indicate the existence of a covalent bond between the two TCNE units in the S_t conformer and the presence of two or three weak intermolecular bonds (hydrogen bonds or van der Waals) between the two TCNE units in the L_c and L_t structures. Since the bond paths connect heavy atoms (C-C and N-C), the intermolecular interaction should be identified as van der Waals. However, the bonds in the L_c and L_t conformers cannot be van der Waals interactions because, as it will be discussed, the intermolecular bonds in L_c and L_t come from the interaction of the singly-occupied orbitals SOMO and not from interactions of doubly-occupied orbitals, such as in van der Waals bonds. The AIM analysis on the L conformers (Table 7.4) identified bond critical points with Laplacian values characteristic of a intermolecular bond, probably due to the long intermolecular C...C distance between the fragments in these conformers. Note that the existence of a critical point is only a necessary condition for the existence of the bonds, but not sufficient. It is also necessary that the structure formed as a result of the new bond is energetically stable. Both the RHF and B3LYP calculations predict that all the conformers are metastable. However, studies with more accurate methods are required before drawing a final conclusion.

The imposition of the double occupancy of the orbitals implied that in the RB3LYP calculations might be a non-physical restriction, particularly at long distances dimers, as those found in the L_c and L_t conformers. We re-calculated the potential energy surface at UB3LYP level. The UB3LYP interaction energy of the L_c and L_t conformers was calculated at RB3LYP optimum geometry for the *closed-shell* and *open-shell* singlet states; the latter using *Broken Symmetry* (BS) methodology. For these geometries, we estimated the orbital occupation by looking at the occupancy of the natural orbitals of the wave function. This was done for the b_{2u} and b_{1g} orbitals of the dimer that result from the combination of the SOMO orbitals of each [TCNE] $^-$ fragment, as well as the anti-bonding virtual b_{2u} orbital which is next in stability to b_{1g} orbital. The occupation numbers of the orbitals b_{2u} , b_{1g} , and b_{2u} are 2.0, 1.7 and 0.3 e^- , respectively, for L_c conformer, and 2.0, 1.5 and 0.5 e^- , respectively, for L_t . These two sets of numbers indicate a significant weight of the *open-shell* singlet S_1 wave function, which requires not doubly occupied orbitals for its description. For comparison, the S_t conformer has the occupation numbers 2.0, 0.0 and 0.0 e^- for the same orbitals,

indicating, in this case, a negligible weight of the *open-shell* S_1 component. Given the significant weight of the S_1 state in the electronic wavefunctions of the L_c and L_t conformers, we can conclude that the potential energy curve along the r coordinate must be computed at UB3LYP level to gain a correct insight into the electronic structure of these two conformers. At short distances, the UB3LYP curve collapses on the closed-shell RB3LYP curve, as expected (see, Figure 7.8). However, at distances longer than 2.5 Å, the BS-UB3LYP (*broken symmetry* UB3LYP) S_1 state becomes more stable. The BS-UB3LYP curve does not show any minimum for the L_c and L_t conformers. Consequently, the minimum calculated at the RB3LYP level is an artifact, *i.e.*, a consequence of the double occupancy restriction imposed to the orbitals. The triplet state curve at the same geometry is also plotted in Figure 7.8. Given that the triplet T_1 curve is higher in energy than the BS-UB3LYP S_1 singlet, the ground state of the L arrangement of dimers is a singlet S_1 , in good agreement with the experimental data.

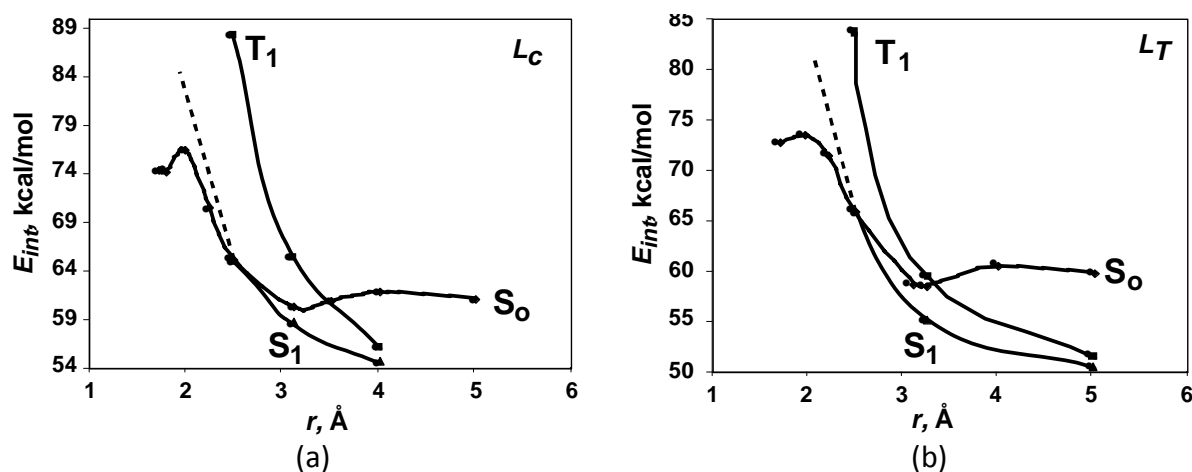


Figure 7.8 Interaction energy as a function of r of S_0 , S_1 and T_1 states for (a) L_c and (b) L_t configurations of the π -[TCNE] $_2^{2-}$ dimers. Notice that S_0 stands for closed-shell $^1A_{1g}$ singlet, S_1 for open-shell $^1B_{1u}$ singlet and T_1 for $^3B_{1u}$ triplet. Note also that the S_0 , S_1 and T_1 data have been calculated at RB3LYP, BS-UB3LYP and UB3LYP level, respectively.

BS-UB3LYP results were confirmed by MCSCF(6,4) calculations at the same geometries using an active space of 6 electrons and 4 orbital. The six electrons considered are those that are part of the π and π^* orbitals of each [TCNE] $^-$ fragment (three per fragment), and the four orbitals are the π and π^* of each fragment (two per fragment). For comparison purpose, these calculations were carried out using a 6-31+g basis set as in previous UB3LYP calculations. For any given geometry, the population of the b_{2u} , b_{1g} , and b_{2u} orbitals in these MCSCF calculations differ in less than $\pm 0.1 e^-$, regarding the UB3LYP results for the same geometry. The shape of the S_0 and S_1 curves calculated using MCSCF are also similar to those found at UB3LYP level. In addition, a full optimization of the geometries of the L_c and L_t conformers at MCSCF(6,4) level, starting from the structures optimized with RB3LYP, produces dissociation of the [TCNE] $^-$ fragments. Therefore, both the UB3LYP and MCSCF results indicate that L_c and L_t conformers are not true minimum energy structures in the potential energy surface. The existence of these minima at RB3LYP level for the conformers L is a consequence of the orbital double occupancy imposition in this method. Therefore, the presence of [TCNE] $_2^{2-}$ dimers both in the L_c and L_t conformers, as have been observed,

must be the result of cation-[TCNE] $_2^{2-}$ attractive electrostatic interactions that outweigh the [TCNE] $^{-}\cdots$ [TCNE] $^{-}$ repulsive electrostatic interaction.

7.3.1 Cation--[TCNE] $_2^{2-}$ stabilization of the TCNE dimers

This section aims at assessing whether the [TCNE] $_2^{2-}$ dimer formation is due to cation $^+\cdots$ [TCNE] $^{-}$ attractive electrostatic interaction. This assertion has been confirmed by computer studies carried out on K_2 [TCNE] $_2$ (glyme) $_2$, (Table 7.5). K_2 [TCNE] $_2$ (glyme) $_2$ system is constituted by two μ_4 -[TCNE] $_2^{2-}$ units (Table 7.2), each one bonded to two K^+ ions { K^+ placed at 2.905 ± 0.055 Å to the N, halfway between the two parallel planes containing the [TCNE] $^{-}$ }, (Figure 7.9a), and by two neutral molecules of glimepiride (glyme), which are also bonded to the K^+ ions⁴¹. The intermolecular CC separation ~ 3.0 Å is significantly less than the sum of the van der Waals radii of 3.4 Å^{59,63}, which would imply an intermolecular CC separation of ~ 4.5 Å. At UHF/6-31+g(2d,2p) level, the [TCNE] $_2^{2-}$ dimer with a short intermolecular distance shows a repulsive interaction of 103.0 kcal/mol in its lowest state. However, the $K^+\cdots$ [TCNE] $^{-}$ interactions within the K_2 [TCNE] $_2$ aggregate are attractive by 75.0 kcal/mol. Thus, although the [TCNE] $_2^{2-}$ dimers are energetically unstable with respect to the dissociation, the neutral K_2 [TCNE] $_2$ system is stable in 158.4 kcal/mol with respect to the dissociation. This value is close to the average result found using *ab initio* methods (about 200 kcal/mol) for the interactions present in many ionic molecular crystals involving single-charged ions^{64–66}.

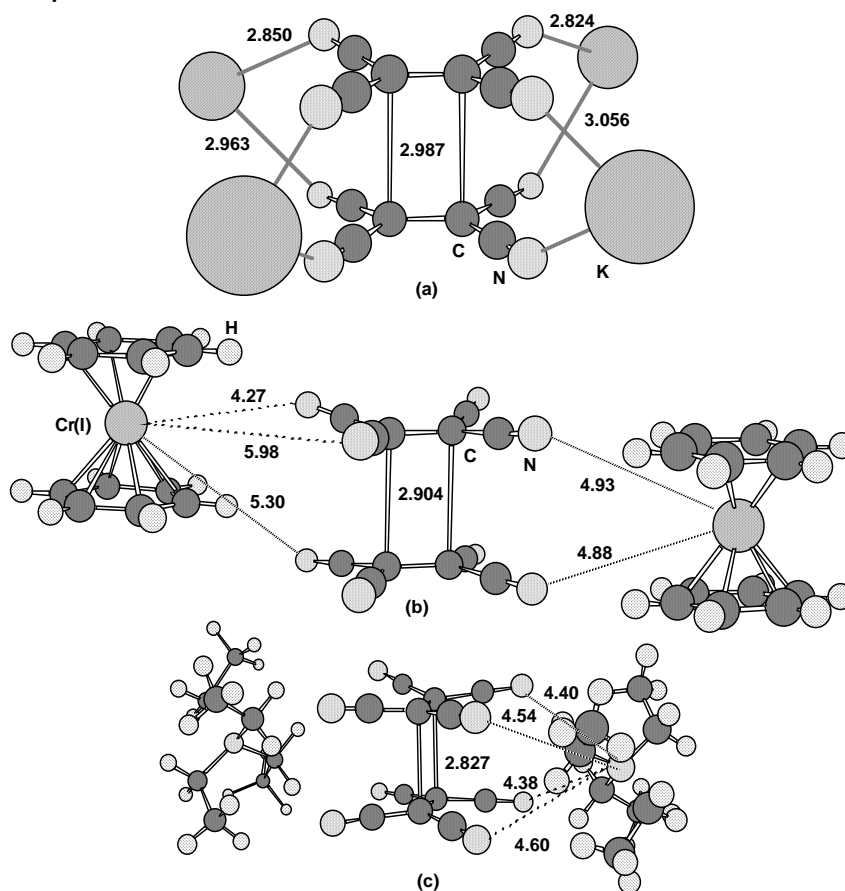


Figure 7.9 Geometry of the neutral (cation) $_2$ [TCNE] $_2$ system used to calculate the energy of the intermolecular interaction in (a) K_2 [TCNE] $_2$ (glyme) $_2$ ⁴¹, (b) $[Cr^I(C_6H_6)_2]_2$ [TCNE] $_2$ ⁴⁰ and (c) $[Et_4N]_2$ [TCNE] $_2$ ⁴⁶. The main intermolecular distances between the fragments are listed in Å. The macromolecular complex unit has a zero net charge.

Table 7.5 Total interaction energy for the $K_2[TCNE]_2(glyme)_2$ ⁴¹, $[Et_4N]_2[TCNE]_2$ ⁴⁶ and $[Cr(C_6H_6)_2]_2[TCNE]_2$ ⁴⁰ systems. The E_{int} is also partitioned into $A^{\cdots}A^-$, $D^{\cdots}D^+$, $A^{\cdots}D^+$ interactions. All calculations were performed at UHF/6-31+g(2d,2p) level.

	$E_{int} A^{\cdots}A^-$ kcal/mol	$E_{int} D^{\cdots}D^+$ kcal/mol	$E_{int} A^{\cdots}D^+$ kcal/mol	Total E_{int} kcal/mol
$K_2[TCNE]_2(glyme)_2$	103.0	30.5	-70.9, -72.1, -75.0 and -73.9	-158.4
$[Et_4N]_2[TCNE]_2$	83.5	19.3	-58.1, -58.0, -66.1 and -66.0	-145.2
$[Cr(C_6H_6)_2]_2[TCNE]_2$	79.9	12.2	-67.5, -68.5, -57.2 and -24.1	-125.2

These observations were also confirmed¹ in the $[Et_4N]_2[TCNE]_2$ ⁴⁶ and $[Cr(C_6H_6)_2]_2[TCNE]_2$ ⁴⁰ systems. These two systems have structures with $[TCNE]_2^{2-}$ dimers in which the cations are placed sideways with respect to the anions (Figure 7.9 b and c). Comparing the results of the UHF/6-31+g(2d,2p) for the three systems $K_2[TCNE]_2$, $[Et_4N]_2[TCNE]_2$ and $[Cr(C_6H_6)_2]_2[TCNE]_2$ (Table 7.5), it is observed that large cations appear to reduce slightly the stability of the $[TCNE]_2^{2-}$ dimers (which decreases from 103.0 kcal/mol in salts of K^+ , to 83.5 kcal/mol in salts of $[Et_4N]^+$, and 79.9 kcal/mol in salts of $[Cr(C_6H_6)_2]^+$) as well as the net stability of the system, that is, respectively 158.4, 145.2, and 125.2 kcal/mol.

The results of the computational studies indicate that the net charge and the geometrical orientations are the most important factors in determining the strength of the interactions in ionic crystals^{64,67,68}. Thus, for instance, if the $[Cr(C_6H_6)_2]^+$ cations of Figure 7.9 are placed perpendicular to the nominal $[TCNE]^-$ planes of the $[TCNE]_2^{2-}$ units, the $[TCNE]_2^{2-}$ dimer is unstable with respect to the dissociation into two $[TCNE]^-$ molecules.

Therefore, despite of the strong inter-anionic repulsive interaction, the supramolecular cation $_2[TCNE]_2$ organization can be formed whenever the cation-anion interactions allow the stabilization of the $[TCNE]_2^{2-}$ dimer at ~ 2.9 Å inter-monomer distance. As a result of this short separation, the singly-occupied orbital (SOMO) π^* of each $[TCNE]^-$ monomer can overlap forming the intermolecular bonding and anti-bonding orbitals of the dimer, which are separated by a non-negligible energy gap, namely Δ . Note that this energy gap is similar to the one observed for energy stable bonds, *e. g.*, H_2 ⁶⁹. Due to this gap, the interactions within the $[TCNE]_2^{2-}$ dimer show all the structural, spectroscopic and magnetic properties characteristic of the bond, as discussed above. Therefore, the inter-monomer CC bond within the $[TCNE]_2^{2-}$ dimer is through cation. On the contrary, other similar cations, for example $[N(n-Bu)_4]^+$ ³³ and $[Fe(C_5Me_5)_2]^+$ ³¹, do not stabilize the $[TCNE]_2^{2-}$ dimer. Note, however, that there may be polymorphic $[TCNE]_2^{2-}$ dimers for these cations, although not detected yet.

7.3.2 TCNE dimers in solvent

It has been mentioned that the metastable minima found in vacuum could be stable in a polar environment. To evaluate this statement, we investigated the dimerization of two TCNE molecules in polar solvents. Preliminary studies were performed at M06L/6-31g(2d,2p) level with continuum solvent methodology (PCM) in acetonitrile and in dichloromethane (Table 7.6). Three L metastable minima [$d \sim 0^\circ$ (L_c), 104° (L_{twist}) and 180° (L_t)] found in vacuum were confirmed as true minima of energy ($E_{int} < 0$) in

acetonitrile. In dichloromethane only two of these three structures ($d \sim 0$ and 103°) were confirmed as minima of energy ($E_{\text{int}} < 0$ respect two separated monomers). The energy of the S_t structure was still above the energy of two separated monomer. It appears that the polar solvent molecules minimize the repulsion between the two TCNE anion molecules and facilitate the stabilization of the long distance dimers L ($r \approx 3 \text{ \AA}$). The E_{int} were lower in acetonitrile than in dichloromethane which can be explained by the higher polarity index (PI) of acetonitrile (PI = 5.8) compared to dichloromethane (PI = 3.1).

Table 7.6 Minima of TCNE $^{2-}$ dimers calculated with M06L and 6-31g(2d,2p) basis set in acetonitrile and dichloromethane

	Acetonitrile			Dichloromethane		
	$r(\text{\AA})$	$d(^{\circ})$	E_{int} (kcal/mol)	$r(\text{\AA})$	$d(^{\circ})$	E_{int} (kcal/mol)
S_t	1.684	180°	10.1	1.685	180°	14.812
L_c	2.959 ^a	4.3°	-5.6	2.942	3.8°	-0.4
L_t	3.320	179.8°	-3.6	3.300	180°	1.4
L_{twist}	3.124	103.8°	-5.0	3.113	103.5°	-0.1

^aAverage of the two C...C values 2.949 \AA and 2.968 \AA .

7.3.3 Pair solvent effect in TCNE dimers

To investigate how the presence of the solvent molecules could affect the interaction of the two ions we carried out several calculations considering explicitly the first solvation sphere of the anions. The interaction between the ions in a solvent can be classified according to three possibilities⁷⁰ (see Figure 7.10): (a) strong ion-pair (or **contact**) where there are no solvent molecules between the two ions and they are in direct contact, (b) **solvent-share** when the two ions share solvent molecules as part of their solvation spheres, and (c) **fully solvated** (or solvent-separated) when each ion has a complete primary solvation sphere that is not shared.

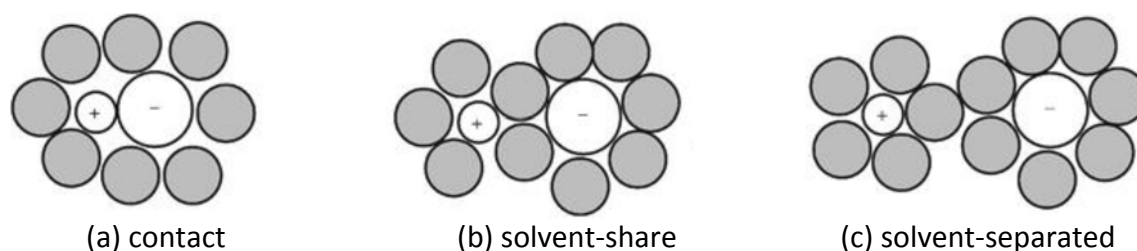


Figure 7.10 Representation of the (a) strong ion-pair (or **contact pair**) when there are no solvent molecules between the two ions, (b) **solvent-share** when the two ions share solvent molecules as part of their solvation spheres and (c) fully solvated (or **solvent-separated**) when each ion has a complete primary solvation sphere.

The study of the dimerization of TCNE considering the pair-solvent was performed following the methodology proposed by da Silve et al⁷¹. To minimize the computational cost, we selected dichloromethane (CH_2Cl_2) as the solvent to carry out this study, since many solvent molecules were incorporated in the calculations.

1. The geometry of the dimer and its solvation shell was obtained from previous molecular simulations of the solute in bulk solvents. We selected several configuration (50031,

- 138551, 182171, 327151, 406691 and 431071) from the Molecular Dynamic (MD) calculations performed by Capdevila-Cortada M. et al.⁷² These configurations were minima of energy in their MD simulations (Figure 7.11a).
2. After investigating all the strong solute-solvent interactions, the first solvation sphere was defined as the solvent molecules that were at distance smaller than 3 Å. The primary solvation sphere selected contained ten solvent molecules (Figure 7.11b) for the monomer and twenty solvent molecules for the dimer (Figure 7.11c).
 3. Initial geometry optimization at UHF/6-31g(d) indicated that higher computational level was required to describe correctly the system. Consequently, all the calculations were carried out at M06L/6-31+g(d) level with Grimme correction, which had been previously identified as a good method to describe this kind of systems⁷².

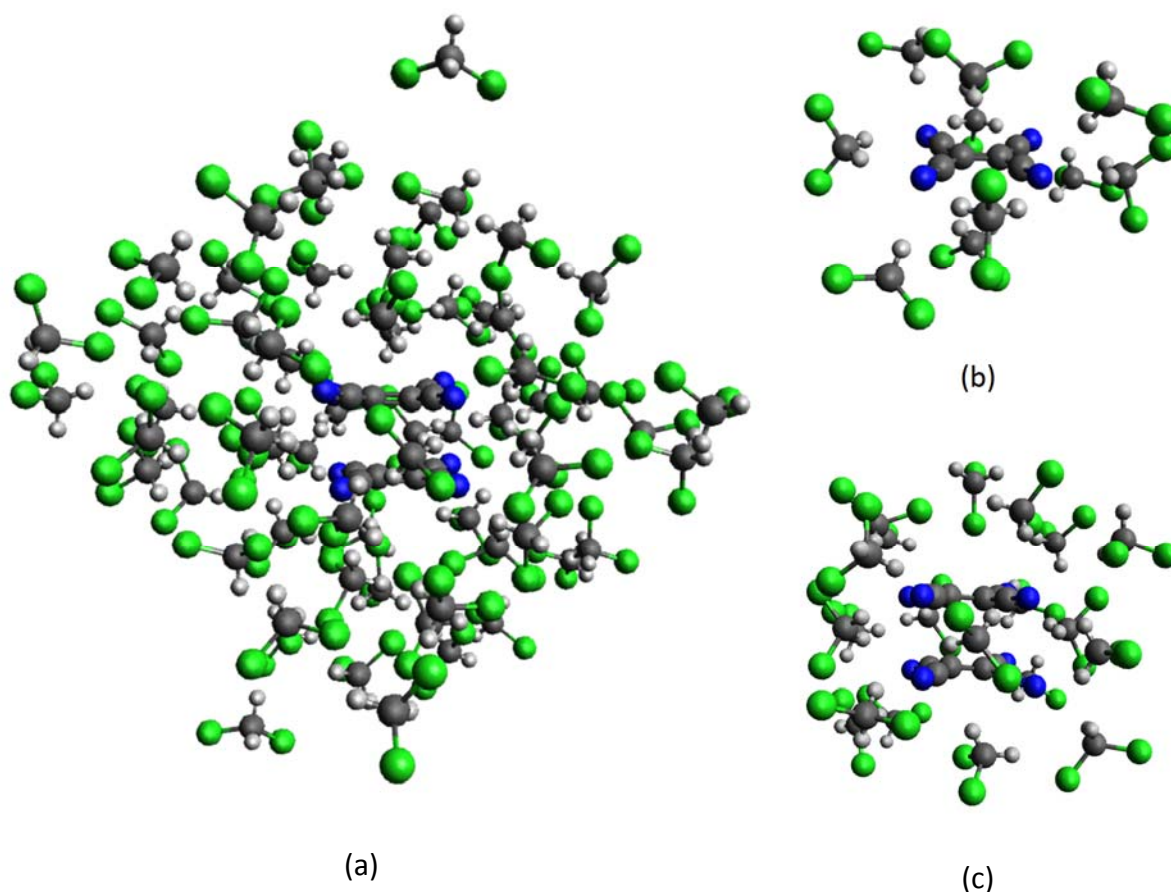


Figure 7.11 (a) Example **50031** configuration extracted from previous MD calculations⁷². (b) TCNE⁻ monomer with its primary solvation sphere containing 10 solvent molecules. (c) TCNE⁻ dimer with its primary solvation sphere containing 20 solvent molecules.

Energy calculations performed at the selected MD orientations⁷² (50031, 138551, 182171, 327151, 406691) estimated that the dimer with its first solvation sphere was more stable than the two separated monomers with their respective solvation spheres (Table 7.7).

The potential energy surface was calculated at M06L/6-31+g(d) level with Grimme correction to obtain the energy at different intermolecular distances, optimizing the geometries of the cluster formed by the dimer and the twenty solvent molecules at each one of these points (Table 7.8). These optimized geometries were used to calculate the single-point energies at M06L/6-31+G(d) level with the continuum solvation method (PCM). Finally, the interaction energies (E_{int}) of these clusters were estimated without and with the continuum solvation method (PCM) both for the singlet and the triplet states.

Table 7.7 Interaction energy (E_{int}) of the TCNE $^-$ dimer with 20 CH $_2$ Cl $_2$ molecules compared to the monomer calculated with M06L and 6-31+g(d) basis set.

System	E_{int} (kcal/mol)
50031	-51.9
138551	-29.1
182171	-55.7
327151	-51.8
406691	-60.1
431071	-51.9

Table 7.8 Interaction energy (E_{int}) of the TCNE $^-$ dimer with 20 CH $_2$ Cl $_2$ molecules calculated with M06L/6-31g(d).

r (Å)	E_{int} (kcal/mol)		$\Delta E^{\text{S-T}}$ (kcal/mol)	
	Optimized Geometry	Single-point calculation with solvation (PCM)	Optimized Geometry	Single-point calculation with solvation (PCM)
2	24.1	-1.1	-33.9	-38.0
3	-22.5	-48.8	-3.7	-15.2
4	-16.0	-40.4	-0.6	-0.9

As a result of these calculations we observed the stabilization of a minimum of energy at $r \sim 3$ Å. In vacuum this was a metastable minimum that needed the counterions to be a real minimum of energy. The presence of the CH $_2$ Cl $_2$ solvent molecules helps in the stabilization of the dimer minimizing the repulsion between the two anion TCNE molecules and facilitating the attractive intermolecular interaction. This stabilizations is higher with the continuum solvation model [$E_{\text{int}}(\text{vacuum}) = -22.5$ kcal.mol vs $E_{\text{int}}(\text{PCM}) = -48.8$ kcal.mol at 3 Å]. In all the cases, the singlet is lower in energy than the triplet, which indicates the antiferromagnetic character of the interaction.

During the optimization at the different points in the curve it was observed the tendency of the dimer to form a strong ionic pair with no solvent molecules between the two ions. We also studied the dimer at intermolecular distances 5 Å, 6 Å (representing the solvent-shared ionic pair) and 10 Å (representing the solvent-separated ionic pair). It was observed that at $r = 5$ Å the initial parallel head-to-head ($d \sim 0^\circ$) orientation is not the preferred minimum and the two molecules of TCNE migrate to a head-to-tail disposition ($d \sim 180^\circ$) with an

intermolecular C-C distance of $r = 4.3 \text{ \AA}$ (Figure 7.12). This structure was identified as metastable minimum in the calculations in vacuum and it is observed in some experimental synthesized crystals (α - and β - [TTF] $_2$ [TCNE] $_2$). The dimer at 6 \AA does not converge and the molecules tend to separate. At 10 \AA the dimer is less stable than the two separated monomers in the continuum solvation model and than the other structures with shorter inter-dimer distances.

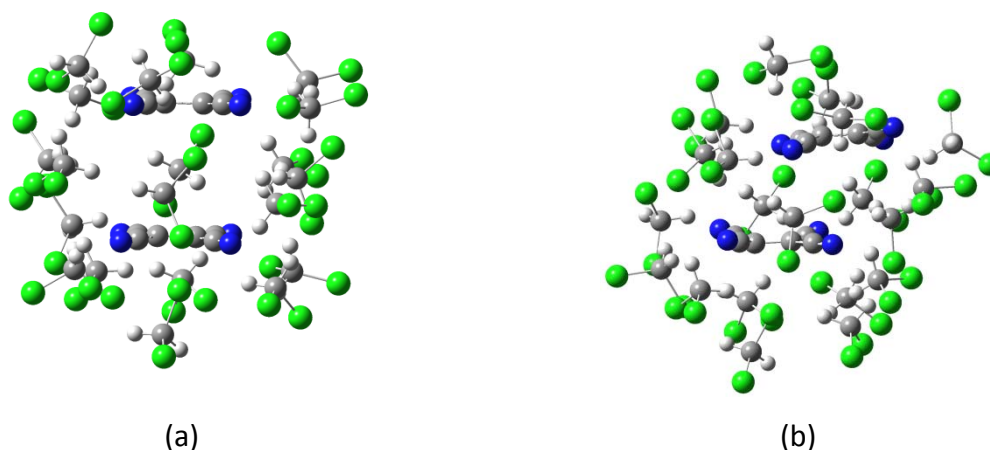


Figure 7.12 (a) Initial optimization step with inter molecular distance $r = 5 \text{ \AA}$ and dihedral angle $\theta \sim 0^\circ$ (b) Optimized structure at $r = 4.3 \text{ \AA}$ and $d = 180^\circ$.

7.4 Nature of the intermolecular interactions within the [TCNE] $_2^{2-}$ dimer

The properties of the $[A]_2^{2-}$ dimers are determined by the anionic nature of the interacting molecules and the existence of an unpaired electron in each of the monomers. As shown in the Figure 7.13, the two main factors that determine the interaction energy (E_{int}) between the anionic monomers are: (i) the electrostatic Coulomb repulsion (E_{coul}) between the two anionic fragments $[A]^-$, and (ii) the attraction forces generated by the unpaired electrons (E_{bond}), that are trying to build an intermolecular σ or π bond. In thus follows that the total interaction energy is the sum of both contributions $E_{int} = E_{coul} + E_{bond}$. If the E_{coul} term dominates ($|E_{coul}| > |E_{bond}|$), the two $[A]^-$ units repel each other at all distances, and no structure will be a minimum of the potential energy surface. On the other hand, if $|E_{bond}| > |E_{coul}|$, a stable energy minimum will exist (Figure 7.13). Finally, when $|E_{bond}| \sim |E_{coul}|$, metastable dimers will form: the energy of such minima will be above the energy corresponding to two $[A]^-$ monomers. However, the dimer will not dissociates into the two molecules due to the presence of an energy barrier (Figure 7.13). If the E_{coul} decreases or the bond between the two $[A]^-$ monomers enlarges, the stability of the metastable dimer increases and, at some point, the dimer can go from being metastable to stable (Figure 7.13). Metastable species cannot form in phase gas at finite temperature, as the thermal energy is less than the barrier for the formation of the dimer from its fragments. However, the formation of metastable species can occur in a crystal if the electrostatic cation $^+$ - $[A]^-$ interaction is enough to overcome the energy associated with the repulsive Coulomb interaction between the $[A]^-$ - $[A]^-$ anions. Although the existence of the $[A]_2^{2-}$ dimer (represented by [TCNE] $_2^{2-}$) in solid phase suggests the formation of a stable or metastable^{30,38-51} species, a calculation of the energy at the experimental geometry is required to characterize them, both isolated and as in the crystal. Stabilization can also

occur in solution if the solvent-anion interactions overcome the Coulomb anion-anion repulsion. Note that in fact the shape of the two energy profiles shown in Figure 7.4 at RB3LYP level indicate $E_{coul} > E_{bond}$, since they agree qualitatively with Figure 7.13.

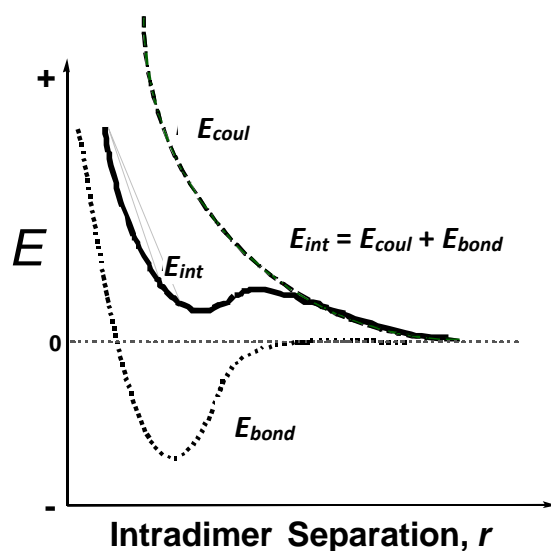


Figure 7.13 Diagram that shows the total interaction energy (E_{int}) curve composed by the addition of the coulombic (E_{coul}) and bond (E_{bond}) components.

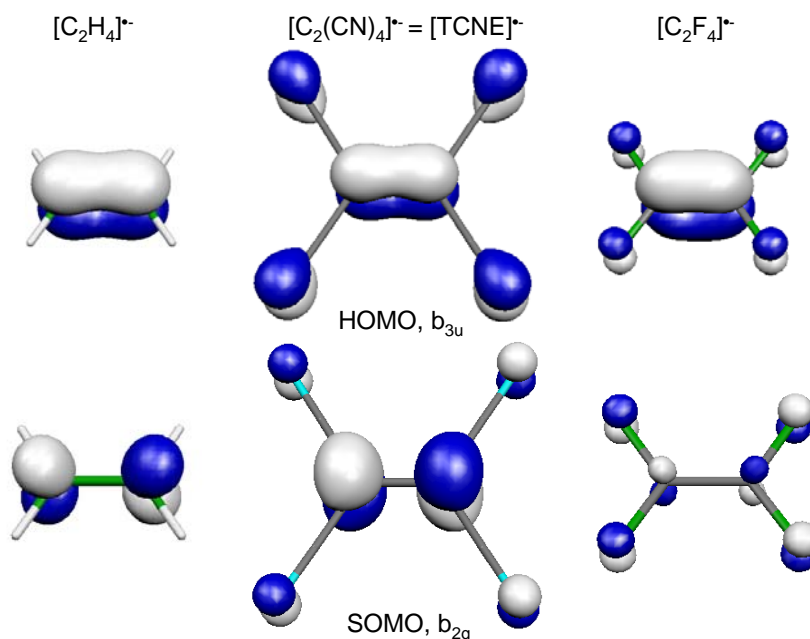


Figure 7.14 HOMO and SOMO orbitals for $[C_2H_4]^{•-}$, $[C_2(CN)_4]^{•-} = [TCNE]^{•-}$ and $[C_2F_4]^{•-}$

UBLYP/6-31+G(2d,2p) calculations performed on the isolated fragments $[TCNE]^{•-}$ and $TCNE^0$ show that the structure of the $[TCNE]^{•-}$ anion is planar and similar to $TCNE^0$ ^{73–76}, except that the central CC distance increases from 1.358 Å in the $TCNE^0$ to 1.392 Å in the $[TCNE]^{•-}$ anion, while the $C\equiv N$ distance experiences just a small increase from 1.158 to 1.167 Å, respectively. The extra electron in the $[TCNE]^{•-}$ anion is placed in the b_{2g} SOMO of π symmetry (Figure 7.14). This orbital is mainly located in the central C ($C_{central}$) atoms and the terminal N atoms,

with similar weights. The Mulliken population analysis of [TCNE] $^-$ (Table 7.9) indicates that C_{central} and N atoms share similar weight of the charge of the extra electron, each one holds $0.18 e^-$ (this value is obtained subtracting the atomic charge in [TCNE] $^-$ monomer from TCNE 0 , Table 7.9). This is consistent with the experimental data obtained from the single-crystal polarized neutron diffraction studies³³. Therefore, the charge tends to delocalize in the peripheral atoms of [TCNE] $^-$. UB3LYP/6-31+g(2d,2p) calculations performed on [C $_2$ H $_4$] $^-$ and [C $_2$ F $_4$] $^-$ (see Table 7.9 and Figure 7.14) indicate that these two systems do not show any charge delocalization trend. We can thus conclude that this trend cannot be entirely attributed to the electronegativity of the CN group, since the fluorine atom (F) is more electronegative than the cyanide group (CN). Therefore, such behavior may only be associated with delocalization due to the presence of low energy resonance forms, according to which the unpaired electron is delocalized over the CN groups (Figure 7.15).

Table 7.9 Net atomic charge obtained after a Mulliken population analysis with B3LYP/6-31+g(2d,2p). The analysis was performed for the atoms of three neutral and monoanionic molecules [C $_2$ X $_4$] n (X = H, F, CN, n = 0, -1)

Molecule	Atom	Charge	
		n = 0	n = -1
C $_2$ H $_4$	C	-0.237	-0.737
	H	0.119	0.119
C $_2$ F $_4$	C	0.590	-0.217
	F	-0.295	-0.141
C $_2$ (CN) $_4$, (TCNE)	C (CCN)	0.996	0.820
	C (CN)	-0.294	-0.272
	N (CN)	-0.203	-0.387

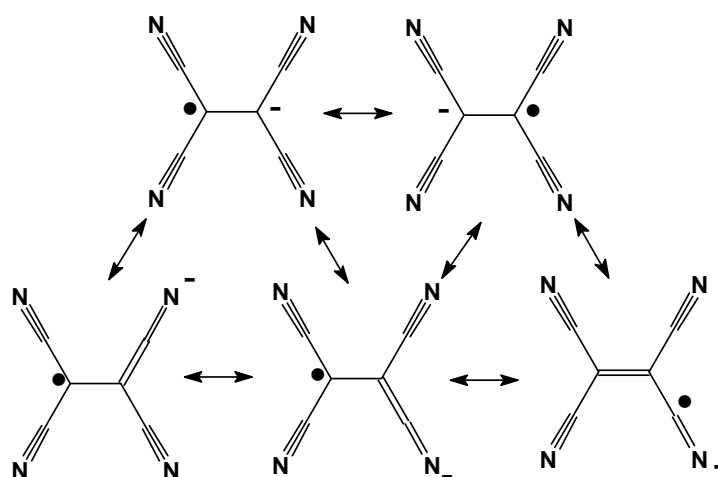


Figure 7.15 Representation of the possible electronic configurations of the TCNE $^-$ anion.

When the SOMO orbital of one [TCNE] $^-$ interacts with the SOMO orbital of the another [TCNE] $^-$ in a L_c structure, they combine to form bonding and antibonding orbitals of b_{2u} and b_{1g} symmetry, respectively (Figure 7.16). If the gap of energy, Δ , between these two orbitals is small, as it is the case at large values of r , each orbital will be partially occupied. $b_{2u}^1 b_{1g}^1$

configuration is then expected to have the lowest energy, which is similar to what happens when two H atoms interact to form the H₂ molecule⁶⁹. This configuration results in an open-shell singlet (S_1) or a triplet (T_0) state, either of which would dissociate into two equivalent [TCNE] $^-$ fragments. As shown in Figure 7.17, the energies of S_1 and T_0 states increase when r decreases, consequently no new bond will be formed between the two fragments for any of these two states. The $b_{2u}^1 b_{1g}^1$ configuration is then expected to have the lowest energy, which is similar to what happens when two H atoms interact to form the H₂ molecule⁶⁹. This configuration results in an open-shell singlet (S_1) or a triplet (T_0) state, either of which would dissociate into two equivalent [TCNE] $^-$ fragments. As shown in Figure 7.17, the energies of S_1 and T_0 states increase when r decreases, consequently no new bond will be formed between the two fragments for any of these two states.

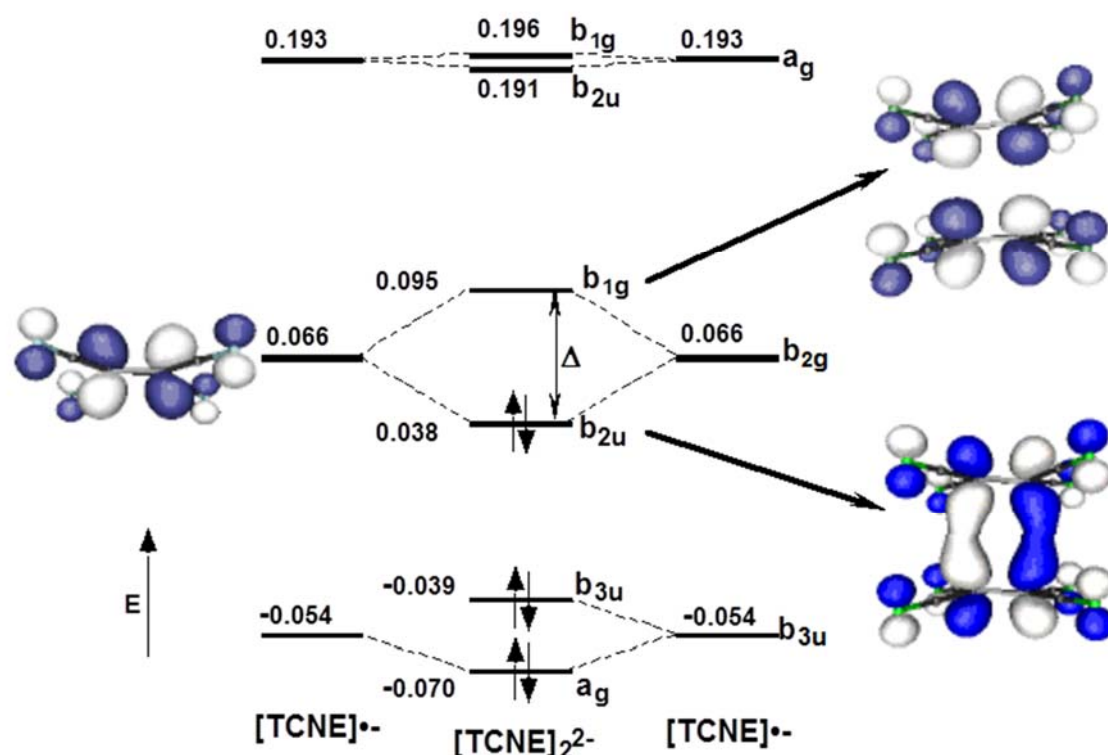


Figure 7.16 Schematic representation of the molecular orbitals of the [TCNE] $_2^{2-}$ dimer generated from the HOMO, SOMO and LUMO orbitals of the [TCNE] $^-$ fragments. See inset SOMO of [TCNE] $^-$ and HOMO/LUMO of [TCNE] $_2^{2-}$.

When r decreases (see Figure 7.17), Δ increases and the configuration $b_{2u}^2 b_{1g}^0$ is the most stable. This configuration lies above the configuration $b_{2u}^1 b_{1g}^1$ in the dissociation since it would result in the formation of fragments [TCNE] 0 and [TCNE] $^{2-}$. This is, again, similar to the situation found when two H atoms interact to form H₂³⁴. The configuration $b_{2u}^2 b_{1g}^0$ is associated with the closed-shell singlet state (S_0). Therefore, whenever the E_{bond} contribution predominates at short distances in the absence of the E_{coul} contribution, it gives rise to the formation of a new bond between the fragments.

This bond is unique in three ways: (1) it is a $2e^-$ bond between four carbon atoms chemically equivalent, (2) it involves the π^* orbital of each fragment (see Figure 7.3a), and (3) it is supramolecular, since the attractive cation \cdots anion electrostatic interactions enables two

anions, that otherwise would repel each other, to be sufficiently close so that their SOMOs can overlap. The existence of this bond is thus associated with the overlap of the π^* orbitals of each fragment. Therefore, the bond will occur whenever two fragments of [TCNE] $^-$ are at a short distance, either because the interaction between these two fragments is strongly energetically stabilized, or because some external force place them together. Multicenter bonds of $2e^-$ in 4 centres⁷⁷ have been reported previously for several boranes⁷⁸, as well as the structurally constrained, but not structurally characterized, 1,3-dehydro-5,7-adamantenediy⁷⁹ and the pagodane dications⁸⁰. However, this is the first example for a carbon-based system as well as the first example of a bond residing over four atoms.

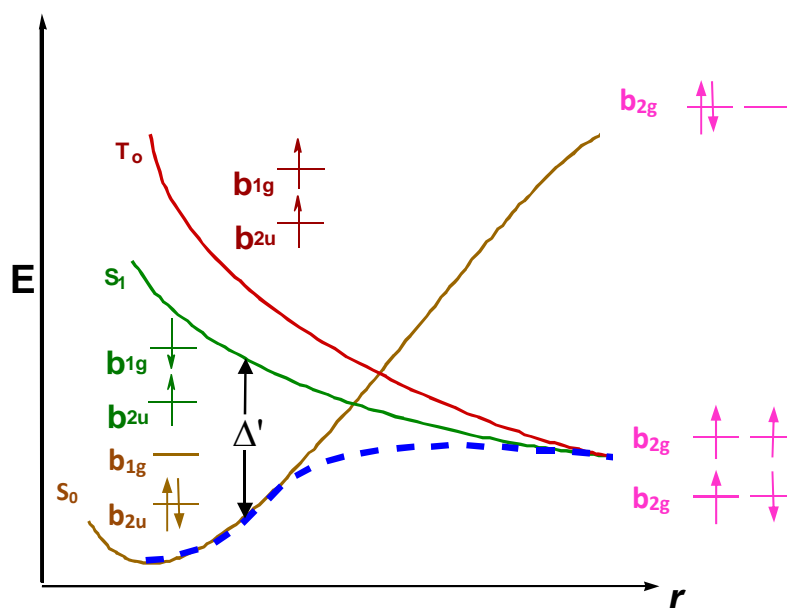


Figure 7.17 Schematic representation of the diabatic energy curves for the closed-shell S_0 singlet, open-shell S_1 singlet and T_0 triplet states for two interacting doublet radicals. The dashed line represents the adiabatic surface obtained after interaction of the diabatic S_0 and S_1 surfaces.

The [TCNE] $^- \cdots [TCNE]^-$ interaction does not meet the characteristics expected for an intermolecular bond of van der Waals type, as these are based on the instantaneous dipole interactions between the different molecular fragments. A van der Waals interaction occurs between closed-shell molecules which have no charge and are regular multipoles. The electronic structure of these interactions can be represented by a diagram in which the doubly occupied orbital of each fragment overlap with each other, and the resulting bonding and antibonding supramolecular orbitals are both doubly occupied (Figure 7.18a). The interaction is stronger when the overlapping orbitals are located on a few atoms of the fragment. Van der Waals interactions are much weaker when the doubly occupied overlapping orbitals are spread out over the entire molecule. This is the case of interactions that involve peripheral H atoms, for example, between molecules of H_2 or alkanes. In the latter case, the interactions could also be considered to be $C-H \cdots C$ ^{61,81}. The key energy term in the van der Waals interactions is the so-called *dispersion*⁸².

There are several differences when comparing the [TCNE] $^- \cdots [TCNE]^-$ interaction with a typical van der Waals bond. First, the electronic structure of the [TCNE] $^- \cdots [TCNE]^-$ interaction (Figure 7.18b) has an open-shell character, that allows to generate an attractive

bonding term (E_{bond}). Likewise, as seen above, the interaction $[\text{TCNE}]^{\cdot-}\cdots[\text{TCNE}]^{\cdot-}$ is dominated by the electrostatic repulsive term (E_{coul}), associated with the anionic nature of $[\text{TCNE}]^{\cdot-}$ fragments. Therefore the $[\text{TCNE}]^{\cdot-}\cdots[\text{TCNE}]^{\cdot-}$ interaction cannot be considered van Waals in nature. Neither can be purely ionic, since ionic interactions are dominated by the electrostatic term, which means that have $E_{bond} = 0$ and are basically repulsive between two anions. Finally, this interaction cannot be considered as a normal covalent bond, since the electrostatic term (E_{coul}) plays an important role defining the shape of the curve of the interaction potential energy. Thus, the $\pi^*-\pi^*$ 2 electrons-4 centers interaction found in the $[\text{TCNE}]_2^{2-}$ dimer, presents a mixture of Coulombic and covalent behaviour.

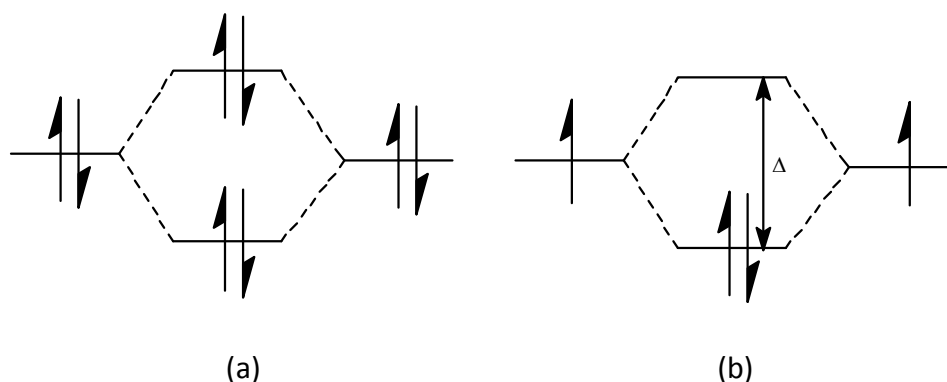


Figure 7.18 Diagrams of the bonding and antibonding orbitals resulting from the interaction of: (a) two doubly occupied orbitals and (b) two semioccupied orbitals.

The S_0 and S_1 diabatic curves intersect in the region between the minimum and the dissociation geometries (Figure 7.17). If the two diabatic curves are allowed to interact, as it occurs when using accurate *ab initio* methods, the adiabatic curve that correctly describes the real physical situation is obtained. This adiabatic curve (dashed line in Figure 7.17) is inferred from the minimum of energy of the two diabatic curves S_0 and S_1 . When the minimum of the S_0 -curve is shallow and both S_0 and S_1 minima are close in energy, there is a transition barrier in the region where the diabatic curves intersect. However, the transition state barrier decreases when the stability of the S_0 state increases and the energy difference between both S_0 and S_1 states rises. The transition barrier may disappear when the S_0 state is stable enough, as it is the case of the majority of chemical bonds due to its high dissociation energy. Both the UHF and UBL3YP methods allow the interaction between the open-shell (S_1) and closed-shell (S_0) singlet states, *i.e.* provide curves of adiabatic potential energy for the interaction of two $[\text{TCNE}]^{\cdot-}$ fragments, which is not the case at RHF or RB3LYP level. It is possible with UHF or UBL3YP methods to determine the relative importance of the S_0 and S_1 contributions to the adiabatic wave function of the singlet. This analysis is performed looking at the occupation numbers of the natural orbitals obtained by diagonalization of the matrix built from *broken symmetry* either UHF or UBL3YP wave functions. If the occupation number of the b_{2u} and b_{1g} orbitals is close to 2 and 0 respectively, the main component is the closed-shell singlet (S_0); while, when the principal component is the open-shell singlet (S_1), the occupation numbers are close to 1 for both orbitals. Additional MCSCF calculations were performed on B3LYP optimized geometries to check the validity of the B3LYP description. The minimum obtained at long intermolecular distance may have a strong diradical character that might not be correctly described at UHF

or UBL3YP level. This analysis only describes the shape of the E_{bond} component of the total interaction energy between two [TCNE] $^-$ fragments. Let us remind that the presence of minima in the E_{int} curve is induced by the minima found in the E_{bond} curve. Therefore, the preliminary qualitative analysis of the E_{bond} component is exceedingly important.

7.5 Experimental evidence of the long intermolecular CC bond

7.5.1 Electronic structure of the [TCNE] $_2^{2-}$ dimer

As noted above, although isolated [TCNE] $_2^{2-}$ dimers are not energetically stable with respect to dissociation, the cation $^+$ -[TCNE] $_2^{2-}$ interaction stabilizes the [cation] $_n$ [TCNE] $_m$ system (Figure 7.9), making the whole aggregate stable with respect to the dissociation into fragments. The cation acts as a "glue" that holds two [TCNE] $^-$ anions at a distance that allows the overlap between orbitals from each fragment.

Ab initio calculations carried out on the [TCNE] $_2^{2-}$ dimers at the range of distances observed for the **S** and **L** conformers show (Figure 7.18) the existence of a energy gap, Δ , between the bonding, b_{2u} , and anti-bonding, b_{1g} , orbitals (Figure 7.16). This energy difference (Δ) between the b_{2u} - b_{1g} orbitals gives rise to two possible singlet states: the *closed-shell*, **S** $_0$ (which comes from the $b_{2u}^2b_{1g}^0$ configuration), and the *open-shell*, **S** $_1$ (configuration $b_{2u}^1b_{1g}^1$). The energy difference between these two states is the reason why there is a new allowed electronic transition observed for [TCNE] $_2^{2-}$ in the visible region of the spectrum. Experimentally, this new absorption is observed in the range of 15000 cm^{-1} (667 nm; 1.86 eV) to 18200 cm^{-1} (549 nm; 2.26 eV) [average value = 16825 cm^{-1} , average standard deviation = 1180 cm^{-1} (594 nm; 2.09 eV)] for nine [TCNE] $_2^{2-}$ dimers (see Table 7.2 and Figure 7.19). According to this absorption, the dimer appears purple via light reflected in it.

These data are consistent with preliminary studies in M[TCNE] systems (where M = Na, K, Rb, Cs) that are not characterized structurally, whose spectrum in solid state at room temperature show a new absorption band at \sim 18500 cm^{-1} (541 nm; 2.29 eV), assigned to the charge transfer between two [TCNE] $^-$ units in the dimer²⁹. Despite the high-energy values of our data, the result is consistent with the absorptions for the structurally characterized [TCNE] $_2^{2-}$ within dimers.

The initial *ab initio* results suggest that the [TCNE] $_2^{2-}$ dimer should be stable in solution at low temperature. The spectrum in solution of the saturated [Et $_4$ N] $_2$ [TCNE] $_2$ dissolved in 2-methyl tetrahydrofuran (MeTHF) only shows the typical spectral features of the [TCNE] $^-$ unit in solution (see Figure 7.20a⁷⁶). However, after a rapid decrease of the temperature to 77 K, when a bright red ice crystal forms, the characteristic [TCNE] $^-$ absorption band disappears, and new absorption bands appear at 18940 and 26000 cm^{-1} (528 nm and 385 nm, respectively; see Figure 7.20b). This is consistent with the equilibrium 2 [TCNE] $^-$ \leftrightarrow [TCNE] $_2^{2-}$ being shifted to the right with decreasing temperature in accordance with entropy considerations such that at 77 K sufficient amounts of the [TCNE] $_2^{2-}$ dimer are present and stable⁹. Hence, [TCNE] $_2^{2-}$ is thermal chromic. Similar solution spectra of [TCNE] $_2^{2-}$ as a 2-methyl-tetrahydrofuran glass at 77 K were also reported [λ_{max} = 18500 cm^{-1} (540 nm)]²⁹.

⁹ The red color of the dimer is also evident for [Et $_4$ N] $_2$ [TCNE] $_2$ dissolved in CH $_2$ Cl $_2$ [mp = 178 K (- 95 °C)] solution at 195 K [- 78.5 °C; dry ice/Me $_2$ CO bath] or 178 K [- 95 °C; PhMe/N $_2$ (l) sush] and the red color is more intense at lower

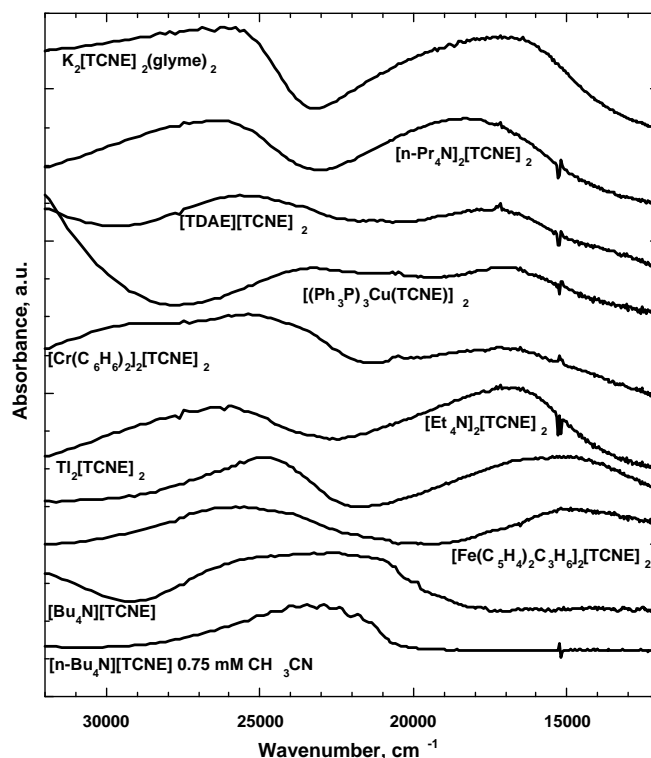
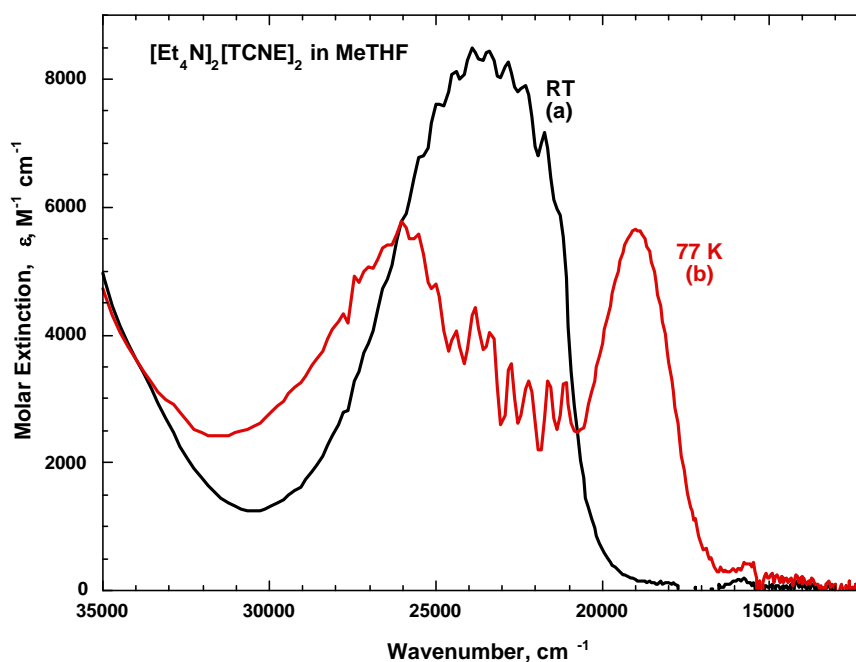


Figure 7.19 Experimental UV-Vis spectra of solid (KBr pellet): $K_2[TCNE]_2(glyme)_2$, $[n-Pr_4N]_2[TCNE]_2$, $[TDAE][TCNE]_2$, $[Cu(PPh_3)_3][TCNE]_2$, $[Cr(C_6H_6)_2][TCNE]_2$, $[Et_4N]_2[TCNE]_2$, $Ti_2[TCNE]_2$, $[Fe(C_5H_4)_2C_3H_6]_2[TCNE]_2$ and $[n-Bu_4N][TCNE]_2$. The absorption bands observed at $\geq 25000\text{ cm}^{-1}$ are assigned to $[TCNE]^-$ transition as observed for $[n-Bu_4N]_2[TCNE]_2$ in solution (75 mM in MeCN).

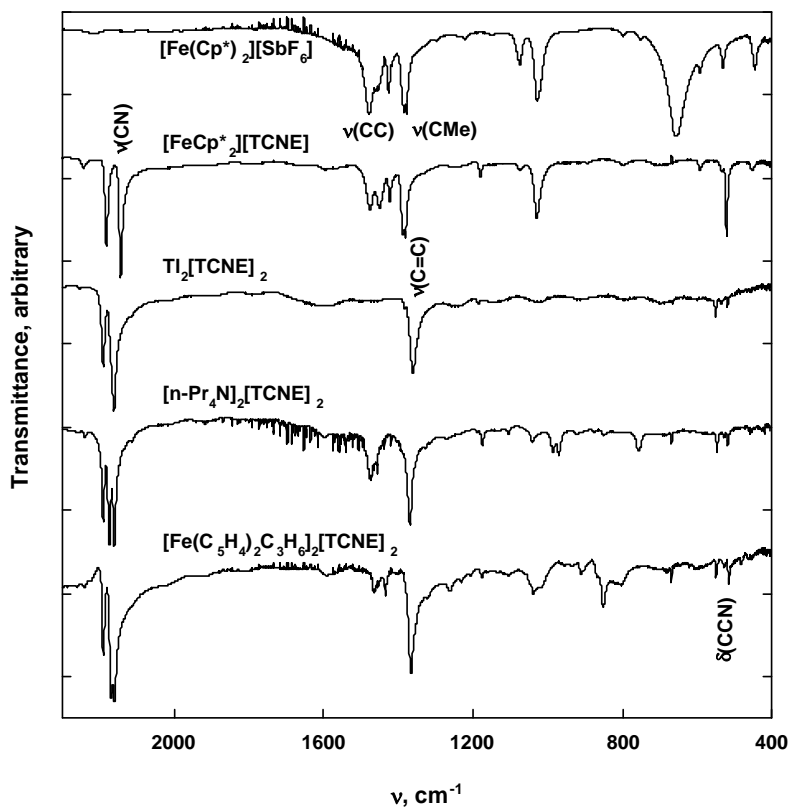


temperatures. On the contrary, the red color of the dimer does not appear when $[n-Bu_4N][TCNE]$, which does not form dimers in the solid state³³, is dissolved in MeTHF and is cooled to 77 K.

Figure 7.20 Experimental UV-Visible electronic absorption spectra of a saturated solution of [Et₄N]₂[TCNE]₂ in MeTHF at (a) room temperature, RT, and at (b) 77 K. Data is recorded as molar extinction (ϵ) per mole of [TCNE]⁻ as a function of energy based on $\epsilon(23375 \text{ cm}^{-1}) = 8425 \text{ M}^{-1}\text{cm}^{-1}$

7.5.2 Vibrational absorption spectra

It is also a demonstration of the intermolecular bond formation that the IR spectrum of the dimer differs with respect to their fragments, as it has been observed. Table 7.4 includes the harmonic stretching frequencies $\nu_{\text{C}\equiv\text{N}}$ of the nitrile C \equiv N groups calculated at RB3LYP/6-31+g level, and their IR intensities. The intensities and frequencies calculated are in agreement with the experimental data in Table 7.2, bearing in mind that the calculated values have been obtained within the harmonic approximation. The calculations on the [TCNE]⁻ fragment displays two strong^{76,10} computed $\nu_{\text{C}\equiv\text{N}} \sim 2200 \text{ cm}^{-1}$, close to the ones observed experimentally at 2183 and 2144 cm^{-1} (Figure 7.21)^{31,76}. Besides, two additional weak peaks ($\sim 10\%$ as intense as the stronger peaks) are also computed at $\sim 2200 \text{ cm}^{-1}$. The RB3LYP/6-31+g calculation on the L_c π -[TCNE] $_2^{2-}$ dimer presents three $\nu_{\text{C}\equiv\text{N}}$ peaks that indicate the bond formation between two [TCNE]⁻ fragments (Figure 7.21). These results are consistent with the average of $\nu_{\text{C}\equiv\text{N}}$ absorptions values [2191 ± 2 (m), 2173 ± 3 (s), and 2162 ± 3 (s) cm^{-1}] observed for eleven [TCNE] $_2^{2-}$ dimers that have been structurally characterized and whose IR spectra are available (Table 7.2). These values differ from those observed for the L_t [2216 ± 2 (m), 2197 ± 3 (m), and 2180 ± 4 (m) cm^{-1}] and S_t [2215 ± 4 (m), 2157 ± 3 (s), and 2107 ± 4 (w) cm^{-1}] arrangements.



¹⁰ Plus two additional weak peaks ($\sim 10\%$ as intense as the stronger peaks) at $\sim 2200 \text{ cm}^{-1}$.

Figure 7.21 IR spectrum of $[\text{Fe}(\text{C}_5\text{Me}_5)_2][\text{SbF}_6]$, $[\text{Fe}(\text{C}_5\text{Me}_5)_2][\text{TCNE}]$, $\text{Ti}_2[\text{TCNE}]_2$, $[n\text{-Pr}_4\text{N}]_2[\text{TCNE}]_2$, and $[\text{Fe}(\text{C}_5\text{H}_4)_2\text{C}_3\text{H}_6]_2[\text{TCNE}]_2$ in a KBr pellet. The IR spectrum includes the spectrum of $[\text{TCNE}]^-$ as salt of $[\text{Fe}(\text{C}_5\text{Me}_5)_2]^+$, as well as the spectrum of the $[\text{Fe}(\text{C}_5\text{Me}_5)_2]^+$.

Furthermore, it has been predicted the appearance of a characteristic absorption peak at $\sim 1400 \text{ cm}^{-1}$ in the IR spectra for the π -[TCNE] $_2^{2-}$ dimer, that is not observed for $[\text{TCNE}]^-$. This new 1400 cm^{-1} absorption is due to the antisymmetric combination of the intrafragment CC stretches of each fragment central CC bond, which becomes allowed and wins intensity due to the electron-vibrational coupling, as the center of symmetry moves from the center of the CC bond in isolated $[\text{TCNE}]^-$ to the center of the $[\text{TCNE}]_2^{2-}$ dimer⁸³. This absorption occurs at $1364 \pm 3 \text{ (s)} \text{ cm}^{-1}$ for the eleven $[\text{TCNE}]_2^{2-}$ dimers from Table 7.2, whose IR spectra are available. In summary, the $\nu_{\text{C=C}}$ absorption, calculated to appear at $\sim 1400 \text{ cm}^{-1}$, is observed at $1364 \pm 3 \text{ cm}^{-1}$ for the L_c class of π -[TCNE] $_2^{2-}$ dimers. This $\nu_{\text{C=C}}$ absorption appears at 1558 cm^{-1} for the TCNE and at 1421 cm^{-1} for the $[\text{TCNE}]^-$, but is only active in Raman spectroscopy. With the change in the location of the center of symmetry in the dimer, it becomes active in IR and appears at $\sim 1364 \text{ cm}^{-1}$ for the L_c arrangement of π -[TCNE] $_2^{2-}$ dimers, further reflecting a reduced central CC bond order and a weaker central CC bond. This trend is further observed for the S_t and L_t arrangements of $[\text{TCNE}]_2^{2-}$ dimers, where the central CC bond absorption is assigned to a band at $1209 \pm 9 \text{ (w)} \text{ cm}^{-1}$ and $1385 \text{ (vs)} \pm 1 \text{ cm}^{-1}$, respectively.

In addition, the bending absorption $\delta_{\text{C-CN}}$, which is observed at $521 \pm 1 \text{ (m)} \text{ cm}^{-1}$ for the TCNE and $[\text{TCNE}]^-$ is split into three weak absorption peaks for S_t , L_c and L_t classes of the $[\text{TCNE}]_2^{2-}$ dimers, appearing at $549 \pm 2 \text{ (w)}$, $530 \pm 4 \text{ (w)}$ and $516 \pm 3 \text{ (w)} \text{ cm}^{-1}$ for L_c ; $557 \pm 1 \text{ (w)}$, $535 \pm 5 \text{ (w)}$ and $508 \pm 3 \text{ (w)}$ for S_t ; and $586 \pm 3 \text{ (w)}$, $535 \pm 1 \text{ (w)}$, and $520 \pm 1 \text{ (w)}$ for L_t .

Therefore the L_c class of π -[TCNE] $_2^{2-}$ dimers can be experimentally identified by (i) an additional strong $\nu_{\text{C=N}}$ absorbance, (ii) the shift of three $\nu_{\text{C=N}}$ absorptions towards higher frequencies, (iii) new absorption at 1364 cm^{-1} , and (iv) splitting of the 521 cm^{-1} $\delta_{\text{C-CN}}$ absorption in three weaker bands at 549 , 530 , and 516 cm^{-1} . In the S_t dimers, the calculated frequency for this $\nu_{\text{C=C}}$ absorption decreases to 1200 cm^{-1} and its intensity decreases by a factor of five compared to those found in the L conformers. In addition, the $\nu_{\text{C=N}}$ vibration for $[\text{TCNE}]_2^{2-}$ dimers in S_t occurs at 2215 (m) , 2157 (s) , and $2107 \text{ (w)} \text{ cm}^{-1}$, which differs from either the L_c and L_t classes of π -[TCNE] $_2^{2-}$ dimers.

7.5.3 Magnetic properties of the $[\text{TCNE}]_2^{2-}$ dimers

When the $[\text{TCNE}]^-$ fragments, which are doublet ($S = \frac{1}{2}$) states, approach to form the π -[TCNE] $_2^{2-}$ dimers, the $\Delta(r)$ value and the singlet-triplet (S-T) energy gap increases. UB3LYP/6-31+g calculations show (Figure 7.8) that the unpaired electron of each $[\text{TCNE}]^-$ fragment couples antiferromagnetically to give a singlet state, which is the ground state at all distances. However, this state changes its character from being mainly *open-shell* singlet, S_1 , at long distances to be *closed-shell* singlet, S_0 , at short distances. UB3LYP/6-31+g results indicate that the triplet is always higher in energy with respect to both singlet states. The S-T energy gap is 5.19 and 0.80 kcal/mol at the optimized L_t and L_c geometries, respectively (Table 7.10). However, for the S_t conformer the triplet state is 70.9 kcal/mol above the *closed-shell* singlet state. It has not been possible to calculate an optimized geometry for the

open-shell singlet for the S_t system with a SCF method, since it always leads to a *closed-shell* solution. These results have been confirmed by MCSCF (6,4) calculations.

The singlet ground state predicted is experimentally demonstrated by values of magnetic susceptibility temperature dependent in the 2 to 350 K range for [Et₄N]₂[TCNE]₂⁴⁶, [n-Pr₄N]₂[TCNE]₂⁵⁰ and [(Me₂N)₂CC(NMe₂)₂]₂[TCNE], [TDAE][TCNE]₂⁴⁴. EPR studies, more sensitive at 380 K, do not show any evidence of population of the triplet state for [Et₄N]₂[TCNE]₂. Therefore, it can be said that these systems only show a *diamagnetic* behavior. This is consistent with the fact that the ground state is a singlet and it is the only populated state at room temperature.

Table 7.10 Summary of the structural and spectroscopic properties of the S_t , L_c and L_t arrangements of [TCNE] $_2^{2-}$ dimers.

	TCNE ⁰	[TCNE] ⁻	S_t	L_c	L_t
Structurally characterized	1	many	2	13	2
Dihedral angle, avg d, [°]	-	-	179.94±0.02	1.65±4.1	179.87±0.06
Intermolecular CC, avg, r, [Å]	-	-	1.61±0.01	2.90±0.05 ^[a]	3.50±0.04 ^[b]
Intermolecular separation, avg, [Å]	-	-	-	2.90±0.05 ^[a]	3.47±0.04 ^[b]
Central CC bond, avg, [Å]	1.357 ³¹	1.39 ³²	1.61±0.01	1.405±0.03 ^[f]	1.399±0.002
NC-C-CN angle, avg, [°]^[c]	116.2 ³¹	117.7 ³²	118.5 ^{[d], 32}	118.4	118.6
CN displacement, avg, [°]	0	0	-	5.0±1.3	-1.9±0.9 ^[g]
Central C hybridization	sp ²	sp ²	sp ³	sp ^{2.17}	sp ^{2.06}
$\nu_{C=N}$ (IR), [cm⁻¹]	2262±1 (m) 2229±1 (w) 2215±1 (vw)	2183±1 (m) 2144±1 (m)	2215±4 (m) 2157±3 (s) 2107±4 (w)	2191±2 (m) 2173±3 (s) 2162±3 (s)	2216±2 (m) 2197±3 (s) 2180±4 (m)
ν_{C-C} (IR), [cm⁻¹]¹	1568±2 ^[e]	1421±1 ^[e]	1209±9 (w) ¹	1364±3 (s)	1385±1 (vs)
δ_{C-CN} (IR), [cm⁻¹]	522±1 (m)	521±1 (m)	557±1 (w) 535±5 (w) 508±3 (w)	549±2 (w) 530±4 (w) 516±5 (w)	586±3 (w) 535±1 (w) 520±1 (w)
¹A_{1g} → ¹B_{1u}, Δ, avg, [cm⁻¹]	-	-	-	16825±1180	
Spin multiplicity	Singlet	Doublet	Singlet	Singlet	Singlet

^[a] Eclipsed. ^[b] Noneclipsed. ^[c] Not metal bonded. ^[d] Terminal nitriles are metal bonded. ^[e] Raman active (IR forbidden). ^[f] Excludes μ_{16} -[TCNE] $_2^{2-}$ dimers. ^[g] Negative value indicates bending toward the center of the dimer.

7.6 Conclusions

Experimentally three classes of [TCNE] $_2^{2-}$ dimers have been observed (see S_t , L_c and L_t , in Figure 7.2b and Table 7.2), which are characterized by the inter-monomers separation, r , and its dihedral angle, d , (Figure 7.2a). All three arrangements have a singlet ground state, but differ due to structural and spectroscopic features (Table 7.10). Compared to the

[TCNE] $^-$ fragment, the L_c π -[TCNE] $_2^{2-}$ dimers can be identified experimentally by (i) a strong additional absorption signal $\nu_{C=N}$, (ii) the existence of three $\nu_{C=N}$ absorption signals at higher frequency values, observed at 2191 ± 2 (m), 2173 ± 3 (s), and 2162 ± 3 (s) cm^{-1} , (iii) new absorption signals at 1364 cm^{-1} assigned to $\nu_{C=C}$, and (iv) the absorption signal δ_{C-CN} is splitted into three peaks at 586 ± 3 (w), 535 ± 1 (w), and 520 ± 1 (w). In addition, in solid state, L_c class of π -[TCNE] $_2^{2-}$ dimers show a new UV-Vis signal at $16825 \pm 1180 \text{ cm}^{-1}$ (594 nm; 2.09 eV) assigned to the transition $^1A_{1g} \rightarrow ^1B_{1u}$. This band appears at 18940 cm^{-1} (528 nm; 2.35 eV) in MeTHF at 77 K for $\{[\text{Et}_4\text{N}]^+\}_2[\text{TCNE}]_2^{2-}$.

The physical properties observed for the L_c class of π -[TCNE] $_2^{2-}$ dimers are consistent with the expected for the formation of a covalent CC bond between the two monomers [TCNE] $^-$. However, due to the repulsive electrostatic interactions, the [TCNE] $^- \cdots [\text{TCNE}]^-$ interaction is energetically unstable in the absence of the neutralizing charge from cations. Therefore, the neutral (cation) $_2$ [TCNE] $_2$ system is energetically stable due to attractive electrostatic cation $^+ \cdots [\text{TCNE}]^-$ interactions that overcome the repulsive electrostatic [TCNE] $^- \cdots [\text{TCNE}]^-$ interactions. This stabilization through the cations facilitates the SOMO orbitals of both [TCNE] $^-$ monomers to overlap via four carbon atoms and, therefore, it is responsible for the existence of a through-cation CC covalent $\pi^*-\pi^*$ bond in the (cation) $_2$ [TCNE] $_2$ aggregates. It should be noted that the formation of cation-mediated π -[TCNE] $_2^{2-}$ dimers does not always happen (e.g. $[(n\text{Bu}_4\text{N})][\text{TCNE}]$ possesses isolated [TCNE] $^-$ radical ions³³). This stabilization has also been predicted to be possible in polar solvents. This two electrons - four centers (2e-/4c) bond arises from the overlap of the [TCNE] $^-$ orbitals, and it is not hypervalent. Therefore, it cannot exist when the HOMO is doubly occupied. It should be noted that, in addition to the short π -CC bonding interactions, longer [TCNE] $^- \cdots [\text{TCNE}]^-$ interactions are frequently present, but at longer distances (> 3.5). At these long distances, the bonding properties disappear, due to the exponential decrease of orbital overlap responsible for Δ . Consequently, the CC bond $\pi^*-\pi^*$ through-cation meets the Pauling definition of a chemical bond; "...there is a chemical bond between two atoms or groups of atoms in the case that the forces acting between them are such as to lead to an aggregate with sufficient stability to make it convenient for the chemist to consider it as an independent molecular species,"⁵⁹ Therefore, it exhibits all physical properties expected for a classic CC covalent bond. As a consequence, this bond is unique since it is a bond involving 2e $^-$ that takes place among four atoms carbon chemically equivalent, and involves the π^* orbitals of each fragment.

7.7 Computational and experimental details

Ab initio UB3LYP/6-31+G(2d,2p) computations were carried out using the non-local B3LYP exchange and correlation DFT functional^{84,85} and the 6-31+G(2d,2p) basis set^{86,87}, using a determinant in which the orbitals are not restricted to be doubly occupied. All the computations were done using the Gaussian-98 suite of programs⁸⁸. The critical point analysis was done using the AIMPAC package⁸⁹.

All calculations taking into account the solvent were performed at M06L⁹⁰/6-31+G(d) level with Grimme⁹¹ correction and the continuum solvation method (PCM)⁹².

All experimental data and interpretation were provided by Prof. J.S. Miller's group. The materials were prepared by routes previously described in a Vacuum Atmospheres Dri-Box

under nitrogen. Infrared spectra were recorded for KBr pellets on a Bio-Rad FTS-40 FTIR spectrophotometer with $\pm 1 \text{ cm}^{-1}$ resolution. Solid state UV-visible spectra were recorded on a Hewlett-Packard 8452A Diode Array Spectrophotometer, also as KBr pellets. A home-built cryostat based upon two 1 in dia quartz windows separated by a ~ 1 mm-thick O-ring/Teflon spacer sample compartment was loaded in a Dri-Box and cooled to 77 K with liquid nitrogen was used for the UV-Vis studies in solution. For these studies [Et₄N]₂[TCNE]₂ was dissolved in dry MeTHF freshly distilled from sodium/benzophenone. Magnetic susceptibility data were obtained on a Quantum Design MPMS 5T magnetometer as previously described⁹³. The EPR spectra were recorded on an IBM/Bruker ER 200 D-SRC spectrometer.

Bibliography

- (1) Del Sesto, R. E.; Miller, J. S.; Lafuente, P.; Novoa, J. J. *Chem. – Eur. J.* **2002**, *8* (21), 4894–4908.
- (2) McConnell, H. M. In *Proc. Robert A. Welch Found. Conf. Chem. Res*; 1967; Vol. 11, pp 144–150.
- (3) Candela, G. A.; Swartzendruber, L. J.; Miller, J. S.; Rice, M. J. *J. Am. Chem. Soc.* **1979**, *101* (10), 2755–2756.
- (4) Miller, J. S.; Zhang, J. H.; Reiff, W. M.; Dixon, D. A.; Preston, L. D.; Reis, A. H.; Gebert, E.; Extine, M.; Troup, J.; et al., . *J. Phys. Chem.* **1987**, *91* (16), 4344–4360.
- (5) Manriquez, J. M.; Yee, G. T.; Mclean, R. S.; Epstein, A. J.; Miller, J. S. *Science* **1991**, *252* (5011), 1415–1417.
- (6) Miller, J. S.; Epstein, A. J. *Mol. Cryst. Liq. Cryst. Sci. Technol. Sect. Mol. Cryst. Liq. Cryst.* **1993**, *233* (1), 133–152.
- (7) Ovcharenko, V. I.; Sagdeev, R. Z. *Russ. Chem. Rev.* **1999**, *68* (5), 345–363.
- (8) Miller, J. S.; Epstein, A. J. *Chem. Commun.* **1998**, No. 13, 1319–1325.
- (9) Plass, W. *Chem. Unserer Zeit* **1998**, *32* (6), 323–333.
- (10) Miller, J. S.; Epstein, A. J. *Angew. Chem. Int. Ed. Engl.* **1994**, *33* (4), 385–415.
- (11) Kinoshita, M. *Jpn. J. Appl. Phys.* **1994**, *33* (Part 1, No. 10), 5718–5733.
- (12) Caneschi, A.; Gatteschi, D. In *Progress in Inorganic Chemistry*; 1991; Vol. 37, p 331.
- (13) Buchachenko, A. L. *Russ. Chem. Rev.* **1990**, *59* (4), 307–319.
- (14) Gatteschi, D. *Adv. Mater.* **1994**, *6* (9), 635–645.
- (15) Kahn, O. *Molecular Magnetism*, 1 edition.; Wiley-VCH: New York, 1993.
- (16) Reynolds, J. R.; Skotheim, T. A.; Elsenbaumer, R. L. *Handbook of conducting polymers*; Marcel Dekker, 1998.
- (17) Nalwa, H. S. *Handbook of Organic Conductive Molecules and Polymers*; Wiley, 1997; Vol. 4 Volume Set.
- (18) Graja, A. *Low-Dimensional Organic Conductors*; World Scientific, 1992.
- (19) Ferraro, J. R.; Williams, J. M. *Introduction to synthetic electrical conductors*; Academic Press, 1987.
- (20) Hünig, S. *J. Mater. Chem.* **1995**, *5* (10), 1469–1479.
- (21) Williams, J. M. *Organic Superconductors (including Fullerenes): Synthesis, Structure, Properties, and Theory*; Prentice Hall, 1992.
- (22) Ishiguro, T.; Yamaji, K.; Saito, G. *Organic Superconductors*; Springer Science & Business Media, 1998.
- (23) Miller, J. S.; Epstein, A. J. *Chem. Eng. News* **1995**, *73* (40).
- (24) Vazquez, C.; Calabrese, J. C.; Dixon, D. A.; Miller, J. S. *J. Org. Chem.* **1993**, *58* (1), 65–81.
- (25) Miller, J. S.; Dixon, D. A. *Science* **1987**, *235* (4791), 871–873.
- (26) Phillips, W. D.; Rowell, J. C.; Weissman, S. I. *J. Chem. Phys.* **1960**, *33* (2), 626–627.
- (27) Chang, R. *J. Phys. Chem.* **1970**, *74* (9), 2029–2030.
- (28) Chesnut, D. B.; Phillips, W. D. *J. Chem. Phys.* **1961**, *35* (3), 1002–1012.
- (29) Itoh, M. *Bull. Chem. Soc. Jpn.* **1972**, *45* (7), 1947–1950.
- (30) Lemervovskii, D. A.; Stukan, R. A.; Tarasevich, B. N.; Slovokhotov, T. L.; Antipin, M. Y.; Kalinin, A. E.; Struchov, Y. T. *Struct. Khim* **1981**, *7*, 240–249.
- (31) Miller, J. S.; Calabrese, J. C.; Rommelmann, H.; Chittipeddi, S. R.; Zhang, J. H.; Reiff, W. M.; Epstein, A. J. *J. Am. Chem. Soc.* **1987**, *109* (3), 769–781.

- (32) Miller, J. S.; Glatzhofer, D. T.; O'Hare, D. M.; Reiff, W. M.; Chakraborty, A.; Epstein, A. J. *Inorg. Chem.* **1989**, *28* (15), 2930–2939.
- (33) Zheludev, A.; Grand, A.; Ressouche, E.; Schweizer, J.; Morin, B. G.; Epstein, A. J.; Dixon, D. A.; Miller, J. S. *J. Am. Chem. Soc.* **1994**, *116* (16), 7243–7249.
- (34) Baukova, T. V.; Ellert, O. G.; Kuz'mina, L. G.; Dvortsova, N. V.; Lemenovskii, D. A.; Rubezhov, A. Z. *Mendeleev Commun.* **1991**, *1* (1), 22–24.
- (35) Flandrois, S.; Ludolf, K.; Keller, H. J.; Nöthe, D.; Bondeson, S. R.; Soos, Z. G.; Wehe, D. *Mol. Cryst. Liq. Cryst.* **1983**, *95* (1–2), 149–164.
- (36) Miller, J. S.; Dixon, D. A.; Calabrese, J. C.; Vazquez, C.; Krusic, P. J.; Ward, M. D.; Wasserman, E.; Harlow, R. L. *J. Am. Chem. Soc.* **1990**, *112* (1), 381–398.
- (37) Barlow, S.; Murphy, V. J.; Evans, J. S. O.; O'Hare, D. *Organometallics* **1995**, *14* (7), 3461–3474.
- (38) Zhang, J.; Sesto, R. E. D.; Gordon, D. C.; Miller, J. S.; Zhang, J.; Liable-Sands, L. M.; Rheingold, A. L.; Burkhart, B. M. *Chem. Commun.* **1998**, No. 13, 1385–1386.
- (39) Olmstead, M. M.; Speier, G.; Szabó, L. *J. Chem. Soc. Chem. Commun.* **1994**, No. 4, 541–543.
- (40) Miller, J. S.; O'Hare, D. M.; Chakraborty, A.; Epstein, A. J. *J. Am. Chem. Soc.* **1989**, *111* (20), 7853–7860.
- (41) Bock, H.; Ruppert, K.; Fenske, D.; Goesmann, H. *Z. Für Anorg. Allg. Chem.* **1991**, *595* (1), 275–284.
- (42) Miller, J. S.; Glatzhofer, D. T.; Vazquez, C.; McLean, R. S.; Calabrese, J. C.; Marshall, W. J.; Raebiger, J. W. *Inorg. Chem.* **2001**, *40* (9), 2058–2064.
- (43) Clemente, D. A.; Marzotto, A. *J. Mater. Chem.* **1996**, *6* (6), 941–946.
- (44) Johnson, M. T.; Campana, C. F.; Foxman, B. M.; Desmarais, W.; Vela, M. J.; Miller, J. S. *Chem. – Eur. J.* **2000**, *6* (10), 1805–1810.
- (45) Fox, J. R.; Foxman, B. M.; Guarrera, D.; Miller, J. S.; Calabrese, J. C.; Reis, A. H. *J. Mater. Chem.* **1996**, *6* (10), 1627–1631.
- (46) Sesto, R. E. D.; Sommer, R. D.; Miller, J. S. *CrystEngComm* **2001**, *3* (47), 222–224.
- (47) Bock, H.; Näther, C.; Ruppert, K. *Z. Für Anorg. Allg. Chem.* **1992**, *614* (8), 109–114.
- (48) Miller, J. S.; Dixon, D. A.; Calabrese, J. C.; Vazquez, C.; Krusic, P. J.; Ward, M. D.; Wasserman, E.; Harlow, R. L. *J. Am. Chem. Soc.* **1990**, *112* (1), 381–398.
- (49) Bock, H.; Ruppert, K. *Inorg. Chem.* **1992**, *31* (24), 5094–5099.
- (50) Del Sesto, R. E.; Botoshansky, M.; Kaftoryb, M.; Miller, J. S. *CrystEngComm* **2002**, *4* (19), 106–108.
- (51) Novoa, J. J.; Lafuente, P.; Del Sesto, R. E.; Miller, J. S. *Angew. Chem. Int. Ed.* **2001**, *40* (13), 2540–2545.
- (52) Kaupp, G.; Boy, J. *Angew. Chem. Int. Ed. Engl.* **1997**, *36* (1–2), 48–49.
- (53) Toda, F. *Eur. J. Org. Chem.* **2000**, *2000* (8), 1377–1386.
- (54) Mikami, S.; Sugiura, K. I.; Miller, J. S.; Sakata, Y. *Chem. Lett.* **1999**, No. 5.
- (55) Zhao, H.; Heintz, R. A.; Dunbar, K. R.; Rogers, R. D. *J. Am. Chem. Soc.* **1996**, *118* (50), 12844–12845.
- (56) Harms, R. H.; Keller, H. J.; Nöthe, D.; Werner, M.; Gundel, D.; Sixl, H.; Soos, Z. G.; Metzger, R. M. *Mol. Cryst. Liq. Cryst.* **1981**, *65* (3–4), 179–196.
- (57) Hoffmann, S. K.; Corvan, P. J.; Singh, P.; Sethulekshmi, C. N.; Metzger, R. M.; Hatfield, W. E. *J. Am. Chem. Soc.* **1983**, *105* (14), 4608–4617.
- (58) Dong, V.; Endres, H.; Keller, H. J.; Moroni, W.; Nöthe, D. *Acta Crystallogr. B* **1977**, *33* (8), 2428–2431.

- (59) Pauling, L. *The Nature of the Chemical Bond and the Structure of Molecules and Crystals: An Introduction to Modern Structural Chemistry*; Cornell University Press, 1960.
- (60) Bader, R. F. W. *Atoms in Molecules, Clarendon*; Oxford, 1990.
- (61) Novoa, J. J.; Lafuente, P.; Mota, F. *Chem. Phys. Lett.* **1998**, *290* (4), 519–525.
- (62) Cioslowski, J.; Mixon, S. T. *J. Am. Chem. Soc.* **1992**, *114* (11), 4382–4387.
- (63) Hunter, C. A.; Sanders, J. K. *J. Am. Chem. Soc.* **1990**, *112* (14), 5525–5534.
- (64) Braga, D.; Grepioni, F.; Novoa, J. J. *Chem. Commun.* **1998**, No. 18, 1959–1960.
- (65) Novoa, J. J.; Nobeli, I.; Grepioni, F.; Braga, D. *New J. Chem.* **2000**, *24* (1), 5–8.
- (66) Howard, J. A. K.; Allen, F. H.; Shields, G. P. *Implications of Molecular and Materials Structure for New Technologies*; Kluwer, Amsterdam, 1999.
- (67) Braga, D.; D’Oria, E.; Grepioni, F.; Mota, F.; Novoa, J. J.; Rovira, C. *Chem. – Eur. J.* **2002**, *8* (5), 1173–1180.
- (68) Braga, D.; Maini, L.; Grepioni, F.; Mota, F.; Rovira, C.; Novoa, J. J. *Chem. Eur. J.* **2000**, *6* (24), 4536–4551.
- (69) Szabo, A.; Ostlund, N. S. *McGraw-Hill N. Y.* **1989**.
- (70) Lacour, J.; Moraleta, D. *Chem. Commun.* **2009**, No. 46, 7073–7089.
- (71) da Silva, E. F.; Svendsen, H. F.; Merz, K. M. *J. Phys. Chem. A* **2009**, *113* (22), 6404–6409.
- (72) Capdevila-Cortada, M.; Ribas-Arino, J.; Novoa, J. J. *J. Chem. Theory Comput.* **2014**, *10* (2), 650–658.
- (73) Becker, P.; Coppens, P.; Ross, F. K. *J. Am. Chem. Soc.* **1973**, *95* (23), 7604–7609.
- (74) Little, R. G.; Pautler, D.; Coppens, P. *Acta Crystallogr. B* **1971**, *27* (8), 1493–1499.
- (75) Drück, U.; Guth, H. Z. *Für Krist. - Cryst. Mater.* **1982**, *161* (1–4), 103–110.
- (76) Dixon, D. A.; Miller, J. S. *J. Am. Chem. Soc.* **1987**, *109* (12), 3656–3664.
- (77) Harcourt, R. D. *J. Phys. Chem.* **1991**, *95* (18), 6916–6918.
- (78) McKee, M. L.; Buehl, M.; Charkin, O. P.; Schleyer, P. v. R. *Inorg. Chem.* **1993**, *32* (21), 4549–4554.
- (79) Bremer, M.; von Ragué Schleyer, P.; Schötz, K.; Kausch, M.; Schindler, M. *Angew. Chem. Int. Ed. Engl.* **1987**, *26* (8), 761–763.
- (80) Prakash, G. K.; Krishnamurthy, V. V.; Herges, R.; Bau, R.; Yuan, H.; Olah, G. A.; Fessner, W. D.; Prinzbach, H. *J. Am. Chem. Soc.* **1986**, *108* (4), 836–838.
- (81) Novoa, J. J.; Whangbo, M.-H.; Williams, J. M. *J. Chem. Phys.* **1991**, *94* (7), 4835–4841.
- (82) Hobza, P.; Zahradnik, R. *Intermolecular complexes*; Elsevier, Amsterdam, 1988.
- (83) Rice, M. J.; Lipari, N. O.; Strässler, S. *Phys. Rev. Lett.* **1977**, *39* (21), 1359–1362.
- (84) Becke, A. D. *J. Chem. Phys.* **1993**, *98* (7), 5648–5652.
- (85) Lee, C.; Yang, W.; Parr, R. G. *Phys. Rev. B* **1988**, *37* (2), 785–789.
- (86) Ditchfield, R.; Hehre, W. J.; Pople, J. A. *J. Chem. Phys.* **1971**, *54* (2), 724–728.
- (87) Clark, T.; Chandrasekhar, J.; Spitznagel, G. W.; Schleyer, P. V. R. *J. Comput. Chem.* **1983**, *4* (3), 294–301.
- (88) Chen, W.; Wong, M. W.; Andres, J. L.; Head-Gordon, M.; Replogle, E. S.; Pople, J. A. *Inc Pittsburgh PA* **1998**.
- (89) Biegler-könig, F. W.; Bader, R. F. W.; Tang, T.-H. *J. Comput. Chem.* **1982**, *3* (3), 317–328.
- (90) Zhao, Y.; Truhlar, D. G. *J. Chem. Phys.* **2006**, *125* (19), 194101.
- (91) Grimme, S. *J. Comput. Chem.* **2006**, *27* (15), 1787–1799.
- (92) Tomasi, J.; Mennucci, B.; Cammi, R. *Chem. Rev.* **2005**, *105* (8), 2999–3094.

- (93) Brandon, E. J.; Rittenberg, D. K.; Arif, A. M.; Miller, J. S. *Inorg. Chem.* **1998**, 37 (13), 3376–3384.

CHAPTER 8

CONCLUSIONS

8 Conclusions

During the development of this thesis, we have discussed the basic premises needed for the design of organic-based molecular magnets. These materials are constituted by (1) organic molecules that have free electrons and permanent magnetic moment, which (2) interact ferromagnetically (3) along the three dimensions of the crystal.

One of the challenges in the design of organic-based molecular magnets is that the organic radicals that are the constitutive units must have permanent magnetic moment. Generally, organic radicals tend to interact forming bonds and canceling the spin moment. We have studied at CASVB, MMVB and *J*-code levels the energy gap between singlet and triplet spin states in several alternant (π -delocalized radicals) and non-alternant (π -localized radicals) biradical hydrocarbons, as well as σ,σ biradicals (like the σ,σ -didehydronaphthalene isomers). As a result of our studies, we have observed that alternant hydrocarbons are more stable than the non-alternant ones. Therefore, in the design of permanent molecular magnets, alternant hydrocarbons would be preferable. Additionally, we have been able to describe the spin preference of the different species based on the different spin interaction contributions: through-bond (TB) and through-space (TS). It has been observed that TB contacts usually involve atoms that are bonded and close, while TS interactions take place between radical centers that are located at long distances. Since the electron-electron interactions are highly dependent on distance, the energy gap between two spin states has been found usually higher when the stabilization of the spin centers occurs by means of TB interactions. Accordingly, if both TB and TS contacts are present in a radical, the TS contribution will define the energy gap between the two lower spin states and their spin distribution.

We have also evaluated the possibility of increasing the spin moment of the molecules following two approaches: (1) the polymerization and (2) the heterogeneous synthesis of spin units (SUs) coupled through coupling units (CUs). In both approaches the constitutive units are stable high-spin biradicals. The polymerization of the high-spin radicals leads to high-spin systems. However, the gap of energy between the first and second spin states decreases with the number of units bonded. Future studies on this field should be addressed to describe the different spin states to further assess the viability of this approach. The study could also be extended to evaluate real macromolecules that result from polymerization of high-spin radicals. On the other hand, we have proved that, when the synthesis of macro-radicals follows the SU-CU-SU methodology, the SU and CU units can be considered as independent units that keep their multiplicity once coupled. The analysis of the spin states of the macromolecule can be performed based on the independent spin states of the constitutive units. Consequently, this approach is valid for the synthesis of macro-radicals. In addition, we have shown that the difference between the high and low spin states is determined by the SU or CU unit with lower energy gap. Therefore, in the design of high-spin macromolecules following this methodology, we can evaluate the energy gap between the spin states of the system looking at the energy gap of the spin states of the constitutive units.

Once the constitutive units are identified, we need to understand the ferromagnetic intermolecular interactions. To this aim the McConnell-I model for through-space magnetic

interactions of two radicals has been revised. This approach proposes that ferromagnetic (FM) interactions are preferred when the main intermolecular contacts are between atoms with opposite spin-densities. Contrarily, if the interacting atoms have the same spin density, the electrons will interact antiferromagnetically (AFM). We have thus explored the magneto-structural relationship in pairs of well-known radicals at different orientations. The dimers we studied were two H_2NO , methyl...allyl and two allyl radicals. The geometry arrangements of these radicals were chosen because they represented actual magnetic contacts in crystals like α -nitronyl nitroxide (α -NN) and other organic-based magnets. It has been demonstrated that the orientation of the radicals is crucial to determine the spin multiplicity of the states. In the studied radicals, the free electrons are located mainly in the p_z orbitals perpendicular to the plane of the molecule. We can conclude that, when the interacting spin-containing radical centers are placed in parallel planes and overlap, the McConnell-I model predicts correctly the spin preference of the ground states. However, whenever there are many interactions involved (i.e. if the spin-containing centers are not placed one on top to the other or they are not located in parallel planes), the prediction of the spin preference becomes very complex, and more detailed quantum calculations are required. It was also observed that, when the through-space interaction involved two perpendicular p_z orbitals, the contribution of this interaction was FM, following a Hund-like mechanism. Overall, we have demonstrated that the McConnell-I model must be used carefully when predicting the multiplicity of the through-space interaction between two radicals.

By means of an Atoms-In-Molecules (AIM) analysis, we have proved that the existence of the bond critical point (BCP) is a necessary, but not a sufficient condition for the identification of attractive intermolecular interactions. We studied the BCP properties of intermolecular hydrogen bonds between molecules with different dipole moment ($\text{H}_2\text{O}\cdots\text{HF}$, $\text{H}_2\text{O}\cdots\text{HCH}_3$, $\text{H}_2\text{O}\cdots\text{HCF}_3$). We can conclude that the Laplacian and electron density in the BCP are larger when the electronegativity of the atoms bound to the hydrogen is higher, denoting a stronger hydrogen bond. Additionally, we investigated how the properties of intermolecular BCPs change depending on whether the BCP relates to either attractive hydrogen bonds or intermolecular repulsive interactions. With this purpose the angular displacement of two water molecules ($\text{H}_2\text{O}\cdots\text{H}_2\text{O}$) was studied. We observed that the electron density and the Laplacian decrease when the intermolecular interaction changes from connecting hydrogen and oxygen (hydrogen bond) to two oxygens. However, a BCP was still observed (with small electron density and Laplacian values) even in the latter case. Further calculations of the interaction between two oxygen atoms in several systems with different properties revealed that intermolecular BCPs could appear even if the interaction energy of the system was positive. We studied the dipole moment and polarizability of the system and the electron density and Laplacian value of these BCPs. However, none of these properties was conclusive to discriminate if the BCP belonged to an attractive interaction. As a result, the AIM analysis should be always accompanied by an energy study of the interaction to recognize whether it describes an intermolecular attractive interaction or is the result of an overlap of spin densities.

Further analysis of the McConnell-I model were performed to evaluate whether it could be applied to assess the magnetic character of real crystals. With this purpose, the subset of experimentally FM crystals within the α -nitronyl nitroxide (α -NN) family was studied. The spin density in these crystals is mainly located on the O, N and C atoms of the α -NN ring

(ONCNO group). For that reason, the closest contacts between two intermolecular ONCNO groups for each chosen crystal were selected. Previous statistical analysis performed with FM and AFM α -NN crystals did not show any clear relationship between the macroscopic magnetic property and the geometrical distribution of the ONCNO groups. The reason is twofold. We first concluded that the ONCNO interactions do not describe entirely the observed macroscopic magnetic property for all the systems. Consequently, we believe that other through-space interactions not considered in the simplistic ONCNO model must play an important role defining the magnetic character. Secondly, it was proved there is not a simple magneto-structural relationship such as the one suggested in McConnell-I model that can be applied to all through-space interactions in the crystals. This conclusion was reached after a twofold statistical analysis (namely, factor and cluster analyses) of the geometrical parameters as a function of the calculated energy gap ΔE^{S-T} .

One of the most successful examples of molecular magnets is charge-transfer salts. These systems have a $[\cdots[D]^+[A]^-][D]^+[A]^-][D]^+[A]^-]\cdots$ structure where D is the donor of electrons and A is the acceptor. However, the formation of $[D]_2^{2+}$ or $[A]_2^{2-}$ diamagnetic dimers in these compounds causes the loss of the magnetic properties. To evaluate the causes that give rise to this dimerization, we studied the formation of TCNE dimers, $[TCNE]_2^{2-}$, which is a prototypical example of an organic acceptor, using the interaction energy (E_{int}). The E_{int} of two charged molecules has two components: the Coulomb contribution (E_{coul}) that represents the repulsion/attraction between two charged molecules with the same/different sign, and the bonding energy (E_{bond}) which is a consequence of the attraction energy and possible bond formation between the two interacting molecules. As a result of these two contributions, metastable minima can be found in the potential energy surface of two approaching molecules. These minima are not stable if the repulsion energy is higher than the bonding energy in absolute value ($|E_{coul}| > |E_{bond}|$). However, if there is any force that counterbalances the repulsion between the two charged molecules (*e.g.* due to cation $\cdots[TCNE]^-$ interactions), the bonding energy could overcome the repulsion energy in absolute value ($|E_{coul}| < |E_{bond}|$), and the metastable minima would become stable ($E_{int} < 0$).

Experimentally three classes of dimers have been observed: the σ -dimer S_t and the two π -dimers L_c and L_t (where S/L stand for short/long distance and t/c for trans/cis configuration of the two molecules). UHF and UB3LYP calculations described three metastable minima that agree with those observed experimentally. Furthermore, extended calculations performed in the presence of cations or polar solvents resulted in the stabilization of the S_t , L_c and L_t dimers, which demonstrates that counterbalance of the repulsive energy is needed for the formation of these long multicenter bonds. As a consequence, this two electrons - four centers ($2e^-/4c$) bond is unique since it involves $2e^-$ and takes place among four carbon atoms chemically equivalent. This bond formation is possible through the overlap of the π^* SOMO orbitals of each fragment if these orbitals are close enough to interact. Besides, the spectroscopic features of each class of these three dimers have been calculated and are in agreement with the available experimental data.

This PhD thesis demonstrates that the Heisenberg effective spin Hamiltonian is a valid approach to estimate the energy difference between two spin states. This effective Hamiltonian is described as a function of the exchange interaction, J_{ij} , and exchange density matrix elements, P_{ij} . These two parameters have been proved to be a useful tool to explain the preference for the spin state of the radical molecules studied. Among computational

chemistry tools, the preferred method to study the systems of interest has been the interaction configuration CASSCF. However, this method is computationally very expensive and for large systems we have used DFT methods, such as B3LYP or M06L, with *broken-symmetry* whenever has been needed. Additionally, the Molecular Mechanics Valence bond (MMVB) method has also been successfully used to describe qualitatively the spin preference and the energy difference between two spin states for very large hydrocarbon systems with a pair number of electrons/orbitals.

CHAPTER 9

RESUMEN

9 Resumen

9.1 Objetivo

El objetivo de esta tesis doctoral ha consistido en estudiar las bases teóricas del magnetismo molecular para poder luego utilizar el conocimiento adquirido en el diseño de materiales magnéticos moleculares.

9.2 Introducción

Para poder entender las bases del magnetismo molecular debemos entender sus principios. Los imanes moleculares están compuestos por moléculas de alto espín (generalmente radicales), denominadas unidades contenedoras de espín, que interaccionan ferromagnéticamente entre ellas y cuya interacción se expande en varias direcciones del espacio para obtener un momento magnético total diferente de cero.

Existen diversos mecanismos que permiten explicar la estabilización de estados de alto espín en radicales orgánicos. En primer lugar, los mecanismos tipo Hund proponen que la interacción entre electrones libres situados en orbitales ortogonales es ferromagnética (Figura 9.1a). Por otro lado, también tendremos en cuenta los mecanismos a través del enlace, también denominado *through-bond*, TB (Figura 9.1b) y a través del espacio, también denominado *through-space*, TS (Figura 9.1c).

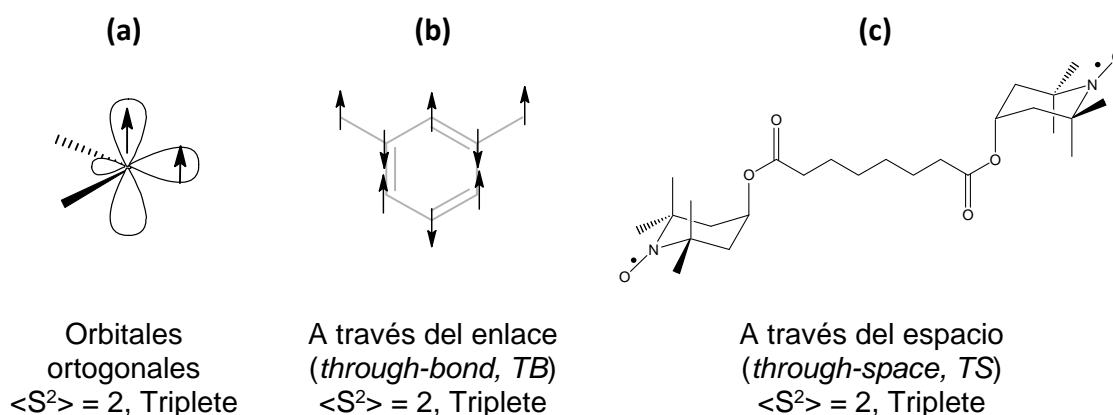


Figura 9.1 Representación de los mecanismos que estabilizan estados de alto espín: (a) mecanismos tipo Hund de orbitales ortogonales, (b) mecanismo a través del enlace (*through-bond*, TB) y (c) mecanismo a través del espacio (*through-space*, TS).

Una de las metodologías ampliamente utilizada para incrementar el momento de espín de un sistema consiste en la polimerización de las moléculas de alto espín. Existen dos estrategias de trabajo que se han aplicado con éxito para crear poliradicales de alto espín: (a) la síntesis por polimerización de radicales de alto espín (Figura 9.2a) y (b) la síntesis heterogénea en base a unidades contenedoras de spin (*spin containing unit*, SU) acopladas a través de otra unidad (*coupling unit*, CU) (Figura 9.2b), siendo ambas SU y CU radicales de alto espín.

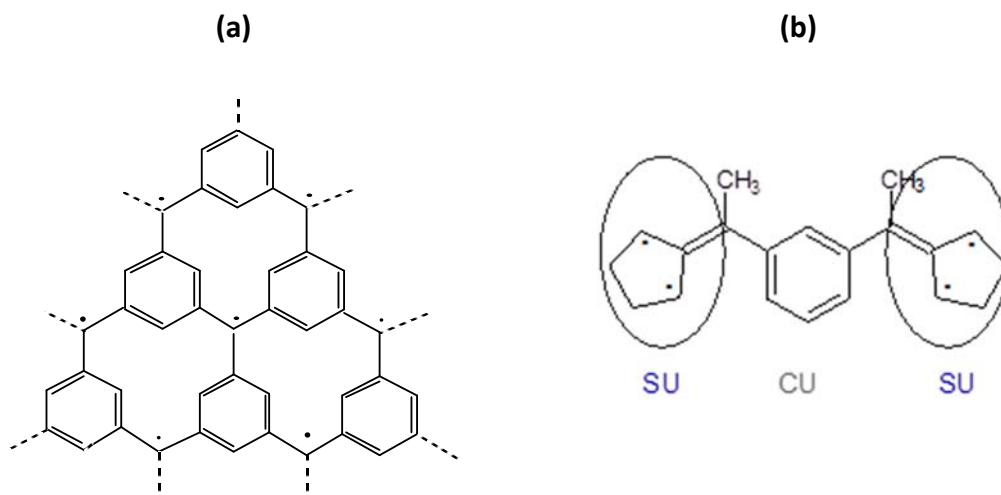


Figura 9.2 Representación de mecanismos de polimerización en la síntesis de oligómeros de alto spin (a) polimerización de moléculas de alto espín; (b) síntesis heterogénea de radicales de alto espín donde unidades contenedoras de spin (SU) están conectadas a través de una segunda unidad acopladora (CU).

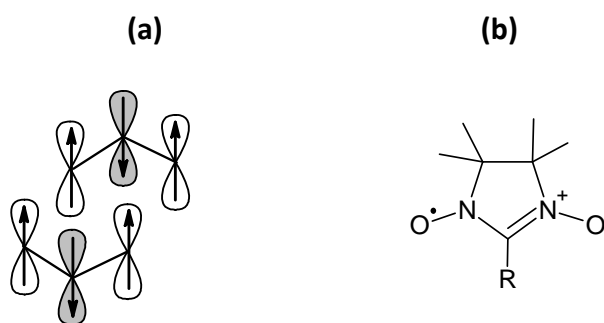


Figura 9.3 Representación de (a) interacción ferromagnética a través del espacio (TS) donde se observa que la interacción de centros de átomos con densidades de espín de signo opuesto da lugar a un sistema de alto spin. (b) Base molecular de los cristales moleculares de la familia de los α -nitronil nitróxidos.

Para estudiar las interacciones intermoleculares que favorecen la estabilización de estados de alto espín, McConnell propuso dos teorías. La denominada McConnell-I establece que la interacción será preferentemente ferromagnética FM (se estabilizará el estado de alto espín) cuando los átomos que interactúan tienen densidades de espín de signo opuesto (Figura 9.3a). La aplicabilidad de esta teoría para estudiar las interacciones intermoleculares de cristales moleculares magnéticos se ha discutido extensamente en cristales de la familia de los α -nitronil nitróxidos (Figura 9.3b).

La teoría denominada de McConnell-II se aplica a compuestos de sales de transferencia de carga, como el complejo $[\text{Fe}(\text{C}_5\text{Me}_5)_2]^+[\text{TCNE}]^-$ (TCNE = tetracianoetileno). En las sales de transferencia de carga una especie dadora [D] dona un electrón a una especie aceptora [A] creándose dos especies radicalarias cargadas $[\text{D}]^+$ y $[\text{A}]^-$ que interactúan formando un complejo con un momento de espín total diferente de cero (Figura 9.4).

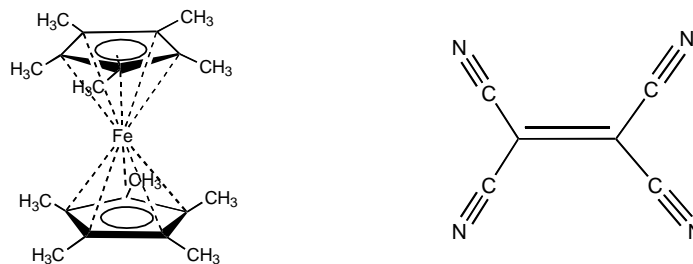


Figura 9.4 Unidades constituyentes de la sal de transferencia de carga $[\text{Fe}(\text{C}_5(\text{CH}_3)_5)_2]^+[\text{TCNE}]^-$ donde la especie dadora, D, es el ferroceno y la aceptora, A, es el tetracianoetileno, TCNE.

9.3 Métodos

En esta tesis doctoral se ha utilizado el Hamiltoniano de espín, tal y como se expresa en la ecuación (9.1), donde \hat{S}_i , \hat{S}_j son los operadores de espín asociados a los electrones i, j de la molécula, \hat{I}_{ij} es el operador identidad de espín, el parámetro Q representa la energía de Coulomb y J_{ij} es la integral de intercambio [ecuación (9.2)].

$$\hat{H}_S = Q - \sum_{i=1}^N \sum_{j>i}^N J_{ij} \left(2\hat{S}_i \cdot \hat{S}_j + \frac{1}{2} \hat{I}_{ij} \right) \quad (9.1)$$

$$J_{ij} = \int \psi_a^*(i) \psi_b^*(j) \hat{H} \psi_a(j) \psi_b(i) d\bar{x}_i d\bar{x}_j \quad (9.2)$$

El parámetro J_{ij} se correlaciona con el acoplamiento de espín de los electrones. En términos de la distribución electrónica de Heitler-London, el parámetro J_{ij} se puede expresar como:

$$J_{ij} = [ij|ji] + 2S_{ij} \langle i|\hat{h}|j \rangle \quad (9.3)$$

donde $[ij|ji]$ representa la integral de repulsión o de intercambio, de valor positivo y pequeño; S_{ij} es el solapamiento entre i y j , siempre positivo; y $\langle i|\hat{h}|j \rangle$ es la integral monoeléctrica, con signo negativo. Generalmente, la magnitud del parámetro J_{ij} está dominada por el término monoeléctrico y es negativa, pero cuando el solapamiento tiende a cero, adopta el valor del término $[ij|ji]$ de valor pequeño y positivo.

El Hamiltoniano de espín de la ecuación (9.1) se puede reescribir como (9.4), donde P_{ij} representan los elementos de la matriz de densidad de intercambio \mathbf{P} [ecuación (9.5)].

$$\langle \hat{H}_S \rangle = Q + \sum_{ij} J_{ij} P_{ij} \quad (9.4)$$

$$P_{ij} = \left\langle - \left(2\hat{S}_i \cdot \hat{S}_j + \frac{1}{2} \hat{I}_{ij} \right) \right\rangle \quad (9.5)$$

En el caso en el que la distribución atómica no cambie entre dos estados de espín, el término de Coulomb Q será equivalente y la diferencia de energía entre el estado de bajo (*low-spin*, LS) y el de alto espín (*high-spin*, HS) se expresa como:

$$\Delta E^{LS-HS} = \langle \hat{H}_S \rangle^{LS} - \langle \hat{H}_S \rangle^{HS} = \left(\sum_{ij} J_{ij} P_{ij} \right)^{LS} - \left(\sum_{ij} J_{ij} P_{ij} \right)^{HS} \quad (9.6)$$

El parámetro J_{ij} depende de la geometría del sistema. Si los dos estados de espín tienen geometrías similares, los valores del parámetro J_{ij} se pueden suponer equivalentes para ambos estados LS y HS. En dicho caso, la ecuación (9.6) se puede aproximar a la expresión de la ecuación (9.7).

$$\Delta E^{LS-HS} = \sum_{ij} J_{ij} \Delta P_{ij}^{LS-HS} \quad (9.7)$$

Los métodos de cálculo utilizados dependen del tipo de sistema estudiado. Se realizaron cálculos **MP2** cuando en la interacción a estudiar era importante incluir correlación dinámica. En cambio, en los sistemas de capa abierta en los que es imprescindible introducir correlación y, generalmente, necesitan ser descritos con más de una configuración se realizaron cálculos **CASSCF(m,n)**. En algunos casos, fue necesario introducir la correlación dinámica y más de una configuración, por lo que el estudio fue del tipo **CASMP2(m,n)**. Asimismo, el método híbrido **Molecular Mechanic Valence Bond** (MMVB) permitió la descripción de hidrocarburos planos con un gran número de electrones en el espacio activo. En aquellos casos en los que fue posible, los cálculos se realizaron con métodos DFT, como **UB3LYP** o **M06L**, por su sencillez y rapidez de cálculo.

9.4 Resultados

9.4.1 Estudio de la estabilización de estados de alto espín en biradicales

Como parte del trabajo de investigación, en esta tesis doctoral se analizó la estabilidad de estados de alto espín en diversos biradicales orgánicos (Tabla 9.1), usando métodos computacionales como CASVB, MMVB y un código desarrollado internamente por el grupo del Prof. M.A Robb, que denominamos **J-code**.

Nuestro estudio demostró que la diferencia de energía entre los estados de alto y bajo espín en hidrocarburos alternados (o π -deslocalizados) es mayor que en los hidrocarburos no alternados (o π -localizados) (Tabla 9.2).

Tabla 9.1 Representación de los sistemas (a) π -deslocalizados y (b) π -localizados

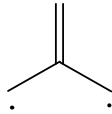
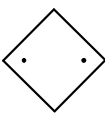
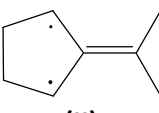
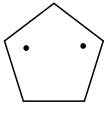
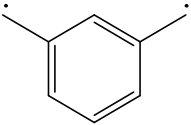
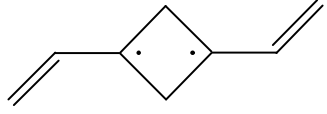
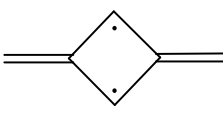
(a) Biradicales π -deslocalizados		(b) Biradicales π -localizados	
SISTEMAS	MULTIPLICIDAD	SISTEMAS	MULTIPLICIDAD
 (I)	Triplete	 (V)	Triplete
 (II)	Triplete	 (VI)	Triplete
 (III)	Triplete	 (VII)	Triplete
 (IV)	Triplete		

Tabla 9.2 Diferencia de energía entre los estados singulete y triplete para los sistemas π -deslocalizados (I, II, III y IV) y π -localizados (V, VI y VII). La diferencia de energía se ha calculado con MMVB y CAS(n,n)/6-31g(d) y se compara con los valores recogidos en la bibliografía. Para los sistemas V-VII no se reportan valores de MMVB porque este método no estima correctamente los valores de energía cuando existen valores de J_{ij} positivos.

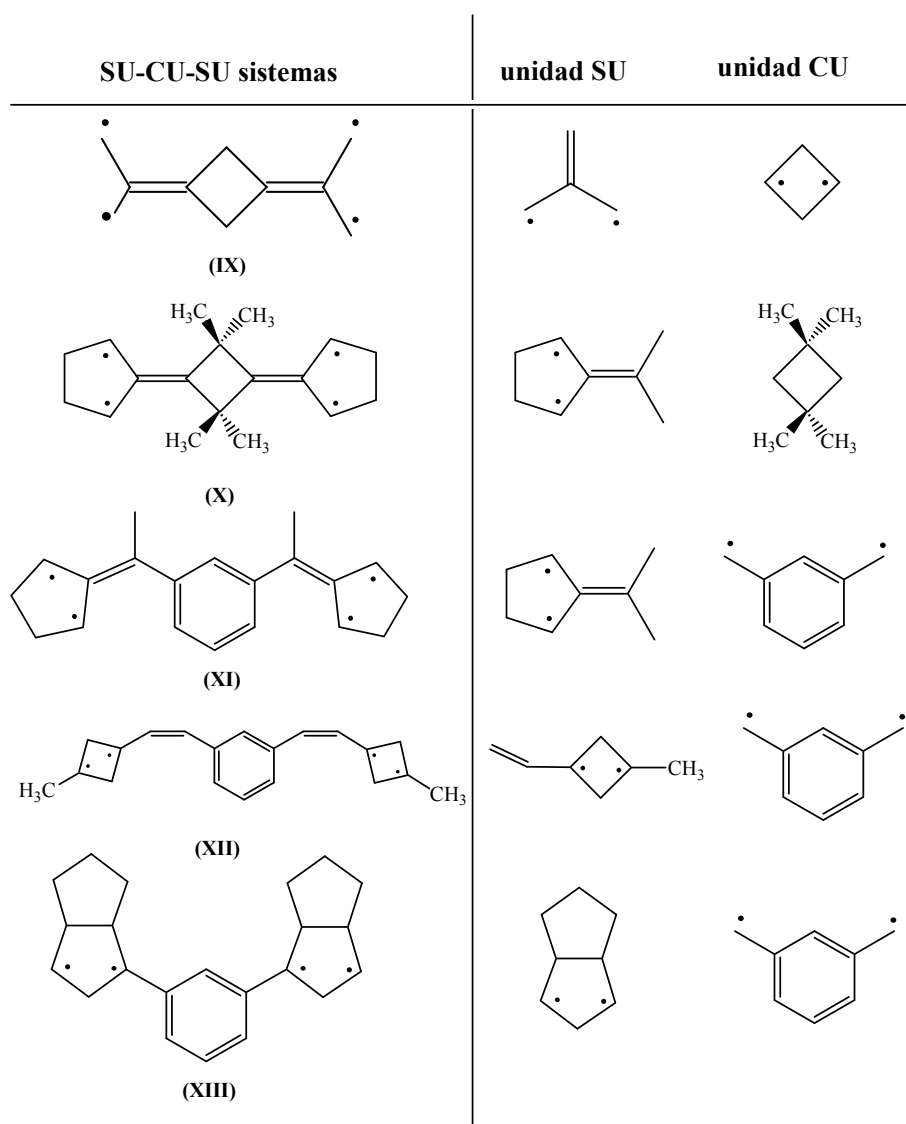
SISTEMAS π -DESLOCALIZADOS	ΔE^{S-T} kcal/mol MMVB	ΔE^{S-T} kcal/mol CAS/6-31g(d)	ΔE^{S-T} kcal/mol bibliografía
I	26.9	25.4	$\approx 15 - 20$
II	26.1	24.4	$\approx 10 - 15$
III	22.5	15.9	$\approx 9 - 10$
IV	24.4	23.5	$\approx 10 - 20$
SISTEMAS π -LOCALIZADOS		ΔE^{S-T} kcal/mol CAS/6-31g(d)	ΔE^{S-T} kcal/mol bibliografía
V		1.5	≈ 1.7
VI		0.9	≈ 1.2
VII		0.5	

Asimismo, se demostró que la metodología empleada se puede extender a sistemas con heteroátomos o con electrones activos que no se encuentren en el entorno π de la moléculas (por ejemplo, σ,σ -didehidronaftaleno). Para estimar correctamente los valores energéticos de los diferentes estados de espín en estos casos es importante tener en cuenta los diferentes valores de los parámetros J_{ij} en cada caso.

9.4.2 Polimerización de biradicales

Entre las metodologías empleadas para incrementar el momento de espín, una ampliamente utilizada consiste en la polimerización de radicales como los estudiados en la sección anterior. Como resultado de los estudios llevados a cabo sobre la polimerización de radicales se observó que la diferencia de energía entre el primer y segundo estados de espín disminuye al incrementar el número de moléculas. De la misma forma, también se incrementa el número de estados de espín posibles.

Figura 9.5 Representación de los sistemas SU-CU-SU estudiados y su descomposición en las unidades constituyentes SU y CU correspondientes.



Otra aproximación para la creación de sistemas macromoleculares de alto espín consiste en la síntesis heterogénea de moléculas contenedoras de espín (*spin containing units*, SU) a través de unidades acopladoras (*coupling units*, CU). En los sistemas SU-CU-SU analizados

(Figura 9.5), como los sintetizados por Dougherty y Adams, las unidades SU y CU son biradicales tripletes como los estudiados en la sección anterior.

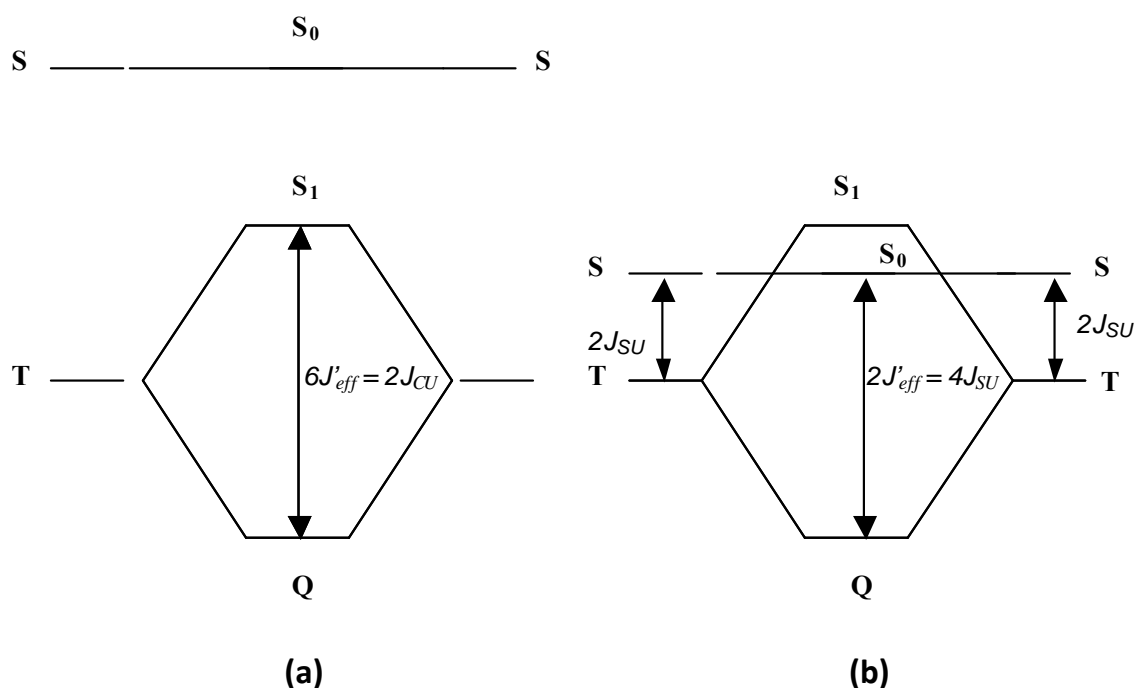


Figura 9.6 Diagramas de energía que incluyen los singuletes S_0 (resultado de la interacción de los estados singulete de dos unidades SU) y S_1 (resultado de la interacción AFM de dos estados triplete de las unidades SU). En el diagrama (a) el estado S_1 es menor en energía que el singulete S_0 . La diferencia de energía entre el estado quintuplete, Q, y el primer estado excitado singulete, S_1 , es $\Delta E(S_1-Q) = 6J'_{eff} = 2J_{CU}$. (b) La energía del estado singulete S_0 es menor que la del singulete S_1 , en cuyo caso la diferencia de energía entre el estado fundamental quintuplete y el primer excitado singulete S_0 es $\Delta E(S_0-Q) = 2J'_{eff} = 4J_{su}$ (si $4J_{su} < 2J_{CU}$ en valor absoluto).

Cuando se diseñan materiales siguiendo esta metodología se ha de considerar si la diferencia de energía entre el primer y segundo estados de espín se puede definir a partir de la diferencia de energía entre los dos estados de espín de las unidades constitutivas. Es decir, cuando dos SU cuyos estados fundamentales son tripletes interaccionan, pueden hacerlo FM, dando como resultado un quintuplete (Q) o AFM, dando lugar a un singulete (S_1) (Figura 9.6a). Se espera que el carácter magnético de la interacción venga determinado por la unidad acopladora, CU.

Como resultado de nuestra investigación observamos que las unidades constitutivas mantienen su espín cuando están formando parte de la macromolécula. Además, se observó que el estado de espín de la macromolécula está caracterizado por las unidades constitutivas de menor diferencia de energía entre estados de espín. Es decir, si la diferencia de energía entre los estados de espín en las unidades SU es menor que en la unidad CU, el estado singulete S_0 de la macromoléculas SU-CU-SU será el resultado de la interacción de los dos singuletes de las unidades SU (Figura 9.6b).

También se ha observado que el estado de alto espín es más estable en aquellos sistemas macromoleculares cuyas unidades constitutivas SU y CU tiene estados de alto espín robustos.

Así pues, se ha demostrado la importancia de los parámetros J_{ij} y P_{ij} para estimar la diferencia de energía entre estados con diferente espín. Estos parámetros han permitido identificar las contribuciones principales de la diferencia de energía entre diferentes estados de espín y comprender los mecanismos que estabilizan estados de espín diferente a cero. Se observó que la diferencia de energía entre dos estados de espín de una molécula está gobernada por los parámetros con menor J_{ij} y que, por tanto, tienen barreras energéticas menores.

9.4.3 Caracterización de interacciones a través del espacio en sistemas bimoleculares

9.4.3.1 Caracterización de interacciones intermoleculares débiles con la metodología *Atoms in Molecules* (AIM)

Las interacciones intermoleculares en sistemas magnéticos generalmente son de carácter débil, por lo que es importante caracterizarlas adecuadamente. La metodología "Atoms in Molecules" (AIM) introducida por Bader propone la descripción de los sistemas moleculares en base a las propiedades topológicas de la densidad de espín. Esta metodología propone analizar las características topológicas de la densidad electrónica y sus propiedades, tales como la Hessiana y la Laplaciana, para definir los núcleos y los enlaces.

Para evaluar la metodología AIM en la descripción de interacciones intermoleculares débiles, hemos estudiado la presencia de puntos críticos de enlace (*bond critical points*, BCP) y sus características con respecto a la distancia y orientación entre dos moléculas.

Los análisis realizados sobre la existencia de BCPs en sistemas bimoleculares $\text{H}_2\text{O}\cdots\text{HF}$, $\text{H}_2\text{O}\cdots\text{CH}_4$, $\text{H}_2\text{O}\cdots\text{CHF}_3$ indican que las características topológicas de la densidad electrónica permiten identificar interacciones intermoleculares débiles como puentes de hidrógeno o interacciones de van der Waals. Estas interacciones se caracterizan por tener una densidad electrónica de pequeña magnitud y un valor de Laplaciana positivo y pequeño.

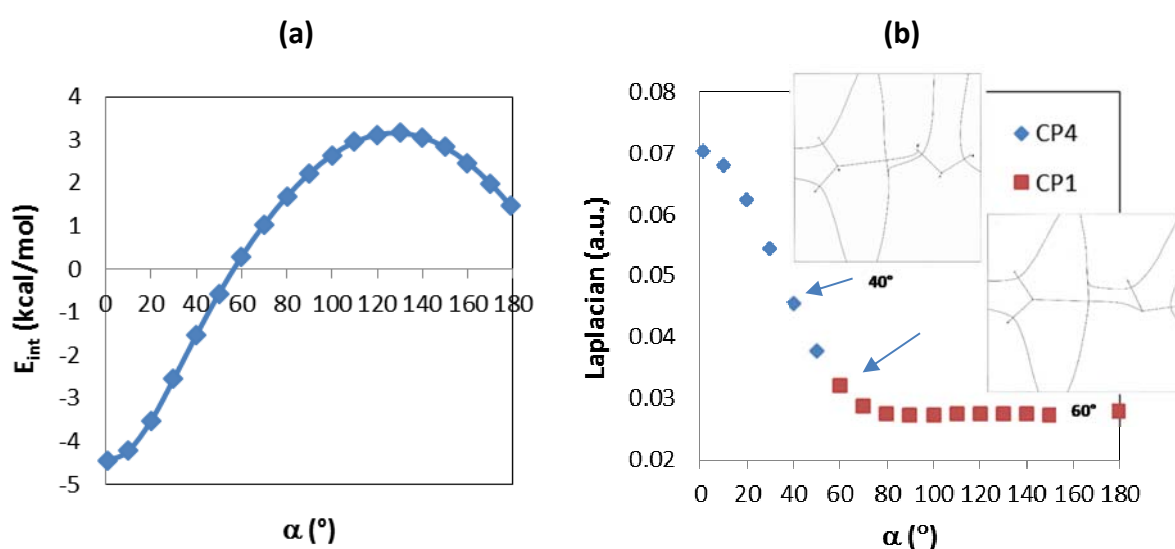


Figura 9.7 (a) E_{int} y (b) Laplaciana del punto crítico (CP) de enlace entre dos moléculas de agua a diferentes ángulos α . Adicionalmente, en (b) se muestran las figuras que indican los caminos de enlace a $\alpha = 40^\circ$ y 60° .

En el estudio sobre la variación angular entre dos moléculas de H₂O, observamos que los parámetros de Bader varían al pasar de una interacción enlazante entre dos moléculas de agua formando un puente de hidrógeno a una interacción no enlazante cuando los dos átomos de oxígeno están enfrentados (Figura 9.7a). El punto crítico de enlace primero se establece entre el hidrógeno de una molécula y el oxígeno de la otra para luego tener lugar entre los dos oxígenos (Figura 9.7b).

Tabla 9.3 Valores de E_{int} , momento dipolar, polarizabilidad, densidad electrónica (ρ_{cp}) y Laplaciana (L_{cp}) en el punto crítico de enlace para los sistemas indicados.

Sistema	E_{int} (MP2) kcal/mol	Momento dipolar	Polarizabilidad	ρ_{cp} a.u.	L_{cp} a.u.
SISTEMAS I					
H ₂ O	2.96	2.084	1.154	$7.33 \cdot 10^{-3}$	$2.54 \cdot 10^{-2}$
HOF	0.64	2.263	1.551	$6.08 \cdot 10^{-3}$	$2.40 \cdot 10^{-2}$
FOF	-0.63	0.253	1.955	$4.75 \cdot 10^{-3}$	$2.15 \cdot 10^{-2}$
CO	-0.61	0.340	1.842	$5.79 \cdot 10^{-3}$	$2.49 \cdot 10^{-2}$
HOCH ₃	2.73	1.956	2.760	$7.65 \cdot 10^{-3}$	$2.59 \cdot 10^{-2}$
(CH ₃) ₂ O	2.07	1.628	4.510	$8.19 \cdot 10^{-3}$	$2.64 \cdot 10^{-2}$
HOCH ₂ F	1.53	0.365	2.930	$7.19 \cdot 10^{-3}$	$2.61 \cdot 10^{-2}$
HOCH ₂ CH ₃	6.09	1.821	4.483	$7.71 \cdot 10^{-3}$	$2.62 \cdot 10^{-2}$
SISTEMAS II					
H ₂ CO	1.55	3.303	2.758	$5.83 \cdot 10^{-3}$	$2.51 \cdot 10^{-2}$
H ₂ NO	2.44	2.913	2.379	$4.85 \cdot 10^{-3}$	$2.30 \cdot 10^{-2}$
HFNO	0.45	2.883	2.496	$4.68 \cdot 10^{-3}$	$2.28 \cdot 10^{-2}$
HCH ₃ NO	3.06			$4.86 \cdot 10^{-3}$	$2.32 \cdot 10^{-2}$
HCH ₂ FNO	1.41			$4.82 \cdot 10^{-3}$	$2.30 \cdot 10^{-2}$
HCH ₂ CH ₃ NO	2.63	3.084	5.613	$4.89 \cdot 10^{-3}$	$2.33 \cdot 10^{-2}$

Finalmente, realizamos un análisis sobre la presencia de BCP intermoleculares en el caso de interacciones repulsivas con la finalidad de encontrar alguna característica de la interacción que permitiera distinguir las interacciones atractivas de las que no lo son. Para ello investigamos las interacciones entre dos moléculas orientadas de forma no enlazante en los siguientes sistemas: H₂O...OH₂, HFO...OFH, F₂O...OF₂, CO...OC, (CH₃)HO...OH(CH₃), (CH₃)₂O...O(CH₃)₂, (CH₂F)HO...OH(CH₂F), (CH₃CH₂)HO...OH(CH₃CH₂), H₂CO...OCH₂, H₂NO...ONH₂, HFNO...ONHF, (CH₃)HNO...ONH(CH₃), (CH₂F)HNO...ONH(CH₂F), (CH₃CH₂)HNO...ONH(CH₃CH₂). Con este análisis se pudo concluir que no se encontró ninguna característica de las analizadas que permitiera discriminar entre interacciones atractivas y repulsivas (Tabla 9.3). En todos los casos encontramos puntos críticos de enlace con valores de densidad electrónica y Laplaciana similares. Como conclusión, podemos afirmar que la presencia de BCP entre dos moléculas es condición necesaria pero no suficiente para definir una interacción intermolecular atractiva. Por tanto, es necesario complementar el estudio con un análisis energético para poder determinar si existe una estabilización del sistema dimérico.

9.4.3.2 Análisis de la teoría de McConnell-I: estudio de la posible correlación magneto-estructural en la interacción entre dos radicales.

McConnell-I es una teoría ampliamente utilizada en el estudio de las interacciones magnéticas entre dos radicales. Esta metodología se basa en un Hamiltoniano fenomenológico de espín [ecuación (9.8)] en el que $\hat{S}_i^A = \hat{S}^A \rho_i$ y $\hat{S}_j^B = \hat{S}^B \rho_j$, donde A y B representan los dos radicales. En el supuesto que el parámetro J_{ij}^{AB} sea equivalente en los dos estados de espín, la diferencia de energía se puede expresar de acuerdo con la ecuación (9.9).

$$\hat{H}^{AB} = - \sum_{\substack{i \in A \\ j \in B}} J_{ij}^{AB} \hat{S}_i^A \cdot \hat{S}_j^B \quad (9.8)$$

$$\begin{aligned} \Delta E^{LS-HS} &= \langle \hat{H}^{AB} \rangle^{LS} - \langle \hat{H}^{AB} \rangle^{HS} = - \sum_{\substack{i \in A \\ j \in B}} J_{ij}^{AB} \left[\langle \hat{S}_i^A \cdot \hat{S}_j^B \rangle^{LS} - \langle \hat{S}_i^A \cdot \hat{S}_j^B \rangle^{HS} \right] = \\ &= - \left[\langle \hat{S}^A \cdot \hat{S}^B \rangle^{LS} - \langle \hat{S}^A \cdot \hat{S}^B \rangle^{HS} \right] \sum_{\substack{i \in A \\ j \in B}} J_{ij}^{AB} (\rho_i^A \rho_j^B) \end{aligned} \quad (9.9)$$

Dado que $\langle \hat{S}^A \cdot \hat{S}^B \rangle^{LS} < \langle \hat{S}^A \cdot \hat{S}^B \rangle^{HS}$ el valor de $\left[\langle \hat{S}^A \cdot \hat{S}^B \rangle^{LS} - \langle \hat{S}^A \cdot \hat{S}^B \rangle^{HS} \right]$ es negativo [ecuación (9.10)(5.5)]. Por lo tanto, McConnell-I postula que la interacción entre dos radicales será FM cuando la interacción principal es entre átomos o grupos de átomos con densidades de espín de signos opuestos $\rho_i^A \rho_j^B < 0$. Por el contrario, si los átomos o grupos de átomos que interaccionan tienen densidades de espín del mismo signo, la interacción será preferentemente AFM.

$$\langle \hat{S}^A \cdot \hat{S}^B \rangle = \frac{1}{2} [S(S+1) - S_A(S_A+1) - S_B(S_B+1)] \quad (9.10)$$

Ahora bien, en varias ocasiones se ha constatado que la teoría de McConnell-I no es capaz de explicar las observaciones experimentales. Para poder determinar en qué casos la teoría de McConnell-I es válida, realizamos un estudio sistemático del efecto de la distancia y la orientación entre radicales en las interacciones intermoleculares. Escogimos para nuestro estudio radicales que representarían interacciones intermoleculares encontradas en cristales moléculas orgánicas: $\text{H}_2\text{NO}\cdot$ (Figura 9.8), $\cdot\text{CH}_3$ (Figura 9.9) y $\cdot\text{C}_3\text{H}_5$ (Figura 9.10).

En la interacción entre dos radicales $\text{H}_2\text{NO}\cdot$ (Figura 9.8) se observó que hay orientaciones que favorecen las interacciones ferromagnéticas, mientras que otras favorecen las antiferromagnéticas. De hecho, la orientación de los orbitales a los que pertenecen los electrones libres determina qué tipo de interacción magnética se estabiliza.

En el análisis de la interacción entre un radical metilo ($\cdot\text{CH}_3$) y uno alilo ($\cdot\text{C}_3\text{H}_5$) se observó que la interacción es AFM cuando los dos radicales están en planos paralelos y el centro de

espín del metilo se localiza sobre los carbonos laterales de los alilos, mientras que si el metilo interacciona principalmente con el átomo central del alilo es FM. Esta observación concuerda con la teoría de McConnell-I ya que el carbono del metilo y los átomos de carbono laterales del alilo tienen densidad de espín del mismo signo, mientras que el átomo de carbono central del alilo tiene densidad de espín de signo contrario. Como resultado del estudio sobre la interacción angular entre ambos radicales (Figura 9.9) se observó que hay zonas de interacción preferentemente FM ($30^\circ - 120^\circ$ y $160^\circ - 180^\circ$) y otras AFM ($0^\circ - 20^\circ$ y $130^\circ - 150^\circ$).

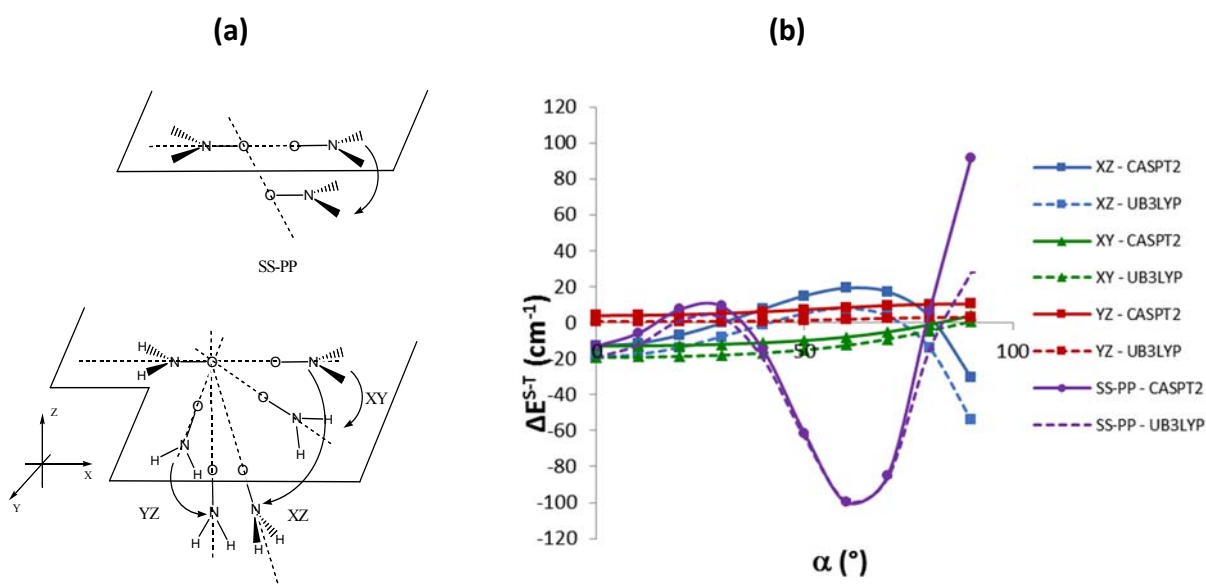


Figura 9.8 (a) Representación de la interacción entre dos H_2NO según SS-PP y los planos XY, XZ e YZ. (b) Diferencia de energía ΔE^{S-T} (cm^{-1}) entre el singulete y el triplete calculada a nivel CASPT2(6,4) y UB3LYP usando la base 6-31+g(2d,2p).

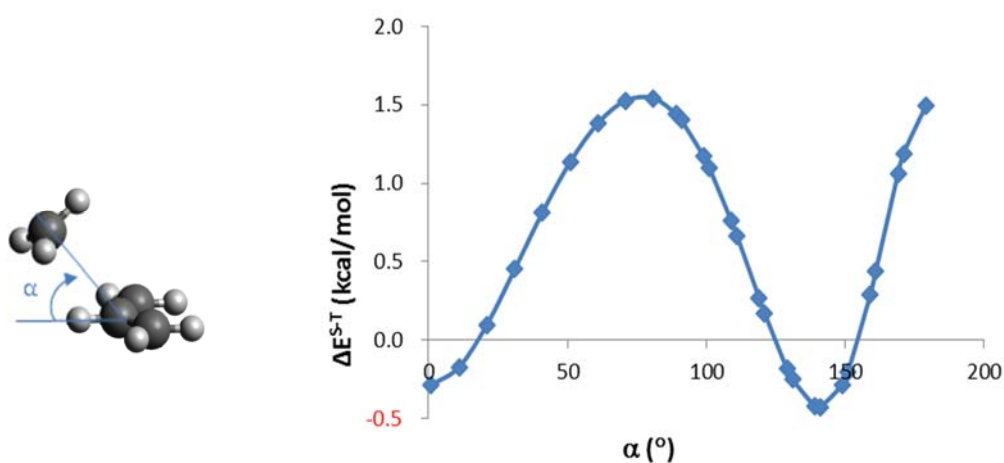


Figura 9.9 Diferencia de energía ΔE^{S-T} (kcal/mol) entre el singulete y el triplete en la interacción metilo...alilo fijando la distancia intermolecular a 3 Å. Los cálculos se realizaron a nivel CAS(4,4)/6-31g(d).

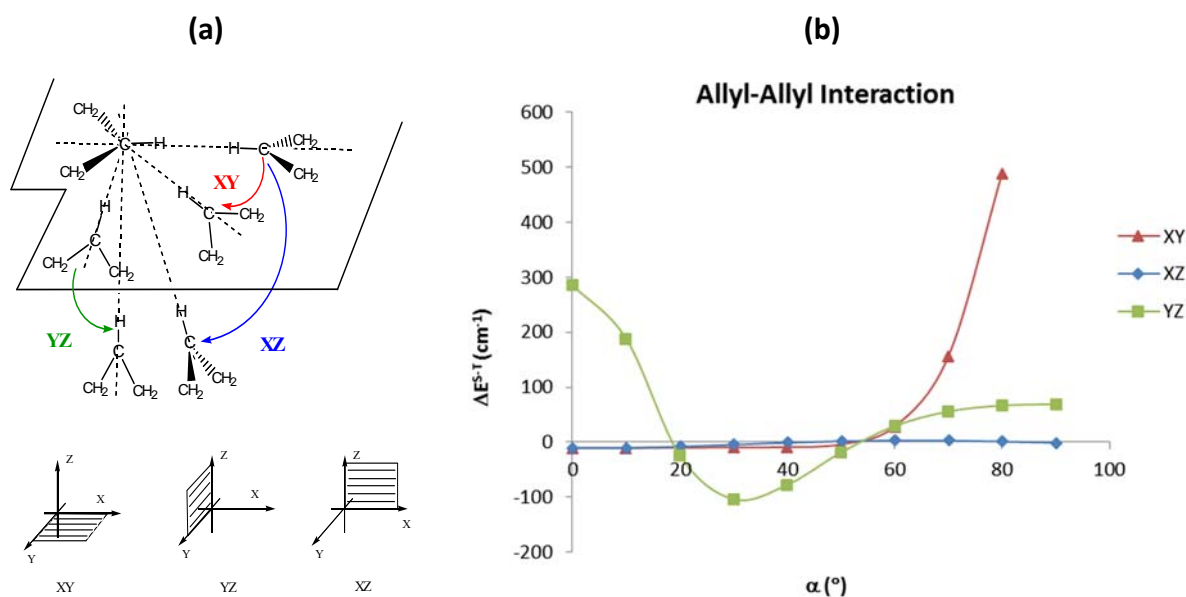


Figura 9.10 (a) Representación de la interacción entre dos alilos según los planos XY, XZ e YZ. (b) Diferencia de energía ΔE^{S-T} (cm⁻¹) entre el singulete y el triplete calculada a nivel CAS(6,6)/6-31g(d)

Si analizamos las contribuciones de las interacciones entre cada par de electrones activos (considerando activos los electrones que pertenecen al entorno π de la molécula), observamos que la interacción es FM cuando la principal interacción (J_{ij} de mayor valor absoluto) se establece entre el metilo y el carbono central (C₂) del alilo (ángulos 45° y 90° en la Tabla 9.4). Por el contrario, la interacción es AFM cuando la interacción principal se establece con los carbonos laterales del alilo (ángulo 135° en la Tabla 9.4). Estas observaciones permiten decir en qué casos la orientación entre los radicales verifica la teoría de McConnell-I.

Tabla 9.4 Valores de J_{ij}^T , ΔP_{ij}^{S-T} , $\Sigma J_{ij}^T \Delta P_{ij}^{S-T}$ y ΔE^{S-T} , calculados a nivel CASSCF(4,4)/6-31g(d) para la interacción metilo...alilo fijando la distancia intermolecular a 3 Å.

	J_{ij}^T kcal/mol			ΔP_{ij}^{S-T} kcal/mol			$\Sigma J_{ij}^T \Delta P_{ij}^{S-T}$ kcal/mol (1)	ΔE^{S-T} kcal/mol
	C ₁	C ₂	C ₃	C ₁	C ₂	C ₃		
0°	0.000	0.000	0.000	1.173	-0.345	1.173	0.0	-0.3
45°	-0.048	-3.853	-0.048	1.181	-0.369	1.181	1.3	1.0
90°	-0.085	-3.998	-0.085	1.184	-0.38	1.184	1.3	1.4
135°	-2.564	-0.106	-2.564	1.164	-0.347	1.164	-5.9	-0.4
180°	0.000	0.000	0.000	1.178	-0.356	1.178	0.0	1.4

(2) Sólo se consideran las interacciones through-space TS

En el análisis de la interacción entre dos radicales alilo observamos que, al igual que en el caso de los otros radicales, existen zonas en las que la interacción es preferentemente FM, mientras que para otras orientaciones es AFM o bien la diferencia entre los dos estados de espín es muy pequeña (Figura 9.10). Al igual que para la interacción metilo...alilo, en cada

caso se pueden identificar las diferentes interacciones entre los seis electrones activos pertenecientes al entorno π de la molécula y definir en términos de J_{ij}^T y ΔP_{ij}^{S-T} qué interacciones favorecen el carácter magnético de la interacción.

Como resultado de nuestras investigaciones se puede decir que existen orientaciones espaciales que favorecen las interacciones ferromagnéticas entre los radicales. Cuando (1) ambos radicales están situados en planos paralelos, (2) sus electrones libres pertenecen al entorno π de la molécula, y (3) la interacción está definida entre un átomo o grupo de átomos de una molécula y la otra, McConnell-I suele poder aplicarse. Pero si existe un ángulo de interacción entre las moléculas o existen otras contribuciones importantes en la interacción entre las moléculas, se requieren cálculos más complejos para poder definir la interacción intermolecular.

9.4.4 Empaquetamiento cristalino

9.4.4.1 Estudio de los cristales HNOBEN y YIMWIA

En el diseño de cristales es importante entender las fuerzas que definen el empaquetamiento cristalino molecular. Así pues, examinamos el empaquetamiento cristalino de dos cristales caracterizados experimentalmente: el cristal hexanitrobenceno (HNOBEN) y el cristal YIMWIA, constituido 1:1 por una molécula de trimetil isocianurato (TMIC) y otra de 1,3,5-trinitrobenceno (1,3,5-TNB) (Figura 9.11). La estructura de estos cristales se obtuvo de la Cambridge Crystallographic Data Centre (CCDC). Para estudiar estos sistemas evaluamos la primera esfera de coordinación tanto intra- como inter-capa e identificamos los pares de moléculas que presentaban las distancias intermoleculares más cortas. Para todos los contactos seleccionados calculamos la energía de interacción entre las dos moléculas a nivel MP2 (BSSE) con bases 6-31(g,d) y 6-31(2g,2p) s.

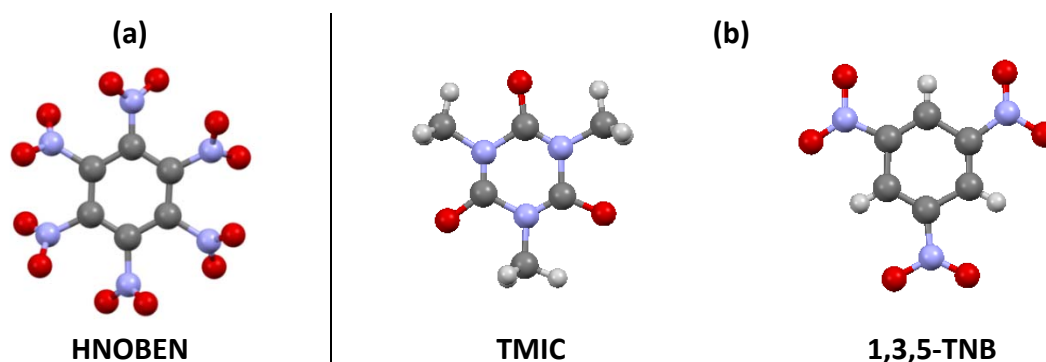


Figura 9.11 (a) Hexanitrobenceno (HNOBEN), molécula que forma el cristal denominado HNOBEN. (b) Trimetil isocianurato (TMIC) y 1,3,5-trinitrobenceno (1,3,5-TNB), las dos moléculas que constituyen el cristal denominado YIMWIA.

En el caso de HNOBEN, tanto las interacciones intra- como inter-capa se estimaron atractivas (Tabla 9.5). Se evaluó que la estabilización inter-capa era resultado de la interacción entre los átomos de oxígeno, ricos en electrones, con el anillo aromático del benceno, cuya densidad electrónica se ve desplazada hacia los seis grupos nitro que tiene enlazados. La interacción inter-capa se ha estimado más enlazante que la intra-capa, ya que

en éste último caso los grupos $-\text{NO}_2$ de ambas moléculas se encuentran frente a frente y existe cierta repulsión intermolecular que disminuye la energía de interacción.

Tabla 9.5 Valores de la energía de interacción ($E_{\text{int}} = E_{\text{dim}} - E_{1+2}$) entre dos moléculas de hexanitrobenceno (HNOBEN) que representan las interacciones (a) intra-capa $\text{mon}_1\text{-mon}_2$ y las dos interacciones inter-capas (b) $\text{mon}_2\text{-mon}_3$ y (c) $\text{mon}_1\text{-mon}_3$ en el cristal HNOBEN.

E_{int} (kcal/mol)	HNOBEN	
	6-31g(d,p)	6-31g(2d,2p)
Intra-capa ($\text{mon}_1\text{-mon}_2$)	-1.9	-2.9
Inter-capa ($\text{mon}_2\text{-mon}_3$)	-5.2	-6.7
Inter-capa ($\text{mon}_1\text{-mon}_3$)	-5.5	-6.8

Tabla 9.6 Valores de la energía de interacción (E_{int}) entre dos moléculas que representan las interacciones inter-capa (a) TMIC-TMIC y (b) TNB-TNB, y la inter-capa (c) TMIC-TNB en el cristal YIMWIA.

E_{int} (kcal/mol)	MP2/ 6-31g(d,p)	MP2/ 6-31g(2d,2p)
Intra-capa TMIC	-1.3	-1.5
Intra-capa 1,3,5-TNB	-0.5	-0.9
Inter-capa TMIC-TNB	-5.7	-7.2

En el caso del cristal denominado YIMWIA, observamos que todas las interacciones intermoleculares de los dímeros que representan las interacciones inter-capa TMIC y 1,3,5-TNB y la inter-capas TMIC-TNB son estabilizantes (Tabla 9.6). La interacción entre moléculas TMIC es posible debido a la presencia de enlaces de hidrógeno entre los grupos metilo de una de las moléculas y el átomo de oxígeno del grupo nitro de la molécula vecina. En el caso de la interacción intra-capa 1,3,5-TNB dedujimos que, a pesar de la presencia de una interacción repulsiva entre los grupos nitro, existe una contribución atractiva entre los grupos $-\text{NO}_2$ de una molécula 1,3,5-TNB e hidrógenos del anillo bencénico desprovisto de densidad electrónica de la otra molécula. El análisis AIM realizado para esta interacción identificó dos puntos críticos de enlace (*Bond Critical Point*, BCP) y un punto crítico de anillo (*Ring Critical Point*, RCP) entre dos moléculas de 1,3,5-TNB. Se realizó un estudio entre fragmentos de las moléculas interaccionantes que confirmó que dichos BCP aparecen como consecuencia de la densidad electrónica de los oxígenos entre los dos grupo $-\text{NO}_2$. Sin embargo, los RCP parecen ser resultado de la interacción atractiva entre las dos moléculas de 1,3,5-TNB y se encuentran camuflados por la presencia de los otros BCP a su alrededor. La interacción inter-capa entre las moléculas TMIC y 1,3,5-TNB es la que presenta un mayor carácter atractivo y, por tanto, se supone que es la encargada de estabilizar la estructura global del cristal. Creemos que la interacción atractiva se ve favorecida por la formación de puentes de hidrógeno entre los átomos de hidrógeno de los grupos metilo de TMIC y los grupos $-\text{NO}_2$ de la molécula 1,3,5-TNB.

9.4.4.2 Estudio magneto-estructural en cristales moleculares de la familia de los α -nitronil nitróxido

Nuestro grupo ha llevado a cabo extensos estudios sobre la aplicabilidad de la teoría de McConnell-I en cristales de la familia de los α -nitronil nitróxido (α -NN) (Figura 9.12a). En concreto, se realizó un extenso análisis de la relación magneto-estructural entre la orientación de los grupos ONCNO (es decir, los átomos que contienen la mayor densidad de espín, Figura 9.12b) de las moléculas de α -NN y la propiedad magnética observada experimentalmente. Como resultado no se observó una relación magneto-estructural clara en los sistemas estudiados. Este hecho podría ser debido a que la interacción seleccionada entre grupos ONCNO no es suficiente para describir el magnetismo obtenido a nivel macroscópico.

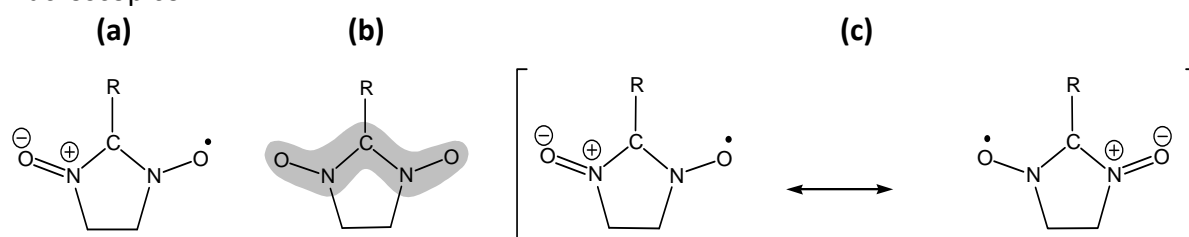


Figura 9.12 (a) Monómero α -nitronil nitróxido, donde R representa grupos orgánicos diferentes. (b) Distribución de la densidad de espín en los átomos ONCNO del monómero α -nitronil nitróxido. (c) Resonancia entre las posibles configuraciones de las moléculas de α -nitronil nitróxido.

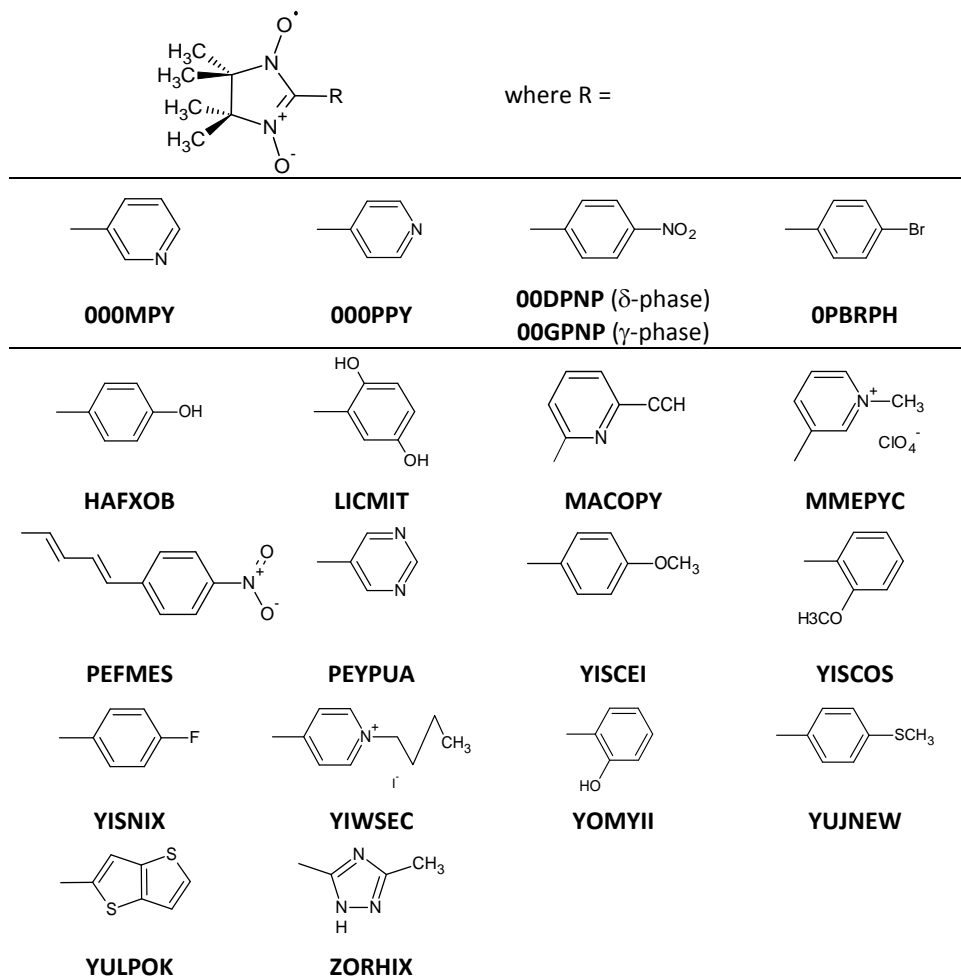


Figura 9.13 Monómeros α -nitronil nitróxido que dan lugar a cristales con propiedades ferromagnéticas.

Para corroborar esta hipótesis, analizamos las interacciones en el subgrupo de cristales que presentan propiedades FM a nivel experimental (Figura 9.13) desde dos puntos de vista. Por un lado evaluamos la diferencia de energía entre el singulete y el triplete entre los grupos ONCNO que representan los contactos más próximos en el espacio. De este estudio se concluye que dentro del subgrupo de cristales FM, los contactos escogidos presentaban tanto interacciones FM ($\Delta E^{S-T} > 0$, en Tabla 9.7) como AFM ($\Delta E^{S-T} < 0$, en Tabla 9.7).

Para analizar en detalle las interacciones entre los grupos ONCNO, se escogieron ciertos contactos dentro del subgrupo de cristales FM que presentaban ambas interacciones, FM ($\Delta E^{S-T} > 0$) y AFM ($\Delta E^{S-T} < 0$) (Table 6.9). Como resultado de este estudio observamos que en las interacciones de carácter FM los contactos principales son entre el C de un grupo ONCNO y el grupo NO del otro (densidades de espín de diferente signo), tal y como se puede observar en la Tabla 9.9. Por el contrario, el carácter de la interacción es AFM cuando las interacciones son principalmente entre grupos NO de ambas moléculas (Tabla 9.9).

Tabla 9.7 Valores de ΔE^{S-T} (en cm^{-1}) calculados a nivel CAS(6,6)/6-31+g(d,p) para la interacción entre dos sistemas ONCNO de los cristales α -nitronil nitróxido estudiados.

	CAS(6,6)		CAS(6,6)		CAS (6,6)
000MPY	9.15	LICMIT1	-2.64	YISCEI	0.06
000PPY	-0.09	LICMIT2	0.14	YISCOS	-0.68
00DPNP	0.08	MACOPY1	0.12	YISNIX	0.01
00GPNP1	0.10	MACOPY2	0.12	YIWSEC	6.75
00GPNP2	0.05	MMEPYC1	-4.85	YUJNEW	-0.46
0PBRPH1	0.04	MMEPYC2	-5.12	YULPOK1	0.06
0PBRPH2	-1.54	PEFMES	-0.07	YULPOK2	-0.49
HAFXOB	-0.20	PEYPUA	35.33	ZORHIX1	12.06
				ZORHIX2	0.00

Tabla 9.8 Valores de ΔE^{S-T} (en cm^{-1}) calculados a nivel CAS(6,6), CASPT2(6,6) y $\sum J_{ij}^T \Delta P_{ij}$, usando la base 6-31+g(d,p) para los dímeros formados por los sistemas ONCNO en los subgrupos FM-FM (**ZORHIX1**, **000MPY**, **PEYPUA** y **YISNIX**) y FM-AFM (**MMEPYC1**, **MMEPYC2** y **0PBRPH**), donde *FM*- es el comportamiento macroscópico del cristal y *-FM/-AFM* el carácter magnético de la interacción estudiada.

<i>FM-FM</i>	CAS(6,6)	CASPT2(6,6)	$\sum J_{ij}^T \Delta P_{ij}$	<i>FM-AFM</i>	CAS(6,6)	CASPT2(6,6)	$\sum J_{ij}^T \Delta P_{ij}$
000MPY	9.2	9.9	1.2	0PBRPH2	-1.5	-1.4	-4.1
PEYPUA	36.9	49.8	58.2	MMEPYC1	-4.8	-6.4	-4.2
YISNIX	6.8	6.8	9.5	MMEPYC2	-5.1	-6.3	-4.2
ZORHIX1	12.0	11.5	4.8				

Tabla 9.9 Desglose de las contribuciones ΔP_{ij} y J_{ij} (en cm^{-1}) con respecto a la diferencia de energía $\Delta E^{\text{S-T}}$ (en cm^{-1}) calculadas a nivel CASVB(6,6)/6-31+g(d,p) para los fragmentos ONCNO en los subgrupos *FM-FM* (**ZORHIX1**, **000MPY**, **PEYPUA** y **YISNIX**) y *FM-AFM* (**MMEPYC1**, **MMEPYC2** y **OPBRPH**) de los cristales α -NN. Las contribuciones más importantes de las interacciones intermoleculares se marcan en cursiva.

<i>FM-FM</i>		ΔP_{ij}			J_{ij}			$J_{ij}\Delta P_{ij}$		
		<i>ON₁</i>	<i>C</i>	<i>ON₂</i>	<i>ON₁</i>	<i>C</i>	<i>ON₂</i>	<i>ON₁</i>	<i>C</i>	<i>ON₂</i>
000MPY	<i>ON₁</i>	0.758	-0.269	0.786	-0.786	-6.148	0	-0.596	<i>1.654</i>	0
	<i>C</i>	-0.256	0.089	-0.257	-0.41	0	0	0.105	0	0
	<i>ON₂</i>	0.682	-0.242	0.709	0	0	0	0	0	0
PEYPUA	<i>ON₁</i>	0.632	-0.266	0.749	4.063	<i>-212.701</i>	-1.2	2.568	<i>56.578</i>	-0.899
	<i>C</i>	-0.232	0.088	-0.276	-0.569	-5.327	-0.656	0.132	-0.469	0.181
	<i>ON₂</i>	0.707	-0.264	0.837	0	-0.517	0	0	0.137	0
YISNIX	<i>ON₁</i>	0.693	-0.256	0.78	0.503	<i>-35.168</i>	0.368	0.349	<i>9.003</i>	0.287
	<i>C</i>	-0.241	0.089	-0.271	0	-1.056	0	0	-0.094	0
	<i>ON₂</i>	0.687	-0.253	0.773	0	0	0	0	0	0
ZORHIX1	<i>ON₁</i>	0.815	-0.251	0.641	-7.715	<i>-45.714</i>	0	-6.288	<i>11.474</i>	0
	<i>C</i>	-0.286	0.088	-0.224	0	-7.353	-0.687	0	-0.647	0.154
	<i>ON₂</i>	0.824	-0.251	0.645	0	-0.471	0	0	0.118	0

<i>FM-AFM</i>		ΔP_{ij}			J_{ij}			$J_{ij}\Delta P_{ij}$		
		<i>ON₁</i>	<i>C</i>	<i>ON₂</i>	<i>ON₁</i>	<i>C</i>	<i>ON₂</i>	<i>ON₁</i>	<i>C</i>	<i>ON₂</i>
OPBRPH2	<i>ON₁</i>	0.683	-0.243	0.717	-2.318	0	-3.602	-1.583	0	-2.583
	<i>C</i>	-0.25	0.089	-0.264	-0.337	-0.595	0	0.084	-0.053	0
	<i>ON₂</i>	0.747	-0.266	0.784	0	0	0	0	0	0
MMEPYC1	<i>ON₁</i>	0.761	-0.245	0.665	-3.655	<i>-7.832</i>	-5.059	-2.782	1.919	-3.365
	<i>C</i>	-0.257	0.088	-0.252	-0.356	-1.112	0	0.091	-0.098	0
	<i>ON₂</i>	0.799	-0.257	0.699	0	0	0	0	0	0
MMEPYC2	<i>ON₁</i>	0.794	-0.25	0.661	-4.762	<i>-3.682</i>	-1.957	-3.781	0.92	-1.294
	<i>C</i>	-0.278	0.087	-0.232	0	-0.647	-0.228	0	-0.056	0.053
	<i>ON₂</i>	0.805	-0.253	0.666	0	0	0	0	0	0

Posteriormente, realizamos un análisis estadístico de los parámetros geométricos intermoleculares que definen la posición relativa de dichos grupos ONCNO. Con esta finalidad, se llevó a cabo un análisis de factores principales y, en segundo lugar, un análisis de formación de agrupaciones (*clusters*). El análisis de factores principales permite encontrar un nuevo sistema de coordenadas en el que el/los factor/es principal/es representan la mayor variabilidad de los parámetros estudiados. De esta manera se reduce un problema de 6 coordenadas utilizadas (una distancia, dos ángulos y tres diedros) a un único factor que represente la mayor variabilidad geométrica. Este análisis identificó un factor principal que describía un 71% de la variabilidad entre los cristales analizados. Este factor está compuesto básicamente por los ángulos diedros entre los dos sistemas ONCNO. Un análisis gráfico de la diferencia de energía entre los dos estados de espín y el factor principal permite visualizar ciertas agrupaciones. Sin embargo, la diferencia es muy sutil y

existen numerosos sistemas que se encuentran en la frontera entre los dos grupos FM y AFM.

En el análisis de agrupaciones, utilizamos las distancias definidas entre los diferentes sistemas ONCNO calculadas según las descripciones de distancias Euclidianas y de Mahalanobis. Se realizó un análisis de agrupaciones de vecinos más cercanos (*nearest neighbor clustering*) para ver si los sistemas se agrupaban según las características magnéticas de la interacción (FM o AFM). El análisis estadístico realizado no encontró ninguna agrupación que diferenciara sistemas de interacciones FM de sistemas que presentaran interacciones AFM.

Como consecuencia de este estudio, concluimos que las interacciones ONCNO no son suficientes para describir las propiedades magnéticas observadas experimentalmente. Otras interacciones –no consideradas en el modelo simplificado de interacciones ONCNO– necesariamente juegan un papel importante a la hora de definir el carácter magnético del sistema. Adicionalmente, se ha demostrado que no hay una relación magneto-estructural sencilla como la que propone el modelo de McConnell-I que pueda ser aplicada de forma generalizada para las interacciones intermoleculares a través del espacio (through-space).

9.4.5 Estudio de dímeros π -[TCNE] $_2^{2-}$ en cristales moleculares

El complejo $[\text{Fe}(\text{C}_5\text{Me}_5)_2]^+[\text{TCNE}]^-$ (TCNE = tetracianoetileno) fue el primer compuesto molecular cuyas propiedades magnéticas fueron descritas. Éste es un ejemplo de los complejos denominados sales de transferencia de carga. En estos sistemas una especie dadora [D] dona un electrón a una especie aceptora [A] creándose dos especies radicalarias cargadas $[\text{D}]^+$ y $[\text{A}]^-$ que pueden interactuar de tal manera que exista un momento de espín total diferente de cero. Sin embargo se han dado casos en los que se ha observado la pérdida de magnetismo por dimerización de las especies dadora $[\text{D}]_2^{2+}$ o aceptora $[\text{A}]_2^{2-}$. Como parte de esta tesis doctoral, se ha estudiado el caso de dimerización de las moléculas de TCNE, al ser un ejemplo sencillo de dímeros de especiesceptoras que permite abordar el problema.

Experimentalmente se han descrito tres clases de dímeros de $[\text{TCNE}]_2^{2-}$ (**St**, **Lc** y **Lt**, en la Figura 9.14a). Estos tres grupos se caracterizan por la separación entre los monómeros, r , y el ángulo diedro, d , entre ellos (Figura 9.14b). Los tres confórmers se distinguen por la distancia y el tipo de enlace entre los monómeros. Aquellos que presentan corta distancia se denominan dímeros σ - $[\text{TCNE}]_2^{2-}$ y los de larga distancia π - $[\text{TCNE}]_2^{2-}$. Los tres grupos tienen como estado fundamental un singulete, pero existen características estructurales y espectroscópicas determinadas experimentalmente que los diferencian.

La energía de interacción E_{int} de dos moléculas cargadas se compone de dos componentes: la energía de Coulomb ($E_{\text{coul}} > 0$ / $E_{\text{coul}} < 0$ para moléculas de diferente/mismo signo de carga) y la energía de enlace ($E_{\text{bond}} < 0$). En el caso de dos moléculas del mismo signo, la contribución de la energía de Coulomb es positiva. Si el valor absoluto de dicha energía es mayor que la energía de enlace ($|E_{\text{coul}}| > |E_{\text{bond}}|$), las dos moléculas se repelen y la formación de dímeros no será estable. Por otro lado, si existen fuerzas iónicas (debidas, por ejemplo, a la presencia de contraiones o disolventes polares) que puedan contrarrestar la

repulsión entre las dos moléculas, la energía de enlace puede llegar a ser mayor que la de Coulomb ($|E_{\text{Coul}}| < |E_{\text{bond}}|$) y se podría llegar a estabilizar la formación de los dímeros (Figura 9.15a).

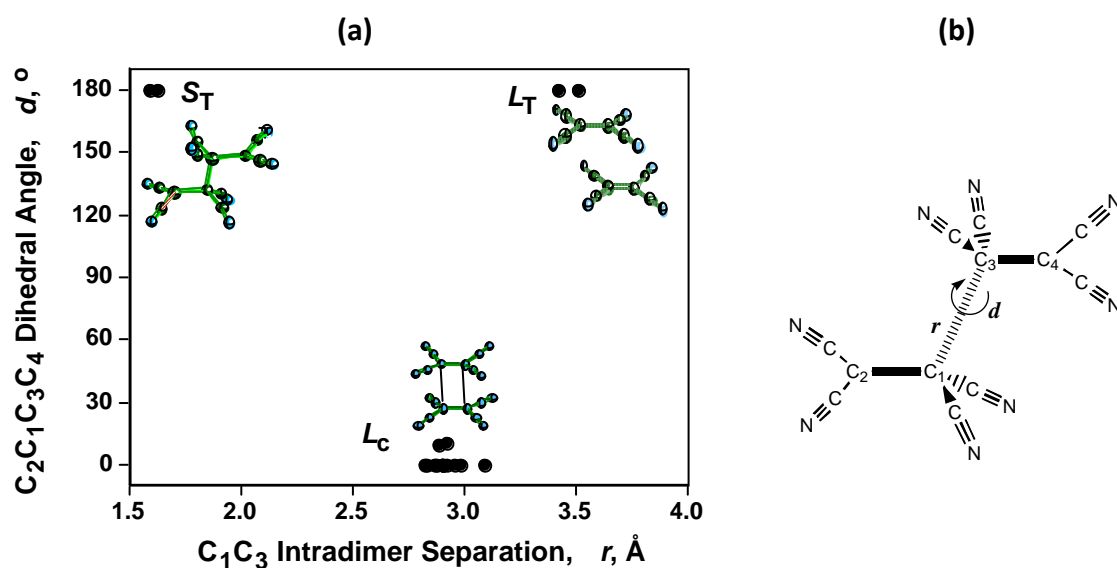


Figura 9.14 (a) Representación de d en función de r para los dímeros de $[\text{TCNE}]_2^{2-}$ caracterizados estructuralmente. (b) Representación gráfica de la distancia $\text{C}\cdots\text{C}$ entre monómeros, r , y el ángulo diedro d .

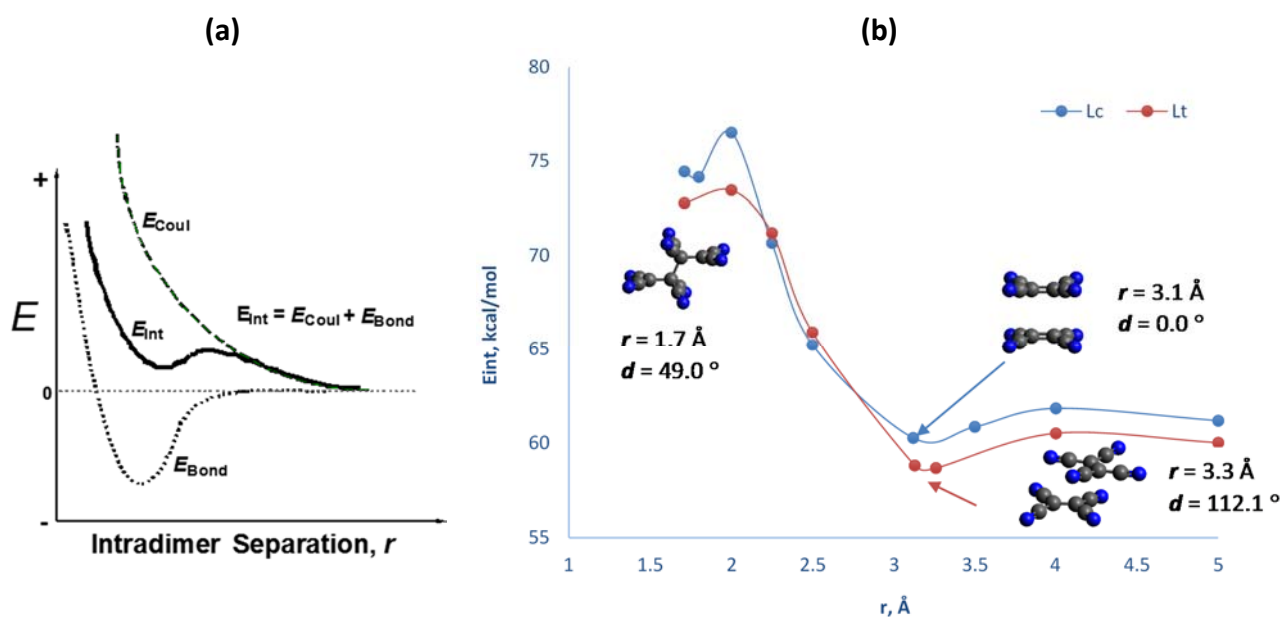


Figura 9.15 (a) Diagrama que muestra la curva de energía de interacción total (E_{int}) compuesta por la adición de la contribución de Coulomb (E_{Coul}) y la de enlace (E_{bond}). (b) Superficie adiabática de energía potencial (E_{int}) calculada en función de la distancia entre los dos monómeros r (en Å) para los conformeros Lc (en azul) y Lt (en rojo). Los cálculos se han realizado a nivel RB3LYP/6-31+g.

Los cálculos que realizamos a nivel RB3LYP describieron la formación de tres mínimos metaestables similares a los observados experimentalmente (Figura 9.15b) y las propiedades espectroscópicas calculadas son análogas a las observadas experimentalmente.

Además, los cálculos realizados a nivel RB3LYP, BS-UB3LYP y UB3LYP describen adecuadamente las curvas de energía potencial de los estados S_0 , S_1 and T_1 , respectivamente (Figura 9.16).

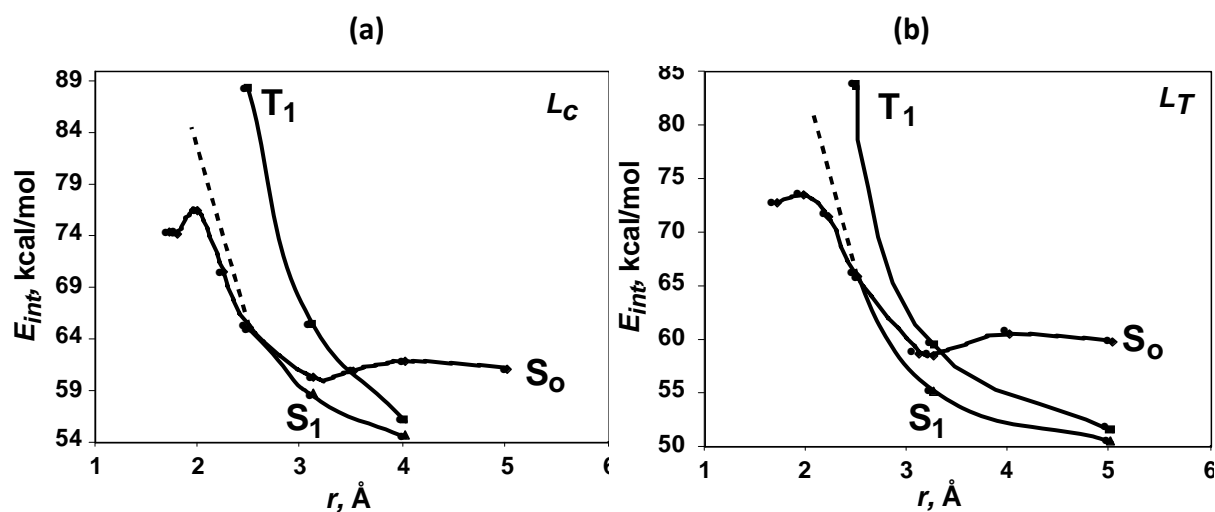
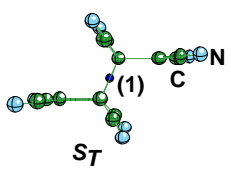
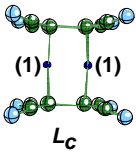
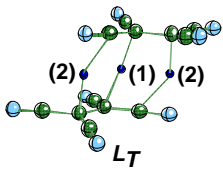


Figura 9.16 Energía de interacción (E_{int}) en función de r de los estados S_0 , S_1 and T_1 para las configuraciones (a) L_c y (b) L_t de los dímeros π -[TCNE] $_2^{2-}$. S_0 representa el singlete de capa cerrada, $^1A_{1g}$; S_1 el singlete de capa abierta, $^1B_{1u}$; y T_1 el triplete, $^3B_{1u}$. Las curvas de energía potencial para los estados S_0 , S_1 y T_1 se han calculado a nivel RB3LYP, BS-UB3LYP y UB3LYP, respectivamente.

Tabla 9.10 Valores de densidad electrónica [$\rho(r_c)$], Laplaciana [$\nabla^2\rho(r_c)$] y ratio $|\lambda_1|/\lambda_3$ de los puntos críticos de enlace (BCP) encontrados en los conforméros S_t , L_c y L_t . Cuando existen diferentes BCP en un mismo conforméromo, estos se indican con diferente numeración.

Conforméromo	#BCP	$\rho(r_c)$	$\nabla^2\rho(r_c)$	$ \lambda_1 /\lambda_3$
 S_t	1	0.167	-0.178	764
 L_c	1	0.012	0.023	0.201
 L_t	1 2	0.011 0.009	0.021 0.021	0.200 0.184

La transición entre los dos conforméromos de larga distancia L_c y L_t supone la ruptura y la formación de nuevos enlaces. Los cálculos realizados muestran un estado de transición para pasar de una conformación *cis* ($d = 0^\circ$, L_c) a una *trans* ($d \approx 120^\circ$) en la que se rompen y

forman enlaces. Asimismo, los BCP que aparecen entre las dos moléculas identifican la existencia de enlaces covalentes en el conformero de corta distancia S_t de tipo σ -[TCNE] $_2^{2-}$ y enlaces débiles en los conformeros de larga distancia L_c y L_t tipo π -[TCNE] $_2^{2-}$ (Tabla 9.10).

Tabla 9.11 Energía de interacción (E_{int}) para los complejos $K_2[TCNE]_2(glyme)_2$, $[Et_4N]_2[TCNE]_2$ y $[Cr(C_6H_6)_2]_2[TCNE]_2$. El valor de E_{int} se descompone en las contribuciones de las interacciones $A^{\cdots}A^-$, $D^+\cdots D^+$, $A^{\cdots}D^+$. Todos los cálculos de realizaron a nivel UHF/6-31+g(2d,2p).

	$E_{int} A^{\cdots}A^-$ kcal/mol	$E_{int} D^+\cdots D^+$ kcal/mol	$E_{int} A^{\cdots}D^+$ kcal/mol	$E_{int} total$ kcal/mol
$K_2[TCNE]_2(glyme)_2$	103.0	30.5	-70.9, -72.1, -75.0 y -73.9	-158.4
$[Et_4N]_2[TCNE]_2$	83.5	19.3	-58.1, -58.0, -66.1 y -66.0	-145.2
$[Cr(C_6H_6)_2]_2[TCNE]_2$	79.9	12.2	-67.5, -68.5, -57.2 y -24.1	-125.2

Cálculos adicionales realizados en presencia de cationes (Tabla 9.11) o en disolventes polares (Tabla 9.12) confirman la estabilización de los mínimos tipo π -[TCNE] $_2^{2-}$, lo que demuestra que al contrarrestar la energía repulsiva se estabiliza la formación de los enlaces a larga distancia.

Tabla 9.12 Mínimos S_t , L_c , L_t y L_{twist} de dímeros de [TCNE] $_2^{2-}$ calculados con el método M06L/6-31g(2d,2p) en acetonitrilo y diclorometano.

	Acetonitrilo			Diclorometano		
	$r(\text{Å})$	$d(^{\circ})$	$E_{int} (kcal/mol)$	$r(\text{Å})$	$d(^{\circ})$	$E_{int} (kcal/mol)$
S_t	1.684	180°	10.1	1.685	180°	14.812
L_c	2.959 ^a	4.3°	-5.6	2.942	3.8°	-0.4
L_t	3.320	179.8°	-3.6	3.300	180°	1.4
L_{twist}	3.124	103.8°	-5.0	3.113	103.5°	-0.1

^a Promedio de dos valores de la distancia intermolecular C \cdots C: 2.949 Å and 2.968 Å.

Tabla 9.13 Energía de interacción (E_{int}) de dímeros de [TCNE] $_2^{2-}$ con 20 moléculas de diclorometano (CH_2Cl_2) calculada a nivel M06L/6-31g(d) usando tanto la geometría optimizada con las moléculas explícitas de disolvente como un algoritmo de disolvente continuo (PCM) con la geometría optimizada.

$r (\text{Å})$	$E_{int} (kcal/mol)$		$\Delta E^{S-T} (kcal/mol)$	
	Geometría opt	PCM	Geometría opt	PCM
2	24.1	-1.1	-33.9	-38.0
3	-22.5	-48.8	-3.7	-15.2
4	-16.0	-40.4	-0.6	-0.9

Para describir la posible formación de dímeros en solución, se realizaron cálculos optimizando la macroestructura del conformero L_c del dímero [TCNE] $_2^{2-}$ con 20 moléculas de disolvente de diclorometano (primera esfera de solvatación). Adicionalmente se calculó

la E_{int} con un método de solvatación continuo (PCM). Como resultado, se observó la estabilización de los dímeros a larga distancia π -[TCNE] $_2^{2-}$ en solución (Tabla 9.13). A distancias intermonoméricas $r = 5 \text{ \AA}$, la orientación inicial *head-to-head* ($d \sim 0^\circ$) se transforma en *head-to-tail* ($d \sim 180^\circ$) con una distancia C-C intermolecular $r = 4.3 \text{ \AA}$. A distancias de 6 \AA , el mínimo no converge y, a 10 \AA , el dímero es menos estable que dos monómeros aislados. Asimismo se puede concluir que en todos los casos el singulete es más estable que el triplete, remarcando el carácter antiferromagnético de la interacción (Tabla 9.13).

El enlace a larga distancia descrito entre dos electrones y cuatro centros ($2e^-/4c$) es único, ya que se da entre $2e^-$ distribuidos entre cuatro átomos de carbono equivalentes.

9.5 Conclusiones

Esta tesis doctoral ha analizado los mecanismos a través del enlace (TB: *through-bond*) y a través del espacio (TS: *through-space*) que estabilizan moléculas de alto espín (radicales) y sus interacciones intermoleculares ferromagnéticas.

Así pues, se ha estudiado la estabilidad de moléculas orgánicas de alto espín y su posible polimerización manteniendo la alta multiplicidad de espín. Se estableció que el mecanismo TS es de menor coste energético que el TB. Por lo tanto, los radicales más estables son aquellos cuyos centros de espín se estabilizan a través del enlace TB. Asimismo, en compuestos que presentan ambos mecanismos, la multiplicidad de espín de los estados fundamental y primer excitado vendrá determinada por el mecanismo a través del espacio TS.

Por otro lado, se estudiaron las interacciones intermoleculares entre radicales, con el objetivo de establecer las condiciones que favorecen la presencia de interacciones ferromagnéticas. En este contexto, se evaluó la teoría denominada McConnell-I. Tras metódicos estudios de la interacción entre dos radicales ($\text{H}_2\text{NO}\cdot$, $\cdot\text{CH}_3$ y $\cdot\text{C}_2\text{H}_5$) en diferentes orientaciones en el espacio, se concluyó que el ámbito de aplicación de esta teoría está limitado. Sólo se podrá aplicar cuando los centros de espín interaccionan en planos paralelos y existe una interacción a través del espacio TS predominante. Estudios adicionales hechos en cristales de la familia de los α -nitronil nitróxidos demostraron que la teoría de McConnell-I no se puede aplicar de forma general a cualquier interacción intermolecular entre radicales. Se observó que esta teoría no predice correctamente el comportamiento magnético de cristales cuando se analiza sólo la interacción entre los átomos que contienen mayoritariamente la densidad de spin (ONCNO). Por tanto, dicho análisis se debe ampliar a otros contactos entre las moléculas interaccionantes para poder describir correctamente el comportamiento magnético observado.

Finalmente, en sales de transferencia de carga, hemos establecido que se dan casos de dimerización de las especies constituyentes, por ejemplo tetracianoetileno $[\text{TCNE}]_2^{2-}$, cuando la repulsión entre especies de la misma carga se minimiza por la presencia de contraiones o disolventes polares. De esta manera, se favorece la formación del enlace en el dímero al permitir la interacción de los electrones desapareados.

